Modelling of Reactive Gas Transport In Unsaturated Soil. A Coupled Thermo-Hydro-Chemical-Mechanical Approach

SHAKIL AL MASUM

Geoenvironmental Research Centre
Cardiff School of Engineering
Cardiff University

Thesis submitted in candidature for the degree of Doctor of Philosophy at Cardiff University

June, 2012

DECLARATION

This work has not previously been accepted in substance for any degree and is not concurrently submitted in candidature for any degree.

Signed ……. (Shakil Al Masum)

Date ……21/06/2012…..…

STATEMENT 1

This thesis is being submitted in partial fulfillment of the requirements for the degree of Doctor of Philosophy (PhD).

Signed ……. (Shakil Al Masum)

Date ……21/06/2012…..…

STATEMENT 2

This thesis is the result of my own independent work/investigation, except where otherwise stated. Other sources are acknowledged by explicit references.

Signed ……. (Shakil Al Masum)

Date ……21/06/2012…..…

STATEMENT 3

I hereby give consent for my thesis, if accepted, to be available for photocopying and for inter-library loan, and for the title and summary to be made available to outside organisations.

Signed ……. (Shakil Al Masum)

Date ……21/06/2012…..…

In The Name of Allah - The Beneficent - The Merciful

Dedicated To

My beloved parents,

Dilara Chowdhury

&

Harun Or Rashid

who have dedicated their life for me and my wellbeing with endless love and support

Acknowledgments

Firstly, I would like to sincerely thank my supervisor Professor Hywel Thomas for his continued support, motivation and invaluable academic guidance throughout this research. I am extremely grateful for the opportunity he has provided me with, allowing me to realise this milestone.

I would also like to express my deepest thanks to my co-supervisor, Dr. Phillip Vardon, for his technical support and guidance during this work. For his contribution, technical comments and encouragement in the last stages of this work, I wish to sincerely acknowledge Dr. Majid Sedighi. The invaluable financial support of this research through PhD fellowships from the Arup and Cardiff School of Engineering and the Geoenvironmental Research Centre is gratefully acknowledged.

I also owe gratitude to all my colleagues at the Geoenvironmental Research Centre for their support; especially Dr. Alexandra, Dr. Tripathy, Dr. Rob Francis, Pauline Welsh, Mojgan Sedighi, Hesham Elgabu, Danothy Bennett, Dr. Manju, Mohammad Irfan, Lee Hosking, Ben Hepburn, Dr. Jamie Lewis. Dr. Ram and Claire Bennett deserve very special thanks for their kind support during this PhD programme.

All my friends who have been so important to finish this work deserve exceptional thanks. I would like to thank Sultanul Islam, Sumi Siddiqua, Monirul Alam, Sadequr Rahman, Shariful Islam, Ziaul Hoque Zico, Zeeshan Mohseen, Shakil Mamun, Ridwanur Rahman, Rahat Khan, Saniul Alam, Bmw Pavel, Reaz, Rajiur Shovon, Hasan Tarek, Mehedi Mamun, Tousif Rahman, Basit Hafeez, Fasiul Alam, Tanima Bari, Kamrul Ahsan, Bulbul Ashraf, Mahjaben Polloby, Sifat Sikandar, Salma Siddika, Shams Ur Rahim, Imtiaz Khan, Rumana Faruque and everyone else who are too numerous to name. A very special mention to Msi Beg, Khaledul Chowdhury, Sharmin Akhter and Faisal Mamun for their cordial support at the very early stage of this academic journey.

For their invaluable kindness and support during my study in the UK, I am truly thankful to my elder brother Tareq Al Mamum Riyadh and younger sister Tasnim Rashid Brinta. Very special thanks to my dearest Sadi Khan and Sanjana Afroz for their enormous support during the toughest years.

Summary

This thesis presents the development of a reactive gas transport equation under coupled framework of thermal, hydraulic, chemical and mechanical (THCM) behaviour of variably saturated soil. The capabilities of theoretical and numerical modelling of THCM processes have been advanced by the successful implementation of various aspects of the new addition. The previously developed THCM model at the Geoenvironmental Research Centre (GRC) has been extended to include the multicomponent gas transport modelling coupled with chemical/geochemical processes.

The mechanisms of advection and diffusion have been considered to define the transport of multicomponent gas and chemicals in respective phases as well as exchange via dissolution and exsolution. The governing mass transfer process is subjected to homogeneous and heterogeneous geochemical reactions under equilibrium condition. Numerical solutions of the governing flow and deformation equations have been achieved by employing finite element method for spatial discretisation and finite difference method for temporal discretisation. Advanced geochemical features of gas-chemical interactions have been incorporated in the transport model, COMPASS by coupling with the geochemical model PHREEQC. A sequential non-iterative approach has been adopted to couple the transport processes and geochemical interactions.

Verification of various aspects of the developed gas transfer equation has been commenced via a number of simulation exercises. Good agreement between the results have been achieved which suggests accurate and successful implementation of the theoretical and numerical formulation.

The model has been implemented to investigate the gas transport processes in variably saturated compacted clay buffers via a number of conceptual simulation scenarios which are representative of high level nuclear waste disposal. Simulation of gas migration through saturated buffer has been intended to investigate the maximum pressure development as well as the dominant flow mechanisms. Demonstration of the modelling capability in context of reactive gas transport has been carried out considering long term isothermal flow of hydrogen through unsaturated clay buffer. The conclusions drawn from the discussions of simulation results has favoured the understanding of some of the key issues associated with gas generation and migration in compacted porous media, particularly, as a case of high level nuclear waste disposal.

Contents

Nomenclature

A	Reactant component of chemical reaction
A_1	Temperature dependent constant
A^+	Exchangeable cation
$\mathbf{A_P}$	Plastic modulus
$\boldsymbol{A_T}$	Thermal vector
$\boldsymbol{A_s}$	Suction vector
B	Reactant component of chemical reaction
B_{ii}	Diagonal elements of binary diffusion matrix
B_{ij}	Cross-diagonal elements of binary diffusion matrix
B_1	Temperature dependent constant
B^+	Exchangeable cation
[B]	Binary diffusion matrix
C	Product of chemical reaction
C_{ps}	Specific heat capacity of solids
C_i	Initial concentration
C_0	Source concentration
$C_{\rho l}$	Specific heat capacity of liquids
C_{pv}	Specific heat capacity of water vapour
C_{pg}	Specific heat capacity of gases, except water vapour
C_{Tl}	Defined in equation (3.150)
C_{TT}	Defined in equation (3.151)
$C^i_{Tc_g}$	Defined in equation (3.152)
$C_{T\mathbf{u}}$	Defined in equation (3.153)
$C^i_{c_d l}$	Defined in equation (3.111)
$C^i_{c_d T}$	Defined in equation (3.112)
$C^i_{c_d^i c_g^j}$	Defined in equation (3.113)

$C^{i}_{c_d c_d}$	Defined in equation (3.114)
$C^{i}_{c_d \mathbf{u}}$	Defined in equation (3.115)
$C^{i}_{c_d s_d}$	Defined in equation (3.119)
C_{ll}	Defined in equation (3.50)
C_{lT}	Defined in equation (3.51)
$C_{lc^{i}_{g}}$	Defined in equation (3.52)
$C_{l\mathbf{u}}$	Defined in equation (3.53)
$\mathbf{C_{c_g l}}$	Defined in equation (4.11)
$\mathbf{C_{c_g T}}$	Defined in equation (4.11)
$\mathbf{C^{i}_{c^{i}_{g} c^{i}_{g}}}$	Defined in equation (4.11)
$\mathbf{C_{c_g u}}$	Defined in equation (4.11)
$\mathbf{C_{ll}}$	Defined in equation (4.19)
$\mathbf{C_{lT}}$	Defined in equation (4.20)
$\mathbf{C^{i}_{lc_g}}$	Defined in equation (4.21)
$\mathbf{C_{lu}}$	Defined in equation (4.22)
$\mathbf{C_{c_d l}}$	Defined in equation (4.28)
$\mathbf{C_{c_d T}}$	Defined in equation (4.29)
$\mathbf{C^{i}_{c_d c_g}}$	Defined in equation (4.30)
$\mathbf{C^{j}_{c_d c_d}}$	Defined in equation (4.31)
$\mathbf{C_{c_d u}}$	Defined in equation (4.32)
$\mathbf{C_{Tl}}$	Defined in equation (4.37)
$\mathbf{C_{TT}}$	Defined in equation (4.38)
$\mathbf{C^{i}_{Tc_g}}$	Defined in equation (4.39)
$\mathbf{C_{Tu}}$	Defined in equation (4.40)
$\mathbf{C_{ul}}$	Defined in equation (4.46)
$\mathbf{C_{uT}}$	Defined in equation (4.47)

$\mathbf{C}^{\mathbf{i}}_{\mathbf{uc_g}}$	Defined in equation (4.48)
$\mathbf{C_{uu}}$	Defined in equation (4.49)
D	Product of chemical reaction
$\mathbf{D}$	Elasticity matrix, defined in equation (3.170)
$\mathbf{[D]}$	Multicomponent diffusion matrix
D_{atms}	Molecular diffusivity of vapour through air
$\mathbf{D_{ep}}$	Elasto-plastic stress-strain matrix
D_d^i	Effective molecular diffusion coefficient
D_{ik}	Knudsen diffusion coefficient
D_{ij}	Multicomponent diffusion coefficient
D_{ij}^0	Effective multicomponent diffusion coefficient
E_{ss}	Sink/source term of water vapour
F	Applied load
F_1	Load collapse curve function
F_2	Suction increase curve function
F_h	Approximate heat flux normal to the boundary surface
G	Shear modulus
H_c	Heat capacity
I	Ionic strength
J_{ad}	Bulk advective gas flux
J_{ad}^i	Advective gas flux of i^{th} gas component
$J_{c_g}^i$	Total flux of i^{th} gas component
J_{od}^i	Diffusive gas flux of i^{th} gas component
J_k^i	Knudsen flux of i^{th} gas component
J_l	Defined in equation (3.57)
$J_{c_d}^i$	Total flux of i^{th} dissolved chemical component
$J_{advective}^i$	Advective flux of i^{th} dissolved chemical component
$J_{diffusive}^i$	Diffusive flux of i^{th} dissolved chemical component

J_Z^i	Defined in equation (3.118)
K_0	At rest stress state of soil
$K_{A/B}$	Equilibrium constant of ion-exchange reaction
K_H	Henry's constant
K_l	Effective permeability of unsaturated soil
K_{eq}	Equilibrium constant of chemical reaction
K_{int}	Intrinsic permeability of porous medium
K_{rg}	Relative permeability
K_{ll}	Defined in equation (3.54)
K_{lT}	Defined in equation (3.55)
$K_{lc_g^i}$	Defined in equation (3.56)
$K_{c_d l}^i$	Defined in equation (3.116)
$K_{c_d c_d}^i$	Defined in equation (3.117)
K_{Tl}	Defined in equation (3.154)
K_{TT}	Defined in equation (3.155)
$K_{Tc_g}^i$	Defined in equation (3.156)
$\mathbf{K}_{\mathbf{c_g^i c_g^i}}^{\mathbf{i}}$	Defined in equation (4.11)
$\mathbf{K}_{\mathbf{ll}}$	Defined in equation (4.23)
$\mathbf{K}_{\mathbf{lT}}$	Defined in equation (4.24)
$\mathbf{K}_{\mathbf{lc_g}}^{\mathbf{i}}$	Defined in equation (4.25)
$\mathbf{K}_{\mathbf{c_d l}}$	Defined in equation (4.33)
$\mathbf{K}_{\mathbf{c_d c_d}}^{\mathbf{j}}$	Defined in equation (4.34)
$\mathbf{K}_{\mathbf{Tl}}$	Defined in equation (4.41)
$\mathbf{K}_{\mathbf{TT}}$	Defined in equation (4.42)
$\mathbf{K}_{\mathbf{Tc_g}}^{\mathbf{i}}$	Defined in equation (4.43)
L	Latent heat of vaporisation
M	The slope of critical state line

M_g^i	Molecular weight of i^{th} gas component.
M_{Fe}	Molecular weight of iron
M_{aq}	Total number of aqueous master species
N	Total number of gas component
N_s	Shape function
N_r	Defined in equation (4.5)
P_0	Preconsolidation stress
$\mathbf{P}$	Strain matrix
P_g^i	Partial pressure of i^{th} gas component
Q	Heat flux
$Q1$	Defined in equation (3.183)
$Q2$	Defined in equation (3.184)
R	Universal gas constant
R_c	Corrosion rate of steel
R_m	Gas generation rate, defined in equation (2.1)
R_v	Specific gas constant of water vapour
$R_{g\leftrightarrow d}^i$	Sink/source term associated with gas phase and liquid phase
$R_{g\leftrightarrow s}^i$	Sink/source term associated with gas phase and solid phase
R_Ω	Weighted residual error over the domain Ω
R_g	Gas influx rate, defined in equation (6.2)
R_w	Water influx rate, defined in equation (6.1)
R	Rate expressions, defined in equation (4.60)
S	Surface area
S_l	Degree of liquid saturation
S_g	Degree of gas saturation
S_e	Effective saturation
S_{lr}	Residual degree of saturation
S_{rc}	Critical degree of saturation
$\hat{T}$	Approximated form of temperature

T	Temperature
T_r	Reference temperature
T_{cr}	Critical temperature of wter
$\mathbf{T}_s$	Defined in equation (4.10)
$\dot{\mathbf{T}}_s$	Time derivative of Temperature
$\mathbf{TL}_{abs}$	Matrix of absolute tolerance
$\mathbf{TL}_{rel}$	Matrix of relative tolerance
V_s	Volume of soil solid
$\mathbf{W}$	Defined in equation (4.50)
X	Charge nutral mineral surface
Z	Axis
a_i^0	Ion-size parameter of hydrated ion
b_{ij}	Binary diffusion coefficient of i and j gas component
b_{iN}	Binary diffusion coefficient of i and N gas component
$\mathbf{b}$	Vector of body force
c	Total molar concentration
c_d^i	Molar concentration of i^{th} dissolved chemical component
c_g^i	Molar concentration of i^{th} gas component
c_r^i	Defined in equation (4.59)
$c_{m,g}^i$	Stoichiometric coefficient of aqueous master species m in species i
$\hat{c}_g$	Approximated form of molar gas concentration
$\mathbf{c}_{\mathbf{c}_g s}$	Defined in equation (4.10)
$\dot{\mathbf{c}}_{\mathbf{g}s}$	Time derivative of molar gas concentration vector
$\dot{\mathbf{c}}_{\mathbf{d}s}$	Time derivative of dissolved chemical concentration
e	Void ratio
f	Flow area factor
f_{Fe}	Fraction of iron in the steel
$f_{c_g}^1$	Approximate flux of 1st gas component normal to boundary

$\mathbf{f}_{c_g}^{i}$	Defined in equation (4.17)
$\mathbf{f}_{l}$	Defined in equation (4.26)
$\mathbf{f}_{c_d}^{j}$	Defined in equation (4.35)
$\mathbf{f}_{T}$	Defined in equation (4.44)
$\mathbf{f}_{u}$	Defined in equation (4.50)
g	The gravitational constant
h	Defined in equation (3.33)
k	Defined in equation (3.181)
k_l	Unsaturated hydraulic conductivity
k_g	Unsaturated gas conductivity
m	Stoichiometry factor, defined in equation (2.1)
m	Aqueous master species, defined in equation (3.127)
m_A	Molality of component A
m_A^0	Molality of component A at a standard state
$\mathbf{m}$	Auxiliary vector
n	Porosity
$\underline{n}$	Direction cosine normal to element boundary surface
p	Net mean stress
p_{atms}	Atmospheric pressure, defined in equation (3.173)
p_0^*	Effective preconsolidation stress of saturated soil
p_c	Reference stress
p_s	Change of soil cohesion with suction
q	Deviatoric stress
q_g	Gas flux boundary, defined in equation (6.2)
q_w	Water flux boundary, defined in equation (6.3)
r	Maximum stiffness controller of soil
r_g^i	Rate of chemical reactions in gas phase
r_d^i	Rate of chemical reactions in liquid phase
s	Suction

s_s^i	Gas phase sink/source term, defined in equation (3.59)
s_d^i	Liquid phase sink/source term, defined in equation (3.98)
s_0	Critical suction, defined in equation (3.182)
$\hat{s}_s$	Approximated form of sink/source term
s_r	Suction at a reference temperature
t	Time
u_l	Porewater pressure
u_g	Pore gas pressure
u_v	Partial vapour pressure
$\hat{u}_l$	Approximated form of porewater pressure
$\mathbf{u_{ls}}$	Defined in equation (4.10)
$\mathbf{u}_s$	Defined in equation (4.10)
$\dot{\mathbf{u}}_s$	Time derivative of deformation
$\mathbf{v_l}$	Darcy's velocity at liquid phase
$\mathbf{v_v}$	Vapour diffusive velocity
$\mathbf{v_g}$	Darcy's velocity at gas phase
x	X-axis coordinate
x_g^i	Mole fraction of i^{th} gas component
y	Y-axis coordinate
z_i	Charge number of ion *i*
z	Elevation
α	Molar mass ratio of porewater to pore gas
α_T	Coefficient of thermal expansion
α_q	A constant derived from the at rest stress state of soil
β	Increase rate of stiffness with soil suction
γ_l	Unit weight of liquid
γ_A	Dimensionless activity coefficient of component *A*.
$\boldsymbol{\varepsilon}$	Total strain vector
$\boldsymbol{\varepsilon}^e$	Elastic strain vector

$\boldsymbol{\varepsilon}^p$	Plastic strain vector
ε_s^p	Volumetric plastic strain at suction increase yield surface
ε_q^p	Deviatoric strain
$\boldsymbol{\varepsilon}_p^e$	Volumetric elastic strain vector due to mean stress
$\boldsymbol{\varepsilon}_s^e$	Volumetric elastic strain vector due to suction
$\boldsymbol{\varepsilon}_T^e$	Volumetric elastic strain vector due to temperature
ε_v^p	Volumetric plastic strain
ε_p^p	Volumetric plastic strain at load collapse yield surface
ζ	Residual force
η_1	Material dependant factor, defined in equation (3.42)
η_2	Material dependant factor, defined in equation (3.42)
θ	Total volumetric water content
θ_l	Volumetric liquid content
θ_v	Volumetric vapour content
θ_g	Volumetric gas content
κ	Slope of the idealised recompression curve
κ_s	Slope of the volumetric suction curve in elastic region
$\lambda(s)$	Stiffness parameter, defined in equation (3.178)
$\lambda(0)$	Stiffness parameter, defined in equation (3.178)
λ_T	Coefficient of thermal conductivity
λ_s	Stiffness parameter, defined in equation (3.193)
μ_l	Absolute viscosity of liquid
μ_g	Absolute viscosity of gas
ν_v	Mass flow factor
ξ	Surface energy at any temperature
ξ_r	Surface energy at reference temperature
π	Integration constant, defined in equation (4.52)
ρ	Density of steel

ρ_v	Density of vapour
ρ_l	Density of liquid
ρ_0	Saturated vapour density
σ''	Net stress
σ	Total stress
τ_g	Tortuosity factor at gas phase
τ_v	Tortuosity factor at vapour phase
υ	Specific volume
υ_0	Initial specific volume
υ_s	Specific volume due to suction
χ_1	Plastic multipliers, defined in equation (3.187)
χ_2	Plastic multipliers, defined in equation (3.187)
ψ	Capillary potential
φ	Defined in equation (4.1)
$\hat{\varphi}$	Defined in equation (4.1)
$\dot{\boldsymbol{\Phi}}$	Time derivative of primary variables
$\boldsymbol{\Phi}$	Vector of primary variables
$\boldsymbol{\Phi}_l$	Defined in equation (4.52)
Ω	Heat flux, defined in equation (3.129)
Ω	Model domain
Γ^e	Element boundary surface
$\wp$	Defined in equation (4.53)
∇	Gradient operator
[ ]	Activities of chemical component, defined in equation (3.121)

1

Introduction

1.1 Introduction

The sustainability of geoenvironment is highly affected by imposing physical, chemical and biological impacts from various man made activities, resulting in an increasing threat to the surface and subsurface environmental quality and the public health (Yong et al., 2006). Hence, developments of better understanding and solutions for appropriate management of our geoenvironmental resources are essential. Advanced knowledge and understanding of various physico-chemical processes in soil are essential to approach sustainable engineering solutions for the management of various hazardous and non-hazardous environmental contaminants.

The capabilities of modelling approaches to study the physico-chemical behaviour should be able to deal with the difficulties associated with the individual processes of transport and reactions. This can involve multiple chemicals and homogenous, heterogeneous reactions with various time-scales in nature. In recent years, the study of reactive gas transport under coupled physical, chemical and mechanical problems has become important in many studies

and research areas and has evolved with developments due to various challenges in various disciplines, e.g. landfill engineering, nuclear waste disposal, carbon sequestration, oil and gas exploration. Such models provide an integrating focus for the wide range of geo-engineering disciplines and represent the basic physical, chemical and mechanical processes which can include the effects of heat, water, chemical processes and mechanical deformation. It is well accepted that numerical simulation can be used to illustrate technical understanding, via development of conceptual models and validation with experimental data. Numerical simulation can then be used to test various scenarios at a reasonable time to predict future behaviour. However, it is critical that models and processes are correctly understood and used only in relevant circumstances; otherwise important processes may be omitted from simulations which can lead to incorrect interpretation of the real scenarios.

The developments in numerical modelling capabilities for simulating gas transport and gas-geochemical processes under coupled behaviour and conditions are among the most important steps forward in the assessment and prediction of geoenvironmental solutions. Understanding the fundamental mechanisms and processes of gas transport in porous media allows numerical models to evaluate and optimise the performance and design of these systems (Ho and Webb, 2006).

The main aim of this research is to advance the knowledge and understanding of multicomponent reactive gas transport in variably saturated soil, under coupled framework of thermal, hydraulic, chemical and mechanical behaviour. The research work is intended to implement the advanced knowledge of gas transport processes and geochemical reactions by developing a multicomponent reactive gas transport model.

The numerical model developed in this thesis will be applicable in simulations of gas reactive transport in several areas of environmental/geoenvironmental engineering, such as high level nuclear waste disposal, deep geological sequestration of carbon dioxide and coal gasification. In general, modelling of transport and fate of gases in porous media coupled with other thermo-hydro-chemical and mechanical processes can be simulated.

In this work, the general development of multicomponent reactive gas transport model is particularly focused on to address some important gas issues associated with High Level nuclear Waste (HLW) disposal. The deep geological disposal facility of high level waste is

subjected to gas generation and migration consequences (Gens et al., 2001; Olivella and Alonso, 2008). Therefore, knowledge and understanding of gas flow processes are of significant importance, to ensure the safety and performance of such a facility for a long period of time.

Repositories of HLW generally depend on a multi-barrier system to isolate the waste from the biosphere (Norris, 2009). In a multi-barrier system the metallic waste canisters are surrounded by engineered barriers which are ultimately encapsulated in the host rock. In most cases, highly expansive smectite clay, has been suggested as the potential barrier or buffer due to its high swelling capacity and very low permeability. In this work, the buffer presumably representative of a MX-80 bentonite clay buffer, unless stated otherwise. After closure of the repository, expected re-saturation might lead the ground water to reach onto the canister surface which possibly initiates the anaerobic corrosion of metallic canisters. Corrosion, together with other mechanisms, such as alpha activity of radioactive waste, water vaporization, water radiolysis, microbial activity and degradation of organic materials could generate several gas species, i.e. hydrogen (H_2), helium (He), water vapour, carbon dioxide (CO_2), methane (CH_4) (Bonin et al., 2000; Norris, 2009). Generation and migration of repository gases could affect the buffering capacity of engineered barrier by altering its physical and chemical properties. Hence, gas transport issues in HLW disposal facility offer an important case study to extend the knowledge and understanding of gas transport processes through porous medium.

The performance assessment of compacted clay buffer includes analysis of complex interactions among coupled thermal, hydraulic, chemical or geochemical and mechanical processes (Yong et al., 2010). Majority of the research work conducted on the thermo-hydro-mechanical (THM) behaviour of barriers concerns the initial transient processes of hydration under the combined action of the infiltrating water from the host rock and the heat generated by the canister (for HLW) and for obvious reasons, experimental information associated with this transient process covers only a minimum time period of the expected lifetime of an engineered buffer (Olivella and Alonso, 2008). The long term behaviours, such as gas transport and geochemical/gas-chemical interactions in the buffer have received less attention (Gens et al., 2001). In context of chemical/geochemical and biological processes, the models require more development to reach to the stage of sophistication to be coupled with THM

platforms (Pusch, 2008). Several experimental research have been carried out by various researchers to understand the dominant mechanisms of gas transport through variably saturated compacted clays (Pusch et al., 1985; Horseman et al., 1999; Galle, 2000; Graham et al., 2002; Harrington and Horseman, 2003 and others). The results of such short term experimental studies are ambiguous, since the complex nature of the problem and require advanced conceptual model and theoretical models encompassing multi-phase and multicomponent processes. Particularly, research studies on gas migration together with gas-chemical/geochemical interaction in the buffer and/or buffer porewater are vital to address the reactive gas transport phenomena and consequent effects on the system.

The study objectives of the thesis have been presented in section 1.2. Section 1.3 describes the background of the research. The scopes of the work and limitations have been presented in section 1.4. Finally an overview of the structure of the thesis and the chapters is given in section 1.5.

1.2 Study objectives

The main objectives of this study are to:

- Develop a theoretical framework for describing the transport of multiple gases through variably saturated soil including the major coupling effects between gas components and geochemical processes under a coupled THCM framework.
- Develop/extend the existing transport model by introducing multicomponent gas transport processes and further integration of an advanced geochemical model into the coupled thermo-hydro-gas-chemical-mechanical model to calculate the geochemical reactions.
- Perform numerical investigations on reactive gas transport through unsaturated clays and its impact on the geochemical state of the clay buffer.
- Carry out numerical simulations for long term predictive purpose in context of gas transport and pressure development in saturated compacted clays related to a generic HLW disposal facility.

1.3 Research background

The current study has been carried out as a part of broad research programs undertaken at the Geoenvironmental Research Centre (GRC) in Cardiff University. One of the significant contributions of GRC in the area of modelling fluid flow through unsaturated soil is the development of the numerical computer code COMPASS (**CO**de for **M**odelling **PA**rtially **S**aturated **S**oils). This section provides the context to this work and neither intended to replace more detailed reviews of literature in chapter 2 nor the theoretical formulation in chapter 3.

A theoretical model of coupled transient heat and moisture (TH) transfer in unsaturated soil was developed by Thomas (1985). The Philip and de Vries (1957) and de Vries (1958) approach have been incorporated in the model to simulate the diffusive flow of vapour and the latent heat of vaporisation was introduced following the approach proposed by Luikov (1966). The principle of mass conservation was employed for moisture flow and the conservation of energy used for heat transfer. The non-linearity of material parameters was then included in the works presented by Thomas (1987), Thomas (1988a) and Thomas

(1988b). Revised time-stepping schemes were investigated under the mentioned coupled TH model by Thomas and Rees (1988) and Thomas and Rees (1990).

Following an experimental investigation into the behaviour of unsaturated sand surrounding a heating rod, Ewen and Thomas (1987) and Ewen and Thomas (1989) modified the vapour transfer diffusivities of the numerical model to simulate coupled heat and moisture transfer processes in unsaturated soil. A numerical simulation in terms of moisture content and temperature was carried out by Ewen and Thomas (1989) including vapour transport via a diffusive mechanism.

Thomas and King (1991) presented a theoretical heat and moisture formulation cast in terms of capillary potential and temperature and found good agreement with the Ewen and Thomas (1987) experiments. Thomas and Sansom (1995) extended this formulation to include elevated pore air pressures and validated via comparison to experimental works on sand and clay. This formulation was presented in three-dimensions including work on pre and post-processing, visualisation and parallel computation by Sloper (1997) and Thomas et al. (1998).

Mechanical behaviour and deformation was introduced examining seasonal ground movements by Thomas and Rees (1990) and Thomas and Rees (1993), with an isothermal coupled hydro-mechanical numerical model presented by Thomas et al. (1992) utilising the non-linear elastic state-surface approach proposed by Lloret and Alonso (1985). This model was applied to seasonal ground movements in the work presented by Thomas and Zhou (1995). An elasto-plastic coupled Thermo-Hydro-Mechanical (THM) model was presented by Thomas and He (1994) and Thomas and He (1995) using the elasto-plastic model of Alonso et al. (1990).

Ramesh (1996) applied the THM model to simulate temperature, moisture and void ratio distributions of montmorillonite subjected to heating/hydration. The work also involved investigation of isothermal volume change behaviour of compacted kaolinite in suction controlled tests. Thomas and Cleall (1999) extended the THM model to include highly expansive behaviour. Using the developed model, a numerical simulation of large scale experiments were presented by Mitchell (2002), Thomas et al. (2003), Melhuish (2004) and Cleall et al. (2006) which included investigation into the microstructure behaviour of bentonite and the effects on re-saturation of the buffer.

Chemical processes were first introduced as non-reactive chemical solute transport for a single species (Thomas and Cleall, 1997). Hashm (1999) developed the model to two-dimensional coupled moisture and reactive multiple chemical solute transport by linking the non-reactive transport code with the geochemical model, MINTEQA2 (Allison et al., 1991). The model was applied to simulate a series of leaching cell experiments to study the migration/sorption behaviour of some of the heavy metals. Seetharam (2003) developed the multicomponent chemicals reactive transport module of the coupled THCM model. The geochemical reactions were calculated by the geochemical model, MINTEQA2 using two different coupling schemes to solve transport and reaction equations. The coupled THCM model was used to simulate the reactive transport of chemicals in a small scale laboratory on compacted bentonite under heating and hydration (Seetharam et al., 2006; Cleall et al., 2007).

A number of theoretical and computational developments have recently been made in the model focusing mainly on the behaviour of compacted bentonite as the buffer in HLW geological repository and to model the large scale THM behaviour of the repository. Singh (2007) presented an experimental and numerical investigation on the heat and moisture transfer in compacted bentonite and kaolinite with special attention to the vapour transfer in compacted clays. Modifications to the existing vapour theory were suggested and introduced in existing THM model. Siddiqua (2008) presented an investigation into the elevated temperature effects (70-200°C) on the THM processes in the model. A pore gas transfer equation and thermo-osmotic effect was developed to account for elevated temperature. Vardon (2009) extended the THM model to accommodate three-dimensional THM behaviour in geological repository, including the development of a high-performance computing algorithm using both multi-threaded and message-passing programming paradigms to enable simulations to be completed in significantly reduced time. The model was utilised for simulation of the THM behaviour of a large-scale experiment, carried out at an underground research laboratory in Sweden. Sedighi (2011) extended COMPASS code by including an advance geochemical model, namely PHREEQC, version 2.0 (hereafter, PHREEQC2) with the transport code. Both equilibrium reactions and kinetically controlled geochemical reactions can be calculated using the geochemical model. The coupled THCM model has been implemented successfully to simulate the transport and fate of multicomponent dissolved chemicals.

More recently, Thomas et al. (2011) presented the inclusion of biological aspects to the coupled THCM model. The work deals with early developments to include some biological impacts on coupled transport phenomena through unsaturated porous media. The presented THCMB model incorporates biodegradation kinetics of organic substrates.

1.4 Scopes and limitations

The scope of the work undertaken in this thesis and in particular the limitations that are anticipated has been listed below:

- Numerical approximation has been used to find a solution to the system of coupled differential equations. In particular, the finite-element method has been used to provide a spatial solution and the finite-difference method used to provide a temporal solution.
- The constitutive relationships presented in the theoretical formulation have been developed for slightly and moderately swelling soils.
- Soil has been assumed as a homogeneous porous medium acknowledging the fact that that soils exhibit some degree of heterogeneity and this may be partly accommodated in this study as the assumption of homogeneity only applies within an individual element. Therefore, different soil types may be used within an analysis.
- It has been assumed that in a mixture of real gases, an individual component behaves as an ideal gas and hence, the component and the mixture follow the ideal gas laws. Although real gases exhibit different properties than that of ideal gases in terms of compressibility effect, molecular attractions, non-equilibrium thermodynamics effect etc. The mixture of gases has been considered as non-separative.
- Although this work is intended to model the transport of multicomponent gases, the water vapour has been considered with the liquid water in the governing moisture flow equation, providing the advantage of cancelling the sink/source term due to condensation/evaporation and long term vapour migration is yet to be understood properly. Therefore, the pore gas is a mixture of dry gases which excludes the water vapour. It has been assumed that the vapour transport is mainly diffusive and does not provide driving contribution to the bulk gas flow but it flows with the bulk movement of the dry gases present in the system.

- It has been assumed that the chemical processes are sufficiently fast comparing to the transport speed. Therefore, the local chemical equilibrium has been considered to exist.
- Isothermal condition has been assumed to prevail during the numerical simulations. It supports the applicability of equilibrium constants at fixed temperatures.

1.5 Overview of the thesis

A brief description of the chapters has been presented below:

Chapter 2 contains a targeted review of current literatures associated with the work contained in the developments presented in the remainder of this thesis. A review of the recent research activities related to gas generation and migration based on experimental and numerical modelling approach has been detailed. A selective review of the developments of numerical strategies for an efficient solution of coupled transport processes and geochemical reactions have also been presented.

Chapter 3 details the development of theoretical formulations of thermal, hydraulic, chemical, gas and mechanical behaviour of porous media. This chapter is primarily focused on to present the newly developed governing equation of multicomponent reactive gas transport. Development of the sink/source term due to geochemical reactions and phase exchange has also been detailed. Chapter 4 deals with the development of numerical formulations of the governing equations. Numerical formulations of the governing differential equations representing heat, moisture, multicomponent gas, multicomponent chemical and deformation behaviour have been presented. The coupling scheme adopted for the solution of gas transport and geochemical reactions has been highlighted in this chapter.

Chapter 5 presents the verification of multicomponent gas transport processes. Depending on the availability of required information, the numerical model has been verified against analytical solutions, alternative numerical solutions and experimental results. It is noted that the numerical model has already been verified for a number of test cases involving coupled moisture flow, heat transfer, dissolved chemical transport and deformation.

Chapter 6 presents an application of the model in case of gas transport through fully saturated compacted clay buffers and the development of maximum pressures in the system. Particularly, the risk of development of pneumatic fractures due to high pressures in the buffer has been investigated. Numerical simulations have been carried out based on a number of representative scenarios similar to a generic HLW disposal facility and under isothermal condition.

Chapter 7 deals with another application of the model in case of reactive gas transport through unsaturated compacted clay buffer. The long term simulations have been carried out under isothermal condition to investigate the transport and fate of a gas component in presence of various chemical components in compacted clay buffer. Since, the porewater of clay buffers contains significant amount of dissolved chemicals, modelling of porewater composition has been performed prior to the numerical simulations. The results of two sets of simulations detail the gas flow patterns and its impact on the THCM behaviour of the clay buffer.

Overall conclusions of the thesis including major findings, analysis of limitations and suggestions for further work have been presented in detail in chapter 8.

References

Allison, J.D., Brown, D.S., Novo-Gradac, K.J., (1991). "MINTEQA2 user manual version 3.0". Environmental Research Laboratory, US EPA.

Alonso, E.E., Gens, A., Josa, A., (1990). "A constitutive model for partially saturated soils". *Geotechnique* **40**, No. 3, pp. 405-430.

Bonin, B., Colin, M., Dutfoy, A., (2000). "Pressure building during the early stages of gas production in a radioactive waste repository". *Journal of Nuclear Materials* **281**, No. 1, pp. 1-14.

Cleall, P.J., Melhuish, T.A., Thomas, H.R., (2006). "Modelling the three-dimensional behaviour of a prototype nuclear waste repository". *Engineering Geology* **85**, No. 2, pp. 212-220.

Cleall, P.J., Seetharam, S.C., Thomas, H.R., (2007). "On the inclusion of some aspects of chemical behaviour of an unsaturated soil in thermo-hydro-chemical-mechanical models: II Application and transport of soluble salts in compacted bentonite". *Journal of Engineering Mechanics, American Society of Civil Engineering* **133**, pp. 348-356.

de Vries, D.A., (1958). "Simultaneous transfer of heat and moisture in porous media", *Transactions American Geophysical Union* **39**, No. 5, pp. 909-916.

Ewen, J., Thomas, H.R., (1987). "The thermal probe – a new method and its use on an unsaturated sand". *Geotechnique* **37**, pp. 91-105.

Ewen, J., Thomas, H.R., (1989). "Heating unsaturated medium sand". *Geotechnique* **39**, No. 3, pp. 455-470.

Galle, C., (2000). "Gas breakthrough pressure in compacted Fo-Ca clay and interfacial gas overpressure in waste disposal context". *Applied Clay Science* **17**, pp. 85-97.

Gens, A., Olivella, S., Vallejan, B., (2001). "Analysis of gas phase transport phenomena in compacted clay barriers". *Proceedings of 10th International Conference of Computational Methods in Advance Geomechanics*, Tucson, AZ, pp. 735–742.

Graham, J., Halayko, K. G., Hume, H., Kirkham, T., Gray, M., Oscarson, D., (2002). "A capillarity-advective model for gas break-through in clays". *Engineering Geology* **64**, No. 2-3, pp. 273-286.

Harrington, J.F., Horseman, S.T., (2003). "Gas migration in KBS-3 buffer bentonite". *SKB Technical Report TR-03-02*, Stockholm, Sweden.

Hashm, A.A., (1999). "A study of the transport of a selection of heavy metals in unsaturated soils". PhD Thesis, University of Wales, Cardiff.

Horseman, S.T., Harrington, J.F., Sellin, P., (1999). "Gas migration in clay barriers". *Engineering Geology* **54**, No. 1-2, pp. 139-149.

Ho, C., Webb, S., (2006). "Gas Transport in Porous Media, Springer". AA Dordrecht, The Netherlands.

Lloret, A., Alonso, E.E., (1985). "State surfaces for partially saturated soils", *Proceedings of the 11th International Conference of Soil Mechanics and Foundation Engineering* **2**, San Francisco, pp. 557-562.

Luikov, A.V., (1966). "Heat and mass transfer in capillary porous bodies". Pergamon Press, Oxford.

Melhuish, T.A., (2004). "An investigation of the three-dimensional thermo/hydro/mechanical behaviour of large scale in-situ experiments". PhD Thesis, Cardiff University, UK.

Mitchell, H.P., (2002). "An investigation into the thermo/hydro/mechanical interactions involved in high level nuclear waste disposal". PhD Thesis, University of Wales, Cardiff.

Norris, S., (2009). "Summary of gas generation and migration current state-of-the art". *FORGE Report D1.2-R-Draft.*

Olivella, S., Alonso, E. E., (2008). "Gas flow through clay barriers". *Geotechnique* **58**, No. 3, pp. 157-176.

Philip, J.R., de Vries, D.A., (1957). "Moisture movement in porous materials under temperature gradients". *Transactions American Geophysical Union* **38**, No. 2, pp. 222-232.

Pusch R, Ranhagen L, Nilsson K., (1985)**.** "Gas migration through Mx-80 bentonite". *Nagra Technical Report NTB 85-36*, Wettingen, Switzerland.

Pusch, R., (2008). "Geological Storage of Highly Radioactive Waste". Springer, New York.

Ramesh, A.D., (1996). "Modelling the thermo/hydraulic/mechanical behaviour of unsaturated soil using an elasto-plastic constitutive relationship". PhD Thesis, University of Wales, Cardiff.

Sedighi, M., (2011). "An investigation of Hydro-geochemical processes in coupled thermal, hydraulic, chemical and mechanical behaviour of unsaturated soils". PhD Thesis, Cardiff University, UK.

Seetharam, S.C., (2003). "An investigation of the thermo/hydro/chemical/mechanical behaviour of unsaturated soils". PhD Thesis, Cardiff University, UK.

Seetharam, S.C., Cleall, P.J., Thomas, H.R., (2006). "Modelling some aspects of ion migration in a compacted bentonitic clay". *Engineering Geology* **85**, pp. 221-228.

Siddiqua, S., (2008). "An investigation of the influence of elevated temperatures on the thermal-hydraulic-mechanical response of unsaturated soils". PhD Thesis, Cardiff University, UK.

Singh, R.M., (2007). "An experimental and numerical investigation of heat and mass movement in unsaturated clays". PhD Thesis, Cardiff University, UK.

Sloper, N.J., (1997). "The development of a new three dimensional numerical model for fully coupled heat, moisture and air flow in unsaturated soil incorporating scientific visualisation and parallel computing techniques". PhD Thesis, University of Wales, Cardiff.

Thomas, H.R., (1985). "Modelling two-dimensional heat and moisture transfer in unsaturated soils, including gravity effects". *International Journal of Analytical Methods in Geomechanics* **9**, pp. 573-588.

Thomas, H.R., (1987). "Non-linear analysis of heat and moisture transfer in partly saturated soil". *Journal of Engineering Mechanics, American Society of Civil Engineering* **113**, pp. 1163-1180.

Thomas, H.R., Rees, S.W., (1988). "The use of Lee's algorithm in the analysis of some ground heat and mass transfer problems". *Proceedings of the 6th International Conference on Numerical Methods in Geomechanics*, Innsbruck, Austria.

Thomas, H.R., (1988a). "A non-linear analysis of two-dimensional heat and moisture transfer in partly saturated soil". *International Journal of Analytical Methods in Geomechanics* **12**, pp. 31-44.

Thomas H.R., (1988b). "The influence of non-linear thermal parameters on moisture content distributions in unsaturated soil". *International Journal of Analytical Methods in Engineering* **26**, pp. 263-279.

Thomas, H.R., Rees, S.W., (1990). "An examination of the performance of a 3-level time stepping algorithm – Coupled heat and mass transfer computing". *Proceedings of the 1st International Conference, Advances in Computer Methods in Heat Transfer*, Southampton, U.K.

Thomas, H.R., King, S.D., (1991). "Coupled temperature/capillary potential variations in unsaturated soil". *Journal of Engineering Mechanics, American Society of Civil Engineers* **117**, No. 11, pp. 2475-2491.

Thomas, H.R., Zhou, Z., He, Y., (1992). "Analysis of consolidation of unsaturated soils", *Proceedings of the 2nd Czechoslovak Conference on Numerical Methods in Geomechanics* **1**, Prague, pp. 242-247.

Thomas, H.R., Rees, S.W., (1993). "The numerical simulation of seasonal soil drying in an unsaturated clay soil". *International Journal of Numerical and Analytical Methods in Geomechanics* **17**, No. 1, pp. 119-132.

Thomas, H.R., He, Y., (1994). "An elasto-plastic analysis of the thermo/hydraulic/mechanical behaviour of unsaturated soil", *Proceedings of the 8th International Conference on Computer Methods and Advances in Geomechanics*, Morgantown, Balkema, Rotterdam, pp. 1171-1176.

Thomas, H.R., He, Y., (1995). "Analysis of coupled heat, moisture and air transfer in a deformable unsaturated soil". *Geotechnique* **45**, No. 4, pp. 677-689.

Thomas, H.R., Sansom, M.R., (1995). "Fully coupled analysis of heat, moisture and air transfer in unsaturated soil". *Journal of Engineering Mechanics, American Society of Civil Engineering* **121**, No. 3, pp. 392-405.

Thomas, H.R., Zhou, Z., (1995). "A comparison of field measured and numerically simulated seasonal ground movement in unsaturated clay". *International Journal for Numerical and Analytical Methods in Geomechanics* **19**, pp. 249-265.

Thomas, H.R., Cleall, P.J., (1997). "Chemico-osmotic effects on the behaviour of unsaturated expansive clays". *Geoenvironmental engineering, Contaminated ground; fate of pollutants and remediation*, Thomas Telford, London, pp. 272-277.

Thomas, H.R., Rees, S.W., Sloper, N.J., (1998). "Three-dimensional heat, moisture and air transfer in unsaturated soils". *International Journal of Numerical and Analytical Methods in Geomechanics* **22**, No. 2, pp. 75-95.

Thomas, H.R., Cleall, P.J., (1999). "Inclusion of expansive clay behaviour in coupled thermo hydraulic mechanical models". *Engineering Geology* **54**, pp. 93-108.

Thomas, H.R., Cleall, P.J., Chandler, N., Dixon, D., Mitchell, H.P., (2003). "Water infiltration into a large-scale in-situ experiment in an underground research laboratory". *Geotechnique* **53**, No. 2, pp. 207-224.

Thomas H.R., Seetharam, S.C., Vardon, P.J., (2011). "On the inclusion of some biological impacts and influences in coupled transport phenomena in unsaturated soil". *Geotechnical and Geological Engineering* **29**, pp. 181-191.

Vardon, P.J., (2009). "A three-dimensional numerical investigation of the therm-hydro-mechanical behaviour of a large-scale prototype repository". PhD Thesis, Cardiff University, UK.

Yong, R.N., Mulligan, C.N., Fukue, M., (2006). "Geoenvironmental Sustainability". CRC Press, Taylor and Francis.

Yong, R.N., Pusch, R., Nakano, M., (2010). "Containment of High-Level Radioactive and Hazardous Solid Wastes with Clay Barriers". Spon Press, New York.

2

Literature Review

2.1 Introduction

The study of flow through porous materials, particularly in soils, has been a subject of interest for many years in wide range of science and engineering applications. Therefore, many of the processes associated with various flows are well established. In recent years, extensive research activities have been carried out to investigate the thermal-hydraulic-chemical-mechanical (THCM) behaviour of compacted soils as buffer materials, via both numerical and experimental investigations. The flow and deformation behaviours of partially saturated soils are more complex than in saturated soils, particularly in highly compacted expansive clay soils which have been considered as buffer materials for contaminated land treatment, higher activity radioactive waste disposal facility etc. To ensure long term safety and functionality of an engineered barrier, it is vital to understand the key processes associated with the THCM behaviour. Along with various flows, such as heat flow, water and vapour flow, dissolved chemical flow and deformation behaviour, it has been strongly suggested that gas flow could provide significant risk against the safety and performance of an engineered barrier.

Since, this study is primarily focused on gas flow through buffer materials and its impact on the coupled THCM behaviours, an up-to-date review of background studies related to gas generation and migration has been presented in this chapter.

A large quantity of literature on coupled THCM behaviour is available in the work of various researchers and in wide range of technical reports. The already existed literature review on coupled THCM behaviour of unsaturated soil has not been repeated here, since it has been discussed at great details in the work of Thomas and He (1995), Cleall (1998), Mitchell (2002), Seetharam (2003), Melhuish (2004), Vardon (2009), Sedighi (2011).

In this study, the literature review primarily focuses on the flow and reactions of gases through a variably saturated porous medium. As explained in previous chapter, one application of the developments under the scope of this thesis is relate the fate of gas in geological disposal of high level radioactive waste. It is expected that significant amount of hydrogen gas could be generated due to corrosion of metallic canisters in a nuclear waste disposal facility. Other processes, such as alpha radioactivity, water radiolysis, microbial activities might also generate helium, methane, carbon dioxide etc. Therefore, apart from a general review presented in this chapter on various processes related to gas transport and reactions in porous media, the majority of this chapter has been devoted to the state of the art of the knowledge on gas generation, transport and behaviour in compacted clay buffer in geological disposal of HLW.

A targeted review of literature associated with corrosion rate and gas generation has been presented in section 2.2. Since the processes of corrosion strongly depends on the availability and chemical composition of porewater, corrosion rates and consequent generation rates have been collected from literature for various types of water in variable chemical environments. Literature review on corrosion rates at ambient temperature to elevated temperature and small scale laboratory experiments to long term experiments have also been presented in this section.

A review of various transport of gases in partially saturated and fully saturated compacted clay buffer has been presented in section 2.3 and section 2.4 respectively. A number of experimental and numerical modelling studies have been conducted to understand the flow of gases through fully saturated buffer. Two major laboratory works reported in the literature

related to gas migration through saturated buffer which has yielded significant results have been discussed in great details. In addition, a brief review of two available theoretical models developed for simulation of gas flow through dry porous medium has been presented in this section.

Background study on porewater composition of compacted clay suggested for the buffer material (i.e. compacted bentonite) has been presented in section 2.5. This section is in support of the simulation work presented in chapter 7. A review of geochemical reactions and processes of special interests, associated with gas flow, has also been presented in this section.

Section 2.6 deals with the review of background study of some computational aspect and recent developments of the reactive transport modelling of chemicals in porous medium. Various schemes to adopt the numerical modelling of the coupled chemical transport and geochemical reactions have been reviewed in this section with the aim for a suitable method to develop the reactive gas transport model. Finally, a detail conclusion section of the literature review has been presented in section 2.7.

2.2 State of the art knowledge on corrosion and gas generation rates

Generation of gases in a high level nuclear waste disposal facility occurs due to water vaporization, water radiolysis, microbial activities, metallic corrosion (e.g. Environment Agency, 2008, Bonin et al., 2000). It is largely thought that the microbial activities are to be suppressed due to the excess pressure from swelling of bentonite (Ortiz et al., 2002). The gas generation due to radiolysis is beyond the scope of this work. In a particular study, in the context of gas generation and migration through Boom Clay, Ortiz et al. (2002) has analysed the experimental results of a hypothetical waste repository in Belgium and suggests that the presence of bacteria in this clay can reduce the potential gas generation due to the bacterial metabolic activities. Therefore, in this section the process and factors related to the hydrogen gas generation due to metallic corrosion which is thought to be the dominant mechanism (Kursten et al., 2004) and has been reviewed in the literature.

The corrosion of the steel canisters under anaerobic conditions produces hydrogen gas (H_2). Another by product of anaerobic corrosion is Magnetite (Fe_3O_4). The reaction involved in anaerobic corrosion is described by the redox reaction, presented in equation (R.1). Other chemical reactions may occur, such as production of ferrous hydroxide i.e. $Fe(OH)_2$. Since, the compound is unstable; it converts into magnetite, water and hydrogen (Ortiz et al., 2002). The total reaction of corrosion under anaerobic condition therefore can be described as:

$$3Fe + 4H_2O \leftrightarrow Fe_3O_4 + 4H_2 \qquad \text{(R.1)}$$

This chemical reaction indicates that for each mole of H_2 gas to be generated equal amount of water has been consumed. That is in fact the amount of water in the form of liquid water or water vapour which is required to maintain the corrosion process (Senger et al., 2008).

In terms of kinetics of the corrosion reaction, Volckaert and Mallants (1999) estimated the rate of hydrogen gas generation for a thin steel plate as:

$$R_m = SR_c \rho m \frac{f_{Fe}}{M_{Fe}/1000} \qquad (2.1)$$

where, R_m is gas generation rate (mol/year), S represents the reactive surface area (m^2), R_c defines corrosion rate (m/year), ρ is the density of steel ($\approx$ 7900 kg/m^3), m is the stoichiometric factor, which for the chemical reaction mentioned above the value can be taken as 4/3 for the generation of hydrogen (based on equation R.1), M_{Fe} stands for the molecular weight, in this case for iron $\approx$ 55.85 g/mol and f_{Fe} is the fraction of iron in the steel, which has been taken as 0.99 for the steel canisters/iron overpack for HLW.

Brown and Masters (1982) stated that experiments on corrosion of iron under atmospheric conditions indicate a decrease in corrosion rate when the relative humidity drops from 90% to 60%. Thermodynamic considerations predict that the gas production stops when hydrogen partial pressure increases above 40 MPa (Neretnieks, 1985). However, these elevated pressures are unlikely to be sustained in a disposal facility.

A wide range of corrosion rate data has been reported by Schenk (1988) and Simpson (1989). Simpson (1989) reported at 50-80˚C and neutral pH level the corrosion rates were in the range of 0.8 to 5.9 μm/year, at pH level 8.5 and similar temperature range the corrosion rates were in the range of 0.6 to 2.8μm/year and at a pH level 10 the corrosion rates were in between less than 0.04 to 2.8 μm/ year (King, 2008).

Experimental evidence of anaerobic corrosion of carbon steel at temperatures related to repository conditions in the thermal period (heat emitting period of high level nuclear wastes) have found the typical corrosion rate to be in the range of 0.2 to 6.5 μm/year and corresponding hydrogen release rate at a pressure of 10 MPa to be in the range between 2.0 to 6.0 dm^3/year and at an worst case scenario of 8.0 dm^3/year (Wikramaratna et al., 1993).

Ortiz et al. (2002) carried out a long term in situ gas migration experiment through artificially created pathway in Boom Clay. Laboratory experiments were carried out at ambient temperature to estimate the corrosion rate of 316L stainless steel and carbon steel in contact with water saturated clay. The metallic powder of 316L stainless steel was mixed with slurry of fresh clay which was prepared by mixing fresh Boom Clay with water at an anaerobic condition. At a pH level of 10.07 the gas production rate and corrosion rate was observed as 4.0×10^{-6} mol/m^2/year and 3.5×10^{-5} μm/year.

The corrosion rate of carbon steel is very small in a highly alkaline environment, with an upper limit of 0.1 μm/year at 30°C (Kursten et al., 2004). Considering the effect of temperature on corrosion rate at the surface of the overpack, which can reach about 90-100°C, it has been suggested that a higher corrosion rate up to 1.0 μm/year may occur.

Smart et al. (2006) carried out a study on the corrosion of steel in bentonite under wider range of conditions. The corrosion rates were measured by collecting hydrogen from the anaerobic corrosion of steel and corrosion in compacted bentonite and artificial bentonite pore water was also experimentally observed. The anaerobic corrosion of steel and consequence generation of hydrogen was measured by using a barometric gas cell technique. Four gas cells were prepared with carbon steel wires in contact with MX-80 bentonite at two test temperatures of 30 and 50ºC, using two water bentonite ratios (bentonite slurry and compacted bentonite). An artificial groundwater, containing 31.56 g/l sodium chloride and 1.06 g/l sodium carbonate maintaining a pH level of 10.4, was used as a test solution for the slurry and for immersing the compacted bentonite test samples. At the end of experimental period, the bentonite had become greenish black and the sample quickly turned brown in air indicating oxidation of ferrous ion to ferric ion (Smart et al., 2006).

Smart et al. (2006) stated that in presence of bentonite, the corrosion product layer was relatively thin compared to fully aqueous conditions, as the ferrous ions released by corrosion exchanged with the bentonite interlayer or attached to the surface of the bentonite grains, rather than forming a separate iron oxide phase. From the gas generation experiments, it has been found that the presence of bentonite exerts some influence on the corrosion reaction at surface of the steel used in the experiment. The corrosion rate of steel has been found to be unaffected by the pH level of the solution. It was also found that the total amount of iron taken up by the bentonite was much greater than any reduction in the concentration of exchangeable cations, suggesting that iron released by the corroding surface was immediately absorbed or adsorbed by the bentonite.

Carbon steel canisters have been selected to dispose high level waste and spent fuel in Swedish repository concept in Opalinus clay. King (2008) prepared a report for Swiss radioactive waste management authority (Nagra), to recommend a range of long term anaerobic corrosion rate for carbon steel canisters and to justify the use of the selected corrosion rate in safety assessment.

King (2008) suggested that it is justifiable to use a constant long-term corrosion rate for safety case assessment. It has been reported that the corrosion rate of carbon steel decreases with time because of the development of protective surface film. In case of bulk solution, the corrosion rate decreases to a steady state rate after a period of six months with a long term rate of 0.1 μm/year. But in compacted clay the rate of decrease in corrosion was slower and a steady state did not attain after several years of exposure. It has also been suggested that significant evidence of well conducted experiments indicated an anaerobic corrosion rate of the order of 1.0-2.0 μm/year. Additional experimental works were reported by King (2008) to investigate the anaerobic corrosion rate of carbon steel and cast iron (Smart et al., 2001, 2002a, 2002b, 2004, 2006).

Smart et al. (2004) presented an experimental approach to measure the corrosion rate of carbon steel and cast iron in contact with bentonite slurry (bentonite-water ratio of 0.3) by measuring the hydrogen production rate. A similar approach was used by Smart et al. (2006) to obtain the anaerobic corrosion rate of carbon steel in compacted bentonite saturated with 1 mol/dm^3 NaCl. By analysing the experimental results of Smart and co-workers, King (2008) has suggested that in presence of bentonite, corrosion rates are higher (1.0-3.0 μm/ year) than that of bulk solution (0.5-1.0 μm/ year) and the long term corrosion rates appeared to be in the order of 0.1-1.0 μm/ year.

King (2008) also reported the work carried out by Kreis and Simpson (1992), Schenk (1988), Simpson (1984), Simpson and Valloton (1986), Simpson and Weber (1992), Simpson et al. (1985) to obtain corrosion rates in Swiss Crystalline rock. In their experiments a range of natural and synthetic groundwater and NaCl solution of different pH level were used at temperature ranges between 25˚C to 140˚C (King, 2008). Simpson et al. (1985) obtained corrosion rates ranges from 5.0-10.0 μm/ year at 80˚C after an exposure period of 260 days in Säckingen and Böttstein (situated in Germany from where the samples were collected) waters (King, 2008). It has been reported that a number of corrosion rates were obtained by Marsh and Taylor (1988) and Marsh et al. (1983) in support of the UK radioactive waste disposal programs in 1980s. The time averaged rates were measured using the mass loss technique.

Using the Volckaert and Mallants (1999) method, Weetjens and Perko (2008) estimated the gas production rate for hydrogen generation rate for the HLW super container (which includes number of components of planned engineered barrier in a single package, pre-

fabricated in a surface facility prior to disposal in underground disposal facility) disposal concept. The rate was reported to be 0.1 mol/year/super container at ambient temperature, increasing up to 1.7 mol/year at high near field temperature.

SKB (1993) reported long term anaerobic corrosion rate of copper/steel canisters as 0.2 µm/year to 6.5 µm/year. Nagra (2004) suggested a lower bound and upper bound corrosion rate ranges between 0.1-1.0 µm/year for steel canisters based on anaerobic corrosion.

Xu et al. (2008) carried out numerical modelling of gas generation and migration through MX80 bentonite buffer. Two types of gas injection rates have been used in their study which ranges from 0.04 m^3/ year to 0.40 m^3/ year per tunnel meter of the disposal facility in Opalinus clay host rock.

The limited experimental work, presented by Horseman et al. (1997) and Harrington and Horseman (2003) experiments, use significantly higher gas injection rates, 375 µL/ hour (nearly two magnitudes higher) than that would likely to occur naturally. These are important works to identify possible flow mechanisms and behaviour of buffer material, but should be considered conservative since the gas injection rates were significantly more than expected in real case scenario and in-line with the observations that a variety of flow mechanisms may occur and are largely dependent upon the rate and pressure of injection, deemed to identify mechanisms related to high gas generation only.

The broad range of corrosion and gas generation rates presented in the aforementioned discussion and in the rest of the chapter have been synthesised in tabular form in Table 6.1, Table 6.2 and Table 6.3 so that an overall observation of the data can be carried out. The corrosion process has been initially examined with the overall reactions. It has been found that the gas generation rates entirely depend on the corrosion rates in a deterministic manner. The rate has been reported dependent upon the conditions of experimental setup, for example water supply, pH and temperature. A quantitative comparison of the generation rates has been presented in chapter 6. It has also been reported that the presence of bentonite may enhance the corrosion process, although the long term corrosion rate is stated to be lower than that the maximum due to a protective surface produced during the corrosion process.

Knowledge of the duration of corrosion process is essential to predict the performance efficiency of a HLW disposal facility. A chronogram of the major phenomena affecting the repository and its geological environment has been detailed by ANDRA (2005) which has been presented in Figure 2.1. It has been suggested in Figure 2.1 that from the point of repository closure the metallic corrosion and consequent hydrogen production possibly continues for approximately 100,000 years.

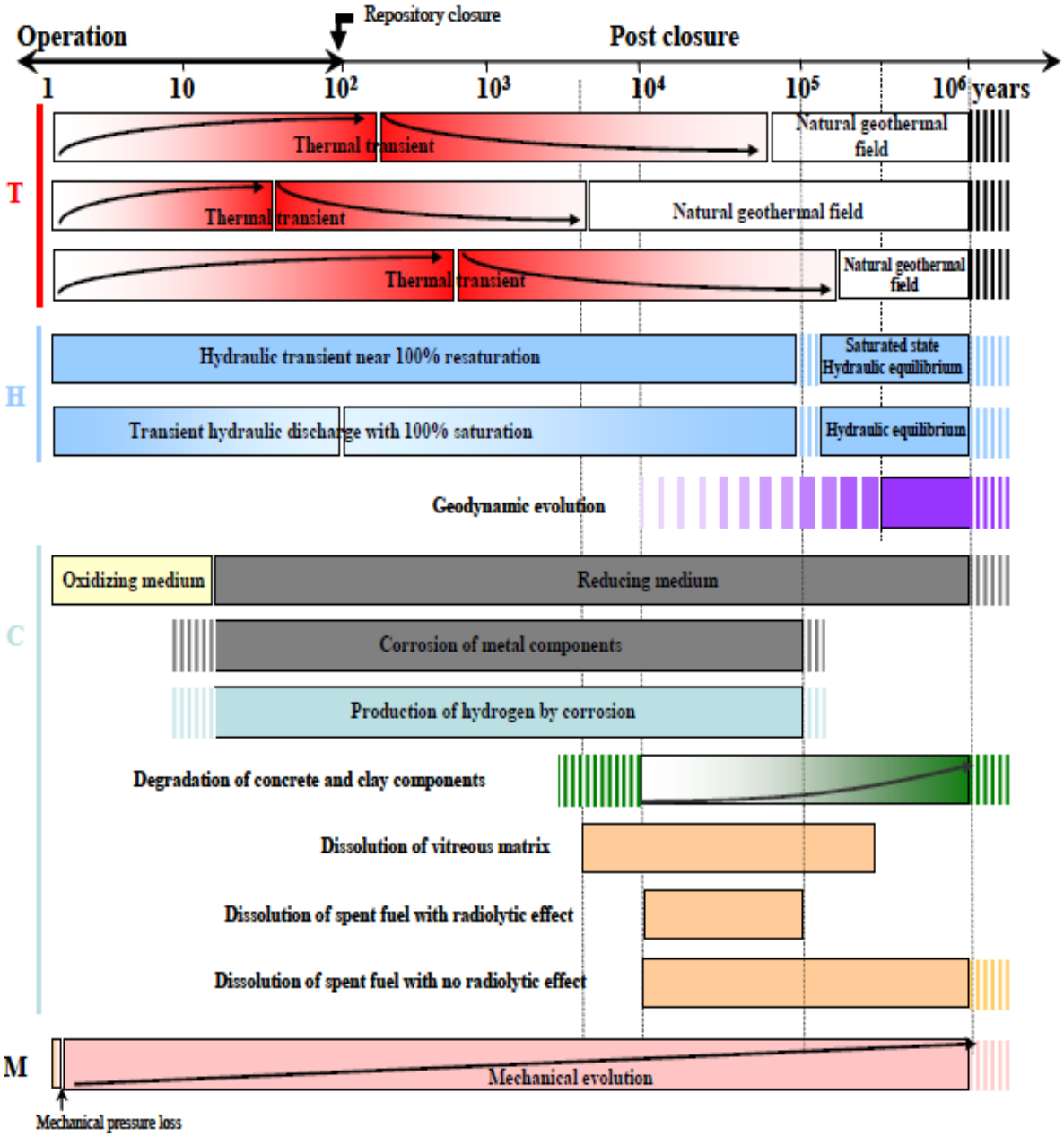

Figure 2.1: Chronogram of the possible thermo-hydro-chemical-mechanical behaviour in a repository (*after* ANDRA, 2005).

2.3 Gas transport through unsaturated porous medium

State of the art review on gas flow through unsaturated soils, in particular compacted clay buffer, has been presented in this section. The section has been divided into four subsections to detail the various aspects of multicomponent gas transport in unsaturated soil. Firstly, literature review has been carried out to investigate the flow mechanisms, e.g. advective flow and diffusive flow through unsaturated soil. Secondly, the validity of Darcy's law to model advective flow has been reviewed in this section. Since, gas flow through unsaturated soil is saturation dependant, two-phase flow phenomena of liquid water and gas components have been investigated. Finally, a review of two available multicomponent gas flow models has been presented.

2.3.1 Principle gas transport processes in unsaturated soil

Fredlund and Rahardjo (1993) stated that gas transport through unsaturated soil generally becomes continuous as the degree of saturation reduced to around 85% or lower. Scanlon et al. (2002) stated that transport of gases in unsaturated porous media can be described by advection and dispersion. Since, the effect of diffusion in gas phase is significantly higher than the mechanical dispersion, it has been mentioned that the mechanical dispersion is ignored.

In unsaturated soil advective flow or bulk flow takes place due to total gas pressure gradient (Fredlund and Rahardjo, 1993) which provides the driving potential for this mechanism and resistance to flow is caused by the viscosity of gas. It has been suggested that if a mixture of gases behaves as ideal gases the pressure gradient can be expressed in terms of concentration gradient and vice versa (Fredlund and Rahardjo, 1993).

Cunningham and Williams (1980) suggested that advective flow due to total pressure gradient dominates when the mean free path of the gas molecules are less than the pore radius and the particle radius, resulting in intermolecular collision being dominant over the collision between gas molecules and the pore walls. The mechanism of collision between gas molecules and pore wall also known free molecule diffusion or Knudsen diffusion. If the mean free path reduced to the level of mean free path of the molecules, Knudsen diffusion or free molecule diffusion becomes important and the molecule-wall collision becomes dominant over advective flow (Ho and Webb, 2006).

Diffusive gas flow through porous media takes place due to concentration gradient of the components (Cussler, 1984; Taylor and Krishna, 1993; Fredlund and Rahardjo, 1993). Bouazza and Vangpaisal (2002) stated that gas diffuse from higher concentrated region to a lower concentrated region due to its concentration gradient.

Binary diffusion of gases through air normally expressed by Fick's law and it can be extended to characterise the multicomponent diffusion behaviour (Taylor and Krishna, 1993). It has been stated that the diffusion of gases takes place due to molecular collisions and the diffusive flow of a component is influenced by the movement of other components present in the system. The multicomponent diffusion is often explained using matrix forms.

It has been identified that the magnitude or order of diffusion coefficients plays important role in case of multicomponent diffusive gas flow (Taylor and Krishna, 1993). It has been demonstrated that in a mixture of gases if the binary diffusion coefficients are of similar order, the multicomponent diffusion matrix is dominated by the diagonal elements, suggesting that the cross diagonal elements which represent the interactions between various gas components are negligible. Taylor and Krishna (1993) concluded that gases with higher order of diffusion coefficients influence the movement of that of lower diffusion coefficients.

Diffusion of gas components in air is faster than the diffusion in liquid water. From experimental results, it has been suggested that the molecular diffusion of gases is approximately four orders of magnitude greater in gas phase than in liquid phase (Cussler, 1984; Taylor and Krishna, 1993).

2.3.2 Validity of Darcy's law

Bulk movement of fluids or advective flow through porous medium is often defined by the Darcy's law. In case of advective gas flow through unsaturated soil, the validity of the law has been reviewed and presented below.

Darcy's law can be used to characterise advective flow in unsaturated porous medium (Fredlund and Rahardjo, 1993). Alzaydi and Moore (1978) reported from flow measurements experiments that Darcy's law could provide a fair approximation of gas flow in low permeability material.

Dullien (1979) suggested that Darcy's law governs the flow of fluids in porous media based on viscous flow which considers velocity along pore wall is zero. Although in case of gases, velocity along the pore wall might be non zero, resulting in slip flow or drift flow. Izadi and Stephenson (1992) confirmed that gas slippage flow thorough clay soils decreases as the degree of saturation decreases suggesting that the magnitude of slip flow is very small relative to viscous flow.

Yu (1985) conducted column experiments to validate Darcy's law in case of airflow and found that the law is valid for Reynolds number less than six. Gas flow through fine porous media should be laminar and usually characterised by a relatively small velocity. McBean et al. (1995) suggested that the Darcy's law is valid for porous mediums with characteristic grain sizes smaller than 2.0 mm.

Darcy's law can be extended to characterise the bulk flow in two-phase conditions, such as liquid and gas phase (Ho and Webb, 2006). It has been suggested that by considering gas or liquid phase relative permeabilities, influence of fluid flow in one phase could be included on the other phase.

2.3.3 Review of two-phase flow in unsaturated soil

Two-phase flow of gas and liquid water in unsaturated soil generally represented by two-phase characteristics curves. de Marsily (1986) stated that the two-phase characteristics curves usually presented as a function of the liquid saturation of the porous medium or the fraction of pore space occupied by liquid. Ho and Webb (2006) mentioned that numerous sets of two-phase characteristics curves are available where relationships for capillary pressure as a function of degree of saturation generally determined based on experimental data. Therefore, expressions for relative permeability are calculated, based on the capillary pressure relationships, using theoretical expressions derived by Burdine (1953) or Mualem (1976).

van Genuchten (1978, 1980) and van Genuchten and Nielsen (1985) suggested that the closed form solutions for the liquid phase relative permeability proposed by Mualem and Burdine, gives similar results but Mualem form is preferred over Burdine due to its more general applicability arises from larger range of curve fitting parameters.

van Genuchten characteristics curves has been developed for liquid phase. Parker et al. (1987) extended the van Genuchten-Mualem characteristics curve to include gas phase relative permeability.

Brooks and Corey (1964, 1966) proposed another two-phase characteristic curves based on experimental observations where the effective saturation has been plotted as a linear function on a log-log plot.

Ho and Webb (2006) highlighted that the linear relationship collapse as the full liquid saturation is approached. Therefore, the Brooks and Corey capillary pressure does not reach to zero at a full degree of liquid saturation (S_l =1.0). This is due to the fact that the straight line fit fails to fit the data in region where capillary pressure is less than bubbling pressure. The bubbling pressure or displacement pressure is the extrapolated capillary pressure which considers the trapped air bubbles at full liquid saturation (Ho and Webb, 2006).

2.3.4 Review of multicomponent gas transport models

A number of attempts have been undertaken in past to model multicomponent gas flow through porous medium including various transport processes. The process of advection and diffusion has been coupled to develop the Dusty Gas Model (DGM) by Evans, Mason and colleagues (Evans et al., 1961; Mason et al., 1963; Mason and Malinauskas, 1983). To develop the model it has been assumed that the porous medium consists of large size and molecular mass, held in space by external forces and can be treated as a component of the gas mixture. Therefore, the kinetic theory of gases is applicable. Darcian type flow has been considered to model advection while multicomponent diffusion has been modelled using Maxwell-Stefan approach for multicomponent diffusion. In case of flow through very low porosity medium, Knudsen diffusion or free molecule diffusion has been considered in the model.

Gas flow through porous medium can also be modelled using Mean Pore Transport Model (MPTM) (Rothwell, 1963; Schneider, 1978; Arnost and Schneider, 1995). The MPTM assumes that the vital part of the gas transport takes place in transport-pores that can be visualised as cylindrical capillaries with radii distributed around a mean value and the width of the distribution is characterised by the mean value of the squared transport-pore radii.

The applicability of these models has seriously been criticised by several researchers in recent years. Young and Todd (2005) stated that none of the authors (in both DGM and MPTM) have been able to resolve the problem of algebraic complexity which besets the subject and cause serious difficulties of understanding. Kerkhof (1996) showed that the addition of a viscous flux to the friction equations, as performed in the DGM, is erroneous, because the viscous friction has already been accounted for in the equations before the addition. Also, the DGM is limited to the flow through Knudsen regime and the multicomponent diffusion matrix based on Maxwell-Stefan approach made it difficult to adopt in governing equations of mass conservations (Jackson, 1977; Kerkhof 1996; Ho and Webb, 2006). Young and Todd (2005) stated that the MPTM theory is not standardised and sometimes it appears that the model assumptions are genuinely different but often because of unclear physical foundations or error from imprecise flux definitions, mass-molar transformation errors, incorrect treatment of the viscous flux.

Various aspects of gas migration through unsaturated soil have been reviewed. It has been reported that the advective and diffusive flow are the dominant mechanisms for gas flow through unsaturated soil. To characterise the multicomponent advective gas flow, validity of Darcy's law has been observed. Multicomponent diffusive gas flow can be explained adequately by implementing the Fick's law. From the review of two-phase flow, it has been understood that gas conductivity of variably saturated soil significantly depends on the degree of saturation of the buffer. Various features of van Genuchten - Mualem characteristics curve have been compared with Brooks and Corey relationships where the former has been found more useful than the later. A brief review of two available models for multicomponent gas transport has been presented including their capabilities and limitations. It has been suggested that the implementation of multicomponent gas flow models, e.g. DGM and MPTM is complex in nature and difficult to adopt in the governing equation of mass conservation.

2.4 Gas transport through saturated compacted clay buffer

Gas flow through saturated porous medium is complex and yet to understand. A number of attempts have been undertaken through laboratory experiments and numerical modelling to identify the flow phenomena in fully saturated compacted clays. A group of researchers have suggested that gas flow through fully saturated buffer takes place by creating tensile fractures or by dilating the pathways while the others consider a capillary flow or classical two phase flow through compacted clay soils. Therefore, in this section, a detail discussion of previously performed experimental and numerical works has been presented.

2.4.1 Gas migration experiments

In the context of gas migration through barrier a number of experimental investigations has been carried out and summarised below. Two experiments with significant results have been discussed in more detail. A summary of key experimental works have been listed in Table 2.1.

The earliest gas migration experiment in saturated MX-80 bentonite was carried out by Pusch and Forsberg (1983) to examine the gas permeability of the clay after gas breakthrough occurred. Hydrogen and nitrogen (as a safe replacement of hydrogen) gases were used to observe the migration phenomena of gas through bentonite. Pusch and Forsberg (1983) stated that highly compacted bentonite, which is more homogenous and less porous after becoming fully saturated, contains continuous passages and these capillary-like passages allow water to flow due to hydraulic gradient, ions to migrate due to concentration gradient and gas to transport due to a pressure gradient.

The hydrogen and nitrogen gas tests were carried out on MX-80 bentonite samples for 4 weeks and 8 weeks respectively. After the tests the samples were examined to observe the water content and density (Pusch and Forsberg, 1983). It was found that the degree of saturation was 100% for the nitrogen gas test samples. It was hypothesised that the gas may have migrated through a small fraction of the cross section. Harrington and Horseman (2003) suggested that as the specimen was found to be 100% degree of saturation, gas flow occurred through a small number of discrete pathways. Data from the hydrogen gas experiment showed a sudden pressure drop after 25 days of successive controlled increases in gas pressure, subsequently the pressure dropped accidentally and could not be raised for a month. After the experiment it was found that the sample was less water saturated and was explained

by the researchers that "some drying took place during the period when there was no gas pressure".

Table 2.1: Summary of key gas migration experiments in compacted clay.

Authors	Year	Sample	Details
Pusch and Forsberg	1983	Bentonite MX-80	Constant gas pressure and incremental pressure was applied to the sample
Pusch et al.	1985	Bentonite MX-80	Incremental pressure was applied to the sample in a constant volume oedometer
Gray et al.	1996	Illite and Sand-Bentonite mixture	Incremental pressure was applied to the specimens in constant volume condition
Horseman and Harrington	1997	Bentonite MX-80 and MX-80 paste	Displacement of gas by water from upstream reservoir; constant isotropic stress in flexible boundary condition
Tanai et al.	1997	Kunigel V1 and Fo-Ca clay	Incremental pressure was applied to the sample in a constant volume cylinder
Galle	2000	Fo-Ca clay	Pressure was increased in a constant volume oedometer
Graham et al.	2002	Avonlea	Pressure was increased in a constant volume oedometer
Harrington and Horseman	2003	Bentonite MX-80	Displacement of gas by water from upstream reservoir; constant volume cylindrical cells were used

Pusch and Forsberg (1983) stated that during the initial 25 days, percolation rates of hydrogen gas were uniform, suggesting that gas did not displace water to flow. Pusch and Forsberg (1983) stated that after the onset of a continuous gas flow, probably the gas passed through the clay without displacing pore water.

Pusch et al. (1985) then carried out experiments on saturated MX-80 specimens and observed that the gas entry in the bentonite take place at some value of critical pressures, which were found to be the same order of magnitude as the swelling pressure.

Gray et al. (1996) carried out experiments on samples of compacted illite and sand-bentonite mixtures to investigate the mechanisms of gas breakthrough and migration in compacted clay buffer. 46 illite specimens and 6 sand-bentonite buffer specimens were tested in the experiments. The illite samples were prepared at dry densities between 1.80 Mg/m^3 and 2.15 Mg/m^3 with a degree of saturation ranging from 55% to 100% and the 50-50 mixture of quartz sand and sodium bentonite buffers were prepared at a dry density of 1.67 Mg/m^3 and degree of saturation between 49% to 93%.

Gray et al. (1996) concluded that when local gas pressure exceeds the total soil pressure gas enters into small pores rather than in capillaries. It was noted that dilation of existing pores is significantly reversible but tensile fissures cause permanent damage in the barrier, developing preferential pathways. An initial backpressure of 200 kPa was applied on illite specimens and then the inflow pressure was increased in a stepwise manner every 5 minutes by an additional 200 kPa. Gas was collected after approximately one hour which has been considered as a gas breakthrough event. From experimental results it was stated that the resistance to gas breakthrough in saturated illite specimens increases curvy-linearly with increasing dry densities. Gas breakthrough pressures in bentonite buffer specimens were found to be significantly higher than the illite specimens and considerably higher than the swelling pressures.

It was thought by Gray et al. (1996) that the experimental evidence indicated that gas pressure gradient decreased along a specimen, indicating a shutdown of previously permitted gas migration pores and prevented accumulation of gas in gas collection circuit. It has been suggested that "this gas flow mechanism might involve some degree of pore dilation". From the results of repeated cycles test, it was found that initial gas breakthrough resistance was slightly higher than the subsequent cycles which indicate the pore structure might be changed to some extent by the gas flow process. It was stated that "gas breakthrough in illite can be explained in terms of capillarity and is related to the porosity and pore size distribution. Pore dilation and tensile fissuring might have also occurred during the tests".

Controlled flow rate gas injection experiments have been carried out by Horseman and Harrington (1997). In their experiment pre-compacted samples of KBS-3 specified MX-80 bentonite was used. Helium was used instead of Hydrogen in the experiments. The use of an inert gas ensured the absence of chemical reaction throughout the buffer. The clay specimens were isotropically consolidated and fully water saturated (degree of saturation, $S_r > 0.99$) under predetermined effective stress conditions. In the experiment the bentonite buffer was subjected to a constant isotropic confining stress and was equilibrated with water at a fixed pressure of 1.01 MPa. A 4.9 × 4.9 cm cylindrical clay specimen was placed between two high air-entry sintered stainless steel porous discs. To exclude confining fluid and to prevent diffusion losses of gas, the bentonite and porous discs were jacketed in a thin walled casing of copper or Teflon heat-shrink tube. An analytical model was also developed to describe gas migration behaviour at post-breakthrough stage.

Under the above mentioned programme four experiments were carried out by Horseman and Harrington (1997). The results of one of the experiments have been discussed in detail here. At the first stage of the experiments the specimen was provided a confining stress 16 MPa and a back pressure of 1.01 MPa. An initial pumping rate of gas at 375 μL/h was used at the upstream of the specimen and gas breakthrough occurred at an excess pressure of 15.19 MPa, which is slightly larger than the swelling pressure: 14.8 MPa at the dry density of 1.669 Mgm^{-3}, of this clay specimen. According to Horseman et al. (1999), the peak excess pressure of 15.30 MPa probably indicates fracturing process and is followed by a spontaneous well defined negative transient which approaches an asymptotic value of 14.22 MPa, as shown in Figure 2.2a. Gas injection was reinstated at a pumping rate of 375 μL/h, with the results shown in Figure 2.2b. But this time no well defined breakthrough was observed and gas flow through specimen commences at an excess pressure substantially lower than that of virgin specimen. The secondary peak excess pressure of 14.25 MPa has been observed which was 1.05 MPa lower than the initial attempt. The specimen was subjected to a descending history of pumping rates of 180 μL/h, 90 μL/h, 45 μL/h, 0 μL/h and each stages has given a negative transient response as detailed in Figure 2.2b. Horseman et al. (1999) observed that the gas flow law was very clearly non-linear or non-Darcian over the experiment leading to variable gas permeability. The maximum permeability of the specimen was observed immediately after the peak pressure.

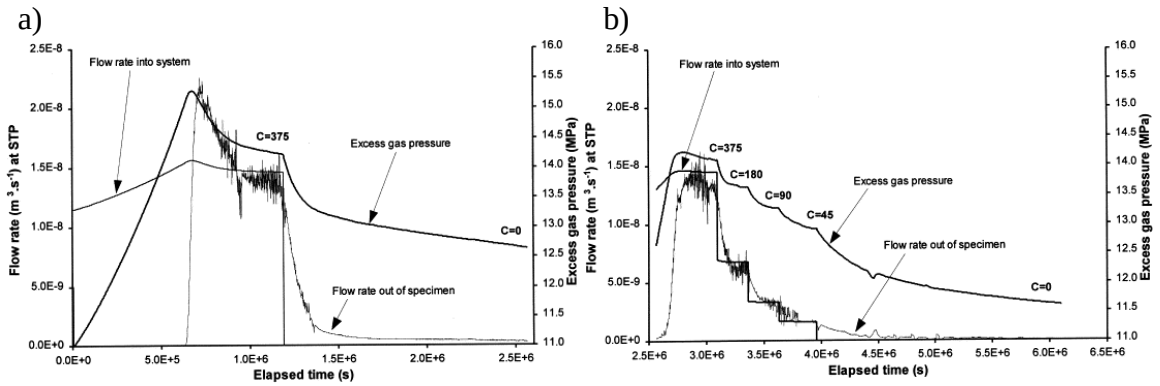

Figure 2.2: Behaviour of migrating gas along the buffer with time (*after* Horseman et al., 1996).

The results of laboratory experiments have been used to predict the behaviour in a real repository conditions. The MX-80 pre-compacted bentonite possesses a swelling pressure of 7.0 MPa at a dry density of 1.6 Mg/m^3 and at a typical repository depth of 500 m, the groundwater pressure is nearly 5 MPa (Horseman et al., 1999). It was stated that the increasing gas pressure at the void space between the canister and the buffer might help the gas to enter into the buffer at a pressure slightly larger than 12 MPa as shown in Figure 2.3 showing gas pressure versus time.

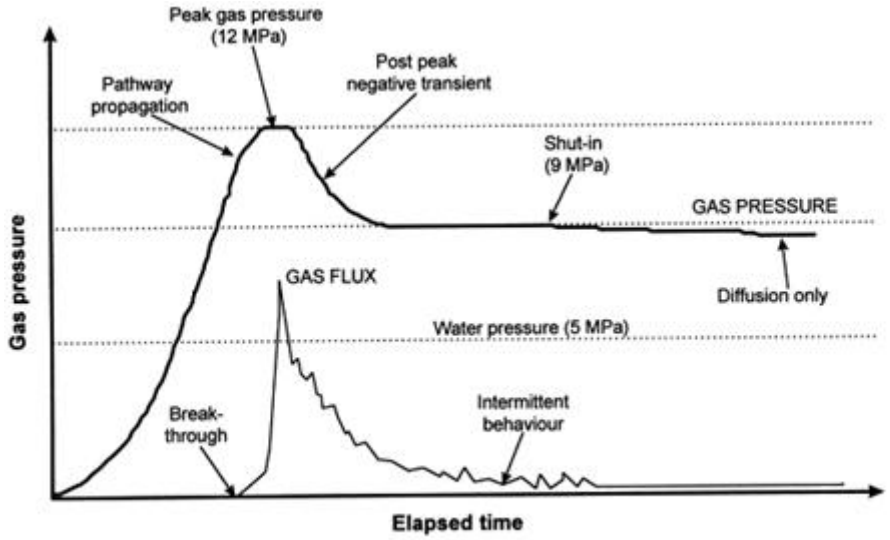

Figure 2.3: Change in gas pressure with time in a repository condition (*after* Horseman et al., 1999)

The change in the slope of the curve before the peak pressure is hypothesised to describe the crack nucleation and propagation, suggesting that the gas would move through a network of crack-like pathways formed by tensile rupture of the clay fabric (Horseman et al., 1999).

If gas generation stopped gas pressure would decline to a lower threshold value which has been termed as shut-in pressure. The shut-in pressure is the lowest value of gas pressure for maintaining an interconnected network of gas permeable pathways in the bentonite. Horseman et al. (1999) stated that the breakthrough pressure at the clay specimen was lower than the virgin clay when the gas injection was re-established in the same specimen. Horseman et al. (1999) explained that this phenomenon took place as the pressure induced pathways did not disappear when the gas injection was stopped. The re-sealing capacity of bentonite could not completely drive away the entrapped air and with the repeated injection, gas could easily find these pathways. Under repository conditions, diffusion of gas away from flow pathways is likely to be more important than flushing by groundwater (Horseman et al., 1999).

Tanai et al. (1997) carried out experimental studies of gas permeability and breakthrough pressures in different types of saturated and unsaturated clays. The gas permeability of Japanese Kunigel V1 bentonite was measured as a function of degree of saturation to validate the conventional two-phase flow models in case of unsaturated soil condition. Cylindrical specimens of 50mm diameter and 10mm thickness were prepared by uniaxial compaction of bentonite powder at 1.6, 1.7, 1.8 Mg/m^3 of dry densities. The intrinsic permeability of the specimens was measured at the value of zero degree of saturation. Tanai et al. (1997) measured the intrinsic permeability of Kunigel V1 saturated bentonite by water permeation tests and obtained results showed about five orders of magnitude lower than that of same dry densities. The differences in intrinsic permeability were obtained due to the change of pore structure by the swelling behaviour of the bentonite. From the experimental evidence it was found that gas permeability of Kunigel V1 approaches to zero at a saturation of about 72%, suggesting at this stage no continuous gas channels were available for flow and therefore gas breakthrough pressure becomes greater than zero.

Controlled H_2 gas injection test was performed by Galle (2000) to detect the threshold pressure for gas entry in cylindrical specimen of Fo-Ca clay. Galle (2000) observed two distinct thresholds for gas entry, i) the pressure when the first appearance of gas at the

downstream end of the specimen observed has been termed as the lower threshold of gas entry pressure and ii) the upper threshold has been characterized by a sharp increase in measured flow rate. The upper threshold which has been termed as breakthrough pressure was always larger than the gas entry pressure and in fully saturated condition these two thresholds were found very close to each other. Based upon experimental evidence Galle (2000) stated that the diffusion mechanism would not be adequate in this experiment to evacuate the generated hydrogen gas which would ultimately initiate the advective flow of gas due to the pressure gradient.

Experiments carried out on Canadian Avonlea bentonite have been reported by Hume (1999) in a MSc thesis and later the results of the experiments were discussed by Harrington and Horseman (2003) in a report prepared for SKB. During the test the unsaturated specimens showed a very low breakthrough pressure when the degree of saturation is below 80-90%. The breakthrough pressure for gas entry showed a sharp increase in case of fully saturated specimens. All the experiments were carried out at constant volume condition. Incident of breakthrough took place in all cases including the saturated soil condition as well but after a long period of time, with a flow mechanism of diffusion hypothesised. Hume hypothesised that the time to breakthrough was likely to be obtained by the time required for water to flow from the specimen to create a passage for gas and postulated an inverse relationship. Harrington and Horseman (2003), however, observed that therefore the breakthrough pressure could be zero for an infinitely large testing period and that this statement denied the existence of finite capillary gas entry pressure governing the flow of gas into a saturated porous medium with very narrow pores. However, it was noted that Hume did not exclude the possibility of a capillary threshold pressure for gas entry in the Canadian constant pressure gas test results.

Laboratory experiments were carried out by Graham et al. (2002) to investigate the gas breakthrough phenomena in illite, bentonite, sand-illite and sand-bentonite mixtures. A range of gas migration mechanisms are considered: i) Two phase advective flow, ii) diffusion of gas through pore fluid, iii) soil fabric deformation providing larger pores to accommodate flow, and iv) fissuring and fracturing. Two phase advective flow which pushes water ahead of the gas phase under the control of a combination of capillarity and hydraulic gradients were considered the most likely transport mechanism in their work. The gas breakthrough mechanisms are deemed to strongly depend on the conditions of the test.

Two types of tests were performed. In the first test, equal increments of gas pressure were applied at constant time intervals until gas breakthrough occurred and in the second test the time required for breakthrough was obtained at constant pressure (Graham et al., 2002). It was observed that gas breakthrough during incremental gas pressure experiments in bentonite specimens was abrupt and ambiguous, indicating a channelling of gas or fracturing of the specimen in a similar way suggested by Pusch and Forsberg (1983) and Horseman et al. (1999) who also used the same procedures. Graham et al. (2002) suggested that macropores in bentonite contain a significant amount of water which possesses higher viscosity than normal water and is not easily available for flow. For gas breakthrough in bentonite this viscous layer has to be disrupted and displaced by gas.

It was reported that the pressure at breakthrough increases with clay density and decreases with degree of saturation (very little resistance to gas migration has been obtained in case of bentonite at degrees of saturation below 93%). Graham et al. (2002) also stated that in a mixture of clay and sand, clay provides very low intrinsic permeability while sand provides resistance against shrinkage and cracking.

Graham et al. (2002) suggested that it would be more appropriate to initiate gas breakthrough research using rigidly confined cells because in disposal vaults of nuclear waste disposal facility, the bentonite will be placed in confined locations between canisters and surrounding host rocks. In such confined specimens it was hypothesised that a combination of capillarity and advective flow mechanism through existing pores is expected to take place, although capillarity might not extend over the whole specimen but possible channelling, flow mechanism (iii) highlighted above, in regions of larger pore sizes is expected. This hypothesis was supported by tests performed on specimens made with non polar paraffin, as opposed to water, experiencing low breakthrough pressures due to lack of bound water in diffusive double layers, hence larger available pore sizes. Delahaye and Alonso (2002) suggested that under rigidly confined test condition, channelling might include local non-homogeneities which allow some compression while other parts are expanding. Breakthrough was observed to be partly time dependent, long durations exhibits breakthrough at low pressure while high pressure development has been observed in the case of short time scales (Graham et al., 2002).

Harrington and Horseman (2003) reported experimental evidence of the sensitivity of the breakthrough and peak gas pressures to the test boundary conditions and suggested that gas entry must be accompanied by dilation of the bentonite fabric. It was found that shut-in pressures in constant volume and radially constrained boundary conditions were of similar magnitude and larger than that of under constant total stress boundary conditions and during shut-in the gas pressure was higher than the internal porewater pressure by a magnitude similar to the capillary pressure. They suggested that in case of undrained constant volume condition dilatancy of the specimen is limited to elastic compression of water and minerals. Harrington and Horseman (2003) suggested that the lower shut-in pressure in constant stress condition specimens occurred due to the ability of inelastic dilatancy in the direction perpendicular to the axis of flow. It was also found that gas entry and gas breakthrough pressures are higher in the constant volume condition experiments than in radially constrained experiments. Sharp pressure drop after the peak in constant volume experiments indicates failure of tensile strength of the bentonite (Harrington and Horseman, 2003). At the end of the experiments, the degree of saturation of the samples were measured and found fully saturated. The authors observed that if the capillaries of bentonite could accommodate the flow of gas, de-saturation of the samples should take place as the water will be displaced by gas from the capillaries but the fully saturated state of the specimens suggests that gas migrated through the bentonite by creating its own paths. Harrington and Horseman (2003) additionally suggested from the analysis of experimental results that the development of pressure induce pathways no ways compromises the sealing capacity of the bentonite barrier.

Large scale tests are important to see if laboratory results can be upscaled to field scale observations and carried forward to design criteria. However, large scale gas migration tests have rarely been performed, although two such large scale tests have been instigated. The Gas Migration Test (GMT) undertaken at the Grimsel underground laboratory in Switzerland (Grimsel Test Site, 2010) aims to investigate the function of the whole engineered barrier system to the impact of gas migration. Olivella and Alonso (2008) suggested from the initial GMT results that large scale experiments are considerably sensitive to minor details, for example, presence of joints, interfaces etc. The Lasgit experiment (SKB, 2007) has been instigated in the Äspö Hard Rock Laboratory, Sweden, to investigate gas migration at full scale. The results of the project have not yet been published.

A targeted review of experimental studies of gas migration through compacted clay barriers has been reported. It has been observed that the major transport phenomena in saturated compacted clays are complex and ambiguous in nature. Laboratory experiments based on flexible boundary condition suggests the flow of gas through pressure induced pathways are necessary for gas flow. Although for volumetrically constrained samples the development of fracture is unlikely. In most of the experiments, high gas injection rates or pressures have been applied on the sample, although such accelerated rates or elevated pressures are beyond that likely to be found in real repository conditions in a short period of time.

2.4.2 Modelling of gas migration in compacted clay buffer

Research has been carried out to predict the long term behaviour of gas migration in a real repository condition. In this context a number of gas generation and migration conceptualisation of flow processes and models have been developed. A summary of some of the modelling attempts have been listed in Table 2.2, with more details provided below.

Pusch and Hokmark (1990) developed a preliminary model for flow and diffusion based on generalized and quantitative microstructural data and basic physical relationships. Pusch and Hokmark (1990) stated that very dense artificially produced Na-montmorillonite clays have their microstructural features formed by the initial arrangement of air-dry bentonite grains that are compressed to yield elements of highly compacted bentonite. It has been assumed that the interlamellar water will not flow under a hydraulic gradient while the external water in the gel fillings of the voids between expanded bentonite grains will flow, provided that the interconnectivity allows for water transport through the compacted clay (Pusch and Hokmark, 1990).

Pusch and Hokmark (1990) reported that one of the most important features of the microstructural model is that the dense grains constitute a basic network with continuous external voids of varying size. Pusch and Hokmark (1990) stated that during hydration of the system under confined conditions the grains expand and reduce the porosity and the remaining voids become filled by soft clay gels (function of the void size) resulting in dense grains which means a significant variation of the hydraulic and gas conductivity over a cross section of the clay. It was suggested that gas penetrates smectite clays in gaseous form when the critical pressure is sufficiently high and the migration takes place through a small number of pathways. From their model it was shown that for very dense clays, the displacement of the gel filling is very small and thus the grains have to be forced aside by the penetrating gas and this then suggests that the critical gas pressure should be of same order of magnitude as the swelling pressure (Pusch and Hokmark, 1990).

Galle (2000) carried out a complementary work focusing on the modelling of gas pressure at the engineered barrier-canister interface and its comparison with the clay gas breakthrough pressures. Galle (2000) found that gas breakthrough pressures are in similar order of magnitude to the interfacial overpressures and that gas would be a key issue for clay engineered barrier performances and thus for disposal safety.

Table 2.2: Summary of important publications regarding numerical simulation of gas migration.

Authors	Year	Details
Pusch and Hokmark	1990	Preliminary model for flow and diffusion based on microstructural data and basic physical relationship.
Galle	2000	Modelling of gas pressure in the canister and engineered buffer interface.
Ortiz et al.	2002	Discussion regarding current status of knowledge relating to gas generation and transport in Boom Clay.
Delahaye and Alonso	2002	Numerical simulations to understand the consequence of soil heterogeneity on the development of preferential pathways
Rodwell et al.	2004	Discussion on various modelling approach
Olivella and Alonso	2008	Model was developed to deal with combined phenomena of two phase flow and generation of discrete paths.
Birgersson et al.	2008	A homogeneous and isotropic model of pressure response in saturated bentonite with high montmorillonite content.
Senger et al.	2008	Modelling using two-phase flow and gas diffusion. Inclusion of water consumption and realistic gas generation rates.
Xu et al.	2008	Follows on from Senger et al. (2008) whereby a reactive source term was utilised. Relied on experimental or conceptual corrosion rates, but allowed water availability and iron consumption to be considered.
Norris	2009	Review of current understanding

Galle (2000) stated that at the end of complete re-saturation of the buffer, generated gases due to canister corrosion and from other sources, would not be able to migrate through the buffer easily which will help in accumulation of gases in the space between the over-pack

and the low permeable clay buffer. The continuous accumulation of gas could initiate an over-pressurization of the entire barrier system leading to damaging the barrier by developing micro-cracks and later the build-up gas might induce host rock fracturing (Galle, 2000)

Galle (2000) stated that formation and propagation of preferential pathways in the clay due to gas pressure may be unstable, leading to intermittent gas flow and this instability was interpreted in terms of gas pathway propagation and collapse. According to Galle (2000) "gas transport in water saturated clay is only possible if the gas pressure exceeds the sum of the clay swelling pressure and the hydraulic backpressure".

According to Ortiz et al. (2002), below the threshold value of gas entry, the Fickian diffusion plays the dominant role for gas migration and when the gas threshold pressure exceeded, gas might accelerate the displacement of pore water by consolidating the clay particles to minimise the free energy of the system. It has been predicted that the increasing gas pressure will simply force the clay minerals apart at the mouth of the largest pathway or where discontinuity exists (Rodwell et al., 1999).

Ortiz et al. (2002) concluded that in the case of gas phase transport mechanisms through continuous Boom Clay formations, all laboratory and field experiments have questioned the validity of generalised Darcy's law at a large scale. The gas flux has been found not proportional to the pressure gradient but exponential. However, the rationale behind this is due to propagation of preferential pathways, where Darcy's Law may be valid. Therefore, this is more a comment on the appropriateness of the modelling assumptions and application of Darcy's Law rather than the flow mechanisms.

Delahaye and Alonso (2002) carried out a number of numerical simulations to understand the consequence of soil heterogeneity on the development of preferential pathways and their impact on the migration of gas. Initially water saturated Boom Clay was considered in their numerical modelling and gas injection process was either at constant pressure or at a constant flow rate. Two types of mechanisms were suggested in their work (Delahaye and Alonso, 2002), firstly natural pre-existing soil heterogeneity allows the development of preferential pathways for gas migration to occur via traditional two-phase flow, where local de-saturation of clay takes place and therefore gas permeability increases rapidly. Secondly, generation of pressure induced gas pathways. Only the first mechanism has been considered in their work

where the procedure describes generation of random fields for soil properties that control the flow of gas through soils. Delahaye and Alonso (2002) found that at an increased gas pressure low stiffness soils experience high gas flow rates due to an increase in porosity or intrinsic permeability. It was stated that soil heterogeneity was likely to lead to the development of preferential pathways in the soil, although it is uncertain due to the lack of experimental evidence. According to Delahaye and Alonso (2002) peak water outflow correspond with the time for gas breakthrough, which is consistent with the two-phase flow model considered.

Rodwell et al. (2004) stated that in highly compacted bentonite intrastack and interstack voids are non-existent and displacement of clay particles, termed micro-fissuring, is required for gas to migrate. If buffers provide significant resistant to gas invasion, at increasing gas pressure macroscopic fracturing of clay is expected, providing fracture pathways for gas flow. It was also reported that gas flow paths generated in bentonite buffer will be sealed by reinvaded water.

It was hypothesised by Alonso et al. (2006) that at high degrees of saturation gas migration might take place as a combined phenomenon of two phase flow and development of pressure induced pathway. Alonso et al. (2006) suggested that the later might play dominant role in low permeability clays, as in low permeability engineered barriers the capillary pressure to initiate de-saturation process would be high and such gas pressures may start the gas fracture processes or enable gas flow through existing discontinuities.

Olivella and Alonso (2008) carried out two sets of numerical simulations to investigate the flow behaviour through preferential paths in porous medium using model developed deal with combined phenomena of two phase flow and generation of discrete fracture paths. In first set of simulations a confined triaxial cell shale specimens were used to simulate the gas flow. The GMT test was simulated in a later attempt. Olivella and Alonso (2008) suggested that to explain the phenomena of irreversible fracture opening an elasto-plastic constitutive model for the soil or rock skeleton needed to be developed. It was stated that the classical framework for THM analysis has been developed based on the equations of mass, heat and momentum balance in system of porous medium is not adequate to explain the development of preferential gas paths in the barrier. A threshold strain parameter was considered to explain the fracture openings. The large GMT test was considered to validate the model. It

was concluded that the results obtained from the numerical simulations are in good agreement with the recorded result during the GMT test, in context of fluid pressures at different points of the sand-bentonite buffer, changes in water content and total stress in several interfaces. It was noted that significant attention to the various components was required to predict the behaviour of saturated and unsaturated buffer zones. It was found that the water pressurisation rate and gas injection rate control the magnitude of interface opening which in turn controls the evolution of pore pressures and stresses within the buffer.

A homogeneous and isotropic model of pressure response in saturated bentonite with high montmorillonite content has been developed by Birgersson et al. (2008). Due to the assumed isotropy, the model considers a single function of swelling pressure in a volumetrically confined system at a water ratio in equilibrium with liquid bulk water. It was concluded by Birgersson et al. (2008) that i) a gas phase does not have access to the pores filled with water because of the strong interaction between water molecules and counter ions, and ii) therefore, for a gas phase to enter into initially saturated clay, consolidation of the clay-water system should be taken place, resulting volume change through which gas can migrate. The model has been verified with the results obtained from the experiments carried out by Harrington and Horseman (2003) and was deemed to have good agreement with the experimental results provided that the model consider a type of clay where montmorillonite content is high enough and the present of secondary minerals are negligible.

Muller and Alkan (2008) reported the limitations of using Darcy's law for gas movement in case of dissolved condition in liquid or as a free gas phase. It was stated that the dominating effect of the capillary forces, the local and global heterogeneities, the interactions of percolating fluids with clay minerals has limited the direct application of Darcy's formulations. Muller and Alkan (2008) suggested that for clay formations and bentonite based buffers, poro-elastic crack dilation due to the effective stress concept causes intermittent, episodic flow processes resulting in non-linearities between flux and hydraulic gradient (Muller and Alkan, 2008).

Nagra (2008) assert clay-rich rock cannot withstand long-term gas pressures higher than the minimum principal stress acting on the rock mass, consequently micro-fractures will form in the host rock. The process of gas-driven micro-fracturing leads to an increase of the pore

space, which is accompanied by a detectable increase in intrinsic permeability and a change in the retention curve.

Senger et al. (2008) carried out numerical modelling to investigate two phase flow phenomena in Opalinus clay. A previously developed model which considered only gas generation phenomena has been extended to observe the gas pressure build up in HLW/SF UDF, considering gas generation and water consumption in clay. It was suggested that desaturation of bentonite by displacement of generated hydrogen is unlikely and requires a pressure of more than 80 MPa. The pressure at this range is significantly higher than the minimum principal stress of Opalinus clay at a repository depth of 650 m. It was reported that the threshold pressure for dilatancy controlled gas flow through Opalinus clay is in the order of 13-15 MPa and potential pathway dilation or fracture development at high pressure might significantly affect the capillary pressure and saturation relationship.

A significant finding was that gas pressure build up was reduced considering the water consumption within the corrosion process, compared to the simulation of considering gas only, as considered by other gas migration experiments and simulations. Senger et al. (2008) reported that very little pore water displacement was been obtained from the barrier at the early stages and the overall water flow has been obtained towards the canister. It was concluded that the gas pressure build-up under realistic corrosion conditions was unlikely to reach the pressures required for the fracture process, however details of the gas migration processes and parameters used included within the model are not given, although both advective and diffusive gas flow are considered.

Xu et al. (2008) presented a reactive chemistry model based on Fe corrosion, coupled with two phase flow phenomena driven by gas pressure buildup related to H_2 generation and water consumption. The model examined specific corrosion reactions and their dependence on hydro-geochemical and two-phase flow conditions at the canister and in the surrounding materials. The geometric configuration and hydraulic parameters of clayey formation were used from the Swiss concept of a nuclear waste disposal facility. The model was not been developed for the purpose of estimating mechanical and chemical impacts on the bentonite buffer and on the host rock but to evaluate the importance of selected physical parameters that affect hydrogen gas generation. The paper presented by a radially-symmetric geometry and a constant temperature of 40 ˚ C was used throughout the model domain and simulation

time. The H_2 gas generation rate and corresponding water consumption rates due to iron corrosion has been dynamically calculated using the simulation software TOUGHREACT which is a non isothermal reactive geo-chemical transport program and able to analyse a range of sub-surface coupled thermal-physical-chemical processes under various thermal-hydrological and geo-chemical conditions. The model has been simulated using initial generation rates of: i) a lower bound H_2 generation rate of 0.04 m^3/year/ tunnel meter (tm) and ii) a higher bound generation rate of 0.4 m^3/year/ tunnel meter (tm) corresponding to Fe dissolution rate constants of 2.0×10^{-12} mol/m^2/sec and 2.0×10^{-11} mol/m^2/sec. The corrosion/gas generation rates were dynamically calculated based upon water availability and reduction of Fe volume.

A review of the most recent understanding of liquid-gas interaction as a result of gas generation and migration in a repository condition has been presented in the draft FORGE report of "Summary of Gas Generation and Migration Current State-of-the-Art" in July 2009 (Norris, 2009).

The sequence of gas generation and migration, through clay soil as characterized by Mallants and Jacques (2004) and Mallants et al. (2007) has been summarized by Norris (2009) into four important stages, which are as follows:

- Stage I: At early stages, the gas generation rate is slow and the generated gas can dissolve into the buffer pore water. At this stage gas can possibly migrate only by diffusion through the barrier and host rock formations.
- Stage II: At this stage, the gas generation rate may exceed the diffusive transport capacity of the dissolved gas which leads to the formation of gas bubbles. Increasing gas pressure results to a gradual de-saturation of the buffer and possibly the host rock. At this stage a small fraction of interstitial water has been expected to be expelled from the buffer.
- Stage III: The continuous gas generation will lead the isolated gas bubbles to form ultimately a continuous gas phase. This stage initiate the two phase flow in the engineered barrier and gas phase mainly flow due to the advection and further expelled of water is expected.

- Stage IV: Gas migration. The process of gas migration is still questionable. One hypothesis originally described by Mallants and Jacques (2004), assumed that some kind of cyclic behaviour of opening and closing of the preferential flow paths will take place and another possibility is dilatancy-controlled gas flow (Norris, 2009). Mallants and Jacques (2004) suggested from experimental evidence that cyclic behaviour of opening and closing of preferential flow paths goes on until the gas production rate becomes small enough to allow dissolved gas to be evacuated by diffusion via the pore-water.

Norris (2009) suggested that in case of high gas generation rate, advective flow would not be adequate to evacuate all the generated gas due to the extreme low permeability of the surrounding buffer and when the increasing gas pressure locally exceeds the minimum component of the principal tensor of total stresses, a preferential pathway would be created in a plane perpendicular to that component. It was thought that the propagation of the fracture will stop when the gas pressure in the fracture becomes less than the value of the minimum principal stress or shut-in stress. Norris (2009) stated that after the development of preferential pathways, gas pressure would drop significantly and the self-healing capacity of clays would help to re-seal the pathways. It was thought that the available continuous fluid flow models would not be able to explain the development of preferential pathways.

Most of the numerical investigations associated with gas migration can be considered as complementary to the experimental research. Long term repository based simulations at realistic generation rates have rarely been conducted. Although it has been suggested the flow of gas through pressure induced fracture is possible, until now, no numerical model has been developed to address this particular issue.

2.5 Compacted bentonite: clay-water-gas system

Bentonite has been envisaged as backfill material for nuclear waste disposal facilities because of its favourable physical and chemical properties (Wersin et al., 2004). Since the material has been considered as a potential barrier for nuclear waste disposal, extensive research has been carried out over the decades to investigate the sealing properties of bentonite buffer. Therefore, large quantity of literature (Pusch and Young, 2006; Wersin, 2003; Wersin et al., 2004; Olivella and Alonso, 2008; Huertas et al., 2000; Rautioaho and Korkiala-Tanttu, 2009; Wilson et al., 2011; and others) is available. A brief review of the porewater composition and associated geochemical reactions have been presented in this section.

In order to provide a clear understanding of gas flow and geochemical interactions, it is essential to predict the porewater chemistry of the buffer material. In this study compacted bentonite MX-80 has been considered as a representative buffer material.

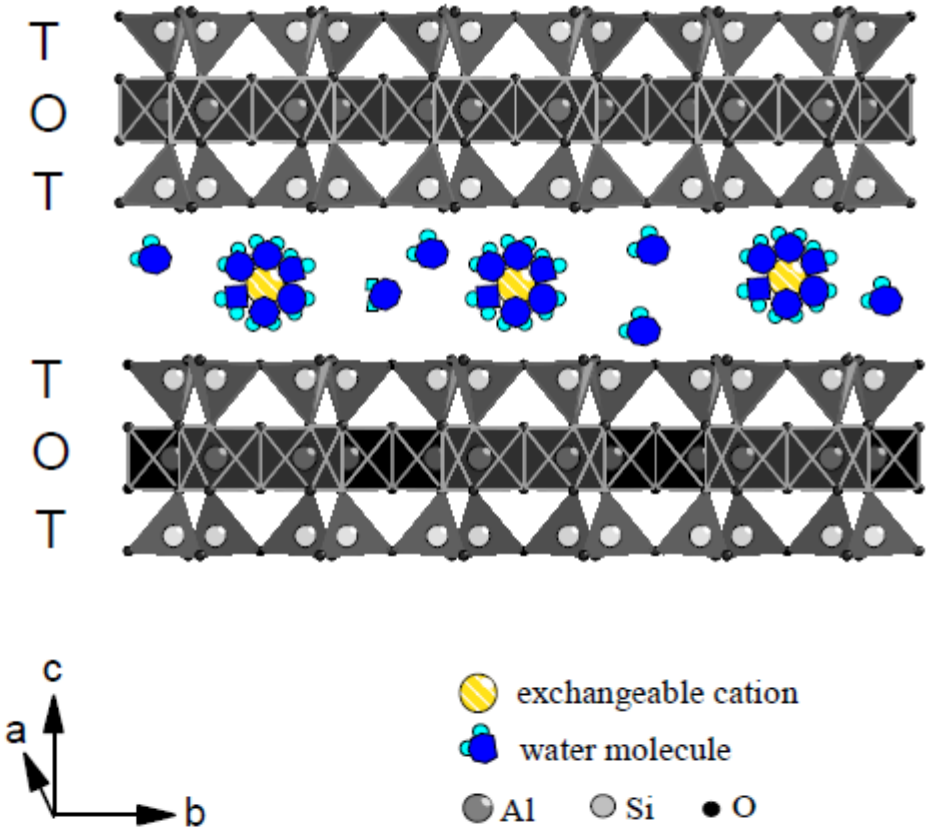

Figure 2.4: Schematic representation of montmorillonite structure (*after* Bradbury and Baeyens, 2002).

Bentonite contains around 65 to 90% montmorillonite and therefore, its properties are largely dominated by this clay mineral (Grauer 1986; Bradbury and Baeyens, 2002). The general structure of montmorillonite consists of an octahedral sheet sandwiched between two silica tetrahedral sheets (Bradbury and Baeyens, 2002). Figure 2.4 shows that the tetrahedral-octahedral-tetrahedral (TOT) layers spaced in the a and b directions of the order of 1000 nm and combine together one above the other in the c direction to form platelets (Bradbury and Baeyens, 2002). Grim (1953) stated that larger particles consist of stacks of these platelets where the number of platelets in each stack varies from three to five in Na-montmorillonite to 10-20 in Ca-montmorillonite (Pusch et al., 1990).

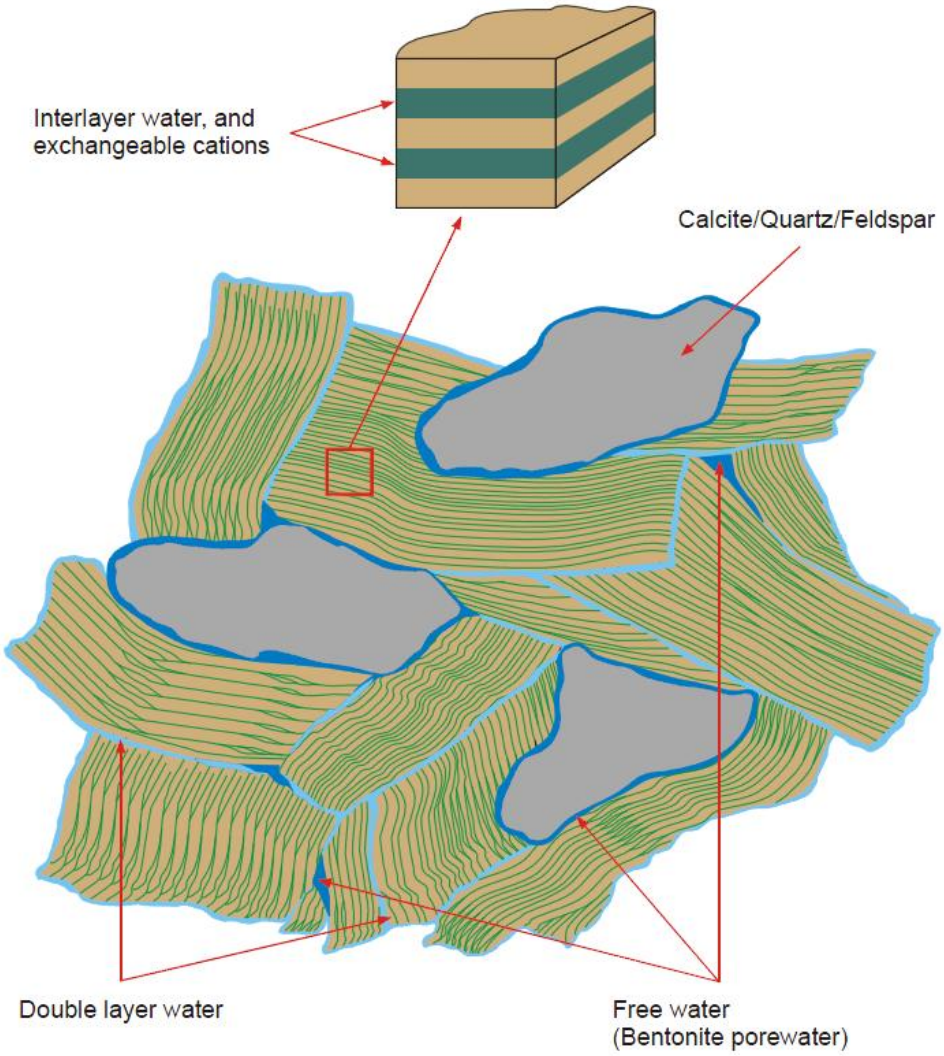

Figure 2.5: Schematic representation of three types of water in compacted bentonite, termed as interlayer water, double layer water and free water (*after* Bradbury and Baeyens, 2002).

The porewater in bentonite can exist in three different forms (Bradbury and Baeyens, 2002). It has been stated that most of the water in re-saturated bentonite, compacted at dry densities more than 1.2 Mg/m^3, under constant volume conditions present in the interlayer space between the individual tetrahedral-octahedral-tetrahedral units and termed as "interlayer water". Rest of the water has been termed as "external water", part of which associated with the external clay surfaces in the electrical double layers known as "double layer water". The remaining portion of water has been described by Bradbury and Baeyens as "free water". A schematic representation of bentonite porewater has been given in Figure 2.5.

Wersin et al. (2004) stated that the swelling capacity of bentonite provides a very efficient diffusion barrier to contaminant transport which makes it difficult to carry out the aqueous phase experiments at compacted conditions. However, the porewater in compacted bentonite is almost impossible to determine experimentally by chemical analysis (Hunter et al., 2007). Therefore, the properties of compacted bentonite porewater can be evaluated through circumstantial experimental evidence or by physico-chemical modelling.

The amount of porewater presents in bentonite is a small fraction of the dry compacted pore volume which decreases with increasing compaction, suggesting that the porewater chemistry in compacted bentonite depends on the initial dry densities (Bradbury and Baeyens, 2002). It has been observed that the bentonite porewater contains relatively high ionic strength and saturated with calcite, gypsum, celestite, quartz etc. Fernandez et al. (2004) suggested that the ion concentrations usually depends on the solid to liquid ratio of the system and the porewater composition is controlled by the dissolution of chlorides, dissolution and/or precipitation of carbonate and sulphate minerals and the cation exchange reactions in the smectite.

Mitchell and Soga (2005) stated that isomorphous substitution of lattice cations by cations of a lower valency creates a permanent negative charge on the surfaces of montmorillonite platelets. Bradbury and Baeyens (2002) suggested that the compensating cations reside within the predominant interlayer space. Therefore, the cations bound to the surfaces due to electrostatic attractions, create the electrical double layer and subjected to stoichiometric exchange with the cations in the solution (Grim, 1953; van Olphen, 1963). The total permanent negative charge defines the cation exchange capacity or CEC of montmorillonite minerals.

Bradbury and Baeyens (2002) explained that the ion capacities of solids are significantly higher than those in the aqueous phase because of large masses of montmorillonite and a tiny fraction of porewater present in bentonite. Therefore, cation loadings and solubility of montmorillonite and other solid phases determines the porewater composition.

The buffering capacity of bentonite towards pH and Eh corresponding to an intrusion of external fluid has been evidenced from a number of experimental studies (Muurinen and Lehikoinen, 1999; Karnland et al., 2000; Fernandez et al., 2004; Muurinen and Carlsson, 2007; Villar et al., 2007; Arcos et al., 2008). It has been concluded from several experimental results that the chemistry of most reactive ions usually governed by mineral precipitation and/or dissolution, cation exchange reactions, redox processes. Some of the important geochemical reactions and the associated processes have been reviewed and has been detailed in the following paragraphs.

Fredlund and Rahardjo (1993) stated that the amount of gas that can be dissolved in a liquid follows the Henry's law which states that at constant temperature, the mass of gas that dissolves in liquid is directly proportional to the absolute pressure of the gas above the solution (Sisler et al., 1953). The dissolution of hydrogen in pure water at equilibrium follows Henry's law and can be expressed as a half reaction suggested by Appelo and Postma (2005):

$$H_{2(g)} \leftrightarrow 2H^{+} + 2e^{-} \qquad \text{(R.2)}$$

The reaction (R.2) suggests that presence of hydrogen gas influence the amount of hydrogen ion and electron activity of a solution. The electron activity or Pe measures the oxidation-reduction capacity of a solution, indicating the tendency of a solution to donate or accept protons (Kehew, 2001). It has been suggested that the higher the value of Pe, there is a strong tendency for the solution to accept protons or the solution is oxidizing. On the other hand, at low Pe the tendency of a solution to donate protons increase or the solution is reducing.

Rankama and Sahama (1950) stated that Pe of a solution affected by hydrogen ion concentration which measures the pH of a system. It has been mentioned that the Pe affects the pH as soon as considerable amount of material precipitate in reactions and no buffer substances are present.

Appelo and Postma (2005) suggested that minerals that react fast with water, such as gypsum, halite, fluorite, carbonate minerals attains equilibrium within a short timestep while other minerals, such as silicates react so sluggishly that at low temperatures equilibrium can never be attained, suggesting that reaction kinetics should be considered.

It is known that carbon dioxide reacts with water to form carbonic acid (H_2CO_3) and the acid provides protons (H^+) which reacts with calcite ($CaCO_3$) to form bicarbonates (HCO_3^-). The overall equilibrium can be presented as:

$$CO_2 + H_2O + CaCO_3 \leftrightarrow Ca^{2+} + 2HCO_3^- \quad \text{(R.3)}$$

Appelo and Postma (2005) mentioned that the reaction is fundamental for understanding the behaviour of calcite precipitation and dissolution at equilibrium. Since, an increase in calcium (Ca^{2+}) or bicarbonate (HCO_3^-) ions or decrease of carbon dioxide helps calcite to precipitate while an increase of carbon dioxide or decrease of calcium and bicarbonate ions results in dissolution of calcites. The dissociation of carbonic acid stepwise releases two protons and therefore, the concentration of dissolved carbonates depend on the pH of the solution. Bicarbonate is the dominant species at pH ranges from 6.3 to 10.3.

Appelo and Postma (2005) explained the processes involved in simultaneous equilibrium with calcite and dolomite combining the dissolution of gypsum ($CaSO_4.2H_2O$) or anhydrite. At equilibrium gypsum/anhydrite dissolution occurs as follows:

$$CaSO_4 \leftrightarrow Ca^{2+} + SO_4^{2-} \quad \text{(R.4)}$$

It has been suggested that the increasing calcium concentration due to gypsum dissolution results calcite to precipitate as it has been described above. Since the carbonate (CO_3^{2-}) concentration decreases due to calcite precipitation, dissolution of dolomite increase magnesium (Mg^{2+}) concentration in the solution. It has been concluded that the dissolution of gypsum in the solution increases the amount of calcium (Ca^{2+}), magnesium (Mg^{2+}) and sulphate (SO_4^{2-}) ions in the solution.

Elrashidi et al. (2010) carried out laboratory based experiment to investigate the effect of gypsum on the solubility of thirteen plant nutrients, such as nitrogen (N_2), phosphorous (P), potassium (K), sodium (Na), calcium (Ca), magnesium (Mg), iron (Fe), manganese (Mn), Boron (B), sulphur (S), chlorine (Cl), cupper (Cu) and Zinc (Zn) on soil samples. A 100 g sample of gypsum-free soil (Sharpsburg Fine, montmorillonitic, mesic type Argiudolls) was treated under increasing amount of gypsum. It has been reported that the addition of gypsum increases magnesium concentration by replacing Mg-exchangeable from clay surfaces. Similarly, the increasing amount of calcium (from dissolution of gypsum) also replaces potassium, manganese from cation exchange zone. An expected increase of sulphate ions have been reported in their result. Elrashidi et al. (2010) observed that the addition of gypsum in a solution reduces pH of the system. It has been reported that an addition of 1.0 g of gypsum to a 100 g soil sample decreased the pH in the extracted water by 0.8 units.

A brief review of the structure and constituents of compacted bentonite have been presented. It has been suggested that the determination of porewater composition of compacted bentonite significantly important for the modelling of reactive transport. It has been noticed that the bentonite porewater contain large amount of dissolved chemicals and minerals. In presence of gases the extent of various geochemical reactions and processes has also been presented.

2.6 Computational and numerical modelling schemes

Advanced computational schemes and numerical methods are essential to develop reactive transport codes. Seetharam (2003) suggested that two main numerical strategies are of paramount importance to develop a reactive transport model. Firstly, numerical methods are required to solve the partial differential equations of transport processes and then non-linear algebraic or partial differential equations representing the equilibrium or kinetically controlled chemical reactions. Secondly, a method is required by which the partial differential equations and non-linear algebraic equations are coupled in an efficient way. Such developments in coupling techniques have been presented here.

Several techniques have been developed by various researchers (Jennings et al., 1982; Lewis et al., 1987; Yeh and Tripathy, 1989; Xu et al., 1999) to solve the coupled transport and reaction equations, e.g. mixed differential and algebraic approach (DAE) , direct substitution approach (DSA), sequential iterative and non-iterative approach (SIA and SNIA). The major computational schemes for solving couple transport and reaction governing equations can be categorised, according to Steefel and MacQuarrie (1996) as:

a. global implicit method, one step or Direct Substitution Approach which simultaneously solves the governing transport and reaction equations, leading to a fully coupled system of equations. The chemical equations are substituted into the transport equations and they are solved by Newton-Raphson method.

b. Operator splitting technique where the transport and reaction equations are decoupled and partial differential equations for chemical transport and chemical reactions are solved sequentially. The sequential approaches, such as SIA and SNIA are the proposed techniques in this category.

The sequential iterative approach (SIA) solves the transport equations first and then using the obtained results, equilibrium values of chemical concentrations are determined by solving chemical equations. The procedure is repeated for every iteration within a time step and therefore, has been termed as sequential iterative approach.

The widely used numerical techniques, such as finite element method and Newton-Raphson method for solving differential and non-linear algebraic equations respectively, can be adopted using efficient algorithms. The sequential non-iterative approach (SNIA) is a special case of SIA where the chemical equations are solved only once in a time step, after the convergence of transport step can be achieved.

It has been suggested that global implicit method provides more accurate results than operator splitting methods but often requires excessive CPU memory and CPU time (Yeh and Tripathy, 1989; Steefel and MacQuarrie, 1996; Saaltink et al., 2001; MacQuarrie and Mayer, 2005). Particularly, for a two and three dimensional problem, DSA and DAE approaches are less efficient in terms of CPU memory and CPU time (Yeh and Tripathy, 1989).

Steefel and MacQuarrie (1996) carried out a comparison study between different coupling schemes including DSA, SIA and SNIA. It has been concluded that in case of multiphase and multicomponent systems, implementation of global implicit methods becomes significantly difficult due to the size of the matrix required for coupling and enlargement of non-linear equations which need to be solved.

Saaltink et al. (2001) performed several tests to observe the efficiency of DSA an SIA. It has been concluded that in case of fast kinetic reaction rates DSA is more robust than the SIA and unlike SIA, the convergence is less sensitive to the size of time step. It has been suggested that although DSA can be applied to solve all coupled reactive transport problems, the SIA is faster and requires less computer memory for large grids and it is computationally more efficient (Steefel and MacQuarrie, 1996; Samper et al., 2009).

Steefel and MacQuarrie (1996) compared the results of some simple case simulations using different sequential coupling methods. It has been concluded that the SIA sometimes gives smallest errors to CPU time ratio, although in other cases SNIA is more efficient. The accuracy of SNIA is strongly dependent on space and time discretisation and the type of chemical reactions.

Xu et al. (1999) adopted SNIA in addition to SIA to compare the accuracy and numerical performance for several test cases. It has been observed that for a specific test case, the SNIA is more efficient and require less CPU time, although noticeable numerical dispersion and

errors have occurred. therefore, it has been concluded that there is no definite proof that SNIA is better than SIA and it mainly depends on the type of chemical reactions, time and space discretisation. Samper et al. (2009) suggested that numerically SNIA is two to three times more efficient than SIA.

The recent development of reactive transport models mainly focused on coupling transport models with well established and advanced geochemical models, such as PHREEQC2 or MINTEQA2. A brief discussion on coupled THCM model has been presented below.

Prommer (2002) presented PHT3D, a computer code, to calculate general reactive transport coupling MODFLOW/MT3DMS for transport and PHREEQC2 for chemical reactions. The algorithm of the coupled code has been developed based on the sequential non-iterative approach.

Seetharam (2003) developed a coupled THCM model by linking transport code COMPASS with geochemical equilibrium code MINTEQA2. The multicomponent reactive transport of dissolved chemicals can be modelled using this coupled code where both the SIA and SNIA have been adopted. The coupled THCM model provides an advantage to compare the results obtained from both SIA and SNIA.

Jacques and Šimůnek (2005) presented reactive transport code HP1 for modelling reactive transport and biogeochemical processes in variably saturated porous media. The HP1 has been developed by combining water and solute transport model HYDRUS-1D and PHREEQC2. HP1 is capable of modelling transient water flow in variably saturated porous medium, transport of multicomponent chemicals, mixed equilibrium/kinetically controlled biogeochemical reactions and heat transport. The transport and geochemical model has been linked by using a sequential non-iterative approach coupling scheme and only limited to one dimensional analysis.

Sedighi (2011) presented a coupled THCM model for multicomponent dissolved chemical transport through highly compacted porous media. The multicomponent chemical transport has been modelled using code COMPASS while the geochemical reactions has been calculated using PHREEQC2.

Both equilibrium and kinetically controlled chemical reactions can be modelled using the coupled COMPASS-PHREEQC2 code. The sequential non-iterative approach has been adopted in this work.

From the aforementioned discussion it has been found that various coupling schemes are available to solve the governing equations for chemical transport and reactions or to link transport and reaction models. The successful implementations of these schemes have been verified in various models. It has been noted that the computational performance and efficiencies of the various suggested coupling schemes are basically affected by the type of the transport problems and the degree of complexity in geochemical reactions.

2.7 Conclusions

The corrosion process has been initially examined, with the overall reactions and a kinetic method to determining gas generation rate reported. It has been found that the gas generation rates entirely depend on corrosion rates in a deterministic manner. A range of corrosion rates and therefore gas generation rates have been presented in this section from experimental work. The rate is reported to differ dependent upon the conditions, for example water supply, pH and temperature. A quantitative comparison of the generation rates has been presented in this chapter. It has also been reported that the presence of bentonite buffers may enhance the corrosion process, although the long term corrosion rate is stated to be lower than that the maximum due to a protective surface produced during the corrosion process.

A comprehensive review of gas transport mechanisms in variably saturated buffer has been presented in this chapter. It has been observed that most of the gas migration experiments and numerical modelling studies consider a fully saturated buffer which has been saturated in uniform manner prior to corrosion process. But in field condition uniform saturation of buffer might not take place, leaving unsaturated or occluded flow paths. Therefore, generated gases, due to corrosion and other mechanisms, might follow the paths of least resistance in the unsaturated zone of buffer materials. Inadequate research has been carried out to address/resolve this subject matter related to gas migration. Multi-phase characteristics curve to define unsaturated gas conductivity has been reviewed in this chapter. Two of the available multicomponent gas flow models, e.g. DGM and MPTM have been presented and their limitation/ complexity of application have been discussed.

A targeted review of experiments into gas migration through compacted clay barriers has been reported. A number of mechanisms were deemed to exist with the some debate over the dominant mechanism. Most research agrees that limited flow can occur prior to a fracture event and for fracture and consequentially elevated flow rates to occur, gas pressures elevated above the swelling pressure is required. Additionally for volumetrically constrained samples the higher gas-pressures are required for fracture to occur. It is noted that in many of the experiments the rate of gas injection is high due to time constraints, elevating the pressure beyond that likely to be found in real repository conditions. However, as the range of flow mechanisms depends upon the pressure regime the experimentation is unable to fully describe the likely conditions within a real disposal facility. Concentrating efforts on the upper end of pressure range may not allow full characterisation of the migration processes occurring at low

pressures and in turn lead to over-conservative assumptions feeding into the safety assessment and design process.

Most of the numerical investigations can be considered as complementary to the experimental research. However, only limited work was available using repository realistic generation rates and inclusion of water consumption in the real corrosion process. Numerical simulation efforts in this field have focused upon the build-up of large pressures and consequential fracture/dilation processes that could occur, although no models to explicitly include fractures and fracture propagation have been developed. The processes and evolution to pressure build-up are reasonably well established. However, at realistic generation rates and low permeabilities, the diffusion of gas through pore-water is likely to be significant and has not been widely considered.

From the review of literatures, it has been found that most of the gas migration experiments through engineered buffers have been carried out using an inert gas or less sensitive (to reaction at normal condition) gases. But various species of gases generated in a waste disposal facility are chemically active which might be involved in geochemical reactions, in presence of other chemical components in aqueous or gas phase. The porewater carries numerous chemical components which could provide possible reaction paths for the gas components present in the system. Literature review on porewater chemical compositions has been presented in this chapter and a detail procedure to calculate porewater composition has been presented in chapter 7. Presence of gases in buffers could possibly influence the solution properties and consequently the geochemical reactions. A background study of such reactions has been carried out and detailed in this chapter.

Background study on development of numerical techniques for efficient solution of coupled transport and geochemical reactions have been presented. In this context a number of coupling methods, such as direct substitution approach, mixed differential approach, sequential iterative and non-iterative approaches has been discussed including their relative merits and drawbacks from the point of view of the chemical nature of the problem. Recent development of some coupled model for reactive transport has also been presented. It has been found that the geochemical model PHREEQC2 provides advanced platform for reactive transport modelling, since the geochemical model is capable of modelling both equilibrium and kinetically controlled reactions.

References

Alzaydi, A.A., Moore, C.A., (1978). "Combined pressure and diffusional transition region flow of gases in porous media". *American Institute of Chemical Engineering Journal* **24**, No. 1, pp. 35-43.

ANDRA, (2005). "Phenomenological evolution of a geological repository". ANDRA Dossier Argile, Report Series.

Appelo, C.A.J., Postma, D., (2005). "Geochemistry, Groundwater and Pollution". A.A. Balkema, Rotterdam.

Arcos,D., Fidel, G., Cristina, D., Fernandez, A. M., Villar, M.V., Muurinen, A., Carlsson, T., Sellin, P., Hernan, P., (2008). "Long-term geochemical evolution of the near field repository: Insights from reactive transport modelling and experimental evidences". *Journal of Contaminant Hydrology* **102**, pp. 196-209.

Arnost, D., Schneider, p., (1995). "Dynamic transport of multicomponent mixtures of gases in porous solids". *Chemical Engineering Journal* **55**, pp. 91-99.

Birgersson, M., Akesson, M., Hokmark, H., (2008). "Gas intrusion in saturated bentonite-A thermodynamic approach". *Physics and Chemistry of Earth* **33**, pp. 248-251.

Bonin, B., Colin, M., Dutfoy, A., (2000). "Pressure building during the early stages of gas production in a radioactive waste repository". *Journal of Nuclear Materials* **281,** No. 1, pp. 1-14.

Bouazza, A., Vangpaisal, T., (2003). "An apparatus to measure gas permeability of geosynthetic clay liners". *Geotextiles and Geomembranes* **21**, pp. 85-101.

Bradbury, M., Baeyens, B., (2002). "Porewater chemistry in compacted re-saturated MX-80 bentonite: physicochemical characterisation and geochemical modelling". *Nagra technical Report NTB 01– 08*, Wettingen, Switzerland.

Brooks, R.H., Corey, A.T., (1964). "Hydraulic Properties of Porous Media". *Hydrology Paper*, No. 3, Fort Collins, Colorado State University, USA.

Brooks, R.H., Corey, A.T., (1966). "Properties of Porous Media Affecting Fluid Flow," *Journal of the Irrigation and Drainage Division, Proceedings of the American Society of Civil Engineers* **92**, No. IR2, pp. 61-88.

Brown, P.W., Masters, L.W., (1982). "Factors affecting the corrosion of metals in the atmosphere". Wiley, New York.

Burdine, N.T., (1953). "Relative Permeability Calculations From Pore Size Distribution Data". *Transactions of the American Institute of Mining and Metallurgical Engineers* **198**, pp. 71-78.

Cleall, P.J., (1998). "An investigation of the thermo/hydraulic/mechanical behaviour of unsaturated soils, including expansive clays". PhD Thesis. University of Wales, Cardiff.

Cleall P.J., Melhuish T.A., Thomas, H.R., (2006). "Modelling of the three-dimensional behaviour of a prototype nuclear waste repository". *Engineering Geology* **85**, pp. 212-220.

Cunningham, R.E., Williams, R.J.J., (1980). "Diffusion in Gases and Porous Media". Plenum Press, New York.

Cussler, E.L., (1984). "Diffusion: Mass Transfer in Fluid Systems". Cambridge University Press, Cambridge.

de Marsily, G., (1986). "Quantitative Hydrology". Academic Press, Inc.

Delahaye, C.H., Alonso, E.E., (2002). "Soil heterogeneity and preferential paths for gas migration". *Engineering Geology* **64, No.** 2-3, pp. 251-271.

Dullien, F.A.L., (1979). "Porous Media: Fluid Transport And Pore Structure". Academic Press, New York

Elrashidi, M.A., West, L.T., Seybold, C.A., Benham, E.C., Schoeneberger, P.J., Ferguson, R., (2010). "Effects of Gypsum Addition on Solubility of Nutrients in Soil Amended With Peat". UDSA/NRCS National Soil Survey Center, Lincoln, USA.

Environment Agency, (2008). "Gas generation and migration from a deep geological repository for radioactive waste, A review of Nirex/NDA's work". Environment Agency, Bristol, UK.

Evans, I.R.B., Watson, G.M., Mason, E.A., (1961). "Gas Diffusion in Porous Media at Uniform Pressure". Journal of Chemical Physics **35**, pp. 2076–2083.

Fernandez, A.M., Baeyens, B., Bradbury, M., Rivas, P., (2004). "Analysis of the pore water chemical composition of a Spanish compacted bentonite used in an engineered barrier". *Physics and Chemistry of the Earth* **29**, pp. 105-118.

Fredlund, D.G., Rahardjo, H., (1993). "Soil Mechanics for Unsaturated Soils", John Wiley & Sons, New York.

Galle, C., (2000). "Gas breakthrough pressure in compacted Fo-Ca clay and interfacial gas overpressure in waste disposal context". *Applied Clay Science* **17**, pp. 85-97.

Graham, J., Halayko, K. G., Hume, H., Kirkham, T., Gray, M., Oscarson, D., (2002). "A capillarity-advective model for gas break-through in clays". *Engineering Geology* **64**, No. 2-3, pp. 273-286.

Grim, R.E., (1953). "Clay Mineralogy". McGraw-Hill, New York.

Grauer, R., (1986). "Bentonite as a backfill material in the high-level waste repository: Chemical aspects". *Nagra Technical Report NTB 86-12E*,Wettingen, Switzerland.

Gray, M., Kirkham, T. J., Lin, A. W.L., Graham, J., (1996). **"**On the gas breakthrough resistance of engineered clay barrier materials proposed for use in nuclear fuel waste disposal". *In: Proeedings of the CNS International Conference on Deep Disposal of Radioactive Waste*, Canadian Nuclear Society, Winnipeg, Manitoba.

Grimsel Test Site., (2010). "Gas Migration in EBS and Geosphere (GMT) – Introduction". [WWW] URL:http://www.grimsel.com/gts-phase-v/gmt/gmt-introduction [Accessed March 2012]

Harrington, J.F., Horseman, S.T., (2003). "Gas migration in KBS-3 buffer bentonite". *SKB Technical Report TR-03-02*, Stockholm, Sweden.

Horseman, S. T., (1996). **"**Generation and migration of repository gases: Some key considerations in radioactive waste disposal". *In: Proc. Int. 2-Day Conference, London, 21–22 Nov. 1996, IBC Technical Services, Energy Division*, pp. 26.

Horseman, S. T., Harrington, J. F., (1997). **"**Study of gas migration in Mx80 buffer bentonite". British Geological Survey, *Technical Report* WE/97/7.

Horseman, S.T., Harrington, J.F., Sellin, P., (1999). "Gas migration in clay barriers". *Engineering Geology* **54**, No. 1-2, pp. 139-149.

Ho, C., Webb, S., (2006). "Gas Transport in Porous Media, Springer". AA Dordrecht, The Netherlands.

Huertas F., Fuentes-Cantillana J.L., Jullien F., Rivas P., Linares J., Farina P., Ghoreychi M., Jockwer N., Kickmaier W., Martines M.A., Samper J., Alonso E., Elorza F.J., (2000). "Full-scale engineered barriers for a deep geological repository for high-level radioactive waste in crystalline host rock (FEBEX project)". European Commission, Nuclear science and technology series, Report EUR 19147 EN.

Hume, H. B., (1999). "Gas breakthrough in compacted Avonlea bentonite". MSc thesis, Department of Soil Science, University of Manitoba, Winnipeg, Canada.

Hunter, F., Bate, F., Heath, T., Hoch, A., (2007). "Geochemical investigation of iron transport into bentonite as steel corrodes". *SKB Technical Report TR-07-09*, Stockholm, Sweden.

Izadi, M.T., Stephenson, R.W., (1992). "Measurement of gas permeability through clay soils". *Current Practices in Ground Water and Vadose Zone Investigations, ASTM STP* **1118**. ASTM, Philadelphia, pp. 3-20.

Jackson, R., (1977). "Transport in Porous Catalysts". *Chemical Engineering Monographs* **4**, Elsevier, Amsterdam.

Jacques, D., and Šimůnek, J., (2005). "User manual of the Multicomponent Variably-Saturated Flow and Transport Model HP1. Description, verification, and examples". *SCK-CEN Report BLG-998*, Belgium.

Jennings, A.A., Kirkner, D.J., Theis, T.L., (1982). "Multicomponent equilibrium chemistry In groundwater quality models". *Water Resources Research* **18**, No.4, pp. 1089-1096.

Karnland, O., Sanden, T., Johannesson, L.E., Eriksen, T.E., Jansson, M.,Wold, S., Pedersen, K., Motamedi, M., Rosborg, B., (2000). "Long term test of buffer material. Final report on the pilot parcels". *SKB Technical Report TR -00-22*, Stockholm, Sweden.

Kehew, A.E., (2001). "Applied Chemical Hydrogeology". Prentice-Hall, Inc.

Kerkhof, J.A.M.P., (1996). "A modified Maxwell-Stefan model for transport through inert membranes: the binary friction model". *The Chemical Engineering Journal* **64**, pp. 319-343.

King, F., (2008). "Corrosion of carbon steel under anaerobic conditions in a repository for SF and HLW in Opalinus clay". *Nagra Technical Report NTB 08-12*, Wettingen, Switzerland.

Kreis, P., Simpson, J.P., (1992). "Hydrogen gas generation from the corrosion of iron in cementitious environments". *In Corrosion Problems Related to Nuclear Waste Disposal, European Federation of Corrosion Publication Number 7 (Institute of Materials, London)*, pp. 57-72.

Kursten, B., Cornelis, B., Labat, S., Van Iseghem, P., (1996). "Geological disposal of conditioned high level and long lived radioactive waste. In situ corrosion experiments". *SCK-CEN Report R-3121*, Belgium.

Kursten, B., Smailos, E., Azkarate, I., Werme, L., Smart, N., Santarini G., (2004). "BECOMA: state of art document on the Corrosion BEhaviour of Container Materials". EC, Luxemburg.

Lewis, F.M., Voss, C.I., Rubin, J., (1987). "Solute transport with equilibrium aqueous complexation and either sorption or ion exchange: Simulation methodology and applications". *Journal of hydrology* **90**, pp. 81-115.

MacQuarrie, K.T.B., Mayer, K.U., (2005). "Reactive transport modeling in fractured rock: A state of the science review". *Earth-Science Reviews* **72**, pp. 189-227.

Mallants, D., Jacques, D., (2004). "Performance assessment for deep disposal of low and intermediate level short-lived radioactive waste in Boom Clay". *SCK-CEN Report R-3793*, Belgium.

Mallants, D., Jacques, D., Perko, J., (2007). "Modelling multi-phase flow phenomena in concrete barriers used for geological disposal of radioactive waste". *Proceedings of the 11th International Conference on Environmental Remediation and Radioactive Waste Management, ICEM07*, September 2-6, 2007, Bruges, Belgium

Marsh, G.P., Bland, I.W., Desport, J.A., Naish, C., Wescott, C., Taylor, K.J., (1983). "Corrosion assessment of metal overpacks for radioactive waste disposal". *European Applied Research Reports-Nuclear Science Technology* **5**, pp. 223-252.

Marsh, G.P., Taylor, K.J., (1988). "An assessment of carbon steel containers for radioactive waste disposal". *Corrosion Science* **28**, pp. 289-320.

Mason, E.A., Evans, I. R.B., Watson, G.M., (1963). "Gaseous diffusion in porous media. III. Thermal transpiration". *Journal of Chemical Physics* **38**, pp. 1808–1826.

Mason, E.A., Malinauskas, A.P., (1983). "Gas Transport in Porous Media: The Dusty-Gas Model". *Chemical Engineering Monograph* **17**, Elsevier, New York.

Matyas, E.L., Radhakrishna, H.S., (1968). "Volume change characteristics of partially saturated soils". *Geotechnique* **18**, No. 4, pp. 432-448.

McBean, E.A., Rovers, F.A., Farquhar, G.J., (1995). "Solid Waste Landfill Engineering And Design". Prentice-Hall PTR, Englewood Cliffs, New Jersey

Melhuish, T.A., (2004). "An investigation of the three-dimensional thermo/hydro/mechanical behaviour of large scale in-situ experiments". PhD Thesis, Cardiff University, UK.

Miller, W., Alexander, R., Chapman, N., McKinley, I., Smellie, J., (2000). "Geological disposal of radioactive wastes & natural analogues". *Waste Management Series* 2, Pergamon, Amsterdam.

Mitchell, H.P., (2002). "An investigation into the thermo/hydro/mechanical interactions involved in high level nuclear waste disposal". PhD Thesis, University of Wales, Cardiff.

Mitchell, J.K., Soga, K., (2005). "Fundamentals of soil behaviour". Third Edition. John Wiley & Sons, Inc., Hoboken, New Jersey.

Mualem, Y., (1976). "A New Model for Predicting the Hydraulic Conductivity of Unsaturated Porous Media". *Water Resources Research* **12**, No. 3, pp. 513–522.

Muller, W., Alkan, H., (2008). "Approaches for modelling gas flow in clay formations as repository systems". *Physics and chemistry of the earth* **33**, pp. 260-268.

Muurinen, A., Lehikoinen, J., (1999). "Porewater chemistry in compacted bentonite". *Engineering Geology* **54**, No. 1, pp. 207-214.

Muurinen, A., Carlsson, T., (2007). "Eh and pH in compacted MX-80 bentonite". NF-PRO EC Integrated Project.

Nagra, (2004). Effects of Post-disposal Gas Generation in a Repository for Spent Fuel, High-level Waste and Long-lived Intermediate Level Waste Sited in Opalinus Clay. *Nagra Technical Report NTB 04-06*, Wettingen, Switzerland.

Nagra (2008). "Corrosion of carbon steel under anaerobic conditions in a repository for SF and HLW in Opalinus Clay". *Nagra Technical Report NTB* 08-12, Wettingen, Switzerland.

Neretnieks, I., (1985). "Some Aspects of the Use of Iron Canisters in Deep Lying Repositories for Nuclear Waste". *Nagra Technical Report NTB 85-35*, Switzerland.

Norris, S., (2009). "Summary of gas generation and migration current state-of-the art". *FORGE Report D1.2-R-Draft.*

Olivella, S., Alonso, E. E., (2008). "Gas flow through clay barriers". *Geotechnique* **58**, No.3, pp. 157-176.

Ortiz, L., Volckaert, G., Mallants, D., (2002). "Gas generation and migration in Boom Clay, a potential host rock formation for nuclear waste storage". *Engineering Geology* **64**, No. 2-3, pp. 287-296.

Papillon, F., Jullien, M., Bataillon, C., (2003). Carbon steel behaviour in compacted clay: two long term tests for corrosion prediction. In Prediction of Long Term Corrosion Behaviour in Nuclear Waste Systems. *European Federation of Corrosion Publication No. 36 (Institute of Materials, Minerals and Mining, London)*, pp. 439–454.

Parker, J.C., Lenhard, R.J., Kuppusamy, T., (1987). "A Parametric Model for Constitutive Properties Governing Multiphase Flow in Porous Media". Water Resources Research, **23**, No. 4, pp 618–624.

Prommer, H., Barry, D.A., and Davis, G.B., (2002). "Modelling of physical and reactive processes during biodegradation of a hydrocarbon plume under transient groundwater flow conditions". *Journal of Contaminant Hydrology* **59**, pp. 113–131.

Pusch, R., Forsberg, T., (1983). "Gas migration through bentonite clay". *SKB Technical Report TR-83-71*, Stockholm, Sweden.

Pusch, R., Hokmark, H., (1990). "Basic Model of Water- and Gas-Flow Through Smectite Clay Buffers". *Engineering Geology* **28**, pp. 379-389.

Pusch, R..,Karnland, O., Hokmark, H., (1990). " GMM - A general microstructural model for qualitative and quantitative studies of smectite clays". *SKB Technical Report TR- 90-43*, Stockholm, Sweden.

Pusch R, Ranhagen L, Nilsson K., (1985)**.** "Gas migration through Mx-80 bentonite"**.** *Nagra Technical Report NTB 85-36*, Wettingen, Switzerland.

Pusch, R., Yong, R.N., (2006). "Microstructure of Smectite Clays and Engineering Performance". Taylor and Francis, New York.

Rankama, K., Sahama, TH.G., (1950). "Geochemistry". The University of Chicago Press, Ltd., London, UK.

Rautioaho, E., Korkiala-Tanttu,L., (2009). "Bentomap: Survey of bentonite andtunnel backfill knowledge: State-of-the-art". VTT Technical Research Centre of Finland, Finland.

Rodwell, W.R., Harris, A.W., Horseman, S.T., Lalieux, P., Muller, W., Ortiz Amaya, L., Pruess, K., (1999). "Gas migration and two-phase flow through engineered and geological barriers for a deep repository for radioactive waste". A Joint ECrNEA Status Report, EUR 19122 EN, European Commission, Nuclear Energy Agency, Brussels, Luxembourg, pp. 429.

Rodwell, R. W., Hoch, A. R., Swift, B. T., (2004). "The modelling of gas migration through compacted bentonite buffers in radioactive waste repositories: the work of the GAMBIT club". *MRS Symposium Proceeding* **807**, Materials Research Society, Warrendale, Pennsylvania.

Rothwell, L.B., (1963). "Gaseous counterdiffusion in catalyst pellets". *American Institute of Chemical Engineering Journal* **9**, pp. 19-24.

Saaltink, M.W., Carrera, J., Ayora, C., (2001). "On the behavior of approaches to simulate reactive transport". *Journal of Contaminant Hydrology* **48**, pp. 213-235.

Samper, J., Xu, T., Yang, C., (2009). "A sequential partly iterative approach for multicomponent reactive transport with CORE2D". *Computers and Geosciences* **13**, pp. 301-316.

Scanlon, B. R., Nicot, J. P., Massmann, J.W., (2002). "Soil Gas Movement in Unsaturated Systems". CRC Press LLC.

Schenk, R., (1988). "Untersuchungen über die Wasserstoffbildung durch Eisenkorrosion unter Endlagerbedingungen". National Cooperative for the Storage of Radioactive Waste Technical Report, *Nagra Technical Report NTB 86-24*, Wettingen, Switzerland.

Schneider, P., (1978). "Multicomponent isothermal diffusion and forced flow of gases in capillaries". *Chemical Engineering Science* **33**, pp. 1311-1319.

Sedighi, M., (2011). "An investigation of Hydro-geochemical processes in coupled thermal, hydraulic, chemical and mechanical behaviour of unsaturated soils". PhD thesis, Cardiff University, UK.

Seetharam, S.C., (2003). "An investigation of the thermo/hydro/chemical/mechanical behaviour of unsaturated soils". PhD Thesis, Cardiff University, UK.

Senger, R., Marschall, P., Finsterle, S., (2008). "Investigation of two phase flow phenomena associated with corrosion in an SF/HLW repository in Opalinus Clay, Switzerland". *Physics and Chemistry of the Earth* **33**, pp. 317-326.

Simpson, J.P., (1984). "Experiments on container materials for Swiss high-level waste disposal projects, Part II. National Cooperative for the Storage of Radioactive Waste". *Nagra Technical Report NTB 84-01*, Wettingen, Switzerland.

Simpson, J.P., Schenk, R., Knecht, B., (1985). "Corrosion rate of unalloyed steels and cast irons in reducing granitic groundwaters and chloride solutions". *Materials Research Society Symposium Proceedings* **50**, pp. 429-436.

Simpson, J.P., Valloton, P.H., (1986). "Experiments on container materials for Swiss high-level waste disposal projects, Part III". *Nagra Technical Report NTB 86-25*, Wettingen, Switzerland.

Simpson, J.P., (1989). "Experiments on container materials for Swiss high-level waste disposal projects, Part IV. National Cooperative for the Storage of Radioactive Waste", *Nagra Technical Report NTB 89-19*, Wettingen, Switzerland.

Simpson, J., Weber, J., (1992). "Steel as a container material for nuclear waste disposal. In Corrosion Problems Related to Nuclear Waste Disposal".*European Federation of Corrosion Publication, Number 7 (Institute of Materials, London)*, pp. 43-56.

Sisler, H.H., Vanderwerf, C.A., Davidson, A.W., (1953). "General Chemistry-A Systematic Approach". Macmillan, New York.

SKB, (1993). "A preliminary assessment of gas migration from the Copper/Steel Canister". *SKB Technical Report TR- 93-31*, Stockholm, Sweden.

SKB, (2007). "RD&D Programme 2007, Programme for research, development and demonstration of methods for the management and disposal of nuclear waste". *SKB Technical Report TR-07-12*, Stockholm, Sweden.

Smart, N.R., Blackwood, D.J., Werme, L.O., (2001). "The anaerobic corrosion of carbon steel and cast iron in artificial groundwaters". *SKB Technical Report TR-01-22*, Stockholm, Sweden.

Smart, N.R., Blackwood, D.J., Werme, L.O., (2002a). "Anaerobic corrosion of carbon steel and cast iron in artificial groundwaters: Part 1 – electrochemical aspects". *Corrosion* **58**, pp. 547-559.

Smart, N.R., Blackwood, D.J., Werme, L.O., (2002b). "Anaerobic corrosion of carbon steel and cast iron in artificial groundwaters: Part 2 – gas generation". *Corrosion* **58**, pp. 627-637.

Smart, N.R., Rance, A.P., Werme, L. O., (2004). "Anaerobic corrosion of steel in bentonite". *Materials Research Society Symposium Proceedings* **87**, pp. 441-446.

Smart, N.R., Rance, A.P., Fennell, A.H., (2006). "Expansion due to the anaerobic corrosion of iron". *SKB Technical Report TR-06-41*, Stockholm, Sweden.

Steefel, C.I., MacQuarrie, K.T.B., (1996). "Approaches to modeling reactive transport in porous media". *Reviews in Mineralogy* **34**, pp. 83-125.

Taylor, R., Krishna, R., (1993). "Multicomponent Mass Transfer". Wiley, New York.

Tanai, K., Kanno, T., Galle C., (1997)**.** "Experimental study of gas permeabilities and breakthrough pressures in clays. Scientific Basis For Nuclear Waste Management XX". *Materials Research Society Symposium Proceedings* 465, Warrendale, Pennsylvania, pp.1003-1010.

Taniguchi, N., Kawasaki, M., Kawakami, S., Kubota, M., (2004). "Corrosion behaviour of carbon steel in contact with bentonite under anaerobic condition". *In Prediction of Long Term Corrosion in Nuclear Waste Systems. Proc. 2nd Int. Workshop, Nice, September 2004 (European Federation of Corrosion and Andra)*, pp. 24-34.

Thomas, H.R., He, Y., (1995). "Analysis of coupled heat, moisture and air transfer in a deformable unsaturated soil". *Geotechnique* **45**, No. 4, pp. 677-689.

van Genuchten, M.Th., (1978). "Calculating The Unsaturated Hydraulic Conductivity With a New Closed-Form Analytical Model". *Water Resources Bulletin 78-WR-08*, Department of Civil Engineering, Princeton University, USA.

van Genuchten, M.Th., (1980). "A Closed-Form Equation for Predicting the Hydraulic Conductivity of Unsaturated Soils". *Soil Science Society of America Journal* **44**, No. 5, pp. 892-898.

van Genuchten, M.Th., Nielsen, D.R., (1985). "On Describing and Predicting the Hydraulic Properties of Unsaturated Soils". *Annales Geophysicae* **3**, No. 5, pp. 615-628.

van Olphen, H., (1963). "An introduction to clay colloid chemistry". Interscience Publishers, J. Wiley and Sons.

Vardon, P.J., (2009). "A three-dimensional numerical investigation of the thermo-hydro-mechanical behaviour of a large-scale prototype repository". PhD Thesis, Cardiff University, UK.

Villar, M.V., Fernandez, A.M., Gomez-Espina, R., (2007). "Effect of heating/ hydration on bentonite: test in a 60-cm long cell". NF-PRO EC Integrated Project.

Volckaert, G., Mallants, D., (1999). "De gasproblematiek bij het bergen van radioactief afval in een diepe geologische berging in de klei van Boom", *SCK-CEN Report R-3287*.

Wersin, P., (2003). "Geochemical modelling of bentonite porewater in high-level waste repositories". *Journal of Contaminant Hydrology* **61**, pp. 405– 422.

Wersin, P., Curti, E., Appelo, C.A.J., (2004). "Modelling bentonite-water interaction at high solid/liquid ratios: swelling and diffuse double layer effects". *Applied Clay Science* **26**, pp. 249-257.

Weetjens, E., Perko J., (2008). "Report on first results of calculations on gas production and transport (PAMINA)". *Contract No FP6-036404*.

Wikramaratna, R.S., Goodfield, M., Rodwell. W.R., Nash, P.J., Agg, P.J., (1993). "A preliminary assessment of gas migration from the copper/steel canister". *SKB Technical Report TR-93-31*, Stockholm, Sweden.

Wilson, J., Savage, D., Bond, A., Watson, S., Pusch, R. Bennett, D., (2011). "Bentonite: A Review of key properties, processes and issues for consideration in the UK context". *Quintessa Report QRS-1378ZG v1.1* for NDA RWMD.

Xu, T., Samper, J., Ayora, C., Manzano, M., and Emilio, C., (1999). "Modeling of non-isothermal multi-component reactive transport in field scale porous media flow systems". *Journal of Hydrology* **214**, pp. 144-164.

Xu, T., Senger, R., Finsterle, S., (2008). "Corrosion-induced gas generation in a nuclear waste repository: Reactive geochemistry and multiphase flow effects". *Applied Geochemistry* **23**, No. 12, pp. 3423-3433.

Yeh, G.T., Tripathi, V.S., (1989). "A critical evaluation of recent developments in hydrogeochemical transport models of reactive multichemical components". *Water Resources Research* **25**, No. 1, pp. 93-108.

Young, J.B., Todd, B., (2005). "Modelling of multi-component gas flows in capillaries and porous solids". *International Journal of Heat and Mass Transfer* **48**, pp. 5338-5353.

Yu, L.L., (1985). "Study of air flow through porous media". MS Thesis, Department of Civil Engineering, University of Connecticut, Storrs, USA.

3

Theoretical Formulation

3.1 Introductions

In this chapter the development of theoretical formulations for thermal/ hydraulic/ mechanical and chemical behavior of a porous media, such as unsaturated soil have been presented. The governing equations have been expressed in terms of primary variables: pore water pressure (u_l), pore gas concentration ($\mathbf{c_g}$), dissolved chemical concentration ($\mathbf{c_d}$), temperature (T), and displacement ($\mathbf{u}$). The pore gas concentration and dissolved chemical concentration have been expressed as vectors to represent any number of chemical species. In the formulation provided, each species has been treated as a primary variable in the model.

The governing equations for coupled liquid, air, temperature and deformation behavior have been developed previously which has been presented in great detail in the work of Thomas and He (1998), Cleall (1998), Mitchell (2002), Melhuish (2004), Vardon (2009). Cleall (1998) has presented the formulation for a single component chemical transport equation. A coupled moisture and reactive chemical transport formulation has been developed by Hashm (1999) but based on a limited number of chemical species, ignoring the coupling with temperature or deformation. Seetharam (2003) developed the formulation of multicomponent dissolved chemical transport. Siddiqua (2008)

developed the pore gas transfer equation in elevated temperature where dry air and water vapor have been considered as pore gas in a non-reactive environment. In these entire previous attempts pore air has been considered as a single component instead of a mixture of multiple gases. Sedighi (2011) developed the multicomponent reactive chemical transport in liquid phase by linking transport process with an advanced geochemical model. The principle of overall charge conservation, such as, electron-neutrality condition, homogeneous and heterogeneous geochemical reactions have been considered in the developed model.

The main objective of this chapter is to present the developed multicomponent reactive pore gas transfer equation (section 3.3) and the geochemical sink/source terms (section 3.5). As the variation of chemicals in the system is coupled with moisture, temperature and deformation, the theoretical formulations of moisture transfer (section 3.2), dissolved chemical transport (section 3.4), heat transfer (section 3.6) and deformation (section 3.7) have also been presented for the sake of completeness.

The governing equations for the transport of dissolved chemicals and pore gas species have been developed considering the mass conservation using the molar balance approach, heat flow equation has been considered by the conservation of energy approach and the mechanical deformation has been developed considering the stress equilibrium approach.

Section 3.2 deals with the theoretical development of moisture transport equation based on the law of conservation of mass. The liquid water flow and water vapour flow in the have been considered simultaneously in the moisture flow equation. Darcy's Law has been used to represent the liquid water flow. The Philip and de Vries (1957) approach has been used to present the diffusive flow of vapour phase.

Section 3.3 deals with the theoretical development of multicomponent reactive gas transport through porous media. The previously developed dry air transfer equation has been replaced with this new development. The formulation has been developed for both isothermal and non-isothermal conditions although this study is focused on multicomponent gas and dissolved chemical transport in isothermal conditions. It has been assumed that in an isothermal condition the pore gas comprises of dry gases that

excludes water vapour which has been considered with the liquid phase. The multi-phase chemical components have been characterized as gas components in gas phase and dissolved chemical components in the liquid phase. Darcy's law has been used to symbolize advective flows in gas and liquid phase. To address the multicomponent diffusion, extended multicomponent Fick's law of diffusion has been used. Section 3.4 represents the development of multicomponent dissolved chemical transport equation. Since, the dissolved chemicals flow with and through the liquid water, Darcy's law and Fick's law of binary diffusion have been considered for advective and diffusive flow respectively. The system has been considered to behave as an isothermal condition; chemicals flow due to temperature gradient has been ignored in this study.

Section 3.5 represents the development of sink/source terms. To account for geochemical reactions, sink/source term has been introduced in both multicomponent pore gas flow equation and dissolved chemical flow equation. This is defined by linking transport model to an advanced geochemical model where possible geochemical reactions have been modelled based on equilibrium chemistry.

Section 3.6 deals with the development of heat transfer equation. The governing equation of heat transfer has been developed based upon the conservation of energy and while developing the theoretical formulation conduction and latent heat of vaporization have been considered as the main modes of transfer. Mechanical formulations have been presented in section 3.7 to represent the elasto-plastic stress-strain behavior of unsaturated soil. The behavior of the soil has been modeled by an elasto-plastic work hardening constitutive model which considers two yield surfaces and suction as a stress variable. A summary of the governing equations has been presented in section 3.8 of this chapter.

3.2 Moisture transfer

In an unsaturated soil, the moisture flow can be considered as a two-phase flow, including the flow of liquid water and water vapour. The volumetric water content, θ, can be expressed as a combination of these two phases, given by:

$$\theta = \theta_l + \theta_v \tag{3.1}$$

where, θ_l and θ_v are volumetric liquid content and volumetric vapour content respectively.

The principle of local thermodynamic equilibrium dictates that at any point, the volumetric liquid water and water vapour are in equilibrium (de Vries, 1958). Accordingly the following relationship can be defined as:

$$\theta_v = \frac{(n - \theta_l)\rho_v}{\rho_l} \tag{3.2}$$

where, n is the porosity, ρ_v is the density of water vapour and ρ_l is the density of liquid water.

The principle of conservation of mass states that, for liquid water phase, the time derivative of the liquid content is equal to the spatial gradient of the liquid flux. Mathematically, this can be expressed as:

$$\rho_l \frac{\partial \theta_l \partial V}{\partial t} = -\rho_l \partial V \nabla \mathbf{v_l} - \rho_l \partial V E_{ss} \tag{3.3}$$

where, ∂V is the incremental volume, t is time, ∇ is the gradient operator, $\mathbf{v_l}$ is the liquid velocity and E_{ss} represents the sink/source term due to the process of vaporisation or condensation.

For the vapour phase, similarly, the conservation of mass dictates that the time derivative of the vapour content is equal to the gradient of the vapour flux and mathematically it can be represented as:

$$\rho_l \frac{\partial \theta_v \partial V}{\partial t} = -\rho_l \partial V \nabla \mathbf{v_v} - \partial V \nabla \left(\rho_v \mathbf{v_g} \right) + \rho_l \partial V E_{ss} \tag{3.4}$$

where, $\mathbf{v_v}$ is the velocity of vapour, ρ_v is the density of vapour and $\mathbf{v_g}$ is the velocity of pore gas. The volumetric gas content, θ_g, can be expressed as:

$$\theta_g = n - \theta_l \tag{3.5}$$

Substituting equations (3.2) and (3.5) into equation (3.4), the law of conservation of mass for water vapour can be written as:

$$\frac{\partial \rho_v \theta_g \partial V}{\partial t} = -\rho_l \partial V \nabla \left(\mathbf{v_v} \right) - \partial V \nabla \left(\rho_v \mathbf{v_g} \right) + \rho_l \partial V E_{ss} \tag{3.6}$$

Combining the equations of conservation of mass for liquid water (3.3) and water vapour (3.6) flow, the equation of mass conservation for moisture transfer can be expressed as:

$$\rho_l \frac{\partial \theta_l \partial V}{\partial t} + \frac{\partial \rho_v \theta_g \partial V}{\partial t} = -\rho_l \partial V \nabla \mathbf{v_l} - \partial V \nabla \left(\rho_l \mathbf{v_v} \right) - \partial V \nabla \left(\rho_v \mathbf{v_g} \right) \tag{3.7}$$

The volumetric liquid content, θ_l, and gas content, θ_g, can be expressed in terms of porosity, *n* and degree of liquid saturation, S_l, and gas saturation, S_g, respectively as:

$$\theta_l = n S_l \tag{3.8}$$

$$\theta_g = n S_g \tag{3.9}$$

The relationship between liquid saturation and gas saturation can be expressed as:

$$S_g = 1 - S_l \tag{3.10}$$

The incremental volume, ∂V , is a summation of the void volume and solid volume, V_s and can be represented as:

$$\partial V = (1+e)\partial V_s \tag{3.11}$$

Substituting equation (3.8), (3.9) and (3.11) into equation (3.7) yields:

$$\begin{aligned} &\frac{\partial\left(\rho_l n S_l (1+e)\partial V_s\right)}{\partial t} + \frac{\partial\left(\rho_v n S_g (1+e)\partial V_s\right)}{\partial t} + \rho_l (1+e)\partial V_s \nabla \mathbf{v_l} \\ &+ \rho_l (1+e)\partial V_s \nabla \mathbf{v_v} + (1+e)\partial V_s \nabla\left(\rho_v \mathbf{v_g}\right) = 0 \end{aligned} \tag{3.12}$$

Since the volume of the solid has been considered to remain constant ∂V_s can be eliminated from the equation (3.12). Also porosity, *n*, can be expressed in terms of void ratio, *e*, as follows:

$$n = e/(1+e) \tag{3.13}$$

Substituting equation (3.13) into equation (3.12) takes the form of:

$$\rho_l \frac{\partial(eS_l)}{\partial t} + \frac{\partial\left(\rho_v S_g e\right)}{\partial t} + \rho_l (1+e)\nabla \mathbf{v_l} + \rho_l (1+e)\nabla \mathbf{v_v} + (1+e)\nabla\left(\rho_v \mathbf{v_g}\right) = 0 \tag{3.14}$$

The spatial derivative terms of equation (3.14) suggests that the moisture flux includes a) liquid flux, b) component of vapour flux due to vapour pressure gradients and c) component of vapour flux arising from the bulk flow of pore gas. It is obvious from equation (3.14) that the movement of moisture is governed by the velocities of the liquid, vapour and gas phases. An explanation of these flow rates and the flow laws that govern them has been presented below.

3.2.1 Mechanisms of liquid water flow

To understand the flow mechanisms of liquid water, it is important to identify the appropriate driving potentials. A detailed discussion about some of the possible driving potentials for water flow through an unsaturated soil has been presented by Fredlund and Rahardjo (1993) and Mitchell (1993).

The plausible mechanisms for water flow have been listed by Mitchell (1993) as follows:

a. Pressure head
b. Elevation head
c. Thermal gradient
d. Chemical gradient or chemo-osmosis
e. Electrical gradient or electro-osmosis

The flow of liquid water due to thermal, chemical and electrical gradients have been neglected in this work.

The combination of pressure head and elevation head termed the hydraulic head has been considered as the driving potential for water flow through unsaturated soils (Fredlund and Rahardjo, 1993). Flow of water due to gradient of hydraulic head can be described by Darcy's Law (1856) and the approach has been used for unsaturated soil by Childs (1969), Neilson et al. (1986) and Fredlund and Rahardjo (1993).

The water flow through unsaturated soil can be expressed by Darcy's law as:

$$\mathbf{v_l} = -\frac{K_l}{\mu_l}\left[\nabla\left(\frac{u_l}{\gamma_l}\right)+\nabla z\right] = -k_l\left[\nabla\left(\frac{u_l}{\gamma_l}\right)+\nabla z\right] \tag{3.15}$$

where, $\mathbf{v_l}$ is the liquid velocity, u_l is the porewater pressure, K_l represents the effective permeability, μ_l stands for the absolute viscosity of pore liquid, k_l is the unsaturated hydraulic conductivity, γ_l is the unit weight of liquid and z represents the elevation.

The absolute viscosity of liquid is temperature dependent and such a relationship has been presented by Kaye and Laby (1973):

$$\mu_l(T)=661.2(T-229)^{-1.562}\times 10^{-3}\pm 0.5\% \qquad (\mathrm{Ns/m^2}) \qquad (3.16)$$

where, T is the temperature, expressed in Kelvin.

Mitchell (1993) suggested that the unsaturated hydraulic conductivity of soil is influenced by a number of factors, such as, the fabric and pore fluid characteristics, particle size and particle distribution, void ratio and mineralogical composition. Hydraulic conductivity is also influenced by degree of saturation and turbulence of flow. The impact of turbulence can be neglected, if the state of flow is slow. Therefore, it can be assumed that the hydraulic conductivity is dependent on two of three possible mass volume properties, such as, void ratio, e, degree of liquid saturation, S_l or volumetric water content, θ_l (Lloret and Alonso, 1980; Fredlund, 1991). Since, the volumetric water content can be expressed in terms of porosity and degree of saturation, the effects of void ratio and degree of liquid saturation have been considered in this formulation, as:

$$k_l=k_l(e,S_l) \qquad (3.17)$$

Matyas and Radhakrishna (1968) proposed that the degree of liquid saturation is a function of the initial void ratio, the initial liquid saturation and the stress parameters mainly, net stress, deviatoric stress and suction. It has been found that the influence of stress on the degree of saturation is relatively insignificant (Alonso et al., 1988). However, if the initial void ratio of a soil sample is controlled and the sample is confined the degree of saturation can be expressed in terms of the suction, s:

$$S_l=S_l(s) \qquad (3.18)$$

Edelfsen and Anderson (1943) have expressed the suction as the free energy state of soil water. The surface energy, ξ, has been expressed as a function of temperature:

$$\xi = 0.1171 - 0.0001516T \qquad \left(\mathrm{J/m^2}\right) \tag{3.19}$$

where, T is in Kelvin.

Therefore, the suction in unsaturated soil has been expressed in terms of surface energy which depends on absolute temperature. If a relationship between suction and degree of saturation at a reference temperature, T_r is known, the suction at any temperature and degree of saturation can be presented as:

$$s = \frac{\xi}{\xi_r} s_r \tag{3.20}$$

where, s_r and ξ_r are the suction and the surface energy at the reference temperature, T_r and s and ξ the suction and surface energy at the temperature T.

Considering the effect of temperature on soil suction, the degree of saturation in equation (3.14) can be expressed in partial derivative form with respect to time as:

$$\frac{\partial S_l}{\partial t} = \frac{\partial S_l}{\partial s}\frac{\partial s}{\partial t} + \frac{\partial S_l}{\partial T}\frac{\partial T}{\partial t} \tag{3.21}$$

The matric suction which is the difference between total pore gas pressure and pore liquid pressure (Fredlund and Rahardjo, 1993), mathematically, can be expressed as:

$$s = u_g - u_l \tag{3.22}$$

where, u_g and u_l are pore gas pressure and pore liquid pressure respectively. Pore gas pressure is the sum of partial pressures of individual gas components and is considered to behave as an ideal gas. According to ideal gas law, the pore gas pressure, u_g, can be written as:

$$u_g = \sum_{i=1}^{N} c_g^i RT \tag{3.23}$$

where, c_g^i is the molar concentration of gas component *i*, *R* is the universal gas constant and T is the temperature in Kelvin, *N* is the total number of gas components, excluding the vapour. Substituting equation (3.23) into equation (3.22) yields:

$$s=\sum_{i=1}^{N} c_g^i RT\text{-}u_l \tag{3.24}$$

Substituting equation (3.24) into equation (3.21), the degree of saturation can be expressed in terms of primary variables as:

$$\frac{\partial S_l}{\partial t}=RT\frac{\partial S_l}{\partial s}\sum_{i=1}^{N}\frac{\partial c_g^i}{\partial t}+\left(R\sum_{i=1}^{N}c_g^i\frac{\partial S_l}{\partial s}+\frac{\partial S_l}{\partial T}\right)\frac{\partial T}{\partial t}-\frac{\partial S_l}{\partial s}\frac{\partial u_l}{\partial t} \tag{3.25}$$

3.2.2 Mechanisms of water vapour flow

It has been considered that vapour transfer in an unsaturated soil takes place due to two main mechanisms which has been termed as diffusive flow and pressure flow or advective flow. The generalised Darcy's law has been used to obtain the bulk flow (Carman, 1956; Alonso et al, 1988). The mechanism of diffusive flow through unsaturated soil has been explained by the theory proposed by Philip and de Vries (1957).

Fredlund and Rahardjo (1993) stated that considering only the bulk gas phase, the main driving potential is the pore gas pressure or the gas concentration where elevation gradient had a negligible effect on gas transfer. Therefore, a generalised Darcy's law for multiphase flow in unsaturated soil has been adopted as:

$$\mathbf{v_g}=-k_g\nabla u_g \tag{3.26}$$

where $\mathbf{v_g}$ is the velocity of pore gas, k_g is the unsaturated pore gas conductivity and u_g is the pore gas pressure.

Substituting equation (3.23) into equation (3.26) yields:

$$\mathbf{v_g} = -k_g \nabla \left(\sum_{i=1}^{N} c_g^i RT \right) \tag{3.27}$$

To define the unsaturated gas conductivity of soils, relationship between the fluid and soil volume/mass properties needs to be established. As the fluid properties generally assumed to be constant during the flow process, it has been considered that the volume/mass properties control the gas conductivity (Olson, 1963). In this study the volume/mass properties chosen are void ratio and degree of pore gas saturation and mathematically can be expressed as:

$$k_g = k_g \left(e, S_g \right) \tag{3.28}$$

Vapour transport due to diffusion can be dealt with by a flow law proposed by Philip and de Vries (1957) and extended by Ewen and Thomas (1989).

Philip and de Vries (1957) proposed that the velocity of vapour $\mathbf{v_v}$ through an unsaturated soil can be defined as:

$$\mathbf{v_v} = -\frac{D_{atms} v_v \tau_v \theta_g}{\rho_l} \nabla \rho_v \tag{3.29}$$

where, D_{atms} is the molecular diffusivity of vapour through air, v_v is a mass flow factor, τ_v is the tortuosity factor and $\nabla \rho_v$ is the vapour density gradient.

Krischer and Rohnalter (1940) proposed an expression for molecular diffusivity due to temperature gradient, in the range of 293-343K. The expression was adopted by Philip and de Vries (1957) as follows:

$$D_{atms} = 5.893 \times 10^{-6} \frac{T^{2.3}}{u_g} \quad (\text{m}^2/\text{s}) \tag{3.30}$$

Philip and de Vries (1957) suggested an expression, for the mass flow factor, which was proposed by Partington and de Vries (1957), who showed that for steady state diffusion in a closed system between an evaporating source and a condensing sink, the factor can be expressed as:

$$v_v = \frac{u_g}{u_g - u_v} \tag{3.31}$$

where u_v is the partial vapour pressure and can be calculated using thermodynamic relationship as:

$$u_v = \rho_v R_v T \qquad \text{(Pa)} \tag{3.32}$$

where R_v is the specific gas constant (Kaye and Laby, 1973) and for water vapour it possesses a value of 461.5 J/KgK.

Philip and de Vries (1957) found that the predicted value of the mass flow factor, v_v in equation (3.31) may not be valid for non-stationary conditions; it would predict the correct order of magnitude and which is close to 1 under normal soil temperatures.

With the aid of psychometric law, Edlefsen and Anderson (1943) proposed the following relationship to obtain the density of water vapour as:

$$\rho_v = \rho_0 h = \rho_0 \exp\left(\frac{\psi g}{R_v T}\right) \qquad \text{(Kg/m}^3\text{)} \tag{3.33}$$

where, ρ_0 represents the density of saturated water vapour, h is relative humidity, g is the gravitational constant and ψ is the capillary potential and can be defined as:

$$\psi = \frac{u_l - u_g}{\gamma_l} \qquad \text{(m)} \tag{3.34}$$

For the density of saturated water vapour, Ewen and Thomas (1989) presented a relationship fitted to standard data (Mayhew and Rogers, 1976), as:

$$\rho_0 = 1/\left\{194.4\exp\left(-0.06374(T-273)+0.1634\times10^{-3}(T-273)^2\right)\right\} \quad (\text{Kg/m}^3) \tag{3.35}$$

Equation (3.33) states that the density of water vapour depends on the saturated soil water vapour density and the relative humidity. From equation (3.35), it is obvious that the saturated water vapour density is dependent on the absolute temperature, *T* and the relative humidity is dependent on both suction and temperature. Therefore, the gradient of vapour density can be expressed as:

$$\nabla\rho_v = h\nabla\rho_0 + \rho_0\nabla h \tag{3.36}$$

According to the aforementioned discussion, equation (3.36) can be expressed as:

$$\nabla\rho_v = \left(h\frac{\partial\rho_0}{\partial T}\right)\nabla T + \rho_0\left(\frac{\partial h}{\partial s}\nabla s + \frac{\partial h}{\partial T}\nabla T\right) \tag{3.37}$$

Substituting equation (3.24) for suction and rearranging the similar terms yields:

$$\nabla\rho_v = \left(h\frac{\partial\rho_0}{\partial T} + \rho_0\frac{\partial h}{\partial T} + \rho_0 R\sum_{i=1}^{N}c_g^i\frac{\partial h}{\partial s}\right)\nabla T + \left(\rho_0 RT\frac{\partial h}{\partial s}\right)\nabla\sum_{i=1}^{N}c_g^i - \left(\rho_0\frac{\partial h}{\partial s}\right)\nabla u_l \tag{3.38}$$

The time derivative of the vapour density can be expressed as:

$$\frac{\partial\rho_v}{\partial t} = \left(h\frac{\partial\rho_0}{\partial T} + \rho_0\frac{\partial h}{\partial T} + \rho_0 R\sum_{i=1}^{N}c_g^i\frac{\partial h}{\partial s}\right)\frac{\partial T}{\partial t} + \left(\rho_0 RT\frac{\partial h}{\partial s}\right)\sum_{i=1}^{N}\frac{\partial c_g^i}{\partial t} - \left(\rho_0\frac{\partial h}{\partial s}\right)\frac{\partial u_l}{\partial t} \tag{3.39}$$

Substituting equation (3.38) into equation (3.29) yields:

$$\mathbf{v_v} = \frac{D_{atms} v_v \tau_v \theta_g}{\rho_l}\left(\rho_0 \frac{\partial h}{\partial s}\right)\nabla u_l - \frac{D_{atms} v_v \tau_v \theta_g}{\rho_l}\left(h\frac{\partial \rho_0}{\partial T} + \rho_0 \frac{\partial h}{\partial T} + \rho_0 R \sum_{i=1}^{N} c_g^i \frac{\partial h}{\partial s}\right)\nabla T \qquad (3.40)$$
$$- \frac{D_{atms} v_v \tau_v \theta_g}{\rho_l}\left(\rho_0 RT \frac{\partial h}{\partial s}\right)\nabla \sum_{i=1}^{N} c_g^i$$

From experimental evidence Philip and de Vries (1957) found that the theory proposed in equation (3.40) was not ideal at increased temperature gradients. Therefore, two refinements to the thermal gradient term have been proposed. A flow area factor, *f* was introduced to obtain a reduction of the vapour flow as the available flow area decreased at higher moisture contents. Also, a microscopic pore temperature gradient factor, $(\nabla T)_a / \nabla T$, was introduced, which represents the ratio of the average temperature gradient in the air filled pores to the overall temperature gradient. This factor considers the microscopic temperature gradients in the fluid filled pores, which might be much higher than the macroscopic temperature gradients across the whole sample. Introducing these two factors in equation (3.40) yields:

$$\mathbf{v_v} = \frac{D_{atms} v_v \tau_v \theta_g}{\rho_l}\left(\rho_0 \frac{\partial h}{\partial s}\right)\nabla u_l - \frac{D_{atms} v_v \tau_v \theta_g}{\rho_l}\left(\rho_0 RT \frac{\partial h}{\partial s}\right)\nabla \sum_{i=1}^{N} c_g^i$$
$$- \frac{D_{atms} v_v \tau_v \theta_g}{\rho_l} f \frac{(\nabla T)_a}{\nabla T}\left(h\frac{\partial \rho_0}{\partial T} + \rho_0 \frac{\partial h}{\partial T} + \rho_0 R \sum_{i=1}^{N} c_g^i \frac{\partial h}{\partial s}\right)\nabla T \qquad (3.41)$$

The microscopic pore temperature gradient factor, $(\nabla T)_a / \nabla T$, has been derived from the work of Preece (1975) which was based on Washington Sand (de Vries, 1966). The aforementioned experimental work was carried out on dense cohesion-less sand. Further research and development is essential to validate the results to analyse the movement of vapour in a highly compacted cohesive soil, such as a bentonite buffer material. Vardon (2009) reported that the form of the vapour flow factor might need to be re-evaluated as a consequence of such work, such as, when considering a case of highly swelling, densely compacted clay. It has been suggested that the application of the original Philip and de Vries (1957) approach, given the mechanistic (constitutive) formulation, might require close re-examination in case of compacted clay materials.

Singh (2007) carried out an initial investigation of experimental and numerical study to obtain vapour flow in highly compacted clays with temperature and hydraulic gradients. It has been suggested by Singh (2007) to include two material dependant factors η_1 and η_2 in equation (3.40) results into:

$$\begin{aligned}\mathbf{v_v} &= \eta_2 \frac{D_{atms} v_v \tau_v \theta_g}{\rho_l}\left(\rho_0 \frac{\partial h}{\partial s}\right)\nabla u_l - \eta_2 \frac{D_{atms} v_v \tau_v \theta_g}{\rho_l}\left(\rho_0 RT \frac{\partial h}{\partial s}\right)\nabla \sum_{i=1}^{N} c_g^i \\ &-\eta_1 \frac{D_{atms} v_v \tau_v \theta_g}{\rho_l} f \frac{(\nabla T)_a}{\nabla T}\left(h \frac{\partial \rho_0}{\partial T} + \rho_0 \frac{\partial h}{\partial T} + \rho_0 R \sum_{i=1}^{N} c_g^i \frac{\partial h}{\partial s}\right)\nabla T\end{aligned} \tag{3.42}$$

3.2.3 Governing equation of moisture flow

The component of liquid and vapour phases have been discussed in the previous sections. To obtain the governing differential equation for water flow the aforementioned flow laws have been adopted in the mass conservation equation (3.14). The resulting equation has been presented in terms of primary variables.

The first two terms of equation (3.14) can be expanded and substituting equation (3.10) yields:

$$\begin{aligned}&e\left(\rho_l - \rho_v\right)\frac{\partial S_l}{\partial t} + e\left(1 - S_l\right)\frac{\partial \rho_v}{\partial t} + \left[\rho_l S_l + \rho_v\left(1 - S_l\right)\right]\frac{\partial e}{\partial t} + \\ &\rho_l (1+e)\nabla \mathbf{v_l} + \rho_l (1+e)\nabla \mathbf{v_v} + (1+e)\nabla\left(\rho_v \mathbf{v_g}\right) = 0\end{aligned} \tag{3.43}$$

Dividing equation (3.43) by (1+e) and substituting equation (3.13) yields:

$$\begin{aligned}&n\left(\rho_l - \rho_v\right)\frac{\partial S_l}{\partial t} + n\left(1 - S_l\right)\frac{\partial \rho_v}{\partial t} + \left[\rho_l S_l + \rho_v\left(1 - S_l\right)\right]\frac{\partial e}{(1+e)\partial t} + \\ &\rho_l \nabla \mathbf{v_l} + \rho_l \nabla \mathbf{v_v} + \nabla\left(\rho_v \mathbf{v_g}\right) = 0\end{aligned} \tag{3.44}$$

First term of equation (3.44) can be expressed using equation (3.25) as:

$$n(\rho_l-\rho_v)\frac{\partial S_l}{\partial t}=-n(\rho_l-\rho_v)\frac{\partial S_l}{\partial s}\frac{\partial u_l}{\partial t}+n(\rho_l-\rho_v)\left[R\sum_{i=1}^{N}c_g^i\frac{\partial S_l}{\partial s}+\frac{\partial S_l}{\partial T}\right]\frac{\partial T}{\partial t}$$
$$+n(\rho_l-\rho_v)RT\frac{\partial S_l}{\partial s}\sum_{i=1}^{N}\frac{\partial c_g^i}{\partial t} \quad (3.45)$$

Second term of equation (3.44) can be expanded using equation (3.39) as:

$$n(1-S_l)\frac{\partial \rho_v}{\partial t}=-n(1-S_l)\left(\rho_0\frac{\partial h}{\partial s}\right)\frac{\partial u_l}{\partial t}+n(1-S_l)\left(\rho_0 RT\frac{\partial h}{\partial s}\right)\sum_{i=1}^{N}\frac{\partial c_g^i}{\partial t}$$
$$+n(1-S_l)\left(h\frac{\partial \rho_0}{\partial T}+\rho_0\frac{\partial h}{\partial T}+\rho_0 R\sum_{i=1}^{N}c_g^i\frac{\partial h}{\partial s}\right)\frac{\partial T}{\partial t} \quad (3.46)$$

Third term of equation (3.44) can be represented as:

$$\left[\rho_l S_l+\rho_v(1-S_l)\right]\frac{\partial e}{(1+e)\partial t}=\left[\rho_l S_l+\rho_v(1-S_l)\right]\mathbf{m}^T\mathbf{P}\frac{\partial \mathbf{u}}{\partial t} \quad (3.47)$$

where,

$$\frac{\partial e}{(1+e)\partial t}=\frac{\partial \varepsilon_v}{\partial t}=(1+e)\frac{\partial n}{\partial t}=\mathbf{m}^T\frac{\partial \varepsilon}{\partial t}=\mathbf{m}^T\mathbf{P}\frac{\partial \mathbf{u}}{\partial t} \quad (3.48)$$

Volumetric strain, ε_v is defined by the rate of change of void ratio with respect to initial volume.

Substituting equations (3.45), (3.46) and (3.47) for the first, second and third terms respectively and equations (3.15), (3.27) and (3.42) for $\mathbf{v_l}$, $\mathbf{v_g}$ and $\mathbf{v_v}$ respectively into equation (3.44) yields the governing differential equation for water transfer in terms of the primary variables as:

$$C_{ll}\frac{\partial u_l}{\partial t}+C_{lT}\frac{\partial T}{\partial t}+C_{lc_g^i}\sum_{i=1}^{N}\frac{\partial c_g^i}{\partial t}+C_{l\mathbf{u}}\frac{\partial \mathbf{u}}{\partial t}= \nabla\left[K_{ll}\nabla u_l\right]+\nabla\left[K_{lT}\nabla T\right]+\nabla\left[K_{lc_g^i}\nabla\sum_{i=1}^{N}c_g^i\right]+J_l \tag{3.49}$$

where, $i = 1,2,\ldots\ldots\ldots\ldots,N$ number of gas components present in the system. The storage terms and flux terms can be presented as:

$$C_{ll}=-n(\rho_l-\rho_v)\frac{\partial S_l}{\partial s}-n(1-S_l)\rho_0\frac{\partial h}{\partial s} \tag{3.50}$$

$$C_{lT}=n(\rho_l-\rho_v)\left(R\sum_{i=1}^{N}c_g^i\frac{\partial S_l}{\partial s}+\frac{\partial S_l}{\partial T}\right)+n(1-S_l)\left(h\frac{\partial \rho_0}{\partial T}+\rho_0\frac{\partial h}{\partial T}+\rho_0 R\sum_{i=1}^{N}c_g^i\frac{\partial h}{\partial s}\right) \tag{3.51}$$

$$C_{lc_g^i}=nRT(\rho_l-\rho_v)\left(\frac{\partial S_l}{\partial s}\right)+nRT(1-S_l)\left(\rho_0\frac{\partial h}{\partial s}\right) \tag{3.52}$$

$$C_{l\mathbf{u}}=\left(S_l\rho_l+(1-S_l)\rho_v\right)\mathbf{m}^T\mathbf{P} \tag{3.53}$$

$$K_{ll}=\frac{\rho_l k_l}{\gamma_l}-\rho_l\frac{\eta_2 D_{atms}\nu_v\tau_v\theta_g}{\rho_l}\left(\rho_0\frac{\partial h}{\partial s}\right) \tag{3.54}$$

$$K_{lT}=\eta_1\rho_l\frac{D_{atms}\nu_v\tau_v\theta_g f(\nabla T)^a}{\rho_l(\nabla T)}\left(h\frac{\partial \rho_0}{\partial T}+\rho_0\frac{\partial h}{\partial T}+\rho_0 R\sum_{i=1}^{N}c_g^i\frac{\partial h}{\partial s}\right)+\rho_v k_g R\sum_{i=1}^{N}c_g^i \tag{3.55}$$

$$K_{lc_g^i}=\eta_2\rho_l RT\frac{D_{atms}\nu_v\tau_v\theta_g}{\rho_l}\left(\rho_0\frac{\partial h}{\partial s}\right)+\rho_v RTk_g \tag{3.56}$$

$$J_l=\nabla\left[(\rho_l k_l)\nabla z\right] \tag{3.57}$$

3.3 Multicomponent pore gas transfer

The governing equations for multicomponent pore gas flow have been derived based on the concept of conservation of mass.

$$\begin{bmatrix} \textit{the net rate of} \\ \textit{change of moles} \end{bmatrix} = \begin{bmatrix} \textit{net rate of} \\ \textit{molar flux} \end{bmatrix} \pm \begin{bmatrix} \textit{net rate of moles gained or lost} \\ \textit{due to the source / sink} \end{bmatrix}$$

In a three phase (solid-gas-liquid) system the components of one phase can be transformed into other phases. Therefore, the sink/ source term calculates the amount of moles gained or lost due to transformation of phases and chemical reactions.

The conservation equation can be expressed in terms of mole concentration of each gas components in the system as follows:

$$\frac{\partial\left(\theta_g c_g^i \partial V\right)}{\partial t} + \frac{\partial\left(\theta_g s_s^i \partial V\right)}{\partial t} = -\nabla J_{c_g}^i \partial V \tag{3.58}$$

where, $J_{c_g}^i$ is the total flux of gas component *i*. s_s^i represents the amount of mass lost or gained due to sink/ source term combining reactions and phase transformations. In a three phase system, it can be expressed as:

$$s_s^i = R_{g\leftrightarrow d}^i + R_{g\leftrightarrow s}^i + r_g^i \tag{3.59}$$

where, $R_{g\leftrightarrow d}^i$ represents the amount of gas components dissolving in liquid phase, $R_{g\leftrightarrow s}^i$ states for amount gas components adsorbing or desorbing into the solid phase and r_g^i is the amount of moles gained/ lost due to the chemical reactions in gas phase. The measurement of sink/source term of multicomponent pore gas flow equation (3.58) has been detailed in section 3.5.

3.3.1 Mechanisms of multicomponent gas flow

The mechanisms of multicomponent gas flow have been discussed in the following sections. The gas species at different phases can be characterised as gas components, dissolved chemical components and sorbed components in gas, liquid and solid phase respectively. Non-reactive gas transport in unsaturated soil is a complex physical process and includes three general transport mechanisms, namely, advection, free molecule diffusion and continuum diffusion (Massmann and Farrier, 1992). The fluxes of gas components in gas phase have been considered based on the following processes:

3.3.1.1 Advection

The advective flow of bulk gases in porous media is driven by pressure gradient and is expressed using Darcy's law. In case of mixture of gases, the advective flux of individual species can be obtained from the proportion of that species in the bulk flow since the mixture is non-separative (Mason and Malinauskas, 1964). The advective flux of i^{th} component in terms of molar flux can be expressed as:

$$J_{ad}^{i} = x_g^i J_{ad} \tag{3.60}$$

where, J_{ad}^{i} is the advection of component i, J_{ad} represents the total advection and x_g^i stands mole fraction of component i which can be presented as:

$$x_g^i = c_g^i / c \tag{3.61}$$

Total molar concentration, c, can be obtained by adding up the individual concentration of the gas components and can be expressed as:

$$c = \sum_{j=1}^{N} c_g^j \tag{3.62}$$

The bulk advective flux according to Darcy's law is

$$J_{ad} = c\mathbf{v_g} = -ck_g \nabla u_g \tag{3.63}$$

where, $\mathbf{v_g}$ is the Darcy's velocity, k_g is the intrinsic permeability, n is porosity and u_g is the total pore gas pressure which has been defined in section 3.2.1.

Substituting equation (3.23) and (3.63) into equation (3.60) yields:

$$J_{ad}^{i} = -c_g^i RTk_g \nabla \sum_{j=1}^{N} c_g^j - c_g^i k_g R \sum_{j=1}^{N} c_g^j \nabla T \tag{3.64}$$

As it has been discussed previously, the unsaturated pore gas conductivity can be expressed in terms of intrinsic permeability, K_{int}, relative gas permeability, K_{rg} and viscosity, μ_g as follows:

$$k_g = \frac{K_{int} K_{rg}}{\mu_g} \tag{3.65}$$

Parker et al. (1987) has modified van-Genuchten characteristics curve to include gas phase relative permeability as:

$$K_{rg} = (1 - S_e)^{1/2} (1 - S_e^{1/m})^{2m} \tag{3.66}$$

where, *m is a* fitting parameter, S_e is the effective saturation and can be expressed in terms of liquid phase degree of saturation, S_l and residual degree of saturation, S_{lr} (the degree of saturation at which changes in matric suction do not alter the saturation state of soil) as follows:

$$S_e = \frac{(S_l - S_{lr})}{(1 - S_{lr})} \tag{3.67}$$

3.3.1.2 Diffusion

The possible forms of diffusion which can take place in a mixture of gases passing through a porous media have been reported by (Bird et al., 1960):

a. Ordinary or Continuum diffusion
b. Free molecule diffusion or Knudsen diffusion
c. Thermal diffusion
d. Pressure diffusion
e. Forced diffusion

In case of multicomponent gas mixture Thermal diffusion is quite small at normal temperature gradients but important in a very steep temperature gradient where separation of mixture is affected (Bird et al., 1960). The pressure diffusion takes place when a pressure gradient is imposed in the system and the tendency for a mixture to separate under a pressure gradient is very small. Therefore has been ignored in this work. Forced diffusion takes place due to the presence of external forces in the system such as gravity. In case of gaseous diffusion this has a negligible effect.

3.3.1.3 Ordinary or continuum diffusion

Diffusive flow of gases takes place in presence of concentration gradient. Fick's law of diffusion is widely applicable in case of systems of binary diffusion. To model diffusion of multicomponent gas mixture Taylor and Krishna (1993) has suggested and extended form of Fick's law of diffusion. For a system of *N*-component gases diffusive fluxes can be expressed as:

$$\left.\begin{aligned} J_{od}^{1} &= -D_{11}\nabla c_g^1 - D_{12}\nabla c_g^2 - D_{13}\nabla c_g^3 \quad . \quad . \quad . - D_{1N}\nabla c_g^N \\ J_{od}^{2} &= -D_{21}\nabla c_g^1 - D_{22}\nabla c_g^2 - D_{23}\nabla c_g^3 \quad . \quad . \quad . - D_{2N}\nabla c_g^N \\ &. \quad . \\ J_{od}^{N} &= -D_{N1}\nabla c_g^1 - D_{N2}\nabla c_g^2 - D_{N3}\nabla c_g^3 \quad . \quad . \quad . - D_{NN}\nabla c_g^N \end{aligned}\right\} \qquad (3.68)$$

The set of linear relationships in equation (3.68) can be expressed in a concise form as follows:

$$J_{od}^{i} = -\sum_{j=1}^{N} D_{ij} \nabla c_g^j \tag{3.69}$$

where, J_{od}^{i} is the diffusive flux of component *i* and D_{ij} represents the multicomponent diffusion coefficients. The multicomponent diffusion matrix, [**D**] can be expressed as:

$$[\mathbf{D}] = [\mathbf{B}]^{-1} \tag{3.70}$$

where, [**B**] is the binary diffusion matrix. The elements of matrix [**B**] can be obtained using mole fraction and binary diffusion coefficients as suggested by Taylor and Krishna (1993):

$$B_{ii} = \frac{x_i}{b_{iN}} + \sum_{k=1}^{N(k\neq i)} \frac{x_k}{b_{ik}} \tag{3.71}$$

$$B_{ij} = -x_i \left(\frac{1}{b_{ij}} - \frac{1}{b_{iN}} \right), i \neq j \tag{3.72}$$

where, B_{ii} and B_{ij} are the diagonal and cross-diagonal elements of [**B**] matrix respectively. b_{ij} is the binary diffusion coefficient of component *i* and *j*. *i,j,k* are gas component counters, *N* represents the total number of gas components. The term b_{iN} stands for the binary diffusion coefficient of i^{th} - N^{th} gas pair. In general, the diffusion coefficients are not symmetric $\left(D_{ij} \neq D_{ji}\right)$ and can take both positive and negative values. The diagonal elements are often termed as "main-term" diffusion coefficients which are usually large in number and similar in magnitude to binary values (Cussler, 1984).

By using the available information of mole fraction and binary diffusion coefficient, the diagonal elements of [**B**] matrix can be calculated using equation (3.71). The cross-diagonal elements of [**B**] matrix can be calculated using equation (3.72). The

multicomponent diffusion matrix [**D**] can be obtained from the developed [**B**] matrix by using matrix inversion scheme.

The above mentioned types of Fick's law are appropriate for free or clear fluids. To model diffusive flow in porous media diffusion coefficients in gases need to be replaced by effective diffusion coefficient which considers the porosity and tortuosity of the porous media. Therefore, effective diffusion coefficient, D_{ij}^{0}, can be expressed as:

$$D_{ij}^{0} = nS_g \tau_g D_{ij} \tag{3.73}$$

A number of models are available to model the tortuosity factor. The widely used model by Millington and Quirk (1961) suggested the gas phase tortuosity factor as:

$$\tau_g = n^{1/3} S_g^{7/3} \tag{3.74}$$

By adopting effective diffusion coefficient, equation (3.73), into equation (3.69) yields:

$$J_{od}^{i} = -nS_g \tau_g \sum_{j=1}^{N} D_{ij} \nabla c_g^{j} \tag{3.75}$$

3.3.1.4 Free molecule diffusion

Free molecule diffusion or Knudsen diffusion becomes important when the gas molecular mean free path becomes of the same order as the capillary tube dimensions (Ho and Webb, 2006). In this case the molecule-molecule collision becomes negligible compared to the molecule-wall collision (Cunningham and Williams, 1980). To describe Knudsen diffusion, an equation similar to the equation (3.75) can be given according to Mason and Malinauskas (1964) as:

$$J_k^{i} = -nS_g D_{ik} \nabla c_g^{i} \tag{3.75a}$$

where, J_k^{i} represents the Knudsen flux and D_{ik} is the Knudsen diffusion coefficient which can be calculated using Klinkenberg coefficient (Thorstenson and Pollock,

1989). Cunningham and Williams (1980) suggested that although in a multicomponent system different species are present but a given species cannot learn about the existence of the other species since there are no molecule-molecule collisions in the Knudsen regime. Knudsen diffusion becomes important in very low porosity materials, such as rock. This process has been mentioned in the formulation to demonstrate the applicability of the model for various types of porous media although it has been ignored in this study.

3.3.2 Governing equations of multicomponent pore gas flow

To obtain the governing equation of multicomponent gas flow in terms of primary variables equations (3.9) and (3.11) has been substituted into equation (3.58) resulting:

$$\frac{\partial\left(nS_g c_g^i\left(1+e\right)\partial V_s\right)}{\partial t}+\frac{\partial\left(nS_g s_s^i\left(1+e\right)\partial V_s\right)}{\partial t}=-\nabla J_{c_g}^i\left(1+e\right)\partial V_s \tag{3.76}$$

Since ∂V_s is constant and using equation (3.13) gives:

$$\frac{\partial\left(eS_g c_g^i\right)}{\partial t}+\frac{\partial\left(eS_g s_s^i\right)}{\partial t}=-\nabla J_{c_g}^i\left(1+e\right) \tag{3.77}$$

Dividing both side of equation (3.77) by (1+e) yields:

$$\frac{\partial\left(eS_g c_g^i\right)}{\left(1+e\right)\partial t}+\frac{\partial\left(eS_g s_s^i\right)}{\left(1+e\right)\partial t}=-\nabla J_{c_g}^i \tag{3.78}$$

It has been assumed that the void ratio remains fixed and expanding the first term of LHS of equation (3.78) yields:

$$\frac{\partial\left(eS_g c_g^i\right)}{\left(1+e\right)\partial t}=nS_g\frac{\partial c_g^i}{\partial t}+nc_g^i\frac{\partial S_g}{\partial t}+S_g c_g^i\frac{\partial e}{\left(1+e\right)\partial t} \tag{3.79}$$

Second term of equation (3.79) can be presented using equation (3.10)

$$nc_g^i \frac{\partial S_g}{\partial t} = -nc_g^i \frac{\partial S_l}{\partial t} \tag{3.80}$$

Substituting equation (3.25) in equation (3.80) yields:

$$-nc_g^i \frac{\partial S_l}{\partial t} = nc_g^i \frac{\partial S_l}{\partial s}\frac{\partial u_l}{\partial t} - nc_g^i \left(R\sum_{i=1}^{N} c_g^i \frac{\partial S_l}{\partial s} + \frac{\partial S_l}{\partial T} \right)\frac{\partial T}{\partial t} - nc_g^i RT \frac{\partial S_l}{\partial s}\sum_{j=1}^{N} \frac{\partial c_g^j}{\partial t} \tag{3.81}$$

Third term of equation (3.79) can be expressed using equations (3.10) and (3.48) as:

$$S_g c_g^i \frac{\partial e}{(1+e)\partial t} = (1-S_l) c_g^i \mathbf{m}^T \mathbf{P} \frac{\partial \mathbf{u}}{\partial t} \tag{3.82}$$

Substituting equations (3.81) and (3.82) into equation (3.79) yields:

$$\begin{aligned} \frac{\partial \left(eS_g c_g^i \right)}{(1+e)\partial t} &= nc_g^i \frac{\partial S_l}{\partial s}\frac{\partial u_l}{\partial t} - nc_g^i \left(R\sum_{i=1}^{N} c_g^i \frac{\partial S_l}{\partial s} + \frac{\partial S_l}{\partial T} \right)\frac{\partial T}{\partial t} + \left(nS_g - nc_g^i RT \frac{\partial S_l}{\partial s} \right)\frac{\partial c_g^i}{\partial t} \\ &- nc_g^i RT \frac{\partial S_l}{\partial s}\sum_{j=1}^{N(i\neq j)} \frac{\partial c_g^j}{\partial t} + S_g c_g^i \mathbf{m}^T \mathbf{P} \frac{\partial \mathbf{u}}{\partial t} \end{aligned} \tag{3.83}$$

Substituting equation (3.83) into equation (3.78) yields:

$$\begin{aligned} &nc_g^i \frac{\partial S_l}{\partial s}\frac{\partial u_l}{\partial t} - nc_g^i \left(R\sum_{i=1}^{N} c_g^i \frac{\partial S_l}{\partial s} + \frac{\partial S_l}{\partial T} \right)\frac{\partial T}{\partial t} + \left(nS_g - nc_g^i RT \frac{\partial S_l}{\partial s} \right)\frac{\partial c_g^i}{\partial t} \\ &- nc_g^i RT \frac{\partial S_l}{\partial s}\sum_{j=1}^{N(i\neq j)} \frac{\partial c_g^j}{\partial t} + nS_g \frac{\partial s_s^i}{\partial t} + S_g c_g^i \mathbf{m}^T \mathbf{P} \frac{\partial \mathbf{u}}{\partial t} = -\nabla J_{c_g}^i \end{aligned} \tag{3.84}$$

Therefore, the LHS of equation (3.84) can be expressed in terms of primary variables as:

$$C^i_{c_g l}\frac{\partial u_l}{\partial t}+C^i_{c_g T}\frac{\partial T}{\partial t}+C^i_{c^i_g c^i_g}\frac{\partial c_{\mathrm{g}}{}^i}{\partial t}+C^i_{c^i_g c^j_g}\sum_{j=1}^{N(i\neq j)}\frac{\partial c_{\mathrm{g}}{}^j}{\partial t}+C^i_{c_g s_g}\frac{\partial s^i_s}{\partial t}+C^i_{c_g \mathbf{u}}\frac{\partial \mathbf{u}}{\partial t} \tag{3.85}$$

RHS of equation (3.78) can be expressed as:

$$=-\left[\nabla J^i_{ad}+\nabla J^i_{od}\right] \tag{3.86}$$

Substituting equations (3.64) and (3.75) into equation (3.86) results:

$$=\nabla\left[c^i_g k_g RT\nabla\left(\sum_{j=1}^{N}c^j_g\right)+nS_g\tau_g\sum_{j=1}^{N}D_{ij}\nabla c^j_g+c^i_g k_g R\sum_{j=1}^{N}c^j_g\nabla T\right] \tag{3.87}$$

Rearranging the similar terms yields:

$$=\nabla\left[c^i_g k_g RT\nabla\sum_{j=1}^{N}c^j_g+\sum_{j=1}^{N}\left(nS_g\tau_g D_{ij}\nabla c^j_g\right)\right]+\nabla\left[c^i_g k_g R\sum_{j=1}^{N}c^j_g\nabla T\right] \tag{3.88}$$

Equation (3.88) can be expressed in terms of primary variables as:

$$=\nabla\left[K^i_{c^i_g c^j_g}\sum_{j=1}^{N}\nabla c_g{}^j\right]+\nabla\left[\sum_{j=1}^{N}\left(K_{c^i_g c^j_g}\nabla c_g{}^j\right)\right]+\nabla\left[K^i_{c_g T}\nabla T\right] \tag{3.89}$$

Combining equation (3.85) and equation (3.89) results the governing equation of multi-component gas flow in terms of principle variables as:

$$\begin{aligned}&C^i_{c_g l}\frac{\partial u_l}{\partial t}+C^i_{c_g T}\frac{\partial T}{\partial t}+C^i_{c^i_g c^i_g}\frac{\partial c_{\mathrm{g}}{}^i}{\partial t}+C^i_{c^i_g c^j_g}\sum_{j=1}^{N(i\neq j)}\frac{\partial c_{\mathrm{g}}{}^j}{\partial t}+C^i_{c_g s_g}\frac{\partial s^i_s}{\partial t}+C^i_{c_g \mathbf{u}}\frac{\partial \mathbf{u}}{\partial t}\\&=\nabla\left[K^i_{c^i_g c^j_g}\sum_{j=1}^{N}\nabla c_g{}^j\right]+\nabla\left[\sum_{j=1}^{N}\left(K_{c^i_g c^j_g}\nabla c_g{}^j\right)\right]+\nabla\left[K^i_{c_g T}\nabla T\right]\end{aligned} \tag{3.90}$$

where, i ,j = 1, 2, ...,N number of gas components.

The flux term and storage term constants can be expressed as:

$$C^i_{c_g l} = nc^i_g \frac{\partial S_l}{\partial s} \tag{3.91}$$

$$C^i_{c_g T} = -nc^i_g \left(R\sum_{i=1}^{N} c^i_g \frac{\partial S_l}{\partial s} + \frac{\partial S_l}{\partial T} \right) \tag{3.92}$$

$$C^i_{c^i_g c^i_g} = nS_g - nc^i_g RT \frac{\partial S_l}{\partial s} \tag{3.93}$$

$$C^i_{c^i_g c^j_g} = -nc^i_g RT \frac{\partial S_l}{\partial s} \tag{3.93a}$$

$$C^i_{c_g s_s} = -nS_g \tag{3.94}$$

$$C^i_{c_g \mathbf{u}} = S_g c^i_g \mathbf{m}^T \mathbf{P} \tag{3.95}$$

$$K^i_{c^i_g c^j_g} = c^i_g k_g RT \tag{3.96}$$

$$K_{c^i_g c^j_g} = nS_g \tau_g D_{ij} \tag{3.96a}$$

$$K^i_{c_g T} = c^i_g k_g R \sum_{j=1}^{N} c^j_g \tag{3.97}$$

3.4 Multicomponent dissolved chemical flow

In this section the development of governing equation of multicomponent dissolved chemicals has been presented. The equation of conservation of chemical solute is utilised to produce the governing equation for chemical transfer. The development of the multicomponent dissolved chemical flow has been detailed in Seetharam (2003) and Sedighi (2011).

3.4.1 Mechanisms of dissolved chemical solute transport

At the subsurface system released contaminants might interact hydrologically, physically and chemically with both the native water and the solid matrix. The main hydrological, physical and chemical processes of interaction include (Diestel, 1976; Yong et al., 1992; Mitchell, 1993):

a. Advective flux
b. Diffusive flux
c. Dispersive flux (Hydrodynamic dispersion)
d. Thermal diffusion
e. Salt sieving
f. Aqueous chemical reactions (Homogenous reactions)
g. Sorption, ion exchange and precipitation/dissolution (Heterogeneous reactions)

The first five processes are involved in hydrological/physical processes and last two processes are involved in key geochemical reactions. Aqueous reactions include aqueous speciation, acid-base and redox reactions (Seetharam, 2003).

In highly compacted clays the flow of liquid is considerably low, coefficient of hydrodynamic dispersion is often controlled by the diffusion coefficient and the coefficient of mechanical dispersion is negligible (Rowe and Booker, 1986). Diestel (1976) stated that the process of salt sieving has been found to be negligible comparing to other accumulation processes such as evaporation and molecular diffusion. Therefore, the effects of hydrodynamic dispersion and salt sieving have been neglected. The combined effect of hydrological, physical and chemical processes on solute transport must satisfy the principles of conservation of mass. The transport processes are usually described by a set of partial differential equations whilst the chemical

reactions, under the assumption of chemical equilibrium, are described by a set of non-linear algebraic equations.

Assuming pore water, as a homogeneous liquid, flowing through a porous rigid media and bearing a given mass of chemical solute, the chemical solute transport equation including sink/source term for phase transformation and chemical reactions can be expressed in molar form as:

$$\frac{\partial\left(\theta_l c_d^i \partial V\right)}{\partial t} + \frac{\partial\left(\theta_l s_d^i \partial V\right)}{\partial t} = -\nabla J_{c_d}^i \partial \mathrm{V} \tag{3.98}$$

where, c_d^i is the molar concentration of dissolved chemical component *i*, $J_{c_d}^i$ represents total flux of dissolved chemical component *i*. In a three phase system the sink/source term for i^{th} component, s_d^i can be expressed as:

$$s_d^i = R_{d\leftrightarrow g}^i + R_{d\leftrightarrow s}^i + r_d^i \tag{3.99}$$

where, $R_{d\leftrightarrow g}^i$ represents the amount of dissolved components transforming into gas phase, $R_{d\leftrightarrow s}^i$ is the amount of dissolved components adsorbing or desorbing into the solid phase and r_d^i represents the amount of moles gained/lost due to the chemical reactions in liquid phase. The mechanisms of dissolved chemicals transport processes have been discussed briefly in the following sections.

3.4.1.1 Advection

The advective flux of individual species of a multi-component system can be calculated from the proportion of that component in the bulk liquid flow. Thus the advective flux, $J_{advective}^i$ can be expressed as:

$$J_{advective}^i = c_d^i \mathbf{v_l} = c_d^i \left[-k_l \left\{ \nabla\left(\frac{u_l}{\gamma_l} \right) + \nabla z \right\} \right] \tag{3.100}$$

3.4.1.2 Diffusion

The process of molecular diffusion is the spreading of the solute molecules through the fluid by virtue of their kinetic motion, even when the fluid is at rest (Crank, 1975). Strictly, diffusive flux is proportional to the gradient of the chemical potential of a substance (Denbigh, 1981), but for most practical applications and for this work, it is taken as proportional to the gradient of concentration. It has been suggested that under non-isothermal conditions, a temperature gradient can facilitate mass movement due to thermal diffusion, also known as Soret effect (Lasaga, 1998; Thomas et al., 2012).

The diffusive flow of multi component dissolved chemicals can be obtained from the Fick's law of binary diffusion. For a multicomponent system the diffusive flux, $J^i_{diffusive}$ can be expressed as:

$$J^i_{diffusive} = -nS_l D^i_d \nabla c^i_d \tag{3.101}$$

where, D^i_d is the effective coefficient of molecular diffusion considering the tortuosity factor due to porous media.

It has been found that if chemicals move with different rate it may cause an electrical potential in the system which affect the diffusion regime as it has been discussed in Sedighi (2011) and Thomas et al. (2012). In this work, the effects of electrical potential on diffusion of chemicals are neglected.

The sink/source term of equation (3.98) has been calculated from geochemical reaction equilibrium and has been detailed in section 3.5.

3.4.2 Governing equation for dissolved chemical flow

Substituting equations (3.8) and (3.11) into equation (3.98) yields:

$$\frac{\partial\left(nS_l c^i_d (1+e)\partial V_s\right)}{\partial t} + \frac{\partial\left(nS_l s^i_d (1+e)\partial V_s\right)}{\partial t} = -\nabla J^i_{c_d}\left(1+e\right)\partial V_s \tag{3.102}$$

Since, ∂V_s is constant and using equation (3.13) into equation (3.102) results:

$$\frac{\partial\left(eS_l c_d^i\right)}{(1+e)\partial t}+\frac{\partial\left(nS_l s_d^i\right)}{\partial t}=-\nabla J_{c_d}^i \tag{3.103}$$

Equation (3.103) can be expanded as:

$$nS_l\frac{\partial c_d^i}{\partial t}+nc_d^i\frac{\partial S_l}{\partial t}+S_l c_d^i\frac{\partial e}{(1+e)\partial t}+nS_l\frac{\partial s_d^i}{\partial t}=-\nabla J_{c_d}^i \tag{3.104}$$

Second term of equation (3.104) can be expressed using equations (3.25) as:

$$nc_d^i\frac{\partial S_l}{\partial t}=nc_d^i RT\frac{\partial S_l}{\partial s}\sum_{j=1}^{N}\frac{\partial c_g^j}{\partial t}+nc_d^i\left(R\sum_{i=1}^{N}c_g^i\frac{\partial S_l}{\partial s}+\frac{\partial S_l}{\partial T}\right)\frac{\partial T}{\partial t}-nc_d^i\frac{\partial S_l}{\partial s}\frac{\partial u_l}{\partial t} \tag{3.105}$$

Third term of equation (3.104) can be expressed using equations (3.48) as:

$$S_l c_d^i\frac{\partial e}{(1+e)\partial t}=S_l c_d^i\mathbf{m}^T\mathbf{P}\frac{\partial\mathbf{u}}{\partial \mathrm{t}} \tag{3.106}$$

Substituting equations (3.105) and (3.106) into LHS of equation (3.104) yields:

$$\begin{aligned}&-nc_d^i\frac{\partial S_l}{\partial s}\frac{\partial u_l}{\partial t}+nc_d^i\left(R\sum_{j=1}^{N}c_g^j\frac{\partial S_l}{\partial s}+\frac{\partial S_l}{\partial T}\right)\frac{\partial T}{\partial t}+nc_d^i RT\frac{\partial S_l}{\partial s}\sum_{j=1}^{N}\frac{\partial c_g^j}{\partial t}+nS_l\frac{\partial c_d^i}{\partial t}\\&+S_l c_d^i\mathbf{m}^T\mathbf{P}\frac{\partial\mathbf{u}}{\partial \mathrm{t}}+nS_l\frac{\partial s_d^i}{\partial t}=-\nabla J_{c_d}^i\end{aligned} \tag{3.107}$$

Substituting equations (3.100) and (3.101) into RHS of equation (3.103) results:

$$-\nabla J_{c_d}^i=\nabla\left[c_d^i k_l\left(\nabla\frac{u_l}{\gamma_l}+\nabla z\right)\right]+\nabla\left[nS_l D_d^i\nabla c_d^i\right] \tag{3.108}$$

Equation (3.108) can be rearranged as:

$$-\nabla J^i_{c_d} = \nabla\left[c^i_d \frac{k_l}{\gamma_l} \nabla u_l \right] + \nabla\left[nS_l D^i_d \nabla c^i_d \right] + \nabla\left[c^i_d \frac{k_l}{\gamma_l} \nabla z \right] \tag{3.109}$$

Substituting equation (3.109) into equation (3.107) and expressing the variables in terms of primary variables yields:

$$\begin{aligned} &C^i_{c_d l} \frac{\partial u_l}{\partial t} + C^i_{c_d T} \frac{\partial T}{\partial t} + C^i_{c^i_d c^j_g} \sum_{j=1}^{N} \frac{\partial c_g{}^j}{\partial t} + C^i_{c_d c_d} \frac{\partial c^i_d}{\partial t} + C^i_{c_d \mathbf{u}} \frac{\partial \mathbf{u}}{\partial t} + C^i_{c_d s_d} \frac{\partial s^i_d}{\partial t} \\ &= \nabla\left[K^i_{c_d l} \nabla u_l \right] + \nabla\left[K^i_{c_d c_d} \nabla c^i_d \right] + J^i_Z \end{aligned} \tag{3.110}$$

where, i = *1,2,……,M* number of dissolved chemical components and j = *1,2,……,N* number of gas components. The storage and flux constants can be expressed as:

$$C^i_{c_d l} = -nc^i_d \frac{\partial S_l}{\partial s} \tag{3.111}$$

$$C^i_{c_d T} \frac{\partial T}{\partial t} = nc^i_d \left(R \sum_{j=1}^{N} c^j_g \frac{\partial S_l}{\partial s} + \frac{\partial S_l}{\partial T} \right) \tag{3.112}$$

$$C^i_{c^i_d c^j_g} = nc^i_d RT \frac{\partial S_l}{\partial s} \tag{3.113}$$

$$C^i_{c_d c_d} = nS_l \tag{3.114}$$

$$C^i_{c_d \mathbf{u}} = S_l c^i_d \mathbf{m}^T \mathbf{P} \tag{3.115}$$

$$K^i_{c_d l} = c^i_d \frac{k_l}{\gamma_l} \tag{3.116}$$

$$K^i_{c_d c_d} = nS_l D^i_d \tag{3.117}$$

$$J^i_Z = \nabla\left(c^i_d \frac{k_l}{\gamma_l} \nabla z \right) \tag{3.118}$$

$$C^i_{c_d s_d} = nS_l \tag{3.119}$$

3.5 Geochemical sink/source term

The sink/source terms of mass conservation equations for multicomponent pore gas flow, equation (3.58) and dissolved chemical flow, equation (3.98) have been detailed in this section. The sink/source term has been obtained considering the equilibrium chemistry of the geochemical reactions. The geochemical processes in porous media, such as compacted clays inundated with complex phenomena and some of the important features have been explained later in details.

In this study the chemical reactions, such as, ion exchange, precipitation and/or dissolution of solids, surface complexation, gas phase equilibrium and redox reactions has been prioritised. Ion-exchange, which is important for clayey soils, occurs due to an affinity of a solid surface for that particular chemical (Sharma and Reddy, 2004). These reactions are involved in exchange of a portion or all of the adsorbed ions of one type by that of another type. Mitchell and Soga (2005) stated that the exchange reactions generally do not affect the structures of the clay particles but significant changes in the physical and physicochemical properties of the soil might take place. Surface complexation considers two important processes. Firstly, chemical interactions between the participating ions and the surface atoms and secondly, an electrostatic effect which depends on the charge condition of the surface (Appelo and Postma, 2005). Precipitation and dissolution reactions involve chemicals in solid phases and generally expressed by equilibrium constant. Mangold and Tsang (1991) suggested that the dissolution or precipitation of minerals or solutes could take place due to the presence of dissolved gases and related minerals and ionic strength of the solution. Gas-liquid equilibrium might favours dissolution or exsolution of gases while altering the chemical environment of the system.

The above mentioned processes are generally expressed mathematically by the law of mass action and relating the thermodynamic equilibrium constant to the activities of the reactants and products (Mangold and Tsang, 1991). The law of mass action can be expressed for a reaction taking place in a solution as:

$$aA + bB \leftrightarrow cC + dD \tag{3.120}$$

where, A, B are the reactants and C, D represents the products of the reaction. a, b, c and d represents the stoichiometric coefficients of the components A, B, C and D respectively. Distribution of the reaction species at equilibrium can be obtained by:

$$K_{eq} = \frac{[C]^c [D]^d}{[A]^a [B]^b} \tag{3.121}$$

where, K_{eq} is the equilibrium constant and the quantities in the [ ] brackets denote activities. Appelo and Postma (2005) stated that the activity of mass action equation is a measure for the effective concentration which represents the behaviour of an ion at infinite diluted solution when there are no interactions with other ions considered. Effective concentration of a chemical species can be defined with the molal concentration of that species and a dimensionless activity coefficient. Mathematically, it can be expressed as:

$$[A] = \gamma_A \frac{m_A}{m_A^0} \tag{3.122}$$

where, m_A is the molality (mol/Kg H_2O) of component A. m_A^0 represents the molality at a standard state, i.e. 1 mol/Kg H_2O and γ_A is the dimensionless activity coefficient of component A. The activity coefficients for a species *i* can be calculated using Debye-Hückel theory. Firstly, the ionic strength, I, can be written as :

$$I = \frac{1}{2}\Sigma\left(\frac{m_i}{m_i^0} z_i^2\right) \cong \frac{1}{2}\Sigma\left(m_i z_i^2\right) \tag{3.123}$$

where, z_i represents the charge number of ion *i*. Secondly, the electrostatic interactions can be presented as:

$$log\gamma_i = -\frac{A_1 z_i^2 \sqrt{I}}{1 + B_1 a_i^0 \sqrt{I}} \tag{3.124}$$

where, A_1 and B_1 are temperature dependent constants. Langmuir (1997) presented the dependency of these constants on a range of temperatures. At 25°C the A_1 = 0.5085 and B_1 = 0.3285×10^{10}/m (Appelo and Postma, 2005). The ion-size parameter, a_i^0 determines the effective diameter of hydrated ion. For a number of cations and anions, the value of a_i^0 has been presented by Garrels and Christ (1965).

Ion exchange reaction models usually assume that the surface site is initially occupied by an exchangeable ion which might release into the solution during exchange process. The exchange of cation (B^+) for a cation (A^+) on a natural mineral surface (X) can be expressed as:

$$A^+ + B\text{-}X \leftrightarrow \text{A}\text{-}X + B^+ \tag{3.125}$$

Therefore, the distribution of species can be given by the law of mass action as:

$$K_{A\backslash B} = \frac{\left[A\text{-}X\right]\left[B^+\right]}{\left[B\text{-}X\right]\left[A^+\right]} \tag{3.126}$$

Activities of equation can be obtained using the aforementioned Debye-Hückel theory.

The equilibrium between a multicomponent gas phase and an aqueous phase can be modelled with heterogeneous mass-action equations (Parkhurst and Appelo, 1999). It has been stated that at equilibrium the amount of a gas component can be calculated from the activities of aqueous master species. By assuming the activity or fugacity of a gas component is similar to its partial pressure, Henry's law can be adopted to relate the partial pressure of the gas component to the activity of aqueous species. Therefore, the partial pressure of a gas component in terms of aqueous phase activities can be presented as (Parkhurst and Appelo, 1999):

$$P_g^i = \frac{1}{K_H}\prod_m^{M_{aq}} a_m^{c_{m,g}^i} \tag{3.127}$$

where, P_g^i is the partial pressure of component *i*, K_H represents Henry's constant, $c_{m,g}^i$ stands for stoichiometric coefficient of aqueous master species *m* in species *i*. M_{aq} is the total number of aqueous master species.

To calculate the chemical equilibrium, a variety of mathematical models encompassing years of research are available to describe the overall behaviour of a system to reach equilibrium. Therefore, in this study, geochemical model PHREEQC, version 2, has been linked with transport model COMPASS to obtain the sink/source terms of the governing equations of mass conservation. The geochemical model, PHREEQC2 (Parkhurst and Appelo, 1999) considers equilibrium chemistry of aqueous solutions reacting with minerals, gases, exchangers and sorption surfaces. The program is based on ion-association aqueous model and capable of speciation and saturation index calculation, batch reactions.

Prior to geochemical modeling, an expression of sink/source term for gas/liquid interface in the transport code has been used. The amount of gas that can be dissolved into liquid has been derived from dimensionless Henry's constant (Ho and Webb, 2006) which can be expressed as:

$$c_d^i = K_H c_g^i \tag{3.128}$$

where, c_d^i is the dissolved concentration of gas species *i*. Later, this term has been compared with the geochemical model and has showed a good agreement.

3.6 Heat transfer

Jakob (1949) has acknowledged three principle mechanisms of heat transfer named conduction, convection and radiation. In developing the theoretical formulation for heat transfer, it has been assumed that the radiation has negligible effect (Mitchell, 1993).

The law of conservation of energy for heat flow states that the temporal derivative of the heat content, Ω is equal to the spatial derivative of the heat flux, Q and can be expressed as:

$$\frac{\partial(\Omega \partial V)}{\partial t} = -\nabla Q(\partial V) \tag{3.129}$$

The heat content for a partially saturated soil, per unit volume can be considered as the sum of soil heat storage capacity and the contribution resulting from the latent heat of vaporisation and can be defined as:

$$\Omega = H_c (T - T_r) + L\theta_g \rho_v \qquad \left(\mathrm{J/m^3}\right) \tag{3.130}$$

where, L is the latent heat of vaporisation, T_r represents reference temperature and H_c represents heat capacity.

The latent heat of vaporisation and specific heat capacities are a function of temperature and based on the Watson formula (Reid et al., 1987), the latent heat can be expressed as:

$$L = 2.672 \times 10^5 \left(T_{cr} - T\right)^{0.38} \qquad \text{(J/Kg)} \tag{3.131}$$

where, $T_{cr} = 647.3K$ is the critical temperature of water. The total change in latent heat is approximately 16% when temperature is raised from 25˚C to 150˚C.

The heat capacity, H_c at reference temperature, T_r, has been presented by Ewen and Thomas (1989) as:

$$H_c = (1-n)C_{ps}\rho_s + n\left(C_{\rho l}S_l\rho_l + C_{pg}S_g\rho_g + C_{pv}S_g\rho_v\right) \tag{3.132}$$

Where C_{ps}, $C_{\rho l}$, C_{pv} and C_{pg} are the specific heat capacities of the solid, liquid, water vapour and gas components respectively. ρ_s is the density of the solid. Equation (3.132) can be adopted for a multicomponent gas system as:

$$H_c = (1-n)C_{ps}\rho_s + n\left(C_{\rho l}S_l\rho_l + \sum_{j=1}^{N} C_{pg}^{j}S_g\rho_g^{j} + C_{pv}S_g\rho_v\right) \tag{3.133}$$

Thomas and He (1995) have defined the heat flux as:

$$\begin{aligned} Q = &-\lambda_T\nabla T + \left(\mathbf{v_v}\rho_l + \mathbf{v_g}\rho_v\right)L \\ &+\left(C_{pl}\mathbf{v_l}\rho_l + C_{pv}\mathbf{v_v}\rho_l + C_{pv}\mathbf{v_g}\rho_v + \sum_{j=1}^{N} C_{pg}^{j}\mathbf{v_g}\rho_g^{j}\right)(T - T_r) \end{aligned} \tag{3.134}$$

where, λ_T is the coefficient of thermal conductivity with the unit of W/mK. The mechanisms of heat transportation can be seen in equation (3.134) where the first term describes the conduction and the last term represents the convection. The second term of the above equation represents the latent heat flow due to the vapour movement. It has been suggested by Fredlund and Rahardjo (1993) and Mitchell (1993) that heat flow in soil entirely dominated by conduction with negligible contribution from convection. Therefore, cancelling the effect of convection, equation (3.134) can be expressed as:

$$Q = -\lambda_T\nabla T + \left(\mathbf{v_v}\rho_l + \mathbf{v_g}\rho_v\right)L \tag{3.135}$$

In a previous attempt Thomas and King (1991) has considered the coefficient of thermal conductivity for an unsaturated soil as a function of the degree of saturation and mathematically can be represented as:

$$\lambda_T = \lambda_T(S_l) \tag{3.136}$$

The law of conservation of energy as defined in equation (3.129) has been modified by substituting the equations (3.130) and (3.135) as:

$$\frac{\partial}{\partial t}\left[\left(H_c\left(T-T_r\right)+L\theta_g\rho_v\right)\partial V\right] = -\nabla\left[-\lambda_T\nabla T + L(\mathbf{v_v}\rho_l + \mathbf{v_g}\rho_v)\right]\partial V \tag{3.137}$$

Substituting equation (3.6) into equation (3.137) and cancelling the ∂V_s yields:

$$\frac{\partial}{\partial t}\left[\left(H_c\left(T-T_r\right)+L\theta_g\rho_v\right)(1+e)\right] = -\nabla\left[-\lambda_T\nabla T + L(\mathbf{v_v}\rho_l + \mathbf{v_g}\rho_v)\right](1+e) \tag{3.138}$$

LHS of equation (3.138) can be expanded as:

$$\begin{aligned}&\frac{\partial}{\partial t}\left[\left(H_c\left(T-T_r\right)+L\theta_g\rho_v\right)(1+e)\right] = \left(T-T_r\right)\frac{\partial}{\partial t}\left[H_c\left(1+e\right)\right] \\ &+H_c\left(1+e\right)\frac{\partial T}{\partial t} + \frac{\partial}{\partial t}\left[L\theta_g\rho_v\left(1+e\right)\right]\end{aligned} \tag{3.139}$$

Substituting equation (3.133) in the first term of equation (3.139) yields:

$$\begin{aligned}&\left(T-T_r\right)\frac{\partial}{\partial t}\left[H_c\left(1+e\right)\right] = \\ &\left(T-T_r\right)\frac{\partial}{\partial t}\left[\left(C_{ps}\rho_s + n\left(-C_{ps}\rho_s + C_{\rho l}S_l\rho_l + \sum_{j=1}^{N} C_{pg}^{j}S_g\rho_g^{j} + C_{pv}S_g\rho_v\right)\right)(1+e)\right]\end{aligned} \tag{3.140}$$

Expanding equation (3.140) and then substituting equation (3.3) and (3.8) results:

$$\left(T-T_r\right)\frac{\partial}{\partial t}\left[H_c\left(1+e\right)\right]=$$
$$\left(T-T_r\right)\left[\begin{array}{l} C_{ps}\rho_s\frac{\partial e}{\partial t}+\left(-C_{ps}\rho_s+C_{pl}S_l\rho_l+C_{pv}S_g\rho_v+\sum_{j=1}^{N}C_{pg}^{j}S_g\rho_g^{j}\right)\frac{\partial e}{\partial t}+ \\ e\left(\begin{array}{l} C_{pl}\rho_l\frac{\partial S_l}{\partial t}-C_{pv}\rho_v\frac{\partial S_l}{\partial t}+C_{pv}(1-S_l)\frac{\partial \rho_v}{\partial t} \\ +\sum_{j=1}^{N}C_{pg}^{j}(1-S_l)\frac{\partial \rho_g^{j}}{\partial t}-\sum_{j=1}^{N}C_{pg}^{j}\rho_g^{j}\frac{\partial S_l}{\partial t} \end{array}\right) \end{array}\right] \tag{3.141}$$

It can be shown that:

$$\frac{\partial e}{\partial t}=\left(1+e\right)^2\frac{\partial n}{\partial t} \tag{3.142}$$

Substituting equation (3.142) into equation (3.141) and rearranging the similar terms yields:

$$\left(T-T_r\right)\frac{\partial}{\partial t}\left[H_c\left(1+e\right)\right]=$$
$$\left(T-T_r\right)\left[\begin{array}{l} C_{ps}\rho_s(1+e)^2\frac{\partial n}{\partial t}+(1+e)^2\left(-C_{ps}\rho_s+C_{pl}S_l\rho_l+C_{pv}S_g\rho_v+\sum_{j=1}^{N}C_{pg}^{j}S_g\rho_g^{j}\right)\frac{\partial n}{\partial t} \\ +e\left(C_{pl}\rho_l-C_{pv}\rho_v-\sum_{j=1}^{N}C_{pg}^{j}\rho_g^{j}\right)\frac{\partial S_l}{\partial t}+eC_{pv}(1-S_l)\frac{\partial \rho_v}{\partial t} \\ +e\sum_{j=1}^{N}C_{pg}^{j}(1-S_l)\frac{\partial \rho_g^{j}}{\partial t} \end{array}\right] \tag{3.143}$$

The third term of equation (3.139) can be represented using equation (3.8) as:

$$\frac{\partial}{\partial t}\left[nS_gL\rho_v\left(1+e\right)\right]=\frac{\partial}{\partial t}\left[eLS_g\rho_v\right] \tag{3.144}$$

Therefore, equation (3.144) can be expanded as:

$$\frac{\partial}{\partial t}\left[nS_gL\rho_v\left(1+e\right)\right]=L(1-S_l)e\frac{\partial \rho_v}{\partial t}-Le\rho_v\frac{\partial S_l}{\partial t}+L(1-S_l)\rho_v\frac{\partial e}{\partial t} \tag{3.145}$$

Substituting equation (3.142) into equation (3.145) results:

$$\frac{\partial}{\partial t}\left[nS_g L\rho_v\left(1+e\right)\right]=L(1-S_l)e\frac{\partial \rho_v}{\partial t}-Le\rho_v\frac{\partial S_l}{\partial t}+L(1-S_l)\rho_v\left(1+e\right)^2\frac{\partial n}{\partial t} \tag{3.146}$$

Substituting equations (3.139), (3.143) and (3.145) into equation (3.138) results the governing equation for heat flow as:

$$\begin{aligned}&\left(T-T_r\right)\left[\begin{array}{l}\left((1+e)^2\left(-C_{ps}\rho_s+C_{pl}S_l\rho_l+C_{pv}S_g\rho_v+\sum_{j=1}^{N}C_{pg}^{j}S_g\rho_g^j\right)\right)\frac{\partial n}{\partial t}\\ +C_{ps}\rho_s(1+e)^2\frac{\partial n}{\partial t}+e\left(C_{pl}\rho_l-C_{pv}\rho_v-\sum_{j=1}^{N}C_{pg}^{j}\rho_g^j\right)\frac{\partial S_l}{\partial t}\\ +eC_{pv}(1-S_l)\frac{\partial \rho_v}{\partial t}+e\sum_{j=1}^{N}C_{pg}^{j}(1-S_l)\frac{\partial \rho_g^j}{\partial t}\end{array}\right]\\ &+H_c(1+e)\frac{\partial T}{\partial t}+L(1-S_l)e\frac{\partial \rho_v}{\partial t}-Le\rho_v\frac{\partial S_l}{\partial t}+L(1-S_l)\rho_v\left(1+e\right)^2\frac{\partial n}{\partial t}\\ &=\nabla\left[-\lambda_T\nabla T+L(\mathbf{v_v}\rho_l+\mathbf{v_g}\rho_v)\right](1+e)\end{aligned} \tag{3.147}$$

Dividing both side of equation (3.147) by *(1+e)* and substituting equation (3.142) yields:

$$\begin{aligned}&\left(T-T_r\right)\left[\begin{array}{l}\left(-C_{ps}\rho_s+C_{pl}S_l\rho_l+C_{pv}S_g\rho_v+\sum_{j=1}^{N}C_{pg}^{j}S_g\rho_g^j\right)(1+e)\frac{\partial n}{\partial t}\\ +n\left(C_{pl}\rho_l-C_{pv}\rho_v-\sum_{j=1}^{N}C_{pg}^{j}\rho_g^j\right)\frac{\partial S_l}{\partial t}\\ +nC_{pv}(1-S_l)\frac{\partial \rho_v}{\partial t}+n\sum_{j=1}^{N}C_{pg}^{j}(1-S_l)\frac{\partial \rho_g^j}{\partial t}\end{array}\right]\\ &+H_c\frac{\partial T}{\partial t}+L(1-S_l)n\frac{\partial \rho_v}{\partial t}-Ln\rho_v\frac{\partial S_l}{\partial t}+L(1-S_l)\rho_v\left(1+e\right)\frac{\partial n}{\partial t}\\ &=\nabla\left[-\lambda_T\nabla T+L(\mathbf{v_v}\rho_l+\mathbf{v_g}\rho_v)\right]\end{aligned} \tag{3.148}$$

Substituting the time derivative of porosity, equation (3.142); vapour density, equation (3.39), degree of liquid saturation, equation (3.25) and expressing the mass density of gas components in molar density ($c_g=\rho_g M_g$, where M_g is the molecular weight of gas

component) in left hand side and equation (3.27) for advective gas flow, equation (3.42) for diffusive vapour flow in right hand side of equation (3.148) yields the governing heat flow equation in terms of primary variables as:

$$C_{Tl}\frac{\partial u_l}{\partial t}+C_{TT}\frac{\partial T}{\partial t}+\sum_{i=1}^{N}C^i_{Tc_g}\frac{\partial c^i_g}{\partial t}+C_{T\mathbf{u}}\frac{\partial \mathbf{u}}{\partial t}=\nabla\left[K_{Tl}\nabla u_l\right]+\nabla\left[K_{TT}\nabla T\right]+\nabla\left[\sum_{i=1}^{N}K^i_{Tc_g}\nabla c^i_g\right] \tag{3.149}$$

where, $i = 1,2,\ldots\ldots\ldots,N$ number of gas components.

$$C_{Tl}=\left(T-T_r\right)\left[-n\left(C_{pl}\rho_l-C_{pv}\rho_v-\sum_{j=1}^{N}C^j_{pg}\rho^j_g\right)\frac{\partial S_l}{\partial s}-nC_{pv}S_g\left(\rho_0\frac{\partial h}{\partial s}\right)\right] \tag{3.150}$$
$$-LnS_g\left(\rho_0\frac{\partial h}{\partial s}\right)+Ln\rho_v\frac{\partial S_l}{\partial s}$$

$$C_{TT}=H_c+\left(T-T_r\right)\left[\begin{array}{l} n\left(C_{pl}\rho_l-C_{pv}\rho_v-\sum_{j=1}^{N}C^j_{pg}\rho^j_g\right)\left(R\sum_{i=1}^{N}c^i_g\frac{\partial S_l}{\partial s}+\frac{\partial S_l}{\partial T}\right)\\ +nC_{pv}S_g\left(h\frac{\partial \rho_0}{\partial T}+\rho_0\frac{\partial h}{\partial T}+\rho_0R\sum_{i=1}^{N}c^i_g\frac{\partial h}{\partial s}\right)\end{array}\right] \tag{3.151}$$
$$+LnS_g\left(h\frac{\partial \rho_0}{\partial T}+\rho_0\frac{\partial h}{\partial T}+\rho_0R\sum_{i=1}^{N}c^i_g\frac{\partial h}{\partial s}\right)-Ln\rho_v\frac{\partial S_l}{\partial T}$$

$$C^i_{Tc_g}=\left(T-T_r\right)\left[nRT\left(C_{pl}\rho_l-C_{pv}\rho_v-C^i_{pg}\rho^i_g\right)\frac{\partial S_l}{\partial s}+nC_{pv}S_g\left(\rho_0RT\frac{\partial h}{\partial s}\right)\right] \tag{3.152}$$
$$+LnS_g\left(\rho_0RT\frac{\partial h}{\partial s}\right)-Ln\rho_v\left(RT\frac{\partial S_l}{\partial s}\right)+C^i_{pg}M^i_gS_g$$

$$C_{Tu}=\left(T-T_r\right)\left(C_{pl}S_l\rho_l+C_{pv}S_g\rho_v+\sum_{j=1}^{N}C^j_{pg}S_g\rho^j_g\right)\mathbf{m}^T\mathbf{P}+LS_g\rho_v\mathbf{m}^T\mathbf{P} \tag{3.153}$$

$$K_{Tl}=-L\rho_l\frac{D_{atms}\nu_v\tau_v\theta_g}{\rho_l}\left(\rho_0\frac{\partial h}{\partial s}\right) \tag{3.154}$$

$$K_{TT}=\lambda_T-L\rho_l\frac{D_{atms}\nu_v\tau_v\theta_g}{\rho_l}\frac{\left(\nabla T\right)_a}{\left(\nabla T\right)}\left(h\frac{\partial \rho_0}{\partial t}+\rho_0\frac{\partial h}{\partial t}+\rho_0R\sum_{i=1}^{N}c^i_g\frac{\partial h}{\partial s}\right) \tag{3.155}$$

$$K^i_{Tg}=L\rho_l\frac{D_{atms}\nu_v\tau_v\theta_g}{\rho_l}\left(\rho_0RT\frac{\partial h}{\partial s}\right)+L\rho_vk_gRT \tag{3.156}$$

3.7 Deformation

An elasto-plastic constitutive model has been used to predict the deformation behaviour of soils. Initially developed by Alonso et al. (1990), the model is known as Barcelona Basic Model (BBM). The model and its formulation have been previously presented in the work of Thomas and He (1998), Cleall (1998), Mitchell (2002), Melhuish (2004), Seetharam (2003) and Vardon (2009). Therefore, a brief discussion on the model has been carried out in this work.

It has been assumed that deformation and therefore volume changes are a result of applied stress, suction and temperature changes. It has been suggested that the stress state of a soil in relation to volume change behaviour can be described by two independent stress-state parameters (Fredlund and Rahardjo, 1993). Alonso et al (1990) has assumed and used the two independent stress-state variables, net stress, σ'' and suction, *s*. The net stress can be defined as:

$$\sigma''=\sigma - u_g \tag{3.157}$$

where, σ has been defined as the total stress. Current formulation considers a positive sign convention for tensile stress (σ).

In case of a three-dimensional stress-state, the stress invariants which represent the volume change behaviour are the net mean stress, *p*, suction, *s*, with the deviatoric stress, *q*, utilised for the shear deformation behaviour. Therefore, the net mean stress in a system of three-dimensional stress-state can be expressed as:

$$p=\frac{\sigma_1''+\sigma_2''+\sigma_3''}{3} \tag{3.158}$$

And the deviatoric stress can be defined as:

$$q=\sqrt{1/2\left[\left(\sigma_1-\sigma_2\right)^2+\left(\sigma_2-\sigma_3\right)^2+\left(\sigma_3-\sigma_1\right)^2\right]} \tag{3.159}$$

Figure 3.1 represents a three dimensional block of soil element with incremental unit dimension under a system of stresses and forces which also includes two types of external forces, i) body forces acting through the centroid and ii) surface forces acting on the boundary surface of the element.

It has been assumed that the thermodynamic law of local equilibrium exists and the processes are occurring at such a rate that any local point can be described as being in equilibrium.

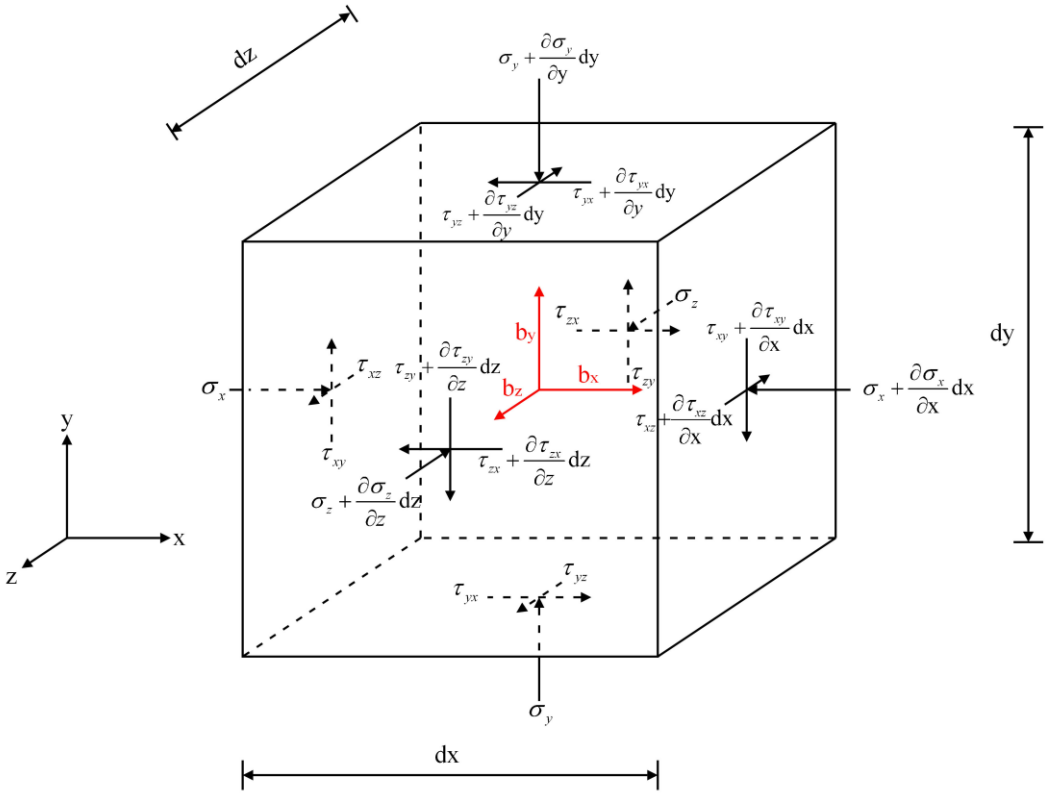

Figure 3.1: Stress and forces on a soil element of infinitesimal dimensions (*after* Fredlund and Rahardjo, 1993). "b" represents the body force.

In line with Newton's First Law and considering that the local equilibrium condition applies, the resultant of forces acting in any direction must be equal to zero. Therefore, along the x-axis it can be shown as:

$$\left(\sigma_x + \frac{\partial \sigma_x}{\partial x} dx\right) dydz + \left(\tau_{zx} + \frac{\partial \tau_{zx}}{\partial z} dz\right) dydx + \left(\tau_{yx} + \frac{\partial \tau_{yx}}{\partial y} dy\right) dxdz$$
$$-\sigma_x dydz - \tau_{zx} dxdy - \tau_{yx} dzdx + b_x dxdydz = 0 \tag{3.160}$$

Substituting equation (3.157) into equation (3.160) and rearranging yields:

$$\left[\frac{\partial \sigma''_x}{\partial x} - \frac{\partial u_g}{\partial x} + \frac{\partial \tau_{zx}}{\partial z} + \frac{\partial \tau_{xy}}{\partial y} + b_x\right] dxdydz = 0 \tag{3.161}$$

Since the term (*dxdydz*) is not equal to zero, equation (3.161) takes the form of:

$$\left[\frac{\partial \sigma''_x}{\partial x} - \frac{\partial u_g}{\partial x} + \frac{\partial \tau_{zx}}{\partial z} + \frac{\partial \tau_{yx}}{\partial y} + b_x\right] = 0 \tag{3.162}$$

Similarly, for y and z directions:

$$\left[\frac{\partial \sigma''_y}{\partial y} + \frac{\partial u_g}{\partial y} + \frac{\partial \tau_{xy}}{\partial x} + \frac{\partial \tau_{zy}}{\partial z} + b_y\right] = 0 \tag{3.163}$$

$$\left[\frac{\partial \sigma''_z}{\partial z} + \frac{\partial u_g}{\partial z} + \frac{\partial \tau_{yz}}{\partial y} + \frac{\partial \tau_{xz}}{\partial x} + b_z\right] = 0 \tag{3.164}$$

The principle of superposition can be applied to equations (3.162), (3.163) and (3.164) to obtain the incremental vector form as suggested by Thomas and He (1997) and Thomas and He (1998) as:

$$\mathbf{P}d\boldsymbol{\sigma}'' + \mathbf{Pm}du_g + d\mathbf{b} = 0 \tag{3.165}$$

where, "*d*" indicates the incremental form. The mechanical formulation has been formulated incrementally, i.e. from one stress step to the next. The total stresses are

then summed at the end of each time step. **b** is the vector of body forces, **P** is the strain matrix and **m** is an auxiliary vector defined in equation for three dimensional analysis:

$$\mathbf{P}=\begin{bmatrix} \frac{\partial}{\partial x} & 0 & 0 & \frac{\partial}{\partial z} & 0 & \frac{\partial}{\partial y} \\ 0 & \frac{\partial}{\partial z} & 0 & \frac{\partial}{\partial x} & \frac{\partial}{\partial y} & 0 \\ 0 & 0 & \frac{\partial}{\partial y} & 0 & \frac{\partial}{\partial z} & \frac{\partial}{\partial x} \end{bmatrix} \tag{3.166}$$

$$\mathbf{m}^T=\begin{bmatrix} 1 & 1 & 1 & 0 & 0 & 0 \end{bmatrix} \tag{3.167}$$

3.7.1 Elasto-plastic constitutive relationships

In case of elasto-plastic soils, the total strain vector, $\boldsymbol{\varepsilon}$ is considered as a product of both recoverable (elastic) and irrecoverable (plastic) strains. Mathematically, it can be expressed as:

$$d\boldsymbol{\varepsilon} = d\boldsymbol{\varepsilon}^e + d\boldsymbol{\varepsilon}^p \tag{3.168}$$

where, $d\boldsymbol{\varepsilon}^e$ is the incremental elastic strain vector and $d\boldsymbol{\varepsilon}^p$ is the incremental plastic strain vector.

To develop a constitutive elasto-plastid model a number of relationships are required which can be defined according to (Britto and Gunn, 1987; Owen and Hinton, 1980) as:

1. A constitutive elastic strain relationship,
2. A yield function which defines the yield surface in a stress space,
3. A flow rule which define the direction and magnitude of strains produced during the period of yielding, and
4. A hardening law which defines the relationship between plastic strain and material hardening.

3.7.1.1 Material behaviour under elastic condition

Alonso et al. (1988) and Thomas and He (1995) adopted the approach taken by Wang (1953) to address the incremental volumetric elastic strain vector which can be written as:

$$d\boldsymbol{\varepsilon}^e = d\boldsymbol{\varepsilon}_p^e + d\boldsymbol{\varepsilon}_s^e + d\boldsymbol{\varepsilon}_T^e \tag{3.169}$$

where, subscripts *p*, *s* and *T* represent vector components due to mean stress, suction and temperature respectively. A generalised Hooke's law has been used to describe the elastic stress-strain relationships as :

$$d\boldsymbol{\sigma}'' = \mathbf{D}\left(d\boldsymbol{\varepsilon} - d\boldsymbol{\varepsilon}^p - d\boldsymbol{\varepsilon}_s^e - d\boldsymbol{\varepsilon}_T^e\right) \tag{3.170}$$

where, $\mathbf{D}$ is the elasticity matrix.

It has been assumed that elastic deformation of unsaturated soil is due to changes in the net stress and the suction under isothermal conditions (Alonso et al., 1990). It has been considered that the suction changes are responsible for volumetric strains and at a constant suction the elastic deformation follows the unloading and reloading curves as demonstrated in Figure 3.2. where, υ is the specific volume. An idealised behaviour of this has been presented in Figure 3.3.

The slope of the idealised compression curve of virgins soils has a value of $-\lambda$ and the slope of the idealised recompression curve has a value of $-\kappa$. Alonso et al. (1990) has suggested that the change in specific volume, υ due to incremental stress change can be expressed as:

$$d\upsilon = -\kappa \frac{dp}{p} \tag{3.171}$$

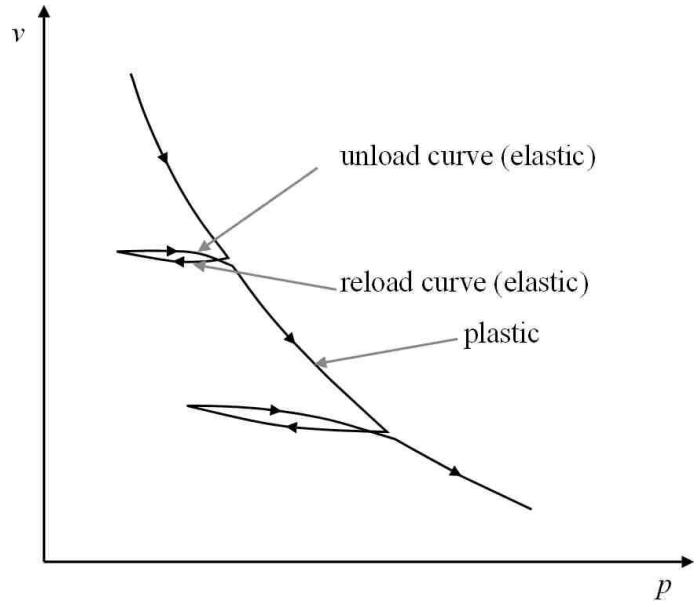

Figure 3.2: Characteristic isotopic compression and recompression curves (Cleall, 1998).

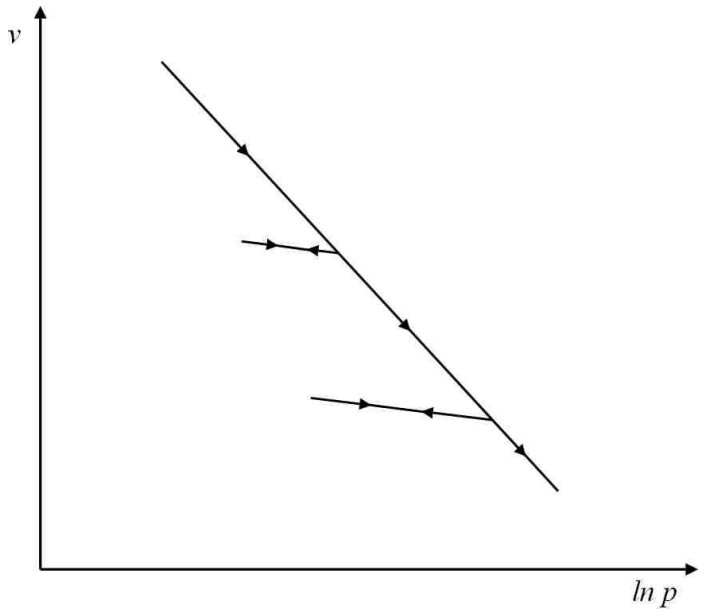

Figure 3.3: Idealised compression and recompression curves (Cleall, 1998).

With the help of equation (3.171), the scalar elastic volumetric strain due to net stress changes can be developed as:

$$d\varepsilon_p^e = \frac{d\upsilon}{\upsilon} = -\frac{\kappa}{\upsilon}\frac{dp}{p} \tag{3.172}$$

Alonso et al. (1990) also suggested that the change in specific volume due to suction change, υ_s at a given stress can be expressed as:

$$d\upsilon_s = -\kappa_s \frac{ds}{(s + p_{atms})} \tag{3.173}$$

where, κ_s is the slope of the volumetric suction curve, in their elastic region. Atmospheric pressure, p_{atms}, has been included to avoid infinite values of strain as suction approaches towards zero.

The elastic volumetric component of strain due to suction change can be expressed as:

$$d\boldsymbol{\varepsilon}_s^e = -\frac{\kappa_s}{\upsilon}\mathbf{m}\frac{ds}{(s + p_{atms})} = \boldsymbol{A}_s ds \tag{3.174}$$

and the suction vector, $\boldsymbol{A}_s$ can be defined as:

$$\boldsymbol{A}_s = -\frac{\kappa_s}{\upsilon(s + p_{atms})}\mathbf{m} \tag{3.174a}$$

The dependence of suction on temperature has been presented in section 3.2. Therefore, the strain component due to temperature should include contributions form both thermal expansion and suction change due to thermal expansion as suggested by Wang (1953) and which can be expressed as:

$$d\boldsymbol{\varepsilon}_T^e = \left(\mathbf{m}\frac{\alpha_T}{\upsilon_0}dT + \boldsymbol{A}_s\frac{\partial s}{\partial T}dT\right) = \left(\boldsymbol{A}_T + \boldsymbol{A}_s\frac{\partial s}{\partial T}\right)dT \tag{3.175}$$

and the thermal vector, $\boldsymbol{A_T}$ can be expressed as:

$$\boldsymbol{A_T} = \mathbf{m}\frac{\alpha_T}{\upsilon_0} \tag{3.175a}$$

where, α_T is the coefficient of thermal expansion and υ_0 is the initial specific volume. The incremental deviatoric strain component, caused by changes in deviatoric stress has been described by Wood (1990) as:

$$d\varepsilon_q^e = \frac{1}{3G}dq \tag{3.176}$$

where, q is the deviatoric stress and G is the shear modulus.

3.7.1.2 Yield function

The yield criteria determine the consequence when material starts to yield. In the BBM, Alonso et al. (1990) has used two yield functions, the load collapse (LC) curve function F_1 and the suction increase (SI) curve function F_2. The LC curve specifies that yielding occurs when stress reaches a critical value. In this case, the critical value is the preconsolidation stress P_0. The SI curve indicates the process of yielding when suction reaches a critical value, s_0. At uniform suction, the LC curve function, F for three-dimensional consolidation can be presented as:

$$F(p, p_0) = p - p_0 = 0 \tag{3.177}$$

The preconsolidation stress is a function of suction (Vardon, 2009). The collapse and swelling behaviour of the soil during wetting and drying processes can be obtained using the following relationship (as detailed in the Figure 3.4):

$$\left(\frac{p_0}{p_c}\right) = \left(\frac{p_0^*}{p_c}\right)^{\left(\frac{\lambda(0)-\kappa}{\lambda(s)-\kappa}\right)} \tag{3.178}$$

where p_0^* is the effective preconsolidation stress of a saturated soil, p_c is a reference stress, $\lambda(s)$ is the stiffness parameter for changes in net mean stress for virgin states of the soil and $\lambda(0)$ is the stiffness parameter for changes in net mean stress for the virgin state of soil at saturation. For virgin soil, an asymptotic expression predicting, $\lambda(s)$, has been proposed by Alonso et al. (1990) as:

$$\lambda(s) = \lambda(0)\left[(1-r)e^{(-\beta s)} + r\right] \tag{3.179}$$

where, r controls the maximum stiffness of the soil and β controls the rate of increase of stiffness with suction. Alonso et al. (1990) extended the model by including the tri-axial stress states and proposed the following LC yield function, shown in Figure 3.5. The yield surface is also valid for three-dimensional stress conditions due to the stress-states p and q are invariants in both tri-axial and three-dimensional stress conditions and this can be expressed as:

$$F_1(p, q, s, p_0^*) = q^2 - M^2(p + p_s)(p - p_0) = 0 \tag{3.180}$$

where, p_s is a parameter to describe the change of soil cohesion with suction, M is the slope of critical state line. If the cohesion of soils increases linearly with suction, the parameter, $p_{s,}$ can be described as:

$$p_s = ks \tag{3.181}$$

where, k is a constant.

The SI yield function represents that the process of yielding occurs when suction reaches a critical value, s_0, which is the previously obtained maximum value of suction and remains parallel to the q-axis when $q>0$. It has been shown graphically on Figure 3.5 and mathematically it has been proposed by Alonso et al. (1990) as:

$$F_2(s, s_0) = s - s_0 = 0 \tag{3.182}$$

3.7.1.3 Flow rule

In order to obtain the relationship between the plastic strain component and the stress increment, it is assumed that the plastic strain is proportional to the outward normal of a plastic potential function. This theoretical assumption is known as flow rule. Alonso et al. (1990) proposed an associated SI plastic flow rule for the SI yield surface and a non-associated plastic flow rule for the LC yield surface. It has been reported that the conventional critical stress models often overestimate K_0 (Gens and Potts, 1982). Therefore, Alonso et al. (1990) proposed a new parameter, α_q.

Thomas and He (1998) proposed the use of plastic potential for LC yield surface *Q1* (non-associated flow rule) and SI yield surface for *Q2* (associated flow rule) as:

$$Q_1 = \alpha_q q^2 - M^2 \left(p + p_s \right)\left(p_0 - p \right) \tag{3.183}$$

$$Q_2 = s - s_0 \tag{3.184}$$

where, Q_1 and Q_2 are the plastic potentials related to the LC and SI flow rules respectively. α_q is a constant derived from K_0, the at rest stress state, when no lateral deformations takes place . Jaky (1948) has suggested this pressure coefficient as:

$$K_0 = \frac{6 - 2M}{6 + M} \tag{3.185}$$

If elastic strain increment approaches to zero, α_q can be defined according to Alonso et al. (1990) as:

$$\alpha_q = \frac{M(M-9)(M-3)}{6(6-M)} \frac{1}{\left(1 - \frac{\kappa}{\lambda(0)}\right)} \tag{3.186}$$

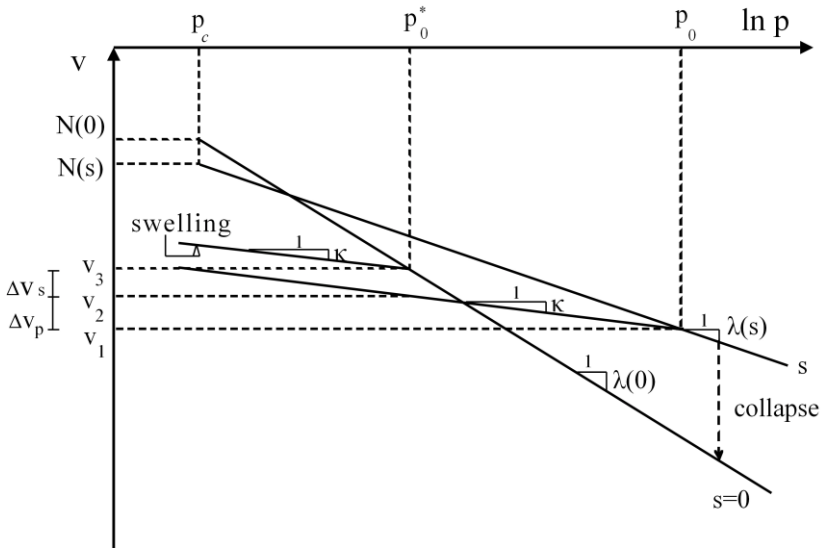

Figure 3.4: Compression curve for saturated and unsaturated soil (*after* Alonso et al., 1990).

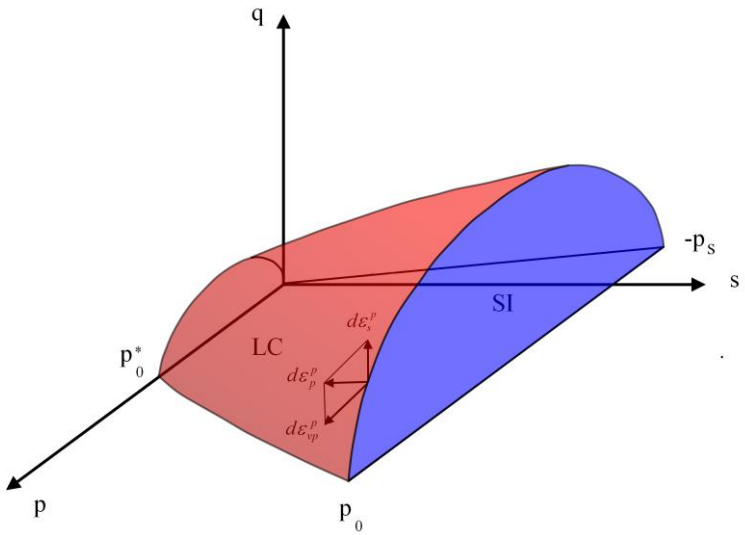

Figure 3.5: Three dimensional view of yield surface in p,q,s stress space (*after* Alonso et al., 1990) where blue represents SI curve and the red for LC curve.

By dividing the plastic strain increment into components due to net stress changes and suction changes while considering that the strain increment is proportional to the stress gradient of the plastic potential results into:

$$d\boldsymbol{\varepsilon}^{p} = \chi_1 \frac{dQ_1}{d\boldsymbol{\sigma}''} + \chi_2 \mathbf{m} \frac{dQ_2}{ds} \tag{3.187}$$

where, χ_1 and χ_2 plastic multipliers defined by Alonso et al. (1990).

The plastic strain increment for changes in stress conditions can be divided into volumetric and deviatoric components. The volumetric plastic strain component associated with the LC yield surface, F_1 which is the load collapse (LC) yield function, can be expressed as:

$$d\varepsilon_p^p = \chi_1 \frac{\partial Q_1}{\partial p} = \chi_1 M^2 (2p + p_s - p_0) \tag{3.188}$$

where, ε_p^p is the volumetric plastic strain component associated with the LC yield surface. The deviatoric strain, ε_q^p can be written as:

$$d\varepsilon_q^p = \chi_1 \frac{\partial Q_1}{\partial q} = \chi_1 2\alpha_q q \tag{3.189}$$

The volumetric plastic strain (ε_s^p) increment associated with the SI yield surface, F_2 is:

$$d\varepsilon_s^p = \chi_2 \frac{\partial Q_2}{\partial s} = \chi_2 \tag{3.190}$$

3.7.1.4 Hardening laws

During the process of plastic deformation, strain hardening takes place. Followed by yielding, the stress level at which further plastic deformation might occur depends on the amount of plastic strain which is available. Josa et al. (1987) found that the process of coupling exist between the hardening of two yield surfaces. The yield surfaces are controlled by the hardening parameters, p_0^* and s_0 and depend on the plastic volumetric strain increment which can be defined as:

$$d\varepsilon_v^p = d\varepsilon_p^p + d\varepsilon_s^p \tag{3.191}$$

where, $d\varepsilon_v^p$ is the volumetric strain increment.

Alonso et al. (1990) gave the hardening laws for yield surfaces F_1 and F_2 as:

$$\frac{dp_0^*}{p_0^*} = \frac{\upsilon}{\lambda(0)-\kappa} d\varepsilon_v^p \tag{3.192}$$

$$\frac{ds_0}{s_0} = \frac{\upsilon}{\lambda_s - \kappa_s} d\varepsilon_v^p \tag{3.193}$$

where, λ_s is the stiffness parameter for changes in suction for virgin soil states.

3.7.2 Governing Equation for deformation

It has been showed previously that the elastic stress-strain relationships can be obtained with the help of incremental elastic constitutive matrix **D**. The elastic matrix is able to envisage the change in stress in relation to change in strain due to the applied load. Meanwhile, if the matrix was developed during the incident of plastic deformation, it might overestimate the change in stresses. Therefore, it should be modified to consider the incident of plastic deformation. Following the approach taken by Owen and Hinton (1980) the constitutive incremental elasto-plastic stress-strain relationship can be expressed as:

$$d\boldsymbol{\sigma}''=\mathbf{D}_{\mathbf{ep}}d\boldsymbol{\varepsilon}^{p} \tag{3.194}$$

Mitchell (2002) has defined the elasto-plastic stress-strain matrix $\mathbf{D_{ep}}$ as:

$$\mathbf{D}_{\mathbf{ep}}=\mathbf{D}-\frac{\mathbf{D}\dfrac{\partial Q_1}{\partial\boldsymbol{\sigma}''}\dfrac{\partial F_1}{\partial\boldsymbol{\sigma}''}\mathbf{D}}{\mathbf{A}_{\mathbf{p}}+\left(\dfrac{\partial Q_1}{\partial\boldsymbol{\sigma}''}\right)^{T}\mathbf{D}\dfrac{\partial F_1}{\partial\boldsymbol{\sigma}''}} \tag{3.195}$$

Where, $\mathbf{A_P}$ is the plastic modulus which can be defined as:

$$\mathbf{A}_{\mathbf{P}}=M^{2}\left(p+p_s\right)\mathbf{m}\frac{\lambda(0)-\kappa}{\lambda(s)-\kappa}p_0\frac{\upsilon}{\lambda(0)-\kappa}\left(M^{2}\left(2p+p_s-p_0\right)\right) \tag{3.196}$$

The elastic form of stress-strain relationship expressed in equation (3.194) can be adopted for elasto-plastic behaviour as follows:

$$d\boldsymbol{\sigma}''=\mathbf{D}_{\mathbf{ep}}\left(d\boldsymbol{\varepsilon}-d\boldsymbol{\varepsilon}_s^{e}-d\boldsymbol{\varepsilon}_T^{e}-d\boldsymbol{\varepsilon}_s^{p}\right) \tag{3.197}$$

Substituting equation (3.174) and equation (3.175) into equation (3.197) gives:

$$d\boldsymbol{\sigma}''=\mathbf{D}_{\mathbf{ep}}\left(d\boldsymbol{\varepsilon}-\boldsymbol{A}_{\mathbf{s}}ds-\left(\boldsymbol{A}_{\boldsymbol{T}}+\boldsymbol{A}_{\mathbf{s}}\frac{\partial s}{\partial T}\right)dT-d\boldsymbol{\varepsilon}_s^{p}\right) \tag{3.198}$$

The term $d\boldsymbol{\varepsilon}$ can be expressed as $\mathbf{P}^{T}d\mathbf{u}$ and using equation (3.22), ds can be presented as $\left(du_g-du_l\right)$.Rewriting the stress equilibrium equation (3.165) with substitution from equation (3.198) gives:

$$\mathbf{P}\left(\mathbf{D}_{\mathbf{ep}}\left(\mathbf{P}^{\mathrm{T}}d\mathbf{u}+\boldsymbol{A}_{\mathbf{s}}du_l-\left(\boldsymbol{A}_{\boldsymbol{T}}+\boldsymbol{A}_{\mathbf{s}}\frac{\partial s}{\partial T}\right)dT-\boldsymbol{A}_{\mathbf{s}}du_g-d\boldsymbol{\varepsilon}_s^{p}\right)\right)+\mathbf{P}\mathbf{m}du_g+d\mathbf{b}=0 \tag{3.199}$$

Substituting equation (3.23) for the term "u_g" and rearranging the similar terms, the governing equation can be written in concise form as:

$$\boldsymbol{C}_{\mathbf{u}l}du_l + \boldsymbol{C}_{\mathbf{u}T}dT + \boldsymbol{C}_{\mathbf{u}c_g^i}d\sum_{i=1}^{N}c_g^i + \boldsymbol{C}_{\mathbf{uu}}d\mathbf{u} - \mathbf{PD}_{\mathbf{ep}}d\varepsilon_s^p + d\mathbf{b} = 0 \tag{3.200}$$

where, i = *1,2,……,N* number of gas components. the coefficients of equation (3.200) can be presented as follows:

$$\boldsymbol{C}_{\mathbf{u}l} = \mathbf{PD}_{\mathbf{ep}}\boldsymbol{A}_s \tag{3.201}$$

$$\boldsymbol{C}_{\mathbf{u}T} = \mathbf{PD}_{\mathbf{ep}}\left(-\boldsymbol{A}_T - \boldsymbol{A}_s\frac{\partial s}{\partial T}\right) \tag{3.202}$$

$$\boldsymbol{C}_{\mathbf{u}c_g^i} = \left(-\mathbf{PD}_{\mathbf{ep}}\boldsymbol{A}_s + \mathbf{Pm}\right)RT \tag{3.203}$$

$$C_{\mathbf{uu}} = \mathbf{PD}_{\mathbf{ep}}\mathbf{P}^{\mathrm{T}} \tag{3.204}$$

3.8 Conclusion

In this chapter, the theoretical development of coupled Thermal-Hydraulic-Chemical-Gas-Mechanical model has been presented in details. The governing equations are based upon the law of mass conservation for moisture flow, dissolved chemical flow and pore gas flow while the law of conservation of energy has been considered for heat flow. The previously developed coupled Thermo-Hydro-Chemical-Mechanical model has been extended by implementing the multicomponent reactive gas transport. Multicomponent advective and diffusive gas flow have been characterised using Darcy's law and Fick's law respectively. The vapour phase has been considered with the liquid water phase in the governing equation of moisture flow. The sink/source term of governing pore gas flow and dissolved chemical flow equation has been calculated using a geochemical model. At equilibrium condition, chemical reactions have been considered for various geochemical processes, such as gas-liquid equilibrium, ion exchange, surface complexation, dissolution and/or precipitation of minerals, redox reactions etc. The formulation has been developed for both isothermal and non-isothermal condition although isothermal condition has been prioritised over non-isothermal condition in this study. The governing equations for moisture flow, multicomponent pore gas flow, multicomponent dissolved chemical flow, heat flow and deformations have been presented in terms of primary variables, such as porewater pressure (u_l), temperature (T), pore gas concentration (c_g^i), dissolved chemical concentration (c_d^j) and deformation ($\mathbf{u}$). *i* and *j* varies from a single component to *N* and *M* number of gas components and dissolved components respectively. The governing equations of coupled Thermo-Hydro-Chemical-gas-Mechanical model have been summarised below:

Moisture flow:

$$C_{ll}\frac{\partial u_l}{\partial t}+C_{lT}\frac{\partial T}{\partial t}+\sum_{i=1}^{N}C_{lc_g^i}\frac{\partial c_g^i}{\partial t}+C_{l\mathbf{u}}\frac{\partial \mathbf{u}}{\partial t}=\nabla\left[K_{ll}\nabla u_l\right]$$
$$+\nabla\left[K_{lT}\nabla T\right]+\nabla\left[\sum_{i=1}^{N}K_{lc_g^i}\nabla c_g^i\right]+J_l$$

Multicomponent gas flow:

$$C^i_{c_g l}\frac{\partial u_l}{\partial t}+C^i_{c_g T}\frac{\partial T}{\partial t}+C^i_{c^i_g c^i_g}\frac{\partial c_{\mathrm{g}}{}^i}{\partial t}+C^i_{c^i_g c^j_g}\sum_{j=1}^{N(i\neq j)}\frac{\partial c_{\mathrm{g}}{}^j}{\partial t}+C^i_{c_g s_g}\frac{\partial s^i_s}{\partial t}+C^i_{c_g \mathbf{u}}\frac{\partial \mathbf{u}}{\partial t}$$
$$=\nabla\left[K^i_{c^i_g c^j_g}\sum_{j=1}^{N}\nabla c_g{}^j\right]+\nabla\left[\sum_{j=1}^{N}\left(K_{c^i_g c^j_g}\nabla c_g{}^j\right)\right]+\nabla\left[K^i_{c_g T}\nabla T\right]$$

Multicomponent dissolved chemical flow:

$$C^i_{c_d l}\frac{\partial u_l}{\partial t}+C^i_{c_d T}\frac{\partial T}{\partial t}+C^i_{c^i_d c^j_g}\sum_{j=1}^{N}\frac{\partial c_g{}^j}{\partial t}+C^i_{c_d c_d}\frac{\partial c^i_d}{\partial t}+C^i_{c_d \mathbf{u}}\frac{\partial \mathbf{u}}{\partial t}+C^i_{c_d s_d}\frac{\partial s^i_s}{\partial t}$$
$$=\nabla\left[K^i_{c_d l}\nabla u_l\right]+\nabla\left[K^i_{c_d c_d}\nabla c^i_d\right]+J^i_Z$$

Heat transfer:

$$C_{Tl}\frac{\partial u_l}{\partial t}+C_{TT}\frac{\partial T}{\partial t}+\sum_{i=1}^{N}C^i_{Tc_g}\frac{\partial c^i_g}{\partial t}+C_{T\mathbf{u}}\frac{\partial \mathbf{u}}{\partial t}=\nabla\left[K_{Tl}\nabla u_l\right]+\nabla\left[K_{TT}\nabla T\right]+\nabla\left[\sum_{i=1}^{N}K^i_{Tc_g}\nabla c^i_g\right]$$

Deformation:

$$\boldsymbol{C}_{\mathbf{u}l}du_l+\boldsymbol{C}_{\mathbf{u}T}dT+\boldsymbol{C}_{\mathbf{u}c^i_g}d\sum_{i=1}^{N}c^i_g+\boldsymbol{C}_{\mathbf{uu}}d\mathbf{u}-\mathbf{PD}_{\mathbf{ep}}d\varepsilon^p_s+d\mathbf{b}=0$$

References:

Alonso, E.E., Battle, F., Gens, A., Lloret, A., (1988). "Consolidation analysis of partially saturated soils- Application to earthdam construction". Numerical Methods in Geomechanics (Innsbruck 1988), pp. 1303-1308.

Alonso, E.E., Gens, A., Josa, A., (1990). "A constitutive model for partially saturated soils", *Geotechnique* **40**, No. 3, pp. 405-430.

Appelo, C.A.J., Postma, D. (2005). "*Geochemistry, Groundwater and Pollution"*. A.A. Balkema, Rotterdam.

Bird, R.B., Stewart, W.E., Lightfoot, E.N., (1960). "Transport Phenomena". John Wiley & Sons, New York.

Britto, A.M., Gunn, M.G., (1987). "Critical State Soil Mechanics via Finite Elements". Ellis Horwood Ltd., Chichester.

Carman, P.C., (1956). "Flow of gases through porous media". Butterworths Scientific Publications, London.

Childs, E.C., (1969). "An introduction to the physical basis of the soil water phenomena".

Cleall, P.J., (1998) "An investigation of the thermo/hydraulic/mechanical behaviour of unsaturated soils, including expansive clays". PhD Thesis, University of Wales, Cardiff.

Crank, J., (1975). "The Mathematics of Diffusion". Second Edition, Clarendon, Oxford.

Cunningham, R.E., Williams, R.J.J., (1980). "Diffusion in Gases and Porous Media". Plenum Press, New York.

Cussler, E.L., (1984). "Diffusion: Mass Transfer in Fluid Systems". Cambridge University Press, Cambridge.

Darcy, H., (1856). "Les fontaines publiques de la ville de Dijon", V. Dalmont, Paris, pp. 590-594.

Denbigh, K.G., (1981). "The Principles of Chemical Equilibrium". Fourth Edition, Cambridge University Press, New York.

de Vries, D.A., (1958). "Simultaneous transfer of heat and moisture in porous media". *Transactions American Geophysical Union* **39**, No. 5, pp. 909-916.

Diestel, H., (1976). "Model experiments on salt displacement mechanisms in unsaturated porous media under temperature gradients". System simulation in water resources, ed. G.C. Vansteenkiste, North-Holland publishing company, pp. 315-328.

Edelfsen, N.E., Andersen, A.B.C., (1943). "Thermodynamics of soil moisture". *Hiigardia* **15**, No. 2, pp. 31-298.

Ewen, J., Thomas, H.R., (1989). "Heating unsaturated medium sand". *Geotechnique* **39**, No. 3, pp. 455-470.

Fredlund, D.G., Rahardjo, H., (1993). "Soil Mechanics for Unsaturated Soils". John Wiley, New York.

Fredlund, D.G., (1991). "Seepage in saturated soils. Panel Discussion : Ground water and seepage problems". *Proceedings of the 10th International Conference on Soil Mechanics and Foundation Engineering*, Stockholm, **4**, pp. 629-641.

Garrels, R.M., Christ, C.L., (1965). "Solutions, Minerals and Equilibria". Harper and Row, New York, pp 450.

Gens, A., Potts, D.M., (1982). "Application of critical state models to the prediction of the behaviour of a normally consolidated low plasticity clay". *Proceedings of the 1st International Symposium on Numerical Modelling and Geomechanics*, Zurich, pp. 312-323.

Ho, C., Webb, S., (2006). "Gas Transport in Porous Media". Springer, AA Dordrecht, The Netherlands.

Jakob, M., (1949). "Heat Transfer: Vol 1", Wiley, New York.

Jaky, J., (1948). "Pressure in soils". *Proceedings of the 2nd International Conference on Soil Mechanics and Foundation Engineering*, **1**, pp. 103-107.

Josa, A., Alonso, E.E., Lloret, A., Gens, A., (1987). "Stress-strain behaviour of partially saturated soils". *Proceedings of the 9th European Conference on Soil Mechanics and Foundation Engineering*, Dublin, **2**, pp. 561-564.

Kaye, G.W.C., Laby, T.M., (1973). "Tables of Physical and Chemical Constants". Fourteenth Edition, Harlow, Longman.

Krischer, D., Rohnalter, H., (1940). "Warmeleitung und Dampfdiffusion in feutchen Gutern". Verein Duet, Ing-Forschungsheft, pp. 402.

Langmuir, D., (1997). "Aqueous Environmental Geochemistry".Prentice-Hall, Englewood Cliffs, pp. 600.

Lasaga, A.C. (1998). "Kinetic Theory in the Earth Sciences". Princeton Series in Geochemistry, Princeton University Press.

Lloret, A., Alonso, E.E., (1980). "Consolidation of unsaturated soils including swelling and collapse behaviour". *Geotechnique* **30**, No. 4, pp. 449-477.

Mangold, D.C., Tsang, C.F., (1991). "A summary of subsurface hydrological and hydrochemical models". *Review of Geophysics* **29**, No. 1, pp. 51-79.

Matayas, E.L., Radhakrishna, H.S., (1968). "Volume change characteristics of partially saturated soils". *Geotechnique* **18**, No. 4, pp. 432-448.

Massmann, J., Farrier, D.F., (1992). "Effects of atmospheric pressures on gas transport in the vadose zone". *Water Resources Research* **28**, No. 3, pp. 777–791.

Mason, E.A., Malinauskas, A.P., (1964). "Gaseous diffusion in porous media. IV. Thermal diffusion". *Journal of Chemical Physics* **41**, pp. 3815.

Melhuish, T.A., (2004) "An investigation of the three-dimensional thermo/hydro/mechanical behaviour of large scale in-situ experiments". PhD Thesis, Cardiff University, UK.

Millington, R.J., Quirk, J.M., (1961). "Permeability of porous solids". *Transactions of Faraday Society* **57**, pp. 1200–1207.

Mitchell, J.K., Soga, K., (2005). "Fundamentals of soil behaviour". Third Edition. John Wiley & Sons, Inc., Hoboken, New Jersey.

Mitchell, H.P., (2002). "An investigation into the thermo/hydro/mechanical interactions involved in high level nuclear waste disposal". PhD thesis. University of Wales, Cardiff.

Mitchell, J.K., (1993). "Fundamentals of soil behaviour". John Wiley, New York.

Nielson, D.R., Van Genuchen, M., Biggar, J.W., (1986). "Water flow and transport processes in the unsaturated zone". *Water Resources Research* **22**, No. 9, pp. 89s-108s.

Olson, R.E., (1963). "Effective stress theory of compaction". *Proceedings of the American Society of Civil Engineering* **81**, pp. 27-44.

Owen, D.R.J., Hinton, E., (1980). "Finite elements in plasticity: Theory and practice". Pineridge Press Ltd., Swansea.

Parker, J.C., Lenhard, R.J., Kuppusamy, T., (1987). "A Parametric Model for Constitutive Properties Governing Multiphase Flow in Porous Media". *Water Resources Research* **23**, No. 4, pp. 618–624.

Parkhurst, D.L., Appelo, C.A.J., (1999). "User's Guide to PHREEQC (version 2)". U.S. Geological Survey, Water Resource Investigation Report, pp. 99-4259.

Partington, J.R., de Vries, D.A., (1957). "Moisture movement in porous materials under temperature gradients". *Transactions American Geophysical Union* **38**, No. 2, pp. 222-232.

Philip J.R., and de Vries D.A., (1957). "Moisture movements in porous materials under temperature gradients". *Transactions American Geophysical Union* **38**, No 2, pp. 222-232.

Preece, R.J., (1975). "The measurement and calculation of physical properties of cable bedding sands. Part 2; specific thermal capacity, thermal conductivity and temperature ratio across 'air' filled pores", *C.E.G.B. Laboratory Note N.*, RD/L/N 231/74.

Reid, R.C., Praunsnitz, J.M., Bruce, E.P., (1987). "The properties of gases and liquids". Fourth Edition, McGraw-Hill, New York.

Rowe, R.K., Booker, J.R. (1986). "A finite layer technique for calculating three dimensional pollutant migration in soil", *Geotechnique* **36**, No. 2, pp. 205-214.

Seetharam, S. C., (2003). "An investigation of the thermo/hydro/chemical/mechanical behaviour of unsaturated soils". PhD Thesis, Cardiff school of Engineering, Cardiff University, UK.

Sedighi, M., (2011). "An investigation of Hydro-geochemical processes in coupled thermal, hydraulic, chemical and mechanical behaviour of unsaturated soils". PhD Thesis, Cardiff University, UK.

Sharma, H.D., Reddy, K.R., (2004). "Geoenvironmental Engineering". John Wiley & Sons, Inc., Hoboken, New Jersey.

Siddiqua, S., (2008). "An investigation of the influence of elevated temperatures on the thermal-hydraulic-mechanical response of unsaturated soils". PhD Thesis, Cardiff University, UK.

Singh, R.M., (2007). "An experimental and numerical investigation of heat and mass movement in unsaturated clays". PhD Thesis, Cardiff University, UK.

Taylor, R., Krishna, R., (1993). "Multicomponent Mass Transfer". Wiley, New York.

Thomas, H.R., He, Y., (1998) "Modelling the behaviour of unsaturated soil using an elasto plastic constitutive relationship". *Geotechnique* **48**, pp. 589-603.

Thomas, H.R., Cleall, P.J., Chandler, N., Dixon, D., Mitchell, H.P., (2003). "Water infiltration into a large-scale in-situ experiment in an underground research laboratory". *Geotechnique* **53**, No. 2, pp. 207-224.

Thomas, H.R., He, Y., (1995). "Analysis of coupled heat, moisture and air transfer in a deformable unsaturated soil". *Geotechnique* **45**, No. 4, pp. 677-689.

Thomas, H.R., He, Y., (1997). "A coupled heat-moisture theory for deformable unsaturated soil and its algorithmic implementation". *International Journal For Numerical Methods In Engineering* **40**, pp. 3421-3441.

Thomas, H.R., King, S.D., (1991). "Coupled temperature/capillary potential variations in unsaturated soil". *Journal of Engineering Mechanics, American Society of Civil Engineers* **117**, No. 11, pp. 2475-2491.

Thorstenson, D.C., Pollock, D.W., (1989). "Gas Transport in Unsaturated Zones: Multicomponent Systems and the Adequacy of Fick's Laws". *Water Resources Research* **25**, pp. 477–507.

Vardon, P.J., (2009). "A three-dimensional numerical investigation of the thermo-hydro-mechanical behaviour of a large-scale prototype repository". PhD Thesis, Cardiff University, UK.

Wang, C., (1953). "Applied Elasticity". McGraw-Hill Book Co.

Wood, D.M., (1990). "Soil behaviour and critical state soil mechanics". Cambridge University Press, Cambridge.

Yong, R.N., Mohamed, A.M.O., Warkentin, B.P., (1992). "Principles of contaminant transport in soils". Elsevier Pub. Amsterdam.

4

Numerical formulations

4.1 Introduction

In this chapter, the numerical formulation of the governing equations for the coupled thermal-hydraulic-chemical-gas-mechanical behaviour has been presented. To achieve a solution to the theoretical formulation presented in last chapter, finite element and finite difference methods have been used. A sequential non-iterative approach has also been implemented in order to couple the geochemical reaction formulation with the transport model.

The numerical formulation of the coupled heat, moisture and deformation has already been presented by Ramesh (1996), Cleall (1998), Seetharam (2003), Vardon (2009). The numerical formulation for dissolved chemical transport has also been presented by Hashm (1999), Seetharam (2003) and Sedighi (2011). In this work the numerical formulation of multicomponent reactive transport of gas chemicals has been developed. The numerical formulations of heat, moisture, dissolved chemical and deformation behaviour have been included in this chapter for the sake of completeness.

Section 4.2 deals with the spatial discretisation method adopted to solve the flow and deformation equations via a finite element approach. The well recognised Galerkin weighted residual approach has been used to carry out the discretisation. Section 4.3 deals with the matrix representation of the flow variables and temporal discretisation of the governing equations. A fully implicit backward difference mid-interval time-stepping algorithm has been used in this work. Section 4.4 explains the coupling between transport and geochemical reactions. An overall conclusion of this chapter has been presented in section 4.5.

4.2 Spatial discretisation of flow and deformation variables

The 'Galerkin weighted residual method' has been adopted in this work to obtain the finite element solutions of the theoretical formulation. This method is a widely accepted tool for spatial discretisation in numerical technique. The method has been well documented and broadly discussed in the literature (Zienkiewicz and Taylor, 1989; Zienkiewicz and Taylor, 2000). Thomas and co-workers (Thomas and He, 1995; Thomas et al., 1998; Cleall, 1998; Seetharam, 2003; Vardon, 2009; Sedighi, 2011) have successfully used this approach for coupled flow and deformation equations. The approach has been used in this work to extend the model for multicomponent gas transport. Therefore, the method has been presented briefly within the scope of work.

The primary variables and their derivatives can be approximated using shape functions as:

$$\varphi \approx \hat{\varphi} = \sum_{s=1}^{n} N_s \hat{\varphi}_s \tag{4.1}$$

and,

$$\nabla\hat{\varphi} = \sum_{s=1}^{n} (\nabla N_s)\hat{\varphi}_s \tag{4.2}$$

where, φ represents any one of the primary variables (u_l, T, c_g^i, c_d^i and **u**), N_s is the shape function expressed in term of independent variables, such as coordinates *x, y, z* etc. The subscript, s represents the nodal points, the symbol, $\hat{}$ indicates an approximated form and *n* is the number of nodes in an element.

As the approximated form is not the exact solution of equation (4.1), it contains a residual error which can be expressed as:

$$R = \varphi - \hat{\varphi} \tag{4.3}$$

where, R is the residual error.

4.2.1 Multicomponent gas transport for a single gas species

In this section, the derivation of the multicomponent gas transport differential equation has been presented. The formulation has been developed for a single gas species. As the derivation process remains similar for any component of a multi-gas system, it has not been repeated for *n* number of components.

The governing equation of multicomponent pore gas, equation (3.90) can be expressed in the approximate form for a single gas component and isothermal condition as:

$$\begin{aligned} &-C^1_{c_g l}\frac{\partial \hat{u}_l}{\partial t} - C^1_{c_g T}\frac{\partial \hat{T}}{\partial t} - C^1_{c^1_g c^1_g}\frac{\partial \hat{c}^1_g}{\partial t} - C^1_{c_g s_g}\frac{\partial \hat{s}^1_s}{\partial t} \\ &-C^1_{c_g \mathbf{u}}\frac{\partial \hat{\mathbf{u}}}{\partial t} + \nabla\left[K^1_{c^1_g c^1_g}\nabla \hat{c}^1_{c_g}\right] = R \end{aligned} \tag{4.4}$$

By considering the weights similar to the shape functions, the integral of weighted residual over the domain, Ω, of the element should be zero.

$$\int_{\Omega^e} N_r R_\Omega d\Omega^e = 0 \tag{4.5}$$

Substituting equation (4.4) into equation (4.5) yields:

$$\int_{\Omega^e} N_r \begin{bmatrix} -C^1_{c_g l}\dfrac{\partial \hat{u}_l}{\partial t} - C^1_{c_g T}\dfrac{\partial \hat{T}}{\partial t} - C^1_{c^1_g c^1_g}\dfrac{\partial \hat{c}^1_g}{\partial t} - C^1_{c_g s_g}\dfrac{\partial \hat{s}^1_g}{\partial t} \\ -C^1_{c_g u}\dfrac{\partial \hat{u}}{\partial t} + \nabla\left[K^1_{c^1_g c^1_g}\nabla \hat{c}^1_{c_g}\right] \end{bmatrix} d\Omega^e = 0 \tag{4.6}$$

Using the theory of integration by parts, the 'weak form' of the equation (4.6) can be attained. The weak forms can be attained by multiplying the equation set by an appropriate arbitrarily chosen function which has same free indices of the actual equation (Zienkiewicz and Taylor, 2000). The 6th term of equation (4.6) can be expanded as:

$$\int_{\Omega^e} N_r \left[\nabla \left(K^1_{c_g c_g} \nabla \hat{c}^1_{c_g} \right) \right] d\Omega^e = \int_{\Omega^e} \nabla \left[N_r K^1_{c_g^1 c_g^1} \nabla \hat{c}^1_{c_g} \right] d\Omega^e - \int_{\Omega^e} K^1_{c_g^1 c_g^1} \nabla \hat{c}^1_{c_g} \nabla N_r d\Omega^e \tag{4.7}$$

Substituting the 'weak forms' into equation (4.6) yields:

$$\int_{\Omega^e} \left[\begin{array}{l} \nabla \left(N_r K^1_{c_g^1 c_g^1} \nabla \hat{c}^1_{c_g} \right) - K^1_{c_g^1 c_g^1} \nabla \hat{c}^1_{c_g} \nabla N_r \\ + N_r \left[-C^1_{c_g l} \dfrac{\partial \hat{u}_l}{\partial t} - C^1_{c_g T} \dfrac{\partial \hat{T}}{\partial t} - C^1_{c_g^1 c_g^1} \dfrac{\partial \hat{c}^1_{c_g}}{\partial t} - C^1_{c_g s_g} \dfrac{\partial \hat{s}^1_{c_g}}{\partial t} - C^1_{c_g \mathbf{u}} \dfrac{\partial \hat{\mathbf{u}}}{\partial t} \right] \end{array} \right] d\Omega^e = 0 \tag{4.8}$$

Using the Gauss-Green Divergence theorem, the second order differential terms can be reduced to first orders and surface integrals can be related to boundary integrals. On adjacent elements, the surface integrals cancel each other and leave a single contribution on the domain boundary. By applying the divergence theorem and rearranging the terms equation (4.8) yields:

$$\int_{\Omega^e} \left[\begin{array}{l} -K^1_{c_g^1 c_g^1} \nabla \hat{c}^1_{c_g} \nabla N_r \\ + N_r \left[-C^1_{c_g l} \dfrac{\partial \hat{u}_l}{\partial t} - C^1_{c_g T} \dfrac{\partial \hat{T}}{\partial t} - C^1_{c_g^1 c_g^1} \dfrac{\partial \hat{c}^1_{c_g}}{\partial t} - C^1_{c_g s_g} \dfrac{\partial \hat{s}^1_{c_g}}{\partial t} - C^1_{c_g \mathbf{u}} \dfrac{\partial \hat{\mathbf{u}}}{\partial t} \right] \end{array} \right] d\Omega^e + \int_{\Gamma^e} N_r \left[K^1_{c_g^1 c_g^1} \nabla \hat{c}^1_{c_g} \right] \underline{n} d\Gamma^e = 0 \tag{4.9}$$

where, Γ^e is the element boundary surface and $\underline{n}$ represents the direction cosine normal to that surface. Addressing the expressions for the derivatives of the primary variables yields:

$$\begin{aligned}
&\int_{\Omega^e}\left[K^1_{c_g^1 c_g^1}\nabla\mathbf{N}^T\nabla\mathbf{N}\right]d\Omega^e\mathbf{c}_{\mathbf{c_g}S}+\int_{\Omega^e}\left[C^1_{c_g l}\mathbf{N}^T\mathbf{N}\right]d\Omega^e\frac{\partial\mathbf{u}_{\mathbf{l}S}}{\partial t}+\int_{\Omega^e}\left[C^1_{c_g T}\mathbf{N}^T\mathbf{N}\right]d\Omega^e\frac{\partial\mathbf{T}_S}{\partial t}\\
&+\int_{\Omega^e}\left[C^1_{c_g^1 c_g^1}\mathbf{N}^T\mathbf{N}\right]d\Omega^e\frac{\partial\mathbf{c}^{\mathbf{i}}_{\mathbf{c_g}S}}{\partial t}+\int_{\Omega^e}\left[C^1_{c_g\mathbf{u}}\mathbf{N}^T\mathbf{N}\right]d\Omega^e\frac{\partial\mathbf{u}_S}{\partial t}+\int_{\Omega^e}\left[C^1_{c_g s_g}\mathbf{N}^T\mathbf{N}\right]d\Omega^e\frac{\partial\mathbf{s}^{\mathbf{i}}_{\mathbf{c_g}S}}{\partial t}\\
&-\int_{\Gamma^e}\mathbf{N}^T\left[f^1_{c_g}\right]d\Gamma^e=0
\end{aligned}\tag{4.10}$$

where, $\mathbf{N}$ represents the shape function matrix; $\mathbf{u}_{\mathbf{l}S}, \mathbf{T}_S, \mathbf{c}_{\mathbf{c_g}S}, \mathbf{u}_S$ represents pore water pressure, temperature, concentration of pore gas and deformation vectors respectively. The term, $f^1_{c_g}$ indicates the approximate flux of gas component *1* normal to the boundary surface.

Equation (4.10) can be expressed for a multicomponent system in concise matrix form as:

$$\mathbf{C}_{\mathbf{c_g l}}\frac{\partial\mathbf{u}_{\mathbf{l}S}}{\partial t}+\mathbf{C}_{\mathbf{c_g T}}\frac{\partial\mathbf{T}_S}{\partial t}+\mathbf{C}^{\mathbf{i}}_{\mathbf{c_g^i c_g^i}}\frac{\partial\mathbf{c}^{\mathbf{i}}_{\mathbf{g}S}}{\partial t}+\mathbf{C}_{\mathbf{c_g u}}\frac{\partial\mathbf{u}_S}{\partial t}+\mathbf{K}^{\mathbf{i}}_{\mathbf{c_g^i c_g^i}}\mathbf{c}^{\mathbf{i}}_{\mathbf{g}S}=\mathbf{f}^{\mathbf{i}}_{\mathbf{c_g}}\tag{4.11}$$

where, i = *1, 2, ……..., N* number of gas components and

$$\mathbf{C}_{\mathbf{c_g l}}=\sum_{e=1}^{m}\int_{\Omega^e}\left[C_{c_g l}\mathbf{N}^T\mathbf{N}\right]d\Omega^e\tag{4.12}$$

$$\mathbf{C}_{\mathbf{c_g T}}=\sum_{e=1}^{m}\int_{\Omega^e}\left[C_{c_g T}\mathbf{N}^T\mathbf{N}\right]d\Omega^e\tag{4.13}$$

$$\mathbf{C}^{\mathbf{i}}_{\mathbf{c_g^i c_g^i}}=\sum_{e=1}^{m}\int_{\Omega^e}\left[C^i_{c_g^i c_g^i}\mathbf{N}^T\mathbf{N}\right]d\Omega^e\tag{4.14}$$

$$\mathbf{C}_{\mathbf{c_g u}}=\sum_{e=1}^{m}\int_{\Omega^e}\left[C_{c_g\mathbf{u}}\mathbf{N}^T\mathbf{N}\right]d\Omega^e\tag{4.15}$$

$$\mathbf{K}^{\mathbf{i}}_{\mathbf{c_g^i c_g^i}}=\sum_{e=1}^{m}\int_{\Omega^e}\left[K^i_{c_g^i c_g^i}\nabla\mathbf{N}^T\nabla\mathbf{N}\right]d\Omega^e\tag{4.16}$$

$$\mathbf{f}^{\mathbf{i}}_{\mathbf{c_g}}=\sum_{e=1}^{m}\int_{\Omega^e}\left[C^i_{c_g s_g}\mathbf{N}^T\mathbf{N}\frac{\partial\mathbf{s}^{\mathbf{i}}_{\mathbf{c_g}S}}{\partial t}\right]d\Omega^e-\int_{\Gamma^e}\mathbf{N}^T\left[f^i_{c_g}\right]d\Gamma^e\tag{4.17}$$

4.2.2 Moisture flow

The process can be repeated to obtain the moisture flow variables. The governing equation of moisture transfer, equation (3.49) can be expressed as:

$$\begin{aligned}&\mathbf{C}_{\mathbf{ll}}\frac{\partial \mathbf{u}_{\mathbf{l}s}}{\partial t}+\mathbf{C}_{\mathbf{lT}}\frac{\partial \mathbf{T}_s}{\partial t}+\sum_{\mathbf{i=1}}^{N}\mathbf{C}^{\mathbf{i}}_{\mathbf{lc_g}}\frac{\partial \mathbf{c}^{\mathbf{i}}_{\mathbf{c_g}s}}{\partial t}+\mathbf{C}_{\mathbf{lu}}\frac{\partial \mathbf{u}_s}{\partial t}\\&+\mathbf{K}_{\mathbf{ll}}\mathbf{u}_{\mathbf{l}s}+\mathbf{K}_{\mathbf{lT}}\mathbf{T}_s+\sum_{\mathbf{i=1}}^{N}\mathbf{K}^{\mathbf{i}}_{\mathbf{lc_g}}\mathbf{c}^{\mathbf{i}}_{\mathbf{g}s}=\mathbf{f}_{\mathbf{l}}\end{aligned} \tag{4.18}$$

where, N is the number of gas components.

$$\mathbf{C}_{\mathbf{ll}}=\sum_{e=1}^{m}\int_{\Omega^e}\left[C_{ll}\mathbf{N}^T\mathbf{N}\right]d\Omega^e \tag{4.19}$$

$$\mathbf{C}_{\mathbf{lT}}=\sum_{e=1}^{m}\int_{\Omega^e}\left[C_{lT}\mathbf{N}^T\mathbf{N}\right]d\Omega^e \tag{4.20}$$

$$\mathbf{C}^{\mathbf{i}}_{\mathbf{lc_g}}=\sum_{e=1}^{m}\int_{\Omega^e}\left[C^i_{lc_g}\mathbf{N}^T\mathbf{N}\right]d\Omega^e \tag{4.21}$$

$$\mathbf{C}_{\mathbf{lu}}=\sum_{e=1}^{m}\int_{\Omega^e}\left[C_{l\mathbf{u}}\mathbf{N}^T\mathbf{N}\right]d\Omega^e \tag{4.22}$$

$$\mathbf{K}_{\mathbf{ll}}=\sum_{e=1}^{m}\int_{\Omega^e}\left[K_{ll}\nabla\mathbf{N}^T\nabla\mathbf{N}\right]d\Omega^e \tag{4.23}$$

$$\mathbf{K}_{\mathbf{lT}}=\sum_{e=1}^{m}\int_{\Omega^e}\nabla\mathbf{N}^T\left[K_{lT}\nabla\mathbf{N}\right]d\Omega^e \tag{4.24}$$

$$\mathbf{K}_{\mathbf{lc_g^i}}=\sum_{e=1}^{m}\int_{\Omega^e}\nabla\mathbf{N}^T\left[K_{lc_g^i}\nabla\mathbf{N}\right]d\Omega^e \tag{4.25}$$

$$\mathbf{f}_{\mathbf{l}}=\sum_{e=1}^{m}\int_{\Omega^e}\left[k_l\rho_l\nabla\mathbf{N}^T\nabla z\right]d\Omega^e-\sum_{e=1}^{m}\int_{\Gamma^e}\mathbf{N}^T\left[f_l\right]d\Gamma^e \tag{4.26}$$

4.2.3 Dissolved chemical flow

The multicomponent dissolved chemical flow governing equation (3.110) can be presented in terms of primary variables as:

$$\mathbf{C}_{\mathbf{c_d l}}\frac{\partial \mathbf{u}_{\mathbf{l}S}}{\partial t}+\mathbf{C}_{\mathbf{c_d T}}\frac{\partial \mathbf{T}_S}{\partial t}+\sum_{\mathbf{i}=1}^{N}\mathbf{C}^{\mathbf{i}}_{\mathbf{c_d c_g}}\frac{\partial \mathbf{c}^{\mathbf{i}}_{\mathbf{c_g}S}}{\partial t}+\sum_{\mathbf{j}=1}^{M}\mathbf{C}^{\mathbf{j}}_{\mathbf{c_d c_d}}\frac{\partial \mathbf{c}^{\mathbf{j}}_{\mathbf{c_d}S}}{\partial t}+\mathbf{C}_{\mathbf{c_d u}}\frac{\partial \mathbf{u}_S}{\partial t}+ \tag{4.27}$$
$$\mathbf{K}_{\mathbf{c_d l}}\mathbf{u}_{\mathbf{l}S}+\sum_{\mathbf{j}=1}^{M}\mathbf{K}^{\mathbf{j}}_{\mathbf{c_d c_d}}\mathbf{c}^{\mathbf{j}}_{\mathbf{c_d}S}=\sum_{\mathbf{j}=1}^{M}\mathbf{f}^{\mathbf{j}}_{\mathbf{c_d}}$$

Where, N and M represents maximum number of gas components and dissolved chemical components respectively.

$$\mathbf{C}_{\mathbf{c_d l}}=\sum_{e=1}^{m}\int_{\Omega^e}\left[C_{c_d l}\mathbf{N}^T\mathbf{N}\right]d\Omega^e \tag{4.28}$$

$$\mathbf{C}_{\mathbf{c_d T}}=\sum_{e=1}^{m}\int_{\Omega^e}\left[C_{c_d T}\mathbf{N}^T\mathbf{N}\right]d\Omega^e \tag{4.29}$$

$$\mathbf{C}^{\mathbf{i}}_{\mathbf{c_d c_g}}=\sum_{e=1}^{m}\int_{\Omega^e}\left[C^i_{c_d c_g}\mathbf{N}^T\mathbf{N}\right]d\Omega^e \tag{4.30}$$

$$\mathbf{C}^{\mathbf{j}}_{\mathbf{c_d c_d}}=\sum_{e=1}^{m}\int_{\Omega^e}\left[C^i_{c_d c_d}\mathbf{N}^T\mathbf{N}\right]d\Omega^e \tag{4.31}$$

$$\mathbf{C}_{\mathbf{c_d u}}=\sum_{e=1}^{m}\int_{\Omega^e}\left[C_{c_d u}\mathbf{N}^T\mathbf{N}\right]d\Omega^e \tag{4.32}$$

$$\mathbf{K}_{\mathbf{c_d l}}=\sum_{e=1}^{m}\int_{\Omega^e}\left[K_{c_d l}\nabla\mathbf{N}^T\nabla\mathbf{N}\right]d\Omega^e \tag{4.33}$$

$$\mathbf{K}^{\mathbf{j}}_{\mathbf{c_d c_d}}=\sum_{e=1}^{m}\int_{\Omega^e}\left[K^i_{c_d c_d}\nabla\mathbf{N}^T\nabla\mathbf{N}\right]d\Omega^e \tag{4.34}$$

$$\mathbf{f}^{\mathbf{j}}_{\mathbf{c_d}}=\int_{\Omega^e}\left[K_l c_d^j\nabla\mathbf{N}^T\nabla z\right]d\Omega^e+\int_{\Omega^e}\left[\mathbf{N}^T\mathbf{N}s_d^j\right]d\Omega^e-\int_{\Gamma^e}\mathbf{N}^T\left[f^{\,j}{}_{c_d}\right]d\Gamma^e \tag{4.35}$$

4.2.4 Heat transfer

The governing equation of heat flow, equation (3.149) can be presented in approximated form as:

$$\begin{aligned}&\mathbf{C}_{\mathbf{Tl}}\frac{\partial \mathbf{u}_{\mathbf{l}s}}{\partial t}+\mathbf{C}_{\mathbf{TT}}\frac{\partial \mathbf{T}_s}{\partial t}+\sum_{\mathbf{i}=1}^{N}\mathbf{C}^{\mathbf{i}}_{\mathbf{Tc_g}}\frac{\partial \mathbf{c}^{\mathbf{i}}_{\mathbf{g}s}}{\partial t}+\mathbf{C}_{\mathbf{Tu}}\frac{\partial \mathbf{u}_s}{\partial t}\\&+\mathbf{K}_{\mathbf{Tl}}\mathbf{u}_{\mathbf{l}s}+\mathbf{K}_{\mathbf{TT}}\mathbf{T}_s+\sum_{\mathbf{i}=1}^{N}\mathbf{K}^{\mathbf{i}}_{\mathbf{Tc_g}}\mathbf{c}^{\mathbf{i}}_{\mathbf{g}s}=\mathbf{f}_{\mathbf{T}}\end{aligned} \tag{4.36}$$

where, N is the number of gas components.

$$\mathbf{C}_{\mathbf{Tl}}=\sum_{e=1}^{m}\int_{\Omega^e}\left[C_{ll}\mathbf{N}^T\mathbf{N}\right]d\Omega^e \tag{4.37}$$

$$\mathbf{C}_{\mathbf{TT}}=\sum_{e=1}^{m}\int_{\Omega^e}\left[C_{lT}\mathbf{N}^T\mathbf{N}\right]d\Omega^e \tag{4.38}$$

$$\mathbf{C}^{\mathbf{i}}_{\mathbf{Tc_g}}=\sum_{e=1}^{m}\int_{\Omega^e}\left[C^i_{Tg}\mathbf{N}^T\mathbf{N}\right]d\Omega^e \tag{4.39}$$

$$\mathbf{C}_{\mathbf{Tu}}=\sum_{e=1}^{m}\int_{\Omega^e}\left[C_{T\mathbf{u}}\mathbf{N}^T\mathbf{N}\right]d\Omega^e \tag{4.40}$$

$$\mathbf{K}_{\mathbf{Tl}}=\sum_{e=1}^{m}\int_{\Omega^e}\left[K_{Tl}\nabla\mathbf{N}^T\nabla\mathbf{N}\right]d\Omega^e \tag{4.41}$$

$$\mathbf{K}_{\mathbf{TT}}=\sum_{e=1}^{m}\int_{\Omega^e}\left[K_{TT}\nabla\mathbf{N}^T\nabla\mathbf{N}\right]d\Omega^e \tag{4.42}$$

$$\mathbf{K}^{\mathbf{i}}_{\mathbf{Tc_g}}=\sum_{e=1}^{m}\int_{\Omega^e}\left[K^i_{Tg}\nabla\mathbf{N}^T\nabla\mathbf{N}\right]d\Omega^e \tag{4.43}$$

$$\mathbf{f}_{\mathbf{t}}=\sum_{e=1}^{m}\int_{\Omega^e}\left[C_{pl}\rho_l K_l\nabla\mathbf{N}^T\nabla z\right]d\Omega^e-\sum_{e=1}^{m}\int_{\Gamma^e}\mathbf{N}^T\left[F_h\right]d\Gamma^e \tag{4.44}$$

In the above, F_h is the approximate heat flux normal to the boundary surface.

4.2.5 Deformation

The governing equation of mechanical deformation (3.200) can be presented as:

$$\mathbf{C_{ul}}\frac{\partial \mathbf{u}_{ls}}{\partial t}+\mathbf{C_{uT}}\frac{\partial \mathbf{T}_s}{\partial t}+\sum_{\mathbf{i}=1}^{N}\mathbf{C}^{\mathbf{i}}_{\mathbf{uc_g}}\frac{\partial \mathbf{c}^{\mathbf{i}}_{\mathbf{c_g}s}}{\partial t}+\mathbf{C_{uu}}\frac{\partial \mathbf{u}_s}{\partial t}=\mathbf{f_u} \tag{4.45}$$

where,

$$\mathbf{C_{ul}}=\sum_{e=1}^{m}\int_{\Omega^e}\left[\mathbf{W}\left[\mathbf{D_{ep}}A_s\right]\mathbf{N}\right]\nabla\, t\, d\Omega^e \tag{4.46}$$

$$\mathbf{C_{uT}}=\sum_{e=1}^{m}\int_{\Omega^e}\left[\mathbf{W}\mathbf{D_{ep}}\left[-A_T-A_s\frac{dS_r}{dt}\right]\mathbf{N}\right]\nabla\, t\, d\Omega^e \tag{4.47}$$

$$\mathbf{C}^{\mathbf{i}}_{\mathbf{ug}}=\sum_{e=1}^{m}\int_{\Omega^e}\left[\mathbf{W}\left[-\mathbf{D_{ep}}A_s-\mathbf{m}\right]\mathbf{N}\right]\nabla\, t\, d\Omega^e \tag{4.48}$$

$$\mathbf{C_{uu}}=\sum_{e=1}^{m}\int_{\Omega^e}\mathbf{W}\mathbf{D_{ep}}\mathbf{B}^T\nabla t d\Omega^e \tag{4.49}$$

$$\mathbf{f_u}=\sum_{e=1}^{m}\left[\int_{\Omega^e}\left[\mathbf{W}\mathbf{D_{ep}}\varepsilon_s^p\right]d\Omega^e+\int_{\Omega^e}\mathbf{N}^T d\mathbf{b}d\Omega^e+\int_{\Gamma^e}\mathbf{N}^T\hat{\underline{T}}_r d\Gamma^e\right] \tag{4.50}$$

Where, $\mathbf{W}$ represents the term "$\mathbf{P}N_r$" and $\mathbf{P}$ has been defined in equation (3.166). $\hat{\underline{T}}_r$ is the approximate traction. Traction is the force per area on a body, normally includes normal and shear forces. In this case, approximated form has been used.

4.3 Matrix representation and temporal discretisation of governing equations

A matrix form of spatially discretised governing equations of flow and deformation behaviour has been developed and presented in Figure 4.1. Time derivative of primary variables has been expressed in the form of $\dot{\boldsymbol{\varphi}}$ which is any one of the primary variables, such as pore water pressure ($\dot{\mathbf{u}}_{ls}$), temperature ($\dot{\mathbf{T}}_s$), gas concentration ($\dot{\mathbf{c}}_{gs}$),

dissolved chemical concentration ($\dot{\mathbf{c}}_{\mathbf{ds}}$) and deformation ($\dot{\mathbf{u}}_s$). The model is capable of dealing with any number of gas species and can be presented in the matrix form.
Thomas and He (1998) stated that various types of boundary conditions can be adopted in the formulation. In the boundary these can be present as:

1. Dirichlet condition: prescribed primary variable $\varphi = \varphi^*$ on boundary Γ^d
2. Neumann condition: prescribed flux $j = j^*$ on boundary Γ^n
3. Cauchy condition: prescribed convection condition on boundary Γ^c
4. In case of stress equilibrium surface traction load is applicable to boundary Γ^f

The matrix form of governing equations can be expressed in the following form:

$$\mathbf{A\Phi} + \mathbf{B}\frac{\partial \mathbf{\Phi}}{\partial \mathrm{t}} + \mathbf{C} = \{\mathbf{0}\} \tag{4.51}$$

where, $\mathbf{\Phi}$ represents the vector of variables and $\mathbf{A}, \mathbf{B}, \mathbf{C}$ are the matrices of coefficients.

A forward difference time-stepping algorithm has been used for time discretisation of spatially discretised governing equations. The algorithm can be expressed as:

$$\mathbf{A}^{\mathbf{\Phi}_l}\left[(1-\pi)\mathbf{\Phi}^{n+1} + \pi\mathbf{\Phi}^n\right] + \mathbf{B}^{\mathbf{\Phi}_l}\left[\frac{\mathbf{\Phi}^{n+1} - \mathbf{\Phi}^n}{\Delta t}\right] + \mathbf{C}^{\mathbf{\Phi}_l} = \{\mathbf{0}\} \tag{4.52}$$

where, π represents an integration constant which varies from 0 for explicit time integration, 0.5 for Crank-Nicholson and 1 for implicit time integrations. The superscript, $\mathbf{\Phi}_l$, represents the level at which the matrices $\mathbf{A}$, $\mathbf{B}$ and $\mathbf{C}$ are evaluated and can be expressed as:

$$\mathbf{\Phi}_l = \wp(n+1) + (1-\wp)(n) \tag{4.53}$$

where, $\wp$ is a constant to define the interval for which the matrices (**A, B** and **C**) are evaluated. In case of a fully implicit mid-interval forward difference time-stepping algorithm π and $\wp$ take the values of 1 and 0.5 respectively.

Substituting the values above, into equation (4.53) yields:

$$\mathbf{A}^{n+1/2}\mathbf{\Phi}^{n+1} + \mathbf{B}^{n+1/2}\left[\frac{\mathbf{\Phi}^{n+1} - \mathbf{\Phi}^{n}}{\Delta t}\right] + \mathbf{C}^{n+1/2} = \{\mathbf{0}\} \tag{4.54}$$

Equation (4.54) can be rearranged as follows:

$$\mathbf{\Phi}^{n+1} = \left[\mathbf{A}^{n+1/2} + \frac{\mathbf{B}^{n+1/2}}{\Delta t}\right]\left[\frac{\mathbf{B}^{n+1/2}\mathbf{\Phi}^{n}}{\Delta t} - \mathbf{C}^{n+1/2}\right] \tag{4.55}$$

Direct solution of equation (4.55) cannot be obtained, since every calculation of $\mathbf{\Phi}^{n+1}$ requires the measurement of coefficients at the mid-interval. Hence, an iterative solution procedure called a predictor - corrector algorithm has been used.

The algorithm considers the steps:

1. Initially the matrices **A**, **B** and **C** are evaluated at time n which yields the predictor.

2. At time $n+1/2$ matrices **A**, **B** and **C** are estimated using the predictor and the values from previous time step. This estimation is the corrector.

3. If elasto-plastic elements are involved in the analysis, a check is carried out for yielding. If the displacement and consequent stress level exceeds the specified tolerance limit, plastic strain will be introduced and hardening parameters need to be estimated.

4. The convergence criteria can be checked by using either of the following conditions:

$$\left|\boldsymbol{\Phi}_{iC}^{n+1} - \boldsymbol{\Phi}_{(i-1)C}^{n+1}\right| \langle \mathbf{TL}_{abs} \tag{4.56}$$

or,

$$\left|\frac{\boldsymbol{\Phi}_{iC}^{n+1} - \boldsymbol{\Phi}_{(i-1)C}^{n+1}}{\boldsymbol{\Phi}_{(i-1)C}^{n+1}}\right| \langle \mathbf{TL}_{rel} \tag{4.57}$$

where, i is the iteration level, $_C$ indicates the corrector has been introduced, $\mathbf{TL}_{abs}$ and $\mathbf{TL}_{rel}$ represents the matrices of absolute and relative tolerances for each variable. To ensure the residual force is within a tolerance limit, the stress equilibrium condition is checked and therefore, residual force, ζ, can be obtained as suggested by (Owen and Hinton, 1980):

$$\int_{\Omega} \mathbf{B}^T \Delta\sigma d\Omega - \Delta F = \zeta \tag{4.58}$$

where, ΔF is the increment of applied force.

If either non-convergence of the variables takes place or large residual stress develops, the algorithm returns to step 2 where the corrector becomes the new predictor. Meanwhile, if convergence takes place or residual force stays within the tolerance limit, the algorithm moves to the next time step where the process repeats.

The number of iterations required for predictor-corrector depends on the simulation conditions, materials parameters and time step size. The model considers a variable time step method for a time efficient solution. When the number of iterations exceeds the specified maximum, the time step size is decreased by a factor and vice-versa. This procedure helps to achieve an efficient solution algorithm.

$$\begin{bmatrix} C_{ll} & C_{lT} & C_{lcd^1} & . & C_{lcd^n} & C_{lcg^1} & . & C_{lcg^n} & C_{lu} \\ C_{Tl} & C_{TT} & C_{Tcd^1} & . & C_{Tcd^n} & C_{Tcg^1} & . & C_{Tcg^n} & C_{Tu} \\ C_{cd^1l} & C_{cd^1T} & C_{cd^1cd^1} & . & C_{cd^1cd^n} & C_{cd^1cg^1} & . & C_{cd^1cg^n} & C_{cd^1u} \\ . & . & . & . & . & . & . & . & . \\ C_{cd^nl} & C_{cd^nT} & C_{cd^ncd^1} & . & C_{cd^ncd^n} & C_{cd^ncg^1} & . & C_{cd^ncg^n} & C_{cd^nu} \\ C_{cg^1l} & C_{cg^1T} & C_{cg^1cd^1} & . & C_{cg^1cd^n} & C_{cg^1cg^1} & . & C_{cg^1cg^n} & C_{cg^1u} \\ . & . & . & . & . & . & . & . & . \\ C_{cg^nl} & C_{cg^nT} & C_{cg^ncd^1} & . & C_{cg^ncd^n} & C_{cg^ncg^1} & . & C_{cg^ncg^n} & C_{cg^nu} \\ C_{ul} & C_{uT} & C_{ucd^1} & . & C_{ucd^n} & C_{ucg^1} & . & C_{ucg^n} & C_{uu} \end{bmatrix} \begin{bmatrix} \dot{u}_{ls} \\ \dot{T} \\ \dot{c}^1_{cd} \\ . \\ \dot{c}^n_{cd} \\ \dot{c}^1_{cg} \\ . \\ \dot{c}^n_{cg} \\ \dot{c}_u \end{bmatrix} + \begin{bmatrix} K_{ll} & K_{lT} & K_{lcd^1} & . & K_{lcd^n} & K_{lcg^1} & . & K_{lcg^n} & K_{lu} \\ K_{Tl} & K_{TT} & K_{Tcd^1} & . & K_{Tcd^n} & K_{Tcg^1} & . & K_{Tcg^n} & K_{Tu} \\ K_{cd^1l} & K_{cd^1T} & K_{cd^1cd^1} & . & K_{cd^1cd^n} & K_{cd^1cg^1} & . & K_{cd^1cg^n} & K_{cd^1u} \\ . & . & . & . & . & . & . & . & . \\ K_{cd^nl} & K_{cd^nT} & K_{cd^ncd^1} & . & K_{cd^ncd^n} & K_{cd^ncg^1} & . & K_{cd^ncg^n} & K_{cd^nu} \\ K_{cg^1l} & K_{cg^1T} & K_{cg^1cd^1} & . & K_{cg^1cd^n} & K_{cg^1cg^1} & . & K_{cg^1cg^n} & K_{cg^1u} \\ . & . & . & . & . & . & . & . & . \\ K_{cg^nl} & K_{cg^nT} & K_{cg^ncd^1} & . & K_{cg^ncd^n} & K_{cg^ncg^1} & . & K_{cg^ncg^n} & K_{cg^nu} \\ K_{ul} & K_{uT} & K_{ucd^1} & . & K_{ucd^n} & K_{ucg^1} & . & K_{ucg^n} & K_{uu} \end{bmatrix} \begin{bmatrix} u_{ls} \\ T \\ c^1_{cd} \\ . \\ c^n_{cd} \\ c^1_{cg} \\ . \\ c^n_{cg} \\ c_u \end{bmatrix} + \begin{bmatrix} f_l \\ f_T \\ f^1_{c_d} \\ . \\ f^n_{c_d} \\ f^1_{c_g} \\ . \\ f^n_{c_g} \\ f_u \end{bmatrix} = 0$$

Figure 4.1: Matrix representation of the numerical formulations of the governing equations in terms of primary variables. $\dot{\mathbf{u}}_{ls}$, $\dot{\mathbf{T}}_s$, $\dot{\mathbf{c}}_{gs}$, $\dot{\mathbf{c}}_{ds}$, $\dot{\mathbf{u}}_s$ represents the time derivative of pore water pressure, temperature, pore gas concentration, dissolved chemical concentration and deformation.

4.4 Coupling between transport and chemical reaction equations

As explained in previous chapter, in order to develop the multicomponent reactive gas transport model, the transport model, COMPASS has been linked with a geochemical model, namely, PHREEQC version 2 (Parkhurst and Appelo, 1999). The approach adopted to link the transport model and the reaction model is based on a sequential approach. Seetharam (2003) implemented both sequential iterative and sequential non-iterative approach to couple the transport model and the geochemical reaction model MINTEQA2 (Alison et al., 1992). Successful implementation of the coupled COMPASS-MINTEQA2, to model reactive transport of multicomponent dissolved chemical, has been reported by Seetharam et al. (2007), Cleall et al. (2007) and Seetharam et al. (2010). Sedighi (2011) has coupled COMPASS with geochemical code PHREEQC version 2, to model the reactive transport of multicomponent dissolved chemicals. Implementation of PHREEQC2 provides an advantage over MINTEQA2, which is based on equilibrium reaction conditions, due to its capability of modelling both equilibrium reactions and kinetically controlled chemical reactions. In this study, the previously coupled COMPASS-PHREEQC module has been modified by implementing the gas phase reactive processes together with the dissolved chemicals. PHREEQC2 is capable of modelling gas phase reactions under fixed pressure or fixed volume condition (Parkhurst and Appelo, 1999).

A sequential non-iterative approach (SNIA) has been used in this study to couple the transport processes and geochemical reactions. The sequences of calculations are as follows:

i) At the beginning transport equations are solved and checked for the convergence. Steefel and MacQuarrie (1996) suggested that under the SNIA coupling scheme transport processes can be presented mathematically as:

$$\frac{\left(c_r^i\right)^{Transport} - \left(c_r^i\right)^n}{\Delta t} = L\left(j_{c_r^i}\right)^n \tag{4.59}$$

where, c is the concentration, subscript, r represents the chemical concentration of either gas components or dissolved chemicals, superscript, n represents the time step. L is the spatial operators applying to the fluxes.

ii) The new values of chemical concentrations associated with the transport processes, this stage is followed by solving equations of chemical reactions as:

$$\frac{\left(c_r^i\right)^{n+1} - \left(c_r^i\right)^{Transport}}{\Delta t} = R_i^{n+1} \tag{4.60}$$

where, R represents the rate expressions for the associated geochemical reactions.

Code COMPASS has been developed on programming language FORTRAN and geochemical code PHREEQC2 has been written in programming language C. These two codes have been linked together using a "Cross-link" subroutine which is written in C. The coupled code runs on a single compiler.

Once the convergence of transport equations takes place, the program proceeds to the geochemical module in COMPASS and connects to "Cross-link" subroutine which prepare and passes the required information for geochemical reactions. From the "Cross-link" subroutine the program calls PHREEQC "Main" function to perform the geochemical analysis. During a single time step, chemical equations are solved only once and therefore, it has been termed as sequential non-iterative approach. The PHREEQC calculates the concentrations of gas components and dissolved chemicals and send the updated results back to "Cross-link" subroutine which passes the newly updated values to COMPASS for the calculations in next time step. A schematic diagram or flowchart of the entire process has been presented in Figure 4.2.

For an efficient and faster coupled code, Seertharam (2003) implemented a relative tolerance level check for the chemical concentrations which has been presented in Figure 2. Mathematically, the relative tolerance, *diff1*, can be expressed as:

$$diff1 = \left(c_r^i\right)^{Transport} - \left(c_r^i\right)^n \tag{4.60}$$

$$diff2 = \left(T\right)^{Transport} - \left(T\right)^n \tag{4.61}$$

If the concentrations of gas components or dissolved chemicals do not vary more than a specific amount during time steps *n* and *n+1*, then the program skips the geochemical analysis.

In this study the numerical formulation of PHREEQC2 has been used without any modification. Two different numerical solution techniques, namely, Newton-Raphson method and Runge-Kutta algorithm have been implemented in PHREEQC2 (Parkhurst and Appelo, 1999). For the chemical reactions under equilibrium condition, a modified Newton-Raphson method has been used for solving a set of non-linear equations while under kinetically controlled reactions Runge-Kutta algorithm has been used to solve the partial differential equations.

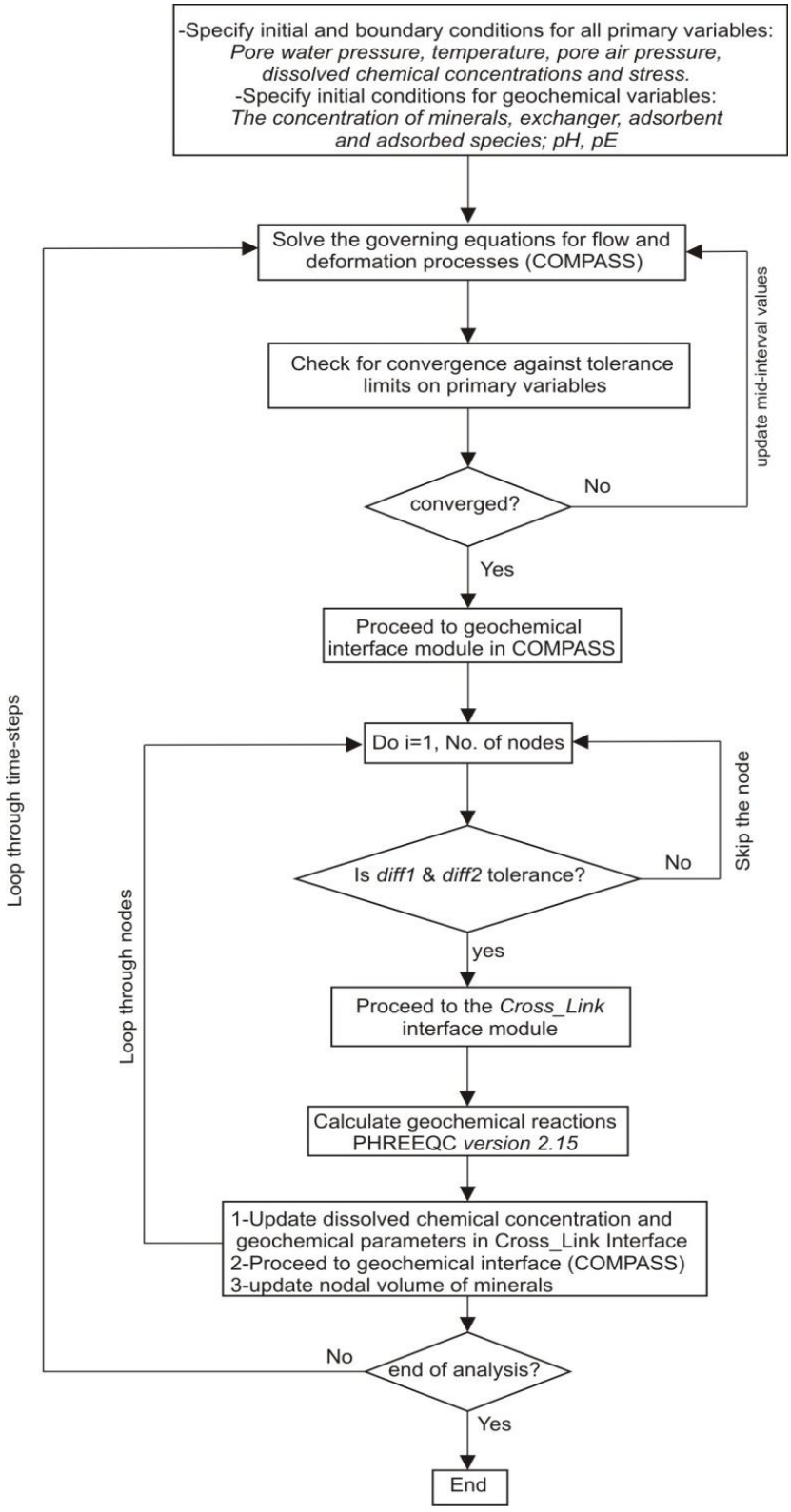

Figure 4.2: Flow chart diagram of sequential non-iterative approach (SNIA) to couple transport model COMPASS and geochemical model PHREEQC2 (*after* Sedighi, 2011).

4.5 Conclusion

Numerical solution of previously developed governing equation of coupled thermo-hydro-chemical-gas-mechanical model has been explained. The procedures to obtain the discretised form of multicomponent gas flow equation have been demonstrated. Galerkin weighted residual approach has been used for spatial discretisation of the governing equations and a forward difference, mid-interval time stepping algorithm has been implemented for temporal discretisation. The sink/source term of the governing pore gas flow and dissolved chemical flow equation has been calculated using geochemical model PHREEQC2. Therefore, it has been essential to link the transport model and the geochemical model. A sequential non-iterative approach has been adopted to couple the transport model COMPASS and geochemical model PHREEQC2. As in a single time step the chemical equations are solved once, after the convergence of transport equations occurs, it has been termed as non-iterative approach. The Fortran based COMPASS code and C based PHREEQC2 code has been linked with a "Cross-link" subroutine and the coupled code executes in a single compiler.

References

Allison, J.D., Brown, D.S., Novo-Gradac, K.J., (1992). "MINTEQA2 User Manual version 3.0". Environmental Research Laboratory, U.S. EPA.

Cleall, P.J., (1998). "An investigation of the thermo/hydraulic/mechanical behaviour of unsaturated soils, including expansive clays". PhD Thesis, University of Wales, Cardiff.

Cleall, P.J., Seetharam, S.C., Thomas, H.R., (2007). "On the inclusion of some aspects of chemical behaviour of an unsaturated soil in thermo-hydro-chemical-mechanical models: I Model development". *Journal of Engineering Mechanics, American Society of Civil Engineers* **133**, pp 338-347.

Hashm, A.A., (1999). "A study of the transport of a selection of heavy metals in unsaturated soils". PhD Thesis, University of Wales, Cardiff.

Owen, D.R.J., Hinton, E., (1980). "Finite Elements in Plasticity: Theory and Practice". Pineridge Press Ltd., Swansea.

Parkhurst, D.L., Appelo, C.A.J., (1999). "User's Guide to PHREEQC (version 2)", U.S. Geological Survey, Water Resource Investigation Report, pp 99-4259.

Ramesh, A.D., (1996). "Modelling the thermo/hydraulic/mechanical behaviour of unsaturated soil using an elasto-plastic constitutive relationship". PhD Thesis, University of Wales, Cardiff.

Sedighi, M., (2011). "An investigation of Hydro-geochemical processes in coupled thermal, hydraulic, chemical and mechanical behaviour of unsaturated soils". PhD Thesis, Cardiff University, UK.

Seetharam, S.C., (2003). "An investigation of the thermo/hydro/chemical/mechanical behaviour of unsaturated soils". PhD Thesis, Cardiff University, UK.

Seetharam, S.C., Thomas, H.R., Cleall, P.J., (2007). "Coupled thermo-hydro-chemical-mechanical model for unsaturated soils-Numerical algorithm". *International Journal of Numerical Methods in Engineering* **70**, pp 1480-1511.

Seetharam, S.C., Thomas, H.R., and Vardon, P.J., (2010). Non-isothermal multi-component reactive transport model for unsaturated soils. *International Journal of Geomechanics, American Society of Civil Engineers*, doi.org/10.1061/(ASCE)GM.1943-5622.0000018.

Steefel, C.I., MacQuarrie, K.T.B., (1996). "Approaches to modeling of reactive transport in porous media". *Reactive Transport in Porous Media, Reviews in Mineralogy* **34**. Mineralogical Society of America, Washington, DC.

Thomas, H.R., He, Y., (1995). "Analysis of coupled heat, moisture and air transfer in a deformable unsaturated soil". *Geotechnique* **45**, No. 4, pp. 677-689.

Thomas, H.R., He, Y., (1998). "Modelling the behaviour of unsaturated soil using an elasto plastic constitutive relationship". *Geotechnique* **48**, pp. 589-603.

Thomas, H.R., Rees, S.W., Sloper, N.J., (1998). "Three-dimensional heat, moisture and air transfer in unsaturated soils". *International Journal of Numerical and Analytical Methods in Geomechanics* **22**, No. 2, pp. 75-95.

Vardon, P.J., (2009). "A three-dimensional numerical investigation of the therm-hydro-mechanical behaviour of a large-scale prototype repository". PhD Thesis, Cardiff University, UK.

Zienkiewicz, O.C., Taylor, R.L., (1989). "The Finite Element Method". McGraw Hill, 4th edition.

Zienkiewicz, O.C., Taylor, R.L., (2000). "The Finite Element Method for Solid and Structural Mechanics". McGraw Hill, 6th edition.

5

Verification of multicomponent gas transport

5.1 Introduction

In this chapter a number of verification and validation exercises have been detailed to acquire confidence of the developed model for predictive purposes. To ensure the accuracy of the solution algorithm it is essential to carry out verification exercises. Similarly, validation is required to ensure that the underlying conceptual model has been implemented correctly or represent the reality. The main objective of this chapter is to verify the theoretical and numerical model, particularly, the developments in the multicomponent gas transport which has been presented in the theoretical and numerical formulation chapter. Based upon the availability of required information, the model has been compared against analytical solutions and/ or alternative numerical solutions and in cases of unavailability of information about analytical or numerical solutions, simple verification methods have been used to verify the developed model.

In the case of coupled moisture flow, heat transfer and deformation behaviour, the numerical model has already been verified and validated by King (1994), Sansom (1995) and Cleall (1998).

In addition to previous efforts, substantial development of COMPASS model has been presented by Thomas and He (1997), Thomas and He (1998), Thomas et al. (1998) and Cleall (1998). The revised code has been therefore re-verified and examined by Mitchell (2002) for coupled thermal, hydraulic and mechanical behaviour. The multicomponent dissolved chemical transport has been extensively verified and validated by Seetharam (2003) and Sedighi (2011). A number of verification exercises on the reactive transport and coupling the transport model with geochemical reaction model have been undertaken and presented by Sedighi (2011). Therefore, the verifications of coupled moisture, heat, deformation and dissolved chemical flow have not been repeated in this study. Instead, verification of the transport processes of newly developed multicomponent reactive gas flow has been presented in details.

Research on multicomponent reactive gas transport through unsaturated soil or in porous medium has rarely been carried out. Due to the lack of required information, a complete validation of the developed model was not possible. Therefore, the individual processes of multicomponent reactive gas transport have been verified separately to ensure implementation accuracy of the processes in the model.

Section 5.2 presents the verification and validation of advective and diffusive flow in one dimension. The developed governing gas flow equation has been verified against the analytical solutions presented by Ogata and Banks (1961). Verification has been carried out considering pure diffusion first and then advective-diffusive process has been verified for a single gas species.

Section 5.3 deals with the verification of the multicomponent advective flow. To obtain the multicomponent advective gas fluxes, approach taken by Mason and Malinauskas (1983) has been considered. Equations have been verified for isothermal condition. A partial validation exercise has also been carried out in this section. The implementation of multicomponent advection has been validated against the results obtained from the numerical model presented by Pini et al. (2011) who developed the model for carbon capture and sequestration in a coal bed.

The verification exercises of multicomponent diffusive flow have been detailed in section 5.4. The Fick's law of diffusion is widely applicable in case of binary diffusion. In multicomponent system, a particular species is simultaneously subjected to a number of binary collisions with other species as it flows. The main objective of this section is to compare the flow behaviour of gas components in a multicomponent system following multicomponent diffusion approach with binary diffusion approach. Since, in a multicomponent system number of species presents with various values of diffusion coefficients, investigation has been carried out on the order of diffusion coefficients to observe its impact on the flow behaviour. Diffusion coefficients obtained from free fluid have been factorised using tortuosity factor to calculate the effective diffusion coefficients in porous medium.

The implementation of the geochemical reaction sink/source term related to the governing equation of transport of gases has been tested in section 5.5. The coupling scheme of COMPASS-PHREEQC has been tested and verified in this section. The coupled set of governing equations describing multicomponent transport and chemical reactions are not easily predictable to analytical solutions except in the very simplest cases. Therefore, a simple verification exercise of the sink/source term has been carried out using Henry's law which measures the amount of gas that can be dissolved in certain amount of liquid at a gas-liquid equilibrium. The verification has been carried out in two steps. Firstly, the simulated results obtained from PHREEQC have been verified against an analytical calculation. Secondly, results have been obtained for a COMPASS simulation and a coupled COMPASS-PHREEQC simulation. An overall conclusion of this chapter has been presented in section 5.6.

5.2 Advection and diffusion in one dimension

This section represents the attempt that has been taken to verify pure diffusion and advection-diffusion components of the governing equation of gas flow in a single dimension. The results obtained from numerical simulation have been compared with the analytical solution of Ogata and Banks (1961) which is applicable for one-dimensional problems only. This exercise demonstrates the transient distribution of a gas species within the soil or porous medium. Fick's law and Darcy's law have been adopted in the model to characterise diffusive and advective flow respectively.

5.2.1 Analytical solution

For a one dimensional gas flow, through homogeneous isotropic porous media, Fetter (1999) suggested that the analytical solution for advective and diffusive flow can be expressed as:

$$\frac{\partial c_g}{\partial t} = D\frac{\partial^2 c_g}{\partial x^2} - \mathbf{v_g}\frac{\partial c_g}{\partial x} \tag{5.1}$$

where, D is coefficient of diffusion, $\mathbf{v_g}$ represents average linear velocity of the gas component, t is time and x is the distance in the direction of flow.

Based on Dirichlet type boundary condition Ogata and Banks (1961) has proposed a solution of the equation above based on the following initial and boundary conditions:

$$c_g(x,0) = C_i \tag{5.2}$$

$$c_g(0,t) = C_0 \tag{5.3}$$

$$\frac{\partial c_g(\infty,t)}{\partial x} = 0 \tag{5.4}$$

where, C_i is the initial concentration and C_0 represents the concentration at the source or at x = 0. The analytical solution has been given as follows:

$$c_g(x,t) = C_i + \frac{C_0 - C_i}{2}\left[erfc\left(\frac{x - \mathbf{v_g}t}{2\sqrt{(Dt)}}\right) + exp\frac{\mathbf{v_g}x}{D}erfc\left(\frac{x + \mathbf{v_g}t}{2\sqrt{(Dt)}}\right)\right] \tag{5.5}$$

The equation (5.5) has been used to obtain the gas concentration profiles and the results are compared with those obtained from the numerical model.

5.2.2 Pure diffusion

Assuming the linear average velocity equals to zero, equation (5.5) reduces to the form of pure diffusive flow. To carry out the numerical simulation a two dimensional soil sample of 30 cm by 3 cm has been used. The model domain has been discretised into 80 equally sized 4-noded quadrilateral elements. Since, there is no flow in the y-direction; the simulated results are representative of one dimensional analysis. A time-step of 3600 seconds has been considered during the simulation.

5.2.2.1 Boundary conditions and material parameters

The initial and boundary conditions have been presented in Figure 5.1. The simulation was carried out under isothermal condition. A dry soil sample has been considered that initially contained no hydrogen gas in the air. A constant gas concentration was considered at one boundary side (x = 0 cm) and the other boundary (x = 30 cm) has been considered impermeable to gas flow.

Boundary condition	Initial condition	Boundary condition
T = 298K c_g = 10.0 mol/m^3	T = 298K c_g = 0.0 mol/m^3	T = 298K c_g = 0 mol/m^3

Figure 5.1: Schematic diagram of the initial and boundary conditions for the simulation of pure diffusion.

The material parameters have been listed in Table 5.1. The parameters are representative of a compacted bentonite sample. Hydrogen has been used as the representative gas component and the binary diffusion coefficient has been collected from Cussler (1984). The effective diffusion coefficient has been obtained using Millington and Quirk (1961) relationship.

Table 5.1: Material parameters for the simulation of pure diffusion.

Material parameters	**Relationship / value**
Porosity, n	0.40
Diffusion coefficient (m^2/s)	6.11×10^{-5}
Tortuosity correlation (Millington and Quirk, 1961)	$n^{1/3}S_g^{7/3}$
Gas saturation, S_g	1.0

5.2.2.2 Results and discussion

Figure 5.2 represents the results obtained from the analytical solution and numerical simulation. From injection face the gas has been distributed along the soil sample due to diffusion only. For one-dimensional, isothermal flow problem the simulated result has showed good agreement with the analytical results.

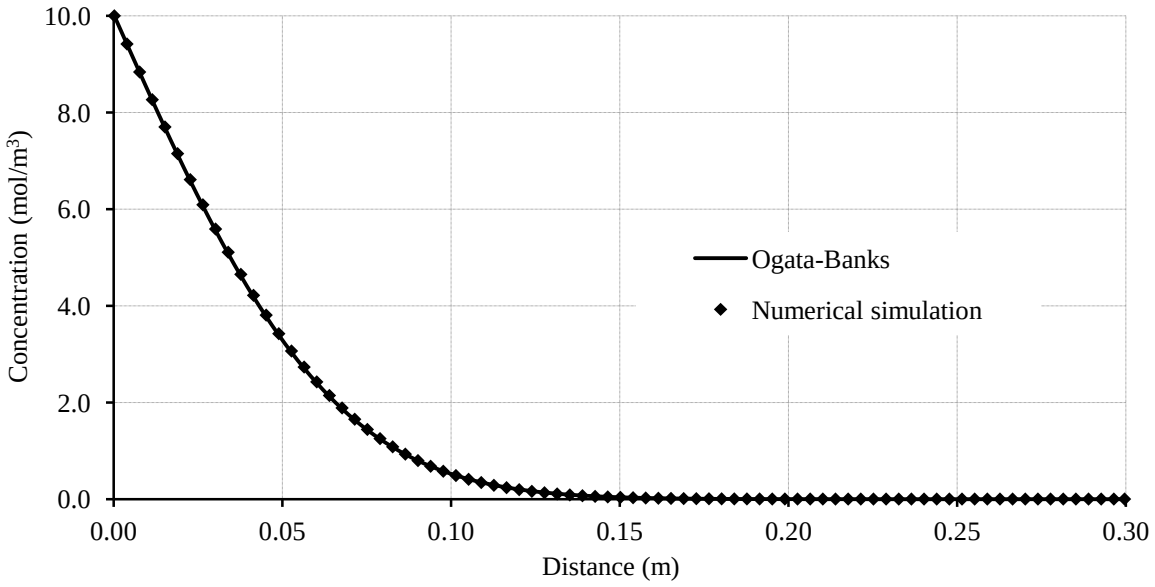

Figure 5.2: Comparison between Ogata-Banks analytical solution and numerical simulation for a pure diffusion problem.

The simulation has also been carried out including three gases in order to test that the multicomponent algorithm has been implemented correctly. The results have been found similar in each case with the assumption that the diffusion of a single gas component is not affected by the presence and movement of the other components. Multicomponent diffusive flow verification exercises have been discussed in details in section 5.4. This exercise therefore demonstrates that the diffusive flow component of the model works correctly.

5.2.3 Advective-diffusive flow

In presence of a bulk gas flow equation (5.5) has been used to calculate the combined advective and diffusive flow of gases. To obtain the average linear velocity, Darcy's law has been used. The constant value of $\mathbf{v_g} = 3.50\times10^{-10}$ m/s has been used in the analytical solution given in equation (5.5). Again a soil sample of 30 cm by 3 cm has been used. The model domain has been discretised into 80 equally sized 4-noded quadrilateral elements with no flow in *y*-direction and a time-step of 3600 seconds has been considered in the simulation.

5.2.3.1 Boundary conditions and material parameters

The boundary conditions of the numerical simulation have been presented in Figure 5.3.

Boundary condition	Initial condition	Boundary condition
T = 298K c_g = 40.0 mol/m^3	T = 298K c_g = 32.0 mol/m^3	T = 298K $\frac{\partial c_g}{\partial x} = 0$

Figure 5.3: Schematic diagram of the initial and boundary conditions of the advective-diffusive flow simulation.

The material parameters for the simulation have been presented in Table 5.2. The domain has been considered fully gas saturated therefore, the gas relative permeability equals to unity.

Table 5.2: Material parameters for the simulation of 1D advective-diffusive flow.

Material parameters	**Relationship / value**
Porosity, n	0.40
Diffusion coefficient (m^2/s)	6.11×10^{-5}
Tortuosity correlation (Millington and Quirk, 1961)	$n^{1/3}S_g^{7/3}$
Gas saturation, S_g	1.0
Gas phase intrinsic permeability, k_{int} (m^2)	1.0×10^{-20}
Dynamic viscosity, μ (Ns/m^2)	1.85×10^{-5}

5.2.3.2 Results and discussion

Considering advective flow together with diffusive flow, the solution of Ogata-Banks analytical solution and numerical simulation has been presented in Figure 5.4. The simulated result shows good agreement with the analytical solution. This represents the processes has been implemented successfully in the model.

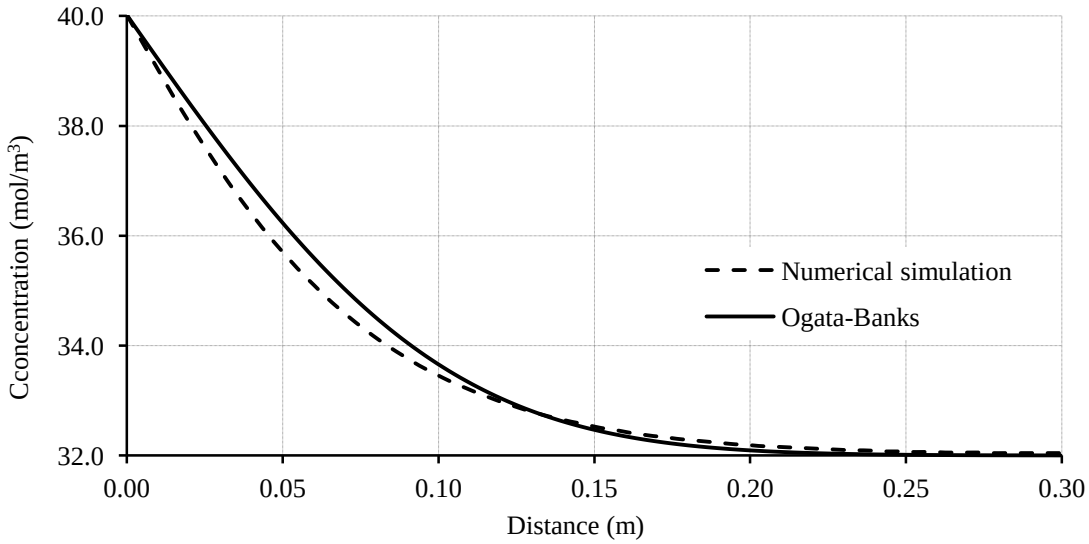

Figure 5.4: Comparison between Ogata-Banks analytical solution and numerical simulation for an advection-diffusion problem.

The slight variation in the analytical solution is due to the assumed average advective velocity in the Ogata-Bank's equation. The velocity has been calculated using equation (3.27) with a concentration difference of 8.0 mol/m^3 over the 30 cm length of the domain. In case of numerical simulations, the advective velocity at each element is calculated using the concentrations (or pressures) at the adjacent nodes. Therefore, numerical simulations measure elemental velocities (which depend on element size and concentrations of the connected nodes) rather than an average advective velocity over the model domain.

5.3 Multicomponent advective gas flow

This section represents the verification exercise of advective flow of multicomponent gases through unsaturated soil. The bulk flow of a gas mixture facilitates the advective flow of individual gas species. A partially saturated soil sample of 30cm by 3cm has been used in the simulation. The two-dimensional finite element domain has been discretised into 80 elements of 4-noded quadrilaterals. Simulation results are checked for spatial and temporal convergence. The simulation has been carried out in isothermal condition for a period of 222 years. A variable time-step regime is used to allow the time-step to increase or decrease depending upon convergence criteria.

5.3.1 Advective flow of gases due to the influx of a particular species in the gas mixture

A mixture of three gas components has been considered in this simulation. In a mixture of gases if the concentration of a particular gas changes it affects the concentration and therefore the pressure of the system causing a change in the bulk flow. Nitrogen (N_2), oxygen (O_2) and hydrogen (H_2) have been used as gas component 1, component 2 and component 3 respectively. A constant flux of hydrogen has been provisioned at the injection face.

5.3.1.1 Boundary conditions and material parameters

The initial and boundary conditions of has been presented in Figure 5.5. The amount of Nitrogen and oxygen has been proportioned to the ratio at the atmosphere and rest space has been taken by hydrogen. At the injection face hydrogen influx is 1.0×10^{-9} mol/m^2/s and the other side of the sample has been made impermeable to any of the gas components.

Boundary condition	Initial condition	Boundary condition
u_l = 0 Pa T = 298K H_2 *flux* = 1.0×10^{-9} mol/m^2/s	u_l = 0 Pa T = 298K $c_g^1(N_2)$ = 112.43 mol/m^3 $c_g^2(O_2)$ = 30.30 mol/m^3 $c_g^3(H_2)$ = 1.44 mol/m^3	u_l = 0 Pa T = 298K $c_g^1(N_2)$ = 0 mol/m^3 $c_g^2(O_2)$ = 0 mol/m^3 $c_g^3(H_2)$ = 0 mol/m^3

Figure 5.5: Schematic of the boundary conditions of multicomponent advective gas flow simulation.

Since the system is under isothermal condition, an initial temperature of 298K has been applied over the domain and maintained during the simulation. For all gas condition, the relative gas permeability is equal to one. The material parameter has been presented in Table 5.2.

Table 5.2: Material parameters for multicomponent advective flow simulation

Material parameters	**Relationship / value**
Porosity, n	0.40
Gas phase intrinsic permeability, k_{int} (m^2)	1.0×10^{-12}
Relative gas permeability	1.0
Dynamic viscosity (Ns/m^2)	1.82×10^{-5}

5.3.1.2 Results and discussions

The results of multicomponent advective flow of gases have been presented in Figure 5.6.

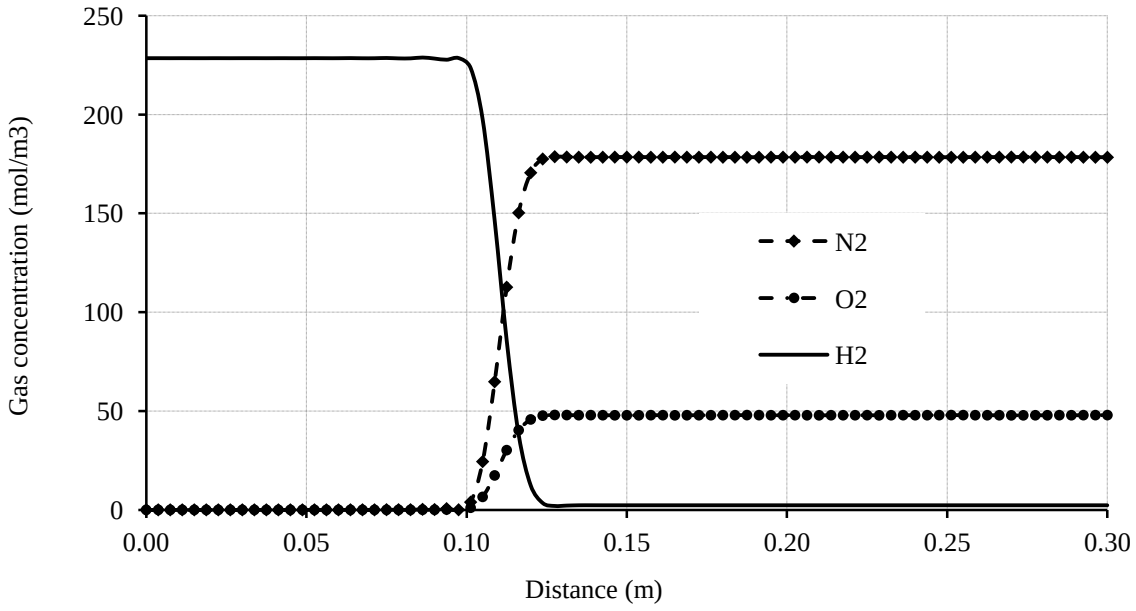

Figure 5.6: Gas concentration profile. The continuous influx of hydrogen has pushed nitrogen and oxygen from the injection face due to advection.

The continuous influx of hydrogen increases its concentration and mole fraction in the model domain. The mole fraction of hydrogen, x_{H_2} can be written using equation (3.61) as:

$$x_{H_2} = \frac{c_{H_2}}{\left(c_{N_2} + c_{O_2} + c_{H_2}\right)}$$

Similar expression can be written for nitrogen and oxygen. From Figure 5.6 it is noticeable that at the injection face hydrogen concentration, at the end of simulation period, is 228.5 mol/m^3 and oxygen and nitrogen concentrations are approximately 4.8×10^{-5} mol/m^3 and 1.8×10^{-4} mol/m^3 respectively. Substituting these values in the above expression results hydrogen mole fraction, $x_{H_2} \approx 1$ and from similar expressions calculated mole fraction of oxygen and nitrogen are $x_{O_2} \approx 0$ and $x_{N_2} \approx 0$ respectively. As the summation of mole fractions ($x_{N_2} + x_{O_2} + x_{H_2}$) equals to one, the verification exercise demonstrates the successful implementation of multicomponent advective flow in the model.

Influx of hydrogen increases the bulk flow of gas mixture according to equation (3.64). The relationship can be expressed in this example as:

$$J = -cRTk_g \nabla\left(c_{N_2} + c_{O_2} + c_{H_2}\right)$$

The bulk flow therefore facilitates the movement of gas components due to advection from the region of high pressure (or concentration) to the region of low pressure. In this case from the injection face to the impermeable face of the soil sample. Figure 5.6 shows that the advective flow of hydrogen gas has pushed away nitrogen and oxygen front from the injection face. Advective flow simulations are often subjected to numerical oscillations which is also observable in Figure 5.6. To minimise the numerical oscillation during the simulation a very small amount of diffusion has been added which has a negligible effect on the overall advective flow. The capability of developed model to simulate multicomponent advection has been presented and the results have shown good agreement with the theory presented in chapter 3.

5.3.2 Partial validation exercise of multicomponent advective gas flow

The following verification exercise has been carried out to validate the multicomponent advective gas flow against the simulated results of Pini et al. (2011) who carried out a numerical simulation on the performance of carbon dioxide storage and coal bed methane recovery with particular emphasis on sorption induced swelling on the coal bed permeability and its consequences on the carbon dioxide storage operation. This exercise is not intended to verify all of their results; rather a part of the simulation that dealt with the advective flow has been compared with the simulated results of currently developed model. The 100m long model domain was initially fully saturated with methane gas and carbon dioxide has been injected to the system. The simulation was carried out under isothermal conditions for 16 days and all other mechanical and physicochemical properties have been assumed to remain constant during the simulation.

In this exercise, the 100m by 1m model domain has been discretised into 100 elements of 4-noded quadrilaterals. A variable time-step regime has been considered to allow the time-step to increase or decrease depending upon the convergence criteria. Simulation has been carried out for 16 days.

5.3.2.1 Boundary conditions and material parameters

The initial and boundary condition of the simulation has been presented in Figure 5.7. The material parameters have been presented in Table 5.3.

Boundary condition	Initial condition	Boundary condition
u_l = 0 Pa T = 318K c_{CO_2} = 1881.84 mol/m^3	u_l = 0 Pa T = 318K c_{CH_4} = 582.43 mol/m^3 c_{CO_2} = 0.0 mol/m^3	$\frac{\partial u_l}{\partial x}$ = 0 T = 318K $\frac{\partial c_{CH_4}}{\partial x}$ = 0 $\frac{\partial c_{CO_2}}{\partial x}$ = 0

Figure 5.7: Schematic diagram of the initial and boundary conditions for the validation exercise.

Table 5.3: Material parameters for the partial validation of multicomponent advective flow

Material parameters	**Relationship / value**
Porosity, *n*	0.08
Permeability (m^2)	9.869233×10^{-15}
Relative gas permeability	1.0
Dynamic viscosity (Ns/m^2)	1.47×10^{-5}

5.3.2.2 Results and discussion

Figure 5.8 presents the results obtained from the numerical simulations in a graphical form. The simulated graphs have been compared with the results reported by Pini et al. (2011) for a 16 day simulation period. The similar trend of graphs in Figure 5.8 suggests a good agreement between the simulated results and the results obtained by Pini et al. (2011).

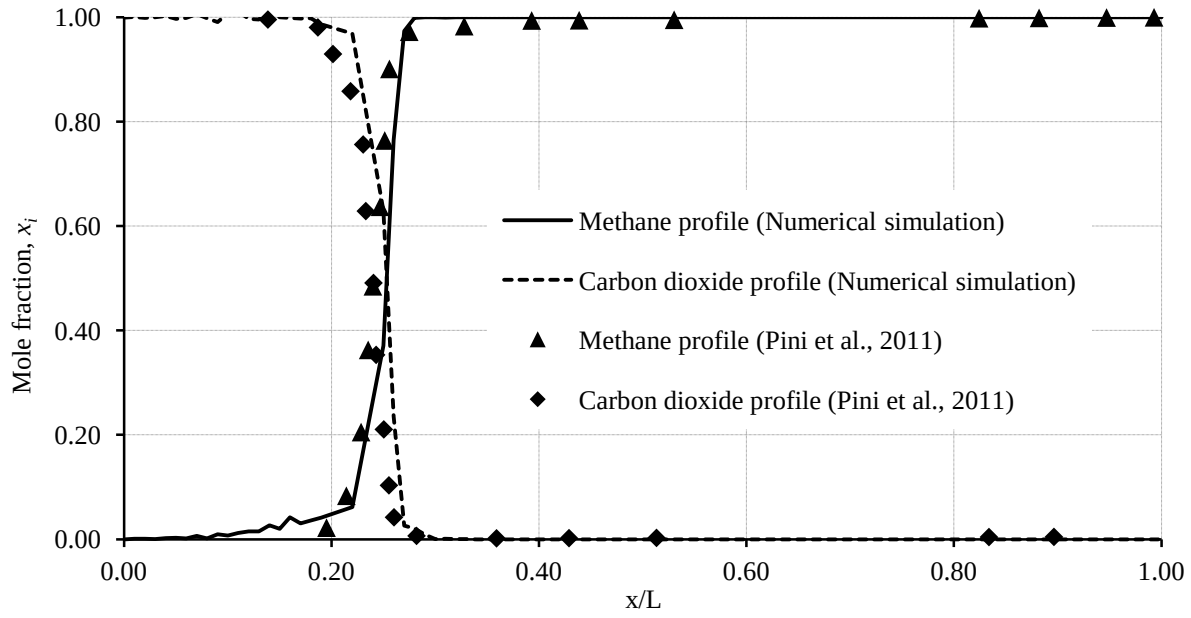

Figure 5.8: Distribution of methane and carbon dioxide along the coal bed. Comparison between the results presented by Pini et al. (2011) and COMPASS simulation. The axial coordinate x is in meter.

Figure 5.8 shows that the advective flow of carbon dioxide has pushed the methane front from the injection face and the mole fractions of carbon dioxide, x_{CO_2} and methane, x_{CH_4} at the injection face are 1.0 and 0.0 respectively. The explanations of the results are similar to that of the previous section, section 5.3.1 and therefore, have not been repeated. To reduce the numerical oscillation a negligible amount of diffusion has been considered in the simulation. The partial validation exercise demonstrates that the multicomponent advective flow phenomena have been successfully adopted in the model.

5.4 Multicomponent diffusive gas flow

Successful implementation of diffusive flow for a single component has already been presented in section 5.2.2. In this section, simulations have been carried out to verify the diffusion phenomena of the multicomponent gas flow equation. Two important aspects of multicomponent diffusive flow have been examined in this exercise. The flow behaviour of gases a) under multicomponent diffusion and binary diffusion approach has been compared b) for various ranges of diffusion coefficients. Therefore, two sets of diffusion coefficients data have been used in this section. The verification exercise also demonstrates the applicability of binary diffusion coefficients to model multicomponent diffusive flow.

In first set of simulations, pore gas has been considered as a mixture of hydrogen, oxygen and carbon dioxide. At standard pressure and temperature (STP) diffusion coefficient of hydrogen is higher than the diffusion coefficient of oxygen and nitrogen. The boundary conditions and material parameters of this simulation have been presented in Figure 5.9 and Table 5.4. In the beginning, concentration of gas components in the buffer has been obtained by considering multicomponent diffusion coefficients which can be calculated using equation (3.70), (3.71) and (3.72). Later, the multicomponent effect has been ignored and simulation has been carried out using binary diffusion coefficients.

The second set of simulations has been carried out using methane which has a similar order of diffusion coefficients like oxygen and carbon dioxide at STP. The initial and boundary conditions of the simulations remain similar to that of the first set except hydrogen which has been replaced by methane in this exercise. Material parameters for this simulation have been presented in table 5.5. Simulations have been carried out under the concept of both multicomponent diffusion and binary diffusion.

A dry soil sample of 30cm by 3cm has been considered as the model domain. The model has been discretised into 80 equally sized 4-noded quadrilateral elements. Simulation has been carried out for 2.5 years and a variable time-step regime has been used allowing the time-step to increase or decrease depending upon the convergence criteria. No advection has been allowed during the simulation.

5.4.1 Boundary conditions and material parameters

The simulations have been carried out under isothermal condition. At one side of the sample, a fixed concentration of 50.0 mol/m^3 for each gas component has been applied while the other side has been impervious to all gas components. The initial and boundary condition of this simulation has been presented in Figure 5.9.

Boundary condition	Initial condition	Boundary condition
T = 298K $\left.\frac{\partial c_{O_2}}{\partial x}\right\|_{x=0}$ = 0.0 $\left.\frac{\partial c_{H_2}}{\partial x}\right\|_{x=0}$ = 0.0 $\left.\frac{\partial c_{CO_2}}{\partial x}\right\|_{x=0}$ = 0.0	u_l = 0 Pa T = 298K c_{O_2} = 25.0 mol/m^3 c_{H_2} = 10.0 mol/m^3 c_{CO_2} = 20.0 mol/m^3	u_l = 0 Pa T = 298K c_{O_2} = 50.0 mol/m^3 c_{H_2} = 50.0 mol/m^3 c_{CO_2} = 50.0 mol/m^3

Figure 5.9: Schematic diagram of the initial and boundary conditions for the simulation of multicomponent diffusive flow.

Table 5.4: Binary diffusion coefficients of oxygen (O_2), hydrogen (H_2) and carbon dioxide (CO_2) at STP. Data has been collected from Cussler (1984).

Binary components	**Diffusion coefficients, ×10^{-5} (m^2/s)**
Air - O_2	1.75
Air - H_2	6.11
Air - CO_2	1.42
O_2 - H_2	6.97
O_2 - CO_2	1.60
H_2 - CO_2	6.40

The material parameter of this simulation is similar to the parameters listed in Table 5.2. Binary diffusion coefficients of oxygen, hydrogen and carbon dioxide has been presented in Table 5.4. Table 5.5 presents the binary diffusion coefficients of oxygen, carbon dioxide and methane. Hdrogen has been replaced by methane later in the second simulation while the other conditions and material parameters remain unchanged. The aim is to observe the behaviour of multicomponent gases when the diffusion coefficients are similar to each other.

Table 5.5: Diffusion coefficients of oxygen (O_2), methane (CH_4) and carbon dioxide (CO_2) at STP. Data has been obtained from Cussler (1984).

Binary components	**Diffusion coefficients, $\times 10^{-5}$ (m^2/s)**
Air - O_2	1.75
Air - CH_4	1.96
Air - CO_2	1.42

5.4.2 Results and discussion

The simulated results for the diffusion data set listed in Table 5.4 have been presented in Figure 5.10 and Figure 5.11. Evolution of gas concentration behaviour along the buffer has been found similar along the buffer. At points near the right edge of the buffer, x = 30 cm, steady state have been achieved earlier than that of left edge. Therefore, the evolution graphs have been obtained at the left hand edge, x = 0, of the model domain. Results plotted in Figure 5.10 consider multicomponent diffusion while Figure 5.11 has been generated based on the binary diffusion. The multicomponent diffusion matrix has been calculated using equations (3.70), (3.71) and (3.72) presented in chapter 3. The binary diffusion coefficients listed in Table 5.4 has been used to calculate the multicomponent diffusion coefficients and can be expressed in matrix form as:

$$[\mathbf{D}] = \begin{bmatrix} 1.96\times10^{-5} & -2.63\times10^{-5} & 9.03\times10^{-7} \\ -4.67\times10^{-7} & 6.67\times10^{-5} & -1.78\times10^{-7} \\ -8.31\times10^{-7} & -2.20\times10^{-5} & 1.76\times10^{-5} \end{bmatrix}$$

It is noticeable that the matrix is dominated by diagonal elements which are similar to the binary diffusion coefficients. Comparing with Figure 5.11, Figure 5.10 suggests that the flow of oxygen and carbon dioxide has been influenced by the diffusive flow of hydrogen which also can be explained using the above matrix. Taylor and Krishna (1993) stated that, if the ratio of the off diagonal terms to diagonal terms of diffusion matrix, is greater than one, such as $\left|D_{12}/D_{11}\right|>1$, the movement of species 1 is influenced by the movement of species 2. In this case the flux of oxygen has been influenced by the diffusive flux of hydrogen. Similarly, movement of carbon dioxide has been affected by the flow of hydrogen, since $\left|D_{32}/D_{33}\right|>1$. The diffusion of hydrogen is faster in the system than the others.

Figure 5.11 represents the results considering the binary diffusion of gases through air only and any kind of multicomponent interaction has been omitted. It is obvious that in absence of multicomponent diffusion the movement of gas components does not influence each other and the diagonal element of the matrix contributes to the major diffusion processes. The graphs of hydrogen, oxygen and carbon dioxide in Figure 5.10 and Figure 5.11 show similar trend in case of multicomponent diffusion and binary diffusion respectively. In both cases hydrogen evolution reaches to a steady state around after 2.0×10^7 seconds. Apart from in the initial variation, oxygen and carbon dioxide flows in same manner in both figures.

Results of numerical simulation for the gases with similar type of diffusion coefficients, Table 5.5, have been presented in Figure 5.12 and Figure 5.13. Following the same approach as mentioned above, binary diffusion coefficients of Table 5.5 has been used to calculate the multicomponent diffusion coefficients matrix which can be expressed as:

$$[D]=\begin{bmatrix} 1.73\times10^{-5} & -7.64\times10^{-7} & 6.68\times10^{-7} \\ -1.85\times10^{-6} & 1.54\times10^{-5} & -8.45\times10^{-7} \\ -7.55\times10^{-7} & 1.17\times10^{-7} & 1.49\times10^{-5} \end{bmatrix}$$

From Figure 5.12 and Figure 5.13 it is noticeable that the multicomponent diffusion and binary diffusion behave very similarly. Since the movement of a single gas component does not affect the flow of others (the ratio of the matrix elements $\left|D_{12}/D_{11}\right|<1$), gases flow due to their individual concentration gradient.

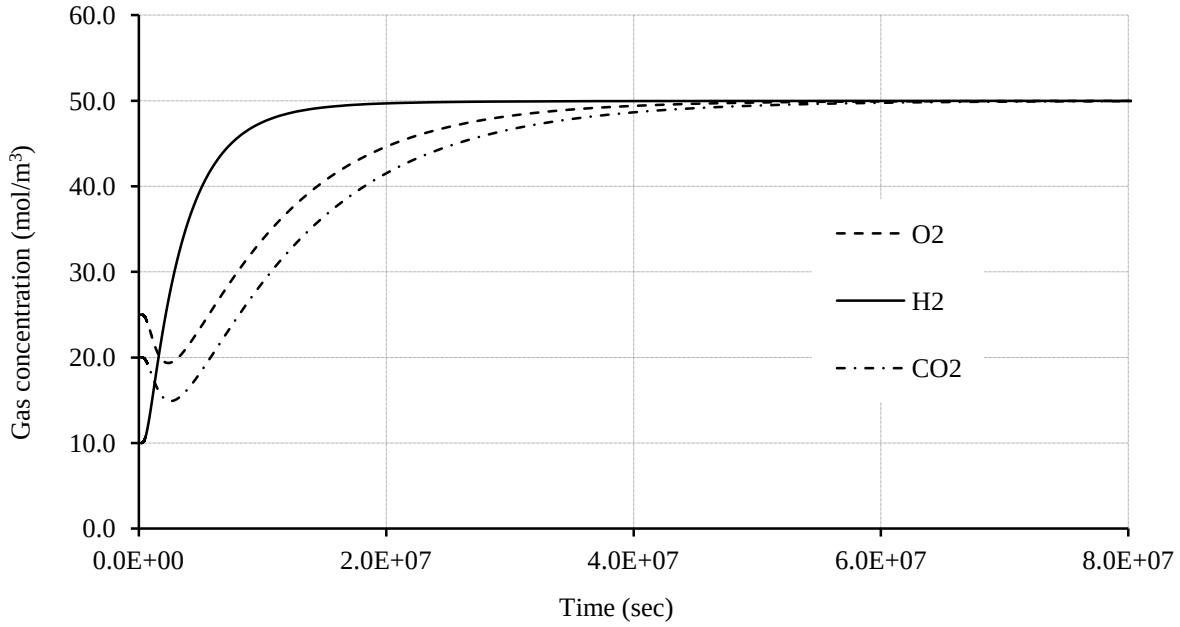

Figure 5.10: Evolution of oxygen, hydrogen and carbon dioxide due to multicomponent diffusive flow (Data: Table 5.4). Hydrogen reaches to steady state prior to oxygen and carbon dioxide due to its higher diffusion rate than the others.

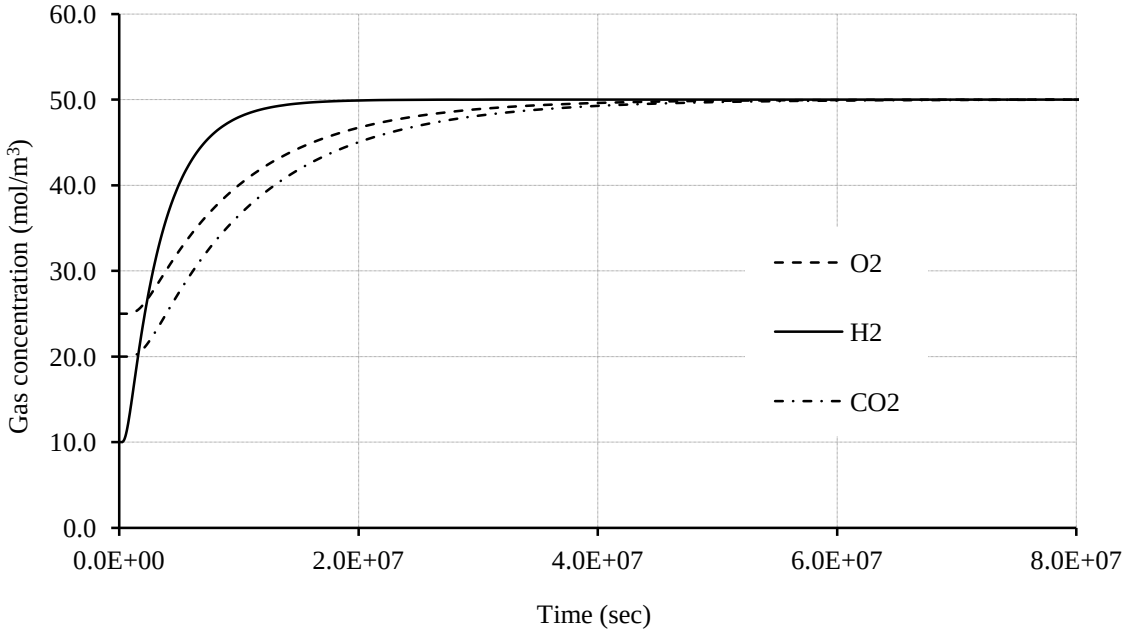

Figure 5.11: Evolution of gas concentrations due to binary diffusion (Data: Table 5.4). The multicomponent diffusion coefficients have been replaced by the Fick's binary diffusion. Simulation has been carried out for 2.5 years.

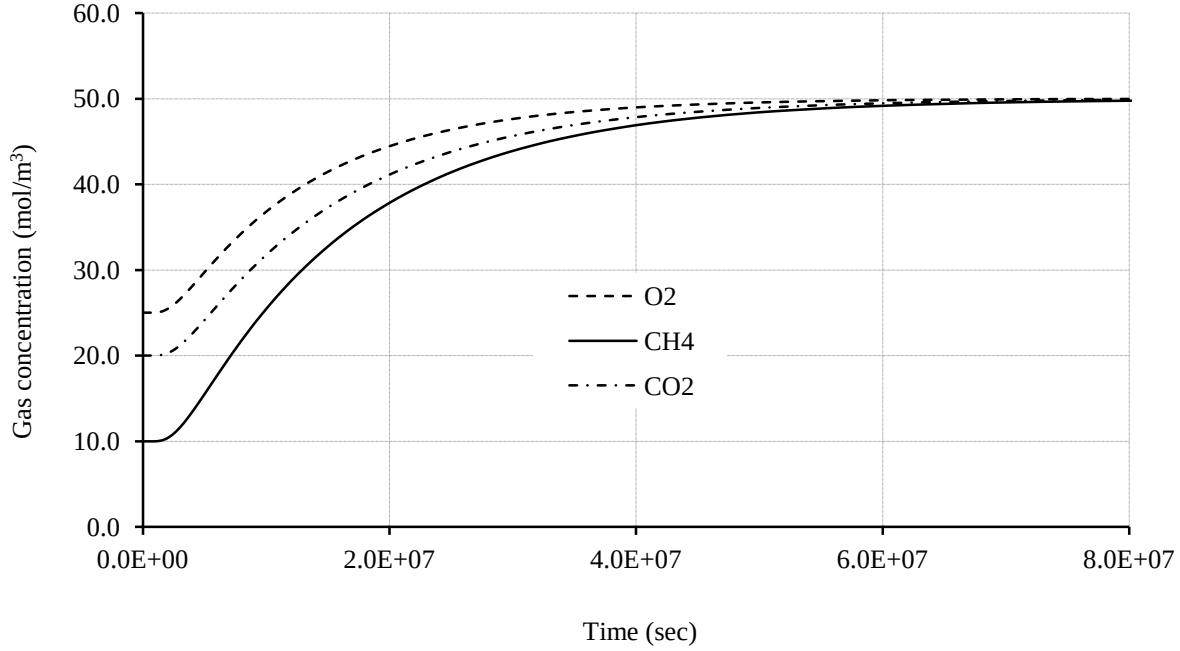

Figure 5.12: Evolution of gas concentrations due to multicomponent diffusion (Data: Table 5.5). The diffusion coefficients of gases are of similar order.

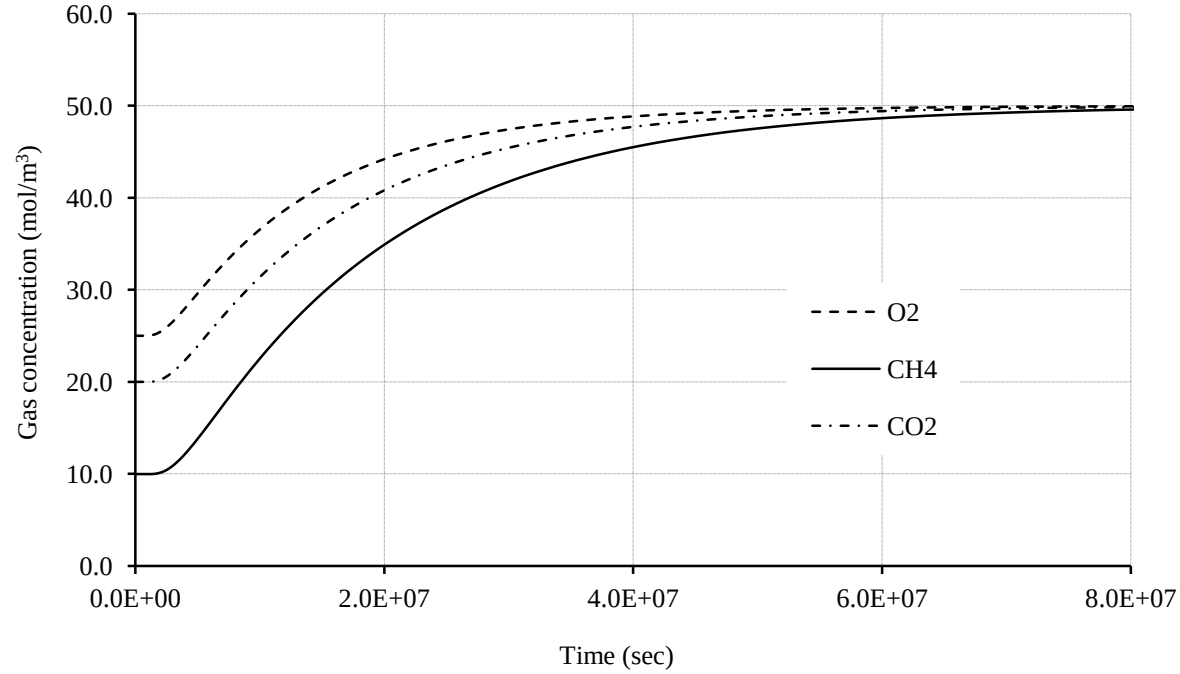

Figure 5.13: Evolution of gas concentrations due to binary diffusion (Data: Table 5.5). The multicomponent diffusion coefficients have been replaced by the Fick's binary diffusion.

From the above discussion it can be summarise that the diffusive flow behaviour of gases in a multicomponent system follows similar trend for multicomponent diffusion coefficients and binary diffusion coefficient. The gases with similar diffusion coefficients do not affect the transport of other components while gases with different order of diffusion coefficients influence the movement of each other and the dominant diagonal diffusion coefficients in the multicomponent diffusion matrix is similar to the binary diffusion coefficients.

It has been observed from this that the diffusive flow of individual components takes place due to their concentration gradient. However, in case of a multicomponent system the flow of a single component might be influenced the movement of other gas components depending on concentration of the gas components and the order diffusion coefficients. The theoretical developments of diffusive flow support the results/observations of these tests, suggesting that the transport process has been successfully adopted in the code.

5.5 Verification of linking the geochemical sink/source term

The objective of this section is to verify whether the sink/ source term has been correctly implemented in the numerical model. As previously mentioned, the sink/source term of the governing equation e.g. equation (3.58) of multicomponent pore gas flow has been calculated using the geochemical code PHREEQC. The amount of a gas component that can be lost from or gained to gas phase due to possible geochemical reactions, such as, ion-exchange, dissolution/precipitation, surface complexation or any gas phase - liquid phase equilibrium. One of the simplest form of the verification exercise can be obtained by calculating the sink/ source term which represent the exchange of the phase e.g. gas phase to liquid phase equilibrium using Henry's law. Two sets of verification exercise have been designed and conducted. First, the implementation of Henry's law in PHREEQC has been tested against a manual calculation. In the second test, theoretically implemented Henry's law as a sink/source term in the developed model, COMPASS has been tested against the linked COMPASS and PHREEQC model. It is noted that the linking approach of the model is based on a sequential non-iterative approach.

5.5.1 Verification of Henry's law with PHREEQC and analytical solution

Henry's law determines the amount of gas that can be dissolved in a solution based on the absolute pressure of the gas above the solution.

Table 5.6: Dissolved hydrogen concentrations at various gas pressures. Henry's constant for hydrogen 7.8×10^{-4} mol/L/atm (Sander, 1999).

Initial gas pressure (atm)	Dissolved gas concentration (mol/L)	Dissolved gas pressure (atm)	Final gas pressure (atm)
.01	7.8×10^{-6}	1.9×10^{-4}	9.8×10^{-3}
.05	3.9×10^{-5}	9.5×10^{-4}	4.9×10^{-2}
.10	7.8×10^{-5}	1.9×10^{-3}	9.8×10^{-2}
.50	3.9×10^{-4}	9.5×10^{-3}	4.9×10^{-1}
1.0	7.8×10^{-4}	1.9×10^{-2}	9.8×10^{-1}
5.0	3.9×10^{-3}	9.5×10^{-2}	4.9×10^{0}
10.0	7.8×10^{-3}	1.9×10^{-1}	9.8×10^{0}

It is obvious from the law that dissolved gas concentration varies proportionally with the gas pressure above the solution. The dissolved concentration of hydrogen has been calculated for various gas pressures, ranges from 0.01 atmospheric to 10 atmospheric pressures. Therefore, from the initial gas pressures (prior to Henry's law), remaining or final hydrogen pressures in the gas phase can be known. For hydrogen, Henry's constant, $K_{H_{cp}}$ of 7.8×10^{-4} mol/L/atm has been proposed by Sander (1999). The results have been presented in Table 5.6. Using PHREEQC, the dissolved hydrogen concentrations in pure distilled water have also been calculated for this pressure range. A comparison between manual calculation and PHREEQC simulation has been presented in Figure 5.15.

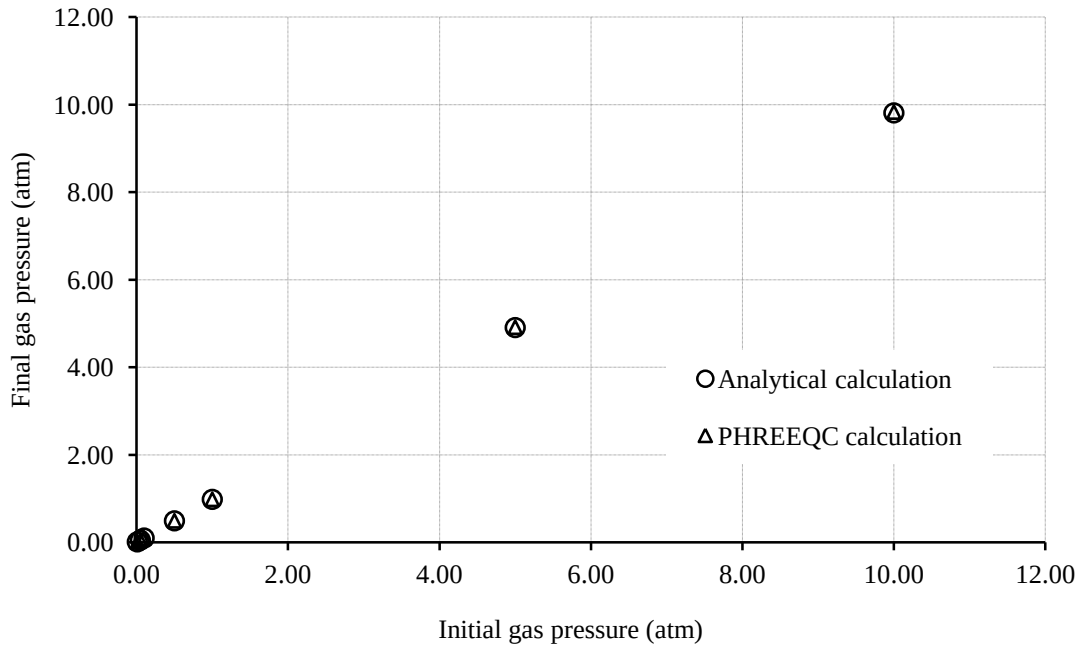

Figure 5.15: Comparison between analytical calculation and PHREEQC simulation to verify Henry's constant at gas-liquid equilibrium.

PHREEQC considers the dissociation of Hydrogen in pure water according to the following reaction.

$$H_2(g) \leftrightarrow 2H^+ + 2e^- \qquad \log K = -3.150 \qquad (5.6)$$

where, logK is the equilibrium constant of the chemical reaction and its value is numerically equal to previously mentioned Henry's constant.

The x-axis and y-axis represent the gas pressures (in atmospheres) before and after the implementation of Henry's law respectively. Figure 5.15 suggests that the results of analytical solution and PHREEQC calculations are in good agreement.

5.5.2 Verification of Henry's law with PHREEQC and analytical solution

As mentioned earlier, the theoretically implemented Henry's law as a sink/source term in the COMPASS model has been tested against the linked COMPASS and PHREEQC model in this exercise. According to law of mass action, the distribution of species at equilibrium can be expressed using an equilibrium constant as:

$$c_{H_{2(aq)}} = K_H c_{H_{2(g)}} \tag{5.7}$$

The dimensionless Henry's constant, $K_{H_{cc}} = 1.70\times10^{-2}$ has been proposed by Sander (1999).

Simulation has been carried out to observe the evolution of gas concentration (or pressure) in the model domain, considering the sink/source term at gas-liquid equilibrium. It has been assumed that isothermal condition prevail during the simulation period of 1000 years. A partially saturated soil sample of 30cm by 3cm has been used in the simulations. The model domain has been discretised into 80 equally sized 4-noded quadrilaterals. Hydrogen gas has been used as the representative gas component.

5.5.2.1 Boundary conditions and material parameters

A schematic diagram of the initial and boundary condition of the simulations have been presented in Figure 5.14. The corresponding pore water pressure represents an unsaturated buffer of a degree of saturation of 48.7%. Table 5.7 presents the material parameters.

Boundary condition	Initial condition	Boundary condition
T = 298K u_l = 0 Pa H_2 *flux* = 1.0×10^{-9} mol/m^2/s	T = 298K u_l = - 50×10^6 Pa c_{H_2} = 0.0 mol/m^3	T = 298K u_l = 0.0 Pa c_{H_2} = 0.0 mol/m^3

Figure 5.14: Schematic of the boundary conditions for the verification of sink/source term.

Table 5.7: Material parameters for the simulation of sink/source term verification.

Material parameters	**Relationship / value**
Porosity	0.40
Unsaturated gas conductivity (m/s)	1.10×10^{-7}
Diffusion coefficient (m^2/s)	6.11×10^{-5}
Henry's constant (dimensionless)	1.70×10^{-2}
Tortuosity correlation	$n^{1/3}S_g^{7/3}$

5.5.2.2 Results and discussion

The results obtained from the "COMPASS analysis" and "COMPASS-PHREEQC analysis" regarding the second test has been presented in Figure 5.16.

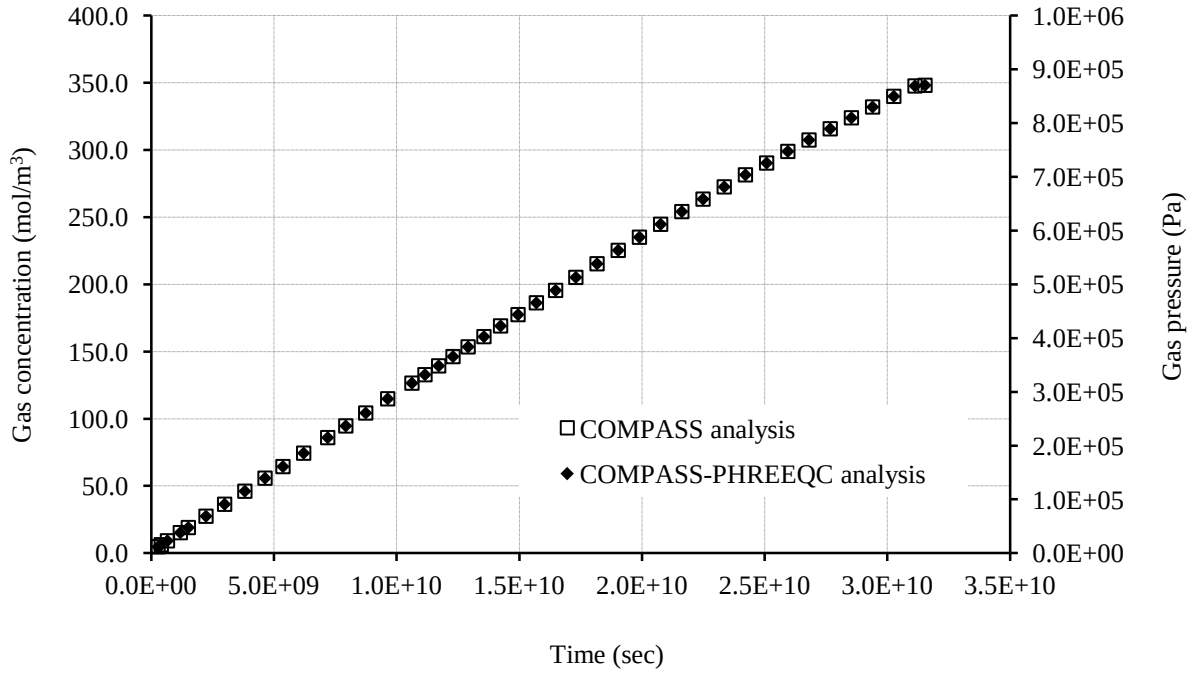

Figure 5.16: The verification of gas pressures or concentrations with time obtained from analysis using COMPASS and COMPASS-PHREEQC.

The continuous flux of hydrogen increases the gas pressure in the soil sample. But in presence of a liquid phase, some of the hydrogen dissolves in porewater following equation (5.7) to maintain the equilibrium. Simulations have been carried out for 1,000 years and the evolution of gas concentration (or pressure) using "COMPASS analysis" follows a similar trend with those obtained by modelling using the linked "COMPASS and PHREEQC analysis". It can be concluded that the approach adopted for linking COMPASS model (transport model) and geochemical model (PHREEQC) via the sequential non iterative approach has been correctly implemented in the code in terms of gas phase exchange. This provides confidence to utilise the linked models for further analysis.

5.6 Conclusion

In this chapter, a number of verification exercises have been presented in order to test the implementation of the governing equations of multicomponent pore gas flow in the model. The key components of gas transport including advective and diffusive flows and the geochemical sink/source term of the governing equations of gas transport have been tested and the results have been presented.

The developed model has been verified against the analytical solutions proposed by Ogata and Banks, for a single gas component, in case of both pure diffusion and advective-diffusive flow. By assuming the linear average velocity to zero the Ogata-Banks analytical solution has been calculated for pure diffusion. The advective-diffusive flow simulation considers Darcy's law to calculate the average linear velocity. The results of both simulations have been compared and have showed a good agreement with the developed theory.

The multicomponent advective flow has been examined and then validated in comparison with the results of an alternative numerical model. It has been found that in a mixture of gases the change of concentration (or pressure) of a particular species influences the flow of other species involved which represents the flow behaviour in cased of advective flow which is in fact in agreement with what can be expected from the theoretical formulation adopted. The simulated results have satisfied the conceptual argument and in comparison with the results of an alternative flow model good correlation has been achieved.

The verification of multicomponent diffusion has been carried out to satisfy two major objectives. In a mixture of gases, how the binary Fickian diffusion varies from that of a multicomponent diffusion and the impact of order of diffusion coefficients on the flow behaviour. It has been found that the multicomponent diffusive gas flow is dominated by the diagonal elements of the multicomponent diffusion coefficient matrix and these values are similar to the binary diffusion coefficients. The simulation considering binary diffusion has shown a similar flow pattern to the multicomponent diffusive flow pattern. In case of similar order diffusion coefficients, negligible difference in flow pattern has been observed in both binary diffusion and multicomponent diffusion.

The implementation of the geochemical sink/source term of the governing equation has also been carried out. Results obtained from the manual calculation, transport model simulation and transport model - chemical model simulations have satisfied the accuracy of implementation of the sequential non-iterative approach adopted for coupling the transport and reaction formulations under the examined condition. This verification exercise has further improved the confidence of coupled transport and reactive model and it can be concluded that the solution algorithm has been correctly implemented in the code.

References

Cleall, P.J., (1998) "An investigation of the thermo/hydraulic/mechanical behaviour of unsaturated soils, including expansive clays". PhD Thesis, University of Wales, Cardiff.

Cussler, E.L., (1984). "Diffusion: Mass transfer in fluid systems". Cambridge University Press.

Fetter, C.W., (1999). "Contaminant Hydrogeology". Prentice Hall. Upper Saddle River, New Jersy.

King, S.D., (1991). "A potential based model of coupled heat and moisture transfer in unsaturated soil". PhD Thesis, University of Wales, Cardiff.

Mason, E.A., Malinauskas, A.P., (1964). "Gaseous diffusion in porous media. IV. Thermal diffusion". *Journal of Chemical Physics* **41**, pp 3815.

Millington, R.J., Quirk, J.M., (1961). "Permeability of porous solids". *Transactions Faraday Society* **57**, pp 1200-1207.

Mitchell, H.P., (2002). "An investigation into the thermo/hydro/mechanical interactions involved in high level nuclear waste disposal". PhD Thesis, University of Wales, Cardiff.

Ogata, A., Banks, R.B., (1961). "A solution of the differential equation of longitudinal disperions in prous media". U.S. Geological survey professional paper, 411-A, pp A1-A9.

Pini, R., Storti, G., Mazzotti, M., (2011). " A model for enhanced coal bed methane recovery aimed at carbon dioxide storage". Springer Science+Business Media, LLC.

Seetharam, S. C., (2003). "An investigation of the thermo/hydro/chemical/mechanical behaviour of unsaturated soils". PhD Thesis, Cardiff University, UK.

Sander, R., (1999). "Compilation of Henry's Law Constants for Inorganic and Organic Species of Potential Importance in Environmental Chemistry". Max-Planck Institute of Chemistry, Mainz, Germany

Sedighi, M., (2011). "An investigation of Hydro-geochemical processes in coupled thermal, hydraulic, chemical and mechanical behaviour of unsaturated soils". PhD thesis, School of Engineering, Cardiff University.

Taylor, R., Krishna, R., (1993). "Multicomponent Mass Transfer". Wiley, New York.

Thomas, H.R., He, Y., (1997). "A coupled heat-moisture transfer theory for deformable unsaturated soil and its algorithmic implementation". *International Journal for Numerical Methods in Engineering* **40**, pp 3421-3441.

Thomas, H.R., He, Y., (1998). "Modelling the behaviour of unsaturated soil using an elasto plastic constitutive relationship". *Geotechnique* **48**, pp 589-603.

Thomas, H.R., He, Y., Onofrei, C., (1998). "An examination of the validation of a model of the hydro/thermo/mechanical behaviour of engineered clay barriers". *International Journal for Numerical and Analytical Methods in Geomechanics* **22**, pp 49-71.

6

Gas migration and pressure development in saturated clay buffer

6.1 Introduction

Compacted clays are often considered as potential buffer materials in various high level nuclear waste disposal concepts. It has been suggested in literature that the underground disposal of high level nuclear waste will be associated with gas generation. Therefore, in multi-barrier systems including waste packages with steel overpack surrounded by clay buffers, gas could accumulate and resulting in high pressure developments which perhaps endanger the safety and performance of the system. In this chapter, numerical simulations have been carried out to investigate gas migration and pressure development in initially saturated compacted clay buffer.

Hydrogen has been considered as the dominant gas species generated under the corrosion process. As explained in chapter 2, gas generation and migration experiments have indicated that there are a range of possibilities for the transport of gas from canisters through the buffers. However these experiments, by the nature of

simulating something that may occur over thousands of years, have accelerated the hydration of the bentonite and the release of gas and therefore the response of the buffer material differ from the reality, as certain physical processes, such as diffusion, are not able to be accelerated accordingly. In this work a number of scenarios, considering repository conditions, have been developed for numerical simulation. The foremost objective of this chapter is to investigate the maximum pressure developments in the buffer at realistic and conservative gas generation rates which have been presented in chapter 2. Also, the impacts of maximum gas pressures on the structural integrity of the system i.e. development of pressure induced fracture or preferential pathways in the buffer. Detailed stress analyses and possible chemical reactions have not been included in this study.

Section 6.2 deals with the development of simulation scenarios. The scenarios have been development based on the geology of host rock, disposal concept, canister, buffer, gas generation rate, gas migration processes and conditions at the boundary. The hydrogen generation rates adopted at the injection face have been collected from chapter 2, section 2.2. A saturation dependent flux boundary condition has been developed in this study. Since, the saturation state of the soil is an important parameter the newly developed flux boundary considers both gas inflow and water outflow due to corrosion reaction.

Section 6.3 deals with the preparation of numerical simulation. A condition for conceptual failure has been detailed in this section. Geometry and discretisation of the model domain, details on material parameters, initial and boundary conditions have also been presented in this section. An assessment of the coefficients of diffusion of hydrogen and air through different types of soil and soil-water have been studied and summarised.

Section 6.4 presents the results and discussions of the numerical simulations. Since a large number of simulation results have been obtained, it has been classified into two main sections based on the host rock condition. The other important variables have then organised and presented in the subsections and compared with the results within the section and with the counter section. An overall conclusion of the chapter has been presented in section 6.5.

6.2 Simulation scenario development

The disposal of radioactive waste is site specific in context of disposal concepts and properties of the host rock formation. The scenarios have been developed considering a series of "generic" repository conditions. A number of key aspects have been considered which are as follows:

- Host rock and disposal concept
- Canisters
- Buffers
- Gas generation and migration
- Boundary conditions

Subsequently these key aspects have been synthesised into a series of simulation scenarios to investigate gas migration and consequent pressure development in the engineered barrier. A detail discussion of the key aspects has been presented in the following subsections.

6.2.1 Host rock and disposal concept

The options for the disposal concepts generally based on high strength crystalline rock formation or lower strength sedimentary rock (clay) formation. The availability and mobility of water in the host rock formation plays major role in gas generation and migration. The disposal concept in high strength rock where natural flow of water primarily occurs in discrete fractures is likely to be different from that of low permeable clay rock formation.

Disposal of high level waste in crystalline hard rock could possibly be performed by using copper canisters with a cast iron insert. In this context, a generic repository could follow the Swedish KBS-3V disposal concept which is highly detailed and mature in nature due to decades of strong research activities. Due to the low hydraulic conductivity of clays, the disposal concept in clay host rock formations (such as the Swiss concept), might consider of using fabricated carbon steel canisters for waste isolation. Geological information, available from these two concepts, such as host rock porosity, hydraulic conductivity, presence of fracture and influences of these

properties to design and predict the lifetime of a canister, could be used for a generic disposal facility. Such scoping information has been converted into material parameters which have been considered in section 6.3.

The properties of a host formation, such as crystalline host rock which has been considered in Sweden for developing the disposal concepts for HLW and SF, is a potential candidate for host formation; similarly, interest has been shown towards clay host formation which has been considered in developing the Swiss disposal concept. The unfractured crystalline host rock hydraulic conductivity has been considered in the range of 10^{-12} m/s and the clay less than 10^{-13} m/s. A representative repository depth of 500m has also been proposed for this work.

6.2.2 Canisters

Two main types of metallic canisters, linked to disposal concepts are proposed. Copper canisters linked to the crystalline rock disposal concept and steel canisters linked to the clay rock disposal concept have been proposed. Copper canisters, preferred in hard rock formations, maintain good resistance against corrosion for a long period of time. Corrosion of steel starts when the cast iron inserts come in contact with water through canister defects and continues until there is no more steel available for corrosion. Initial defects (assumed, 1 mm^2) in copper canisters are assumed to be very small and will become enlarge after a long period of time. It has been suggested by SKB (1999) that the copper shell will fail after about 2.0×10^5 years leading to an increase in gas pressure in the system. In this work this is largely related to two parameters:

i. The initial buffer conditions when gas begins to be generated and
ii. The gas generation rate.

The initial saturation state for this disposal concept will be considered as fully saturated and at equilibrium with the hydrostatic water table, i.e. 5MPa. The gas generation rate has been determined using the steel corrosion rate and has not considered the exact defect as it is thought that this would be difficult to predict. This means that the crystalline rock concept simulations are implicitly conservative.

Carbon steel canisters will start corrosion as soon as it comes in contact with water in an anaerobic condition. The metallic content is of great importance in both types of canisters as this governs the gas production. However, when a steady state is reached in the analyses, conservatism is achieved as corrosion products and carbonates may form a protective layer around the metal and resulting in slow corrosion.

6.2.3 Buffer

Sodium rich bentonite buffers have been considered in context of a generic disposal concept. For a generic repository condition the buffer thickness has been chosen in a range between 300-800 mm for developing the scenarios. A buffer with excessive thickness could better resist erosion but would reduce heat transfer capacity. Increased thickness would also increase the distance whereby diffusion is the dominant migration process. However, if the thickness is small then the time to re-saturate the buffer is short, swelling pressures may be less and therefore, pressure induced fractures could possibly break through the buffer relatively easily. MX-80 bentonite has been considered in this study due to wealth of knowledge of the material behaviour as reported in the literature.

6.2.4 Gas generation and migration

It has been considered that isothermal condition prevails during gas generation period because the corrosion process is envisaged to initiate after the thermal period which prevents the buffer becoming fully saturated. In a repository condition anaerobic corrosion of metallic canisters and iron insert of copper canisters cause the majority of bulk hydrogen gas generation. Type of canister materials, contact area of water with canisters, quality (generation rate is slower in alkaline environment than acidic environment) and quantity of water available for corrosion process are important factors for gas generation and these are specific to site and disposal concept. Temperature and pH are seen to have important impacts as well as the material properties. A number of the studies use clay slurries where water availability may be high and ensured anaerobic conditions thereby providing upper bound estimations of repository gas generation rates, although the disposal concepts often consider compacted bentonite rather than slurries. It has been reported that the presence of bentonite may enhance the corrosion process, although the long term corrosion rate is

stated to be lower than that the maximum due to a protective surface produced during the corrosion process.

Therefore, the rates have been characterised into two categories, namely, realistic and conservative based on the experimental setup, condition and duration. Table 6.1 represents corrosion rates, based on laboratory experiments and natural analogue study, with consequent gas generation rates calculated. The experiments quote the corrosion process in terms of the depth of steel corroded over time and the rates are calculated via the approach of Volckaert and Mallants (1999), presented in equation 2.1. Importantly natural analogue studies (Miller et al., 2000) seem to corroborate laboratory scale test. Generation rates obtained and used by Nagra and SKB have been presented in Table 6.2. The rates quoted for both Nagra and SKB are consistent with the experimental results presented in Table 6.1. A major difference exists on the evolution gas generation. Nagra assume a carbon steel canister, therefore gas is assumed to generate evenly; whereas SKB assume a copper canister and therefore assume a canister defect scenario which is the process that allows water to reach the steel canisters after the failure of copper canisters (e.g. small holes in copper overpack) due to corrosion. For comparison purposes the rate of corrosion of the steel has been converted into gas generation rate per area and therefore represents a conservative approach. The gas generation/injection rates used by different authors in experimental research, for both gas injection tests and corrosion rates, and numerical modelling have been summarised in Table 6.3. Gas generation rates presented in Table 6.1, Table 6.2 and Table 6.3 have been termed as either realistic or conservative. Brief explanation for each term has also been provided in the tables.

For a generic repository condition, to address the gas issues, both realistic and conservative gas generation rates have been in numerical modelling. Although it has been predicted that isothermal conditions are likely to prevail during the gas generation period, gas generation rates at higher temperature has also been considered in the generation rates.

Table 6.1: Summary of gas generation rates and corrosion rates

Author	Corrosion rate (μm/year)	Gas generation rate** (mol/m^2/ year)	Gas generation rate** (kg/m^2/sec)	Buffer	Solution	Comments
Taniguchi et al. (2004)	7.0 to 0.99	1.307 to 0.184	8.35×10^{-12} to 1.18×10^{-12}	Compacted Bentonite	Synthetic sea water pH(7.9-8.4)	Measured corrosion rate after one year* and three-four years* respectively at 80˚C. Anaerobic condition was ensured during the experiment and the range considered as realistic.
Taniguchi et al. (2004)	4.0 to 1.9	0.747 to 0.355	4.77×10^{-12} to 2.26×10^{-12}	Compacted Bentonite	Synthetic sea water pH(7.9-8.4)	Measured corrosion rate after one year* and three-four years* respectively at 50˚C. Anaerobic condition prevailed during the experiment and the range can defined as realistic.
Taniguchi et al. (2004)	4.2 to 0.18	0.784 to 0.034	5.01×10^{-12} to 2.14×10^{-13}	Compacted Bentonite	Synthetic ground water pH(8.3-8.7)	Measured corrosion rate after one year* and three-four years* respectively at 80˚C. Anaerobic condition and the range could be considered as realistic.
Taniguchi et al. (2004)	7.4 to 0.62	1.382 to 0.116	8.83×10^{-12} to 7.40×10^{-13}	Compacted Bentonite	Synthetic ground water pH(9.1-9.2)	Measured corrosion rate after one year* and three-four years* respectively at 80˚C. Anaerobic condition was ensured during the experiment suggesting as in realistic range.

Taniguchi et al. (2004)	< 1.0 to 2.0	<0.1867 to 0.373	1.19×10^{-12} to 2.38×10^{-12}	Compacted Bentonite	Ground water	Realistic long term corrosion rates at 80˚C and 50˚C respectively. Taniguchi et al. (2004) suggested that less corrosion layer at reduced temperature.
Marsh & Taylor(1988); Marsh et al. (1983)	6.0 to 8.0	1.120 to 1.494	7.16×10^{-12} to 9.54×10^{-12}	Bentonite paste	Synthetic sea water	Anaerobic condition was maintained during the tests. Since the immersion tests gives comparatively higher corrosion, Rates could be considered as conservative.
Papillon et al. (2003)	4.0 to 5.0	0.747 to 0.934	4.77×10^{-12} to 5.96×10^{-12}	Compacted Fo-Ca Clay	Synthetic groundwater pH(8.0)	An-aerobic corrosion of carbon steel was measured for six months at ambient temperature. The rate of corrosion could be considered as realistic.
Simpson and Valloton (1986)	4.0 to 10.0	0.747 to 1.867	4.77×10^{-12} to 1.19×10^{-11}	Bentonite slurry/ wet Bentonite	Ground water	Corrosion rate of carbon steel measured at 80˚C. Since the samples were immersed in slurry, the surface area available for corrosion was significantly high. Therefore, the range of rate has been assumed conservative in nature.
Smart et al. (2006)	1.0 to 3.0	0.187 to 0.561	1.19×10^{-12} to 3.58×10^{-12}	Compacted Bentonite	Sodium chloride solution	Anaerobic corrosion rate of carbon steel obtained after six months. The range of corrosion rates could be considered as realistic at ambient temperature.

Smart et al. (2006)	0.5 to 1.0	0.094 to 0.187	5.97×10^{-13} to 1.19×10^{-12}	-	Sodium chloride solution	Anaerobic corrosion rate of carbon steel in bulk solution. In comparison to the previous corrosion rates, it has been found that corrosion rates increase in presence of bentonite (King, 2008).
Simpson et al. (1985)	5.0 to 10	0.94 to 1.867	5.97×10^{-12} to 1.19×10^{-11}	-	Sackingen and Bottstein water	The range of corrosion rates obtained at 80˚C after an exposure period of 260 days. The immersion test result has been considered as conservative.
Miller et al. (2000)	0.1 to 10	0.0187 to 1.867	1.19×10^{-13} to 1.19×10^{-11}	Wide range of soil	Porewater in soil	Corrosion rates of carbon steel up to 2000 years at ambient temperature from natural analogue study. Suggested range can be considered as realistic to over conservative in nature. The observed range covers almost all of the above mentioned corrosion rates.
Kursten et al. (1996)	1.8 to 8.6	0.336 to 1.606	2.14×10^{-12} to 1.02×10^{-11}	Boom Clay	Interstitial water	Under an-aerobic condition interstitial water consists of Mg-Na dominated sulphate solution with dissolved solids (King, 2008). The long term corrosion rates ranges from a realistic value of (2.14×10^{-12} kg/m^2/sec at 16˚C) to a conservative value of (1.02×10^{-11} kg/m^2/sec at 170˚C). The later has been considered as conservative due to the high temperature condition.

* Estimated from the slope of mass loss as a function of time (King, 2008).

** Rates have been measured using equation (2.1) developed by (Volckaert and Mallants, 1999).

Table 6.2: Gas generation rates used by end-users: Nagra and SKB.

Author	Corrosion rate	Gas generation/ flow rate (Units as quoted)	Gas generation/ flow rate ($kg/m^2/sec$)	Comments
Nagra (2004)	0.1 μm/year	0.4 mol/ year/ canister	1.19×10^{-13}	Gas generation rates, based on anaerobic corrosion of carbon steel canisters. The former has been termed as realistic while the later as over conservative by Nagra.
	1.0 μm/year	4.0 mol/ year/ canister	1.19×10^{-12}	
SKB (1993)	0.2 μm/year to 6.5 μm/year	2.0 dm^3/ year to 6.0 dm^3/ year	Based on corrosion rate 2.38×10^{-13} to 7.76×10^{-12}	Rates have been presented for long term anaerobic corrosion of copper/ steel canister. Initial defect in copper canister has been assumed as 5.0 mm^2 (Wikramaratna et al., 1993).

Table 6.3: Gas injection rates used in experimental or numerical modelling

Author	Gas generation/ flow rate (As quoted unit)	Gas generation/ flow rate ($kg/m^2/sec$)	Comments
Bonin et al. (2000)	0.4 mol/year/m^2	2.55×10^{-12}	Numerical modelling based upon gas generation equation provided by Gras (1988), conservative as neglecting water consumption.
Horseman et al. (1997)	375 μL/ hour	4.97×10^{-9}	Gas was injected in saturated specimen of compacted MX80 bentonite at constant isotropic stress condition. Sample 4.9 cm diameter.
Harrington & Horseman (2003)	375 μL/ hour	4.97×10^{-9}	Gas was injected in saturated specimen of compacted MX80 bentonite at constant volume. Change in volume was restricted at every direction.
Xu et al. (2008)	0.04 m^3/ year/ tunnel meter to 0.40 m^3/ year/ tunnel meter	1.45×10^{-11} 1.45×10^{-10}	Rates were used in a chemistry model based on Fe corrosion, coupled with two phase flow phenomena driven by gas pressure buildup related to H_2 generation and water consumption. Bentonite MX80 buffer and Opalinus clay host rock were considered in developing the model. The former generation has been considered as realistic while the later as over conservative.
Ortiz et al. (2002)	5.0×10^{-3} mol/year/m^2 to 5.9×10^{-3} mol/year/m^2	3.19×10^{-14} 3.77×10^{-14}	Fine metallic powder of cast iron was mixed in Boom Clay slurry. The slurry was prepared with pure water with a pH in the range of 9.19-9.85. The rates can be considered as conservative since powder provide more reaction surface area.

Based on the discussion presented above, the following rates have been considered:

Median realistic value: 5.0×10^{-12} kg/m^2/sec
Upper bound realistic value: 2.0×10^{-11} kg/m^2/sec
Conservative value: 2.0×10^{-10} kg/m^2/sec
Upper bound over-conservative value: 1.0×10^{-9} kg/m^2/sec

The conceptualisation of the boundary conditions has been examined. Flux boundary conditions have been considered in this study. Traditional boundary conditions where fixed fluxes are specified have been included and termed 'traditional'; a conservative approach where the water consumption is neglected is examined and compared with a more realistic approach of gas and water consumption. A boundary condition whereby the fluxes are dependent upon the degree of saturation has been developed and will be compared with the 'traditional' flux boundary condition.

The governing equation of multicomponent gas flow through unsaturated soil, presented in Chapter 3, section 3.3, can be adopted for modelling fully saturated condition. Generated gas can initially be dissolved in the porewater and the dissolved gas is taken to be transferred advectively and diffusively within the pore liquid. Henry's law is used to define the proportion of gas contained in the pour liquid. In case of fully saturated buffer, porewater provides an important flow path for diffusive flow, therefore it has been considered in the formulation. Bulk gas transfer is driven by the gradient of gas pressure and is determined by the use of Darcy's law. In a saturated buffer, the relative gas permeability is zero. The advective flux initiates after part of the buffer becomes unsaturated due to gas pressure.

6.2.5 Boundary condition development

As previously discussed in chapter 2, the generation of hydrogen is saturation dependent. Therefore, a boundary condition has been developed in this study where both gas generation and water consumption has been considered. Casting equation (2.1) as generation rate per meter squared area and multiplying by the molecular weight of hydrogen and water respectively gives the maximum flux quantities per m^2:

$$R_g = \frac{R_m M_{H2}}{S} \qquad (\text{kg/year/m}^2) \qquad (6.1)$$

$$R_w = -\frac{R_m M_{H2O}}{S} \qquad (\text{kg/year/m}^2) \qquad (6.2)$$

Additionally the availability of water is a key for the corrosion reaction to occur. For example, Brown and Masters (1982) stated that the laboratory experiments on corrosion of Fe under atmospheric condition indicate a decrease in corrosion rate when the relative humidity drops from 90% to 60%. Senger et al. (2008) states that the maximum corrosion rate occurs at a degree of saturation of approximately 85%.

An assumption in this work is that the water is able to reach the steel at an equal rate independent of time beyond the buffer boundary, i.e. corrosion products do not incrementally impede the water movement over time within the steel.

A joint flux boundary condition has been developed for the gas and water flux with a limitation depending upon the saturation of the buffer at the boundary surface. The boundary condition can be expressed as:

$$q_g = dR_g;\ \ q_w = dR_w = \alpha dR_g \qquad (6.3)$$

where, q_g and q_w are the fluxes of gas and water in kg/year/m^2, $d = f(Sr)$ is a function of degree of saturation allowing for the reduction in flux if saturation levels drop, α is the ratio of molar mass of porewater to pore gas and R_g and R_w are the gas fluxes reported from equation (6.1) and (6.2).

Function *d* has been given two possible forms due to a lack of information. The first is referred to as a step-change condition where above a critical degree of water saturation, S_{rc}, the value of *d* is 1 and below that critical value d = 0. The second is where above the same critical value of degree of saturation the function of *d* increases linearly from 0 to 1 at $S_r=1$. In this case a linear expression has been adopted as a first approximation due to a lack of other data. Mathematically these can be expressed as:

Step-change condition:

$$d = 0 \ if \ \ S_r \le S_{rc}; \ \ d = 1 \ if \ \ S_r > S_{rc} \tag{6.4}$$

Linear function condition:

$$d = 0 \ if \ \ S_r \le S_{rc}; \ \ d = \frac{S_r - S_{rc}}{1 - S_{rc}} \ \ if \ \ S_r > S_{rc}; \tag{6.5}$$

The value of *d* against S_r has been shown schematically on Figure 6.1 for a value of S_{rc} = 0.85.

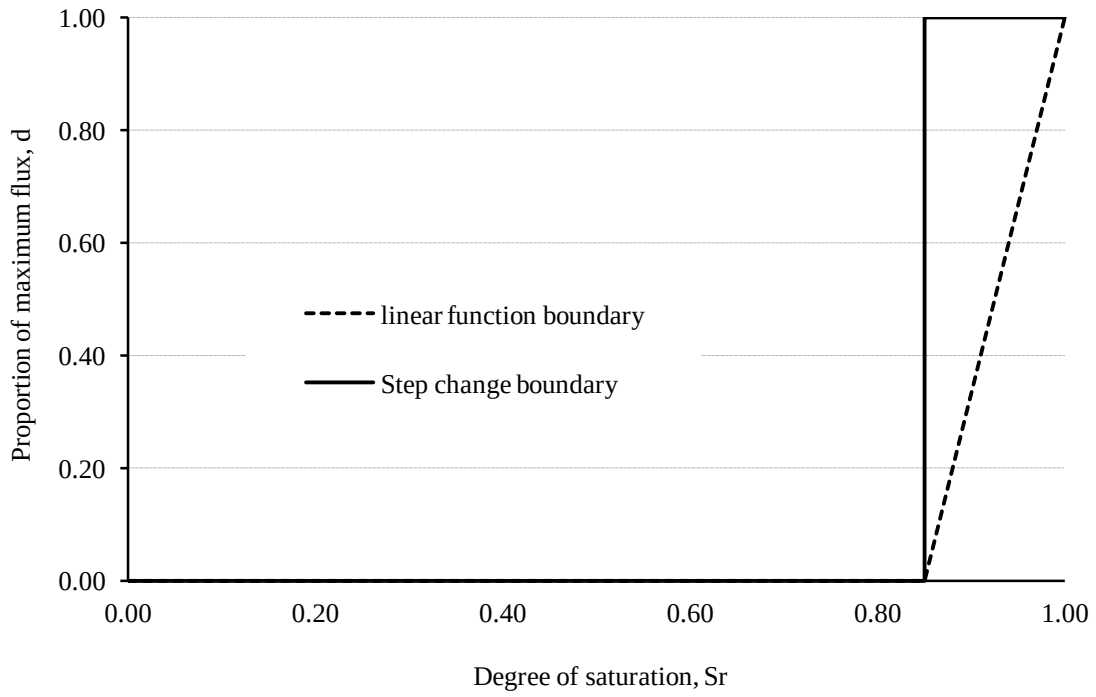

Figure 6.1: Value of the proportion of the maximum gas flux, *d*, against the degree of saturation, S_r, for the two proposed boundary conditions.

6.2.6 Summary of scenario conditions

A summary of the scenario conditions have been presented in Table 6.4. It has been classified into three sections, i.e. concept scenario, corrosion process and material properties. The conditions related to disposal concepts have been presented in section 6.2.1 to section 6.2.3. The corrosion process based water consumption and gas generation on the boundary has been detailed in section 6.2.4 and section 6.2.5. The material parameters have been presented in section 6.3.

Table 6.4: Summary of the conditions considered in developing the scenarios.

Concept scenario	
Host rock	Granite or clay
Canister	Steel or Copper
Steel corrosion start	At S_r > critical value or Canister defect when S_r =1.0
Bentonite	300 – 800 mm
Repository depth	500 m
Corrosion process	
Rate of gas influx	Realistic - 2.0×10^{-11} - 5.0×10^{-12} kg/m^2/s Conservative - 1.0×10^{-9} - 2.0×10^{-10} kg/m^2/s
Boundary condition conceptualisation	Traditional – flux boundaries i) gas in ii) gas in/water out New – variable dependant flux conditions (section 6.2.5), all include both gas and water fluxes i. Step change at critical degree of saturation ii. Linear change in relation to degree of saturation
Material properties	
Diffusion coefficient, D_{ij}	Realistic - 2.0×10^{-11} - 2.0×10^{-13} m^2/s
Intrinsic permeability, k_{int}	1.0×10^{-21} – 1.0×10^{-19} m^2

6.3 Simulation setup

To carry out numerical simulations, the modelling approach used in this investigation has been detailed in this section. The approach follows development of simulation scenarios, establish a failure criterion of the model, time and space discretisation of the model domain, selection of material parameters and setup initial and boundary conditions for the simulations.

6.3.1 Simulation scenarios

The scenarios considered in the modelling have been derived from the representative scenarios developed in section 6.2 and presented in Table 6.4. The influence of the various aspects to the evolution of gas pressures has been investigated. Table 6.5 presents the ranges of parameters considered within the simulations and allocates a code to the various aspects so that they can easily be tracked. For example an analysis with the host rock of 'Granite' will be referred to by the code 'R1'.

6.3.2 Conceptual failure

The failure of the material is likely, where gas flux exceeds the carrying capacity of the porous media. In this case exceptionally high pressures will be calculated and numerically are likely to cause model failure. However, before this stage there is a risk of preferential pathways being created which invalidates the assumptions of the conceptual model and therefore, the continuing evolution. Without a well defined state at which preferential pathways are created in the buffer material a conservative value has been determined. From the literature review it is well accepted that the gas pressure required for fracture propagation exceeds the sum of the pore-water pressure and the swelling pressure. To ensure conservatism, it has been considered that if the pore-gas pressure is equal to the sum of the swelling pressure, set at 5MPa for the minimum in saturated conditions, and the pore-water pressure, hydrostatically at 5MPa at saturation, and then there is a risk of preferential pathways being created. Further experimental investigation of the material properties would be required to confirm the amount that this pressure can be exceeded without risk of fracture. Therefore, in this work, risk of pneumatic fracture in the buffer occurs if pore gas pressure exceeds 10MPa.

Table 6.5: Summary of the scenario variables.

	Simulation scenarios				
	1	2	3	4	Code
Host rock	Granite	Clay	-	-	R
Boundary condition	variable dependant flux conditions	Gas in and water out	Gas inflow only	-	Q
Gas influx ($kg/m^2/s$)	Realistic rate 2.0×10^{-11}	Realistic rate 5.0×10^{-12}	Conservative rate 1.0×10^{-9}	Conservative rate 2.0×10^{-10}	J
Water out-flux ($kg/m^2/s$)	1.8×10^{-10}	4.5×10^{-11}	9.1×10^{-9}	1.8×10^{-09}	W
Diffusion co efficient (m^2/s)	2.0×10^{-11}	2.0×10^{-12}	-	-	D
Buffer thickness (mm)	300	500	800	-	B
Degree of saturation (%)	85	100	-	-	S
Intrinsic permeability (m^2)	1.0×10^{-19}	1.0×10^{-21}	-	-	I

6.3.3 Model domain and time-step

The model domain shown in Figure 6.2 is discretised into a finite element mesh which varied depending upon the buffer dimensions, B (300, 500 and 800 mm). For a typical analysis the buffer is discretised into 20 finite-elements and the host rock into 50 finite-elements with smaller elements nearer to the boundary where higher gradients are expected. A 3.0 m long host rock has been arbitrarily chosen for the simulations Simulation results have been checked for spatial and temporal convergence. A variable time-step regime is used to allow the time-step to increase or decrease depending upon convergence criteria.

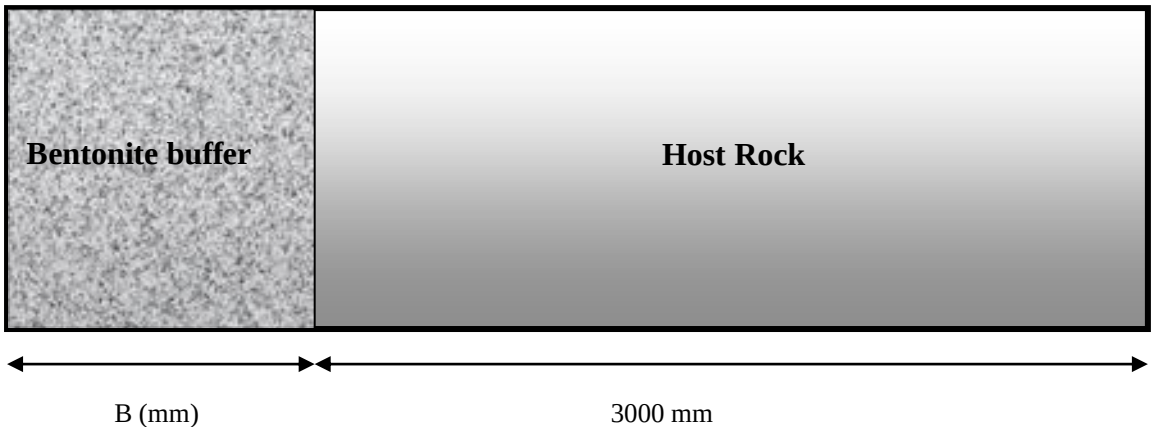

Figure 6.2: Conceptual schematic of the model domain (not to scale).

6.3.4 Material parameters

The material parameters have been selected for generic buffer and rock materials, based upon material data available in literature. For bentonitic buffer materials the data has been based upon the well characterised MX-80 compacted bentonite. Key material parameters, that are likely to have a major impact on this work, have been discussed in detail whereas others have been selected in detail and are presented elsewhere, e.g. Vardon (2009), Cleall et al. (2006), THERESA (2008). All the parameters are presented in Table 6.5.

6.3.4.1 Gas diffusion

Barden and Sides (1967) measured the coefficient of diffusion for air through the water phase in a range of compacted clays and the results have been presented in

Table 6.6. A compilation of quoted coefficients of diffusion for hydrogen through different types of clay pore water has been presented in Table 6.7.

Table 6.6: Coefficient of diffusion of pore air through different clay materials (Barden and Sides, 1967, quoted by Fredlund and Rahardjo, 1993).

Materials	**Coefficient of diffusion, D_{ij} (m^2/s)**
Free water	2.2×10^{-9}
Kaolinite clay consolidated at 414 kPa and 49% water content	4.5×10^{-10}
Kaolinite clay consolidated at 483 kPa and 75% water content	6.2×10^{-10}
Kaolinite clay consolidated at 34.5 kPa and 53% water content	4.7×10^{-10}
Jackson clay and 4% bentonite consolidated at 34.5 kPa and 39% water content	$<1.0\times10^{-11}$

It is noted that there is a wide range of values for the diffusion of gas through clays have been quoted in literature. This is possibly due to the low values being challenging to measure accurately, other transport processes occurring and variability of the materials measured. In general, however, it can be seen that for all materials quoted containing bentonite, the value of diffusion is low. For this work therefore, an upper and lower realistic value has been selected for buffer and clay materials, $\boldsymbol{D_{ij}}$ = 2.0×10^{-11} and 2.0×10^{-12} m^2/s respectively. For the crystalline rock, the pores are likely to be more interconnected. With only limited data available a wide upper and lower bound has been selected of $\boldsymbol{D_{ij}}$ = 2.0×10^{-9} and 2.0×10^{-11} m^2/s respectively. These values of diffusion coefficients of air have been adopted for hydrogen gas because of lack of information available in literature for hydrogen diffusion through host rocks.

Table 6.7: Diffusion coefficients of hydrogen gas through compacted clay buffers.

Medium	Coefficient of diffusion, D_{ij} (m^2/s)	References
Compacted Fo-Ca clay	1.0×10^{-11} to 5.0×10^{-11}	Galle (2000)
Boom clay	4.0×10^{-12} to 5.0×10^{-10}	Norris (2009)
Compacted Bentonite	2.0×10^{-11}	Werme, (1980) Wikramaratna et al. (1993)
Compacted Bentonite	3.6×10^{-12}	Neretnieks and Skagius (1978)
Compacted Bentontie	1.8×10^{-11}	Eriksen and Jacobsson, (1982)

6.3.4.2 Intrinsic permeability

For MX-80 bentonite liquid phase intrinsic permeability has been determined as a function of porosity (THERESA, 2008). Considering a porosity of approximately 0.4, typical for a buffer, a range of approximately 1.0×10^{-21} to 1.0×10^{-19} m^2 has been reported. Other work considering the intrinsic permeability, e.g. Horseman et al. (1999) also report values in this range.

For a crystalline rock material the intrinsic permeability is likely to be considerably higher, in the range of 1.0×10^{-19} to 1.0×10^{-8} m^2 has been reported (e.g. after Rhén and Forsmark, 2001). The implication of this is that the advective flow of water into the repository buffer due to water consumption due to corrosion is likely to be controlled by the buffer, when initially saturated. If larger volumes of water are required the low porosity of virtually intact rock may be important. In this case to reduce the number of variables considered the crystalline rock intrinsic permeability will be set to

1.0×10^{-14} m^2. For crystalline rock Nagra (2002) state that the hydraulic conductivity of the clay rock is less than 1.0×10^{-13} m^2. Therefore, in this work the same value as buffer material will be used.

6.3.4.3 Moisture retention behaviour

Water retention experiments were carried out by EUROGEOMAT on MX-80 bentonite to characterise the water retention behaviour for various initial dry densities (EBS, 2005). It was found that the van Genuchten equation, presented in equation (6.6) matches well to the experimental results.

$$\theta_l = \theta_{lr} + \left(\theta_{ls} - \theta_{lr}\right)\left[\frac{1}{1+(\alpha s)^n}\right]^m \tag{6.6}$$

where θ_l is the volumetric water content, θ_{ls} is the saturated volumetric water content, θ_{lr} is the residual volumetric water content, α, n, are m are constants and s is the matric suction measured in metres height.

It was found that the best fit was achieved using the following constants for benontite of 1.6Mg/m^3: α = 0.00045, $n = 1.75$, $m = 0.43$, $\theta_{lr} = 0.0001$, $\theta_{ls} = porosity$ = 0.4.

The relationship used for crystalline granite rock is based upon Gens et al. (1998) and has been successfully used by Cleall et al. (2007) and Vardon (2009) given as:

$$S_r = \left(1+\left(\frac{s}{P_0}\right)^{1/(1-\beta_l)}\right)^{-\beta_l} \tag{6.7}$$

It was found that the best fit was achieved using the following constants: P_0 = 0.33 MPa and β_l = 0.33.

6.3.4.4 Summary

A summary of the material parameters used is contained in Table 6.8.

Table 6.8: Material parameters used in the simulations.

		Bentonite buffer	Crystalline rock	Clay rock
Density of liquid moisture (kg/m^3)		1000		
Density of soil solids (kg/m^3)		2700		
Specific heat capacity of dry air (J/kg/K)		1000		
Specific heat capacity of liquid (J/kg/K)		4180		
Specific heat capacity of vapour (J/kg/K)		1870		
Specific heat capacity of solid (J/kg/K)		750		
Specific gas constant of dry air (J/kg/K)		287.1		
Specific gas constant of vapour (J/kg/K)		461.5		
Henry's constant for generated gas		0.02		
Latent heat of vaporisation (J/kg/K)		2400000		
Intrinsic permeability (m^2)	k_{int}	See section 6.3.4.2		
Unsaturated hydraulic conductivity (m/s) $K_l = \frac{\rho_l g k_{int} S_r^{\,n}}{\mu_l}$		*n = 3*	*n = 0.33*	*n = 3*
Unsaturated pore gas conductivity (m^2/Pa.s) $K_g = \frac{k_{int}}{\mu_g}\left(1-S_r\right)^{1/2}\left(1-S_r^{1/m}\right)^{2m}$		*m = 0.3*	*m = 0.3*	*m = 0.3*
Diffusion coefficient (m^2/s)	D	See section 6.3.4.1		
Water retention curve based on van Genucthen expression $\theta_l = nS_r = \theta_{lr} + (\theta_{ls} - \theta_{lr})\left[\frac{1}{1+(\alpha s)^n}\right]^m$ where s is matric suction in metres	α	0.00045	-	0.00045
	n	1.16	-	1.16
	m	1.75	-	1.75
	θ_{lr}	0.0001	-	0.0001
	θ_{ls}	0.4	-	0.4
Water retention curve based on Gens et al. (1998) $S_r = \left(1+\left(\frac{s}{P_0}\right)^{1/(1-\beta_l)}\right)^{-\beta_l}$	P_0		0.33	
	β_l		0.33	
Porosity		0.4	0.05	0.4

6.3.5 Initial and boundary conditions

Initial and boundary conditions of the simulations have been presented in Figure 6.3. Fixed porewater pressure and hydrogen concentration has been considered at the right hand side boundary of the model domain, e.g. x = (B/1000 + 3.0 m) where B is the buffer width in millimetre. The fixed porewater pressure at this boundary is equivalent to the water pressure at 500 m depth. Flux boundary condition has been adopted at the injection face (canister-buffer interface) of the buffer. The gas inflow and water outflow varies depending on the simulation scenarios and the values have been presented in Table 6.5. It has been considered that isothermal condition prevails during the simulation which is in equilibrium at 25°C.

Boundary condition	**Initial condition**	**Boundary condition**
T = 298K *Gas inflow,* J (mol/m^2/sec) *water outflow,* W (mol/m^2/sec)	T = 298 K $u_l = 5.0\times10^6$ Pa c_{H_2} = 0.0 mol/m^3	T = 298K $u_l = 5.0\times10^6$ Pa c_{H_2} = 0.0 mol/m^3

Figure 6.3: Schematic of the initial and boundary conditions.

6.4 Results and discussion

In this chapter results of numerical simulations have been presented. The results have been split initially by the host rock and then by other variables that have been discussed.

The gas pressure/concentration results are presented in the form of gas pressure only for consistency and ability to compare, although when dissolved in fully saturated conditions only the concentration will be apparent. The pressure can be converted into concentrations in a straightforward manner using Henry's law.

6.4.1 Granite host rock (R1)

6.4.1.1 Base case

A base case has been selected, which is considered to be within the bounds of realism under repository conditions. This allows the deviation from the base case to investigate the impact of various parameters. The base case variables are reported in Table 6.9.

Table 6.9: Variable values for base case simulation for Granite host rock.

Host rock	Granite	R1
Gas influx ($kg/m^2/s$)	1.25×10^{-11}	Jmid
Water out-flux ($kg/m^2/s$)	1.125×10^{-10}	Wmid
Boundary conditions	saturation dependant flux	Q1
Diffusion coeff. (m^2/s)	1.1×10^{-11}	Dmid
Buffer thickness (mm)	300	B1
Degree of saturation (%)	100	S2
Intrns. perm. (m^2)	5.05×10^{-20}	Imid

The results of the base case for pore gas evolution are shown in Figure 6.4. The degree of saturation remains at 1.0 throughout the buffer and the time evolution which indicates that sufficient gas pressures are not developed to force two-phase flow away from the canister and that the hydraulic conductivity is sufficient to allow recharge of the flow removed from the liquid water flux due to corrosion.

The steady state value of pore-gas pressure is found to be 0.55MPa which is significantly below the risk of fracture. In this case the diffusive mechanism is more capable to transfer the generated pore gas. The steady state conditions occur within approximately 300 years (9.5E+9 seconds) and are seen to persist until the iron is consumed. However, the corrosion rate, hence the gas generation rate, is likely to be retarded due to a protective film on the iron surface.

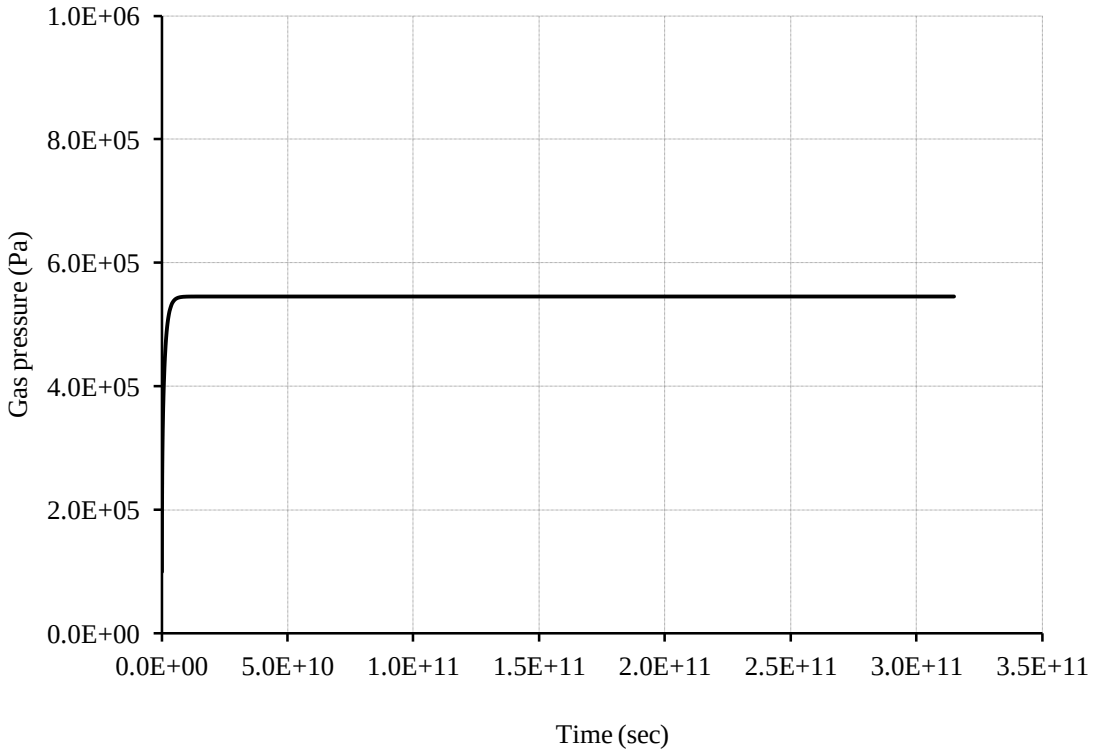

Figure 6.4: Pore gas pressure evolution of the base case scenario for crystalline rock.

6.4.1.2 Generation rate

The effects of the generation rate are presented in Figure 6.5 below, where the upper realistic (J1) and upper (over-) conservative rates (J3) are shown. All other parameters are equal to the base case simulation in section 6. 4.1.1. The mid intrinsic permeability (Imid) and lower intrinsic permeability (I2) are shown for the over-conservative rate and have only negligible impact on the J1 rate. It is seen, as expected, that the higher the generation rate, the higher the gas pressure generated. However, it is also shown on the figure that there is an impact of the intrinsic permeability at the lower intrinsic permeability due to the water consumption flux and limited recharge. It is also seen in this figure that even at the over-conservative generation rate, there is little chance of preferential pathways being generated, although it is noted that the magnitudes are similar.

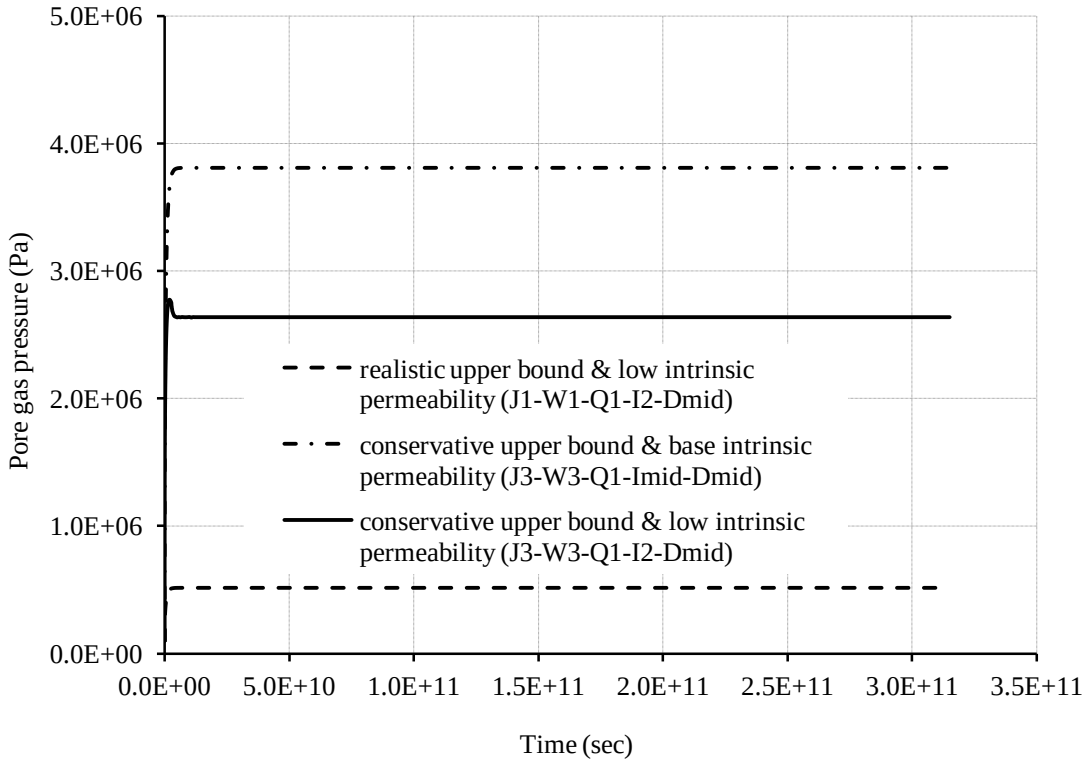

Figure 6.5: Pore gas pressure evolution for upper realistic (J1) and over-conservative (J3) gas generation rates, using the same parameter as the base case, with the exception of the single simulation with a lower intrinsic permeability for comparison.

6.4.1.3 Diffusion rate

Simulations investigating the diffusion rate have been presented in this section. All other parameters are as the base case simulation presented in section 6.4.1.1. The gas pressure evolution has been presented in Figure 6.6 for the upper and lower realistic rates of gas generation (J1 and J2) and for the upper and lower realistic bounds of gas diffusion through the pore water (D1 and D2). The simulation has been carried out at base intrinsic permeability.

For the upper realistic gas generation rate (J1) and for the case of high diffusion (D1) the maximum pore gas pressure has been found around 0.55 MPa and for low diffusion (D2) the maximum reached to 1.61 MPa. The lower diffusion provides more resistance to the flow of gas through the buffer comparing to higher diffusion. For high diffusion, the steady state condition has been reached earlier than that of low diffusion. In both cases the steady state condition has been obtained at or before approximately 1000 years (3.15E+10 seconds). For the lower realistic gas generation rates (J2) the gas pressures achieved were 0.2 MPa and 0.8 MPa for the upper and lower rates of diffusion respectively.

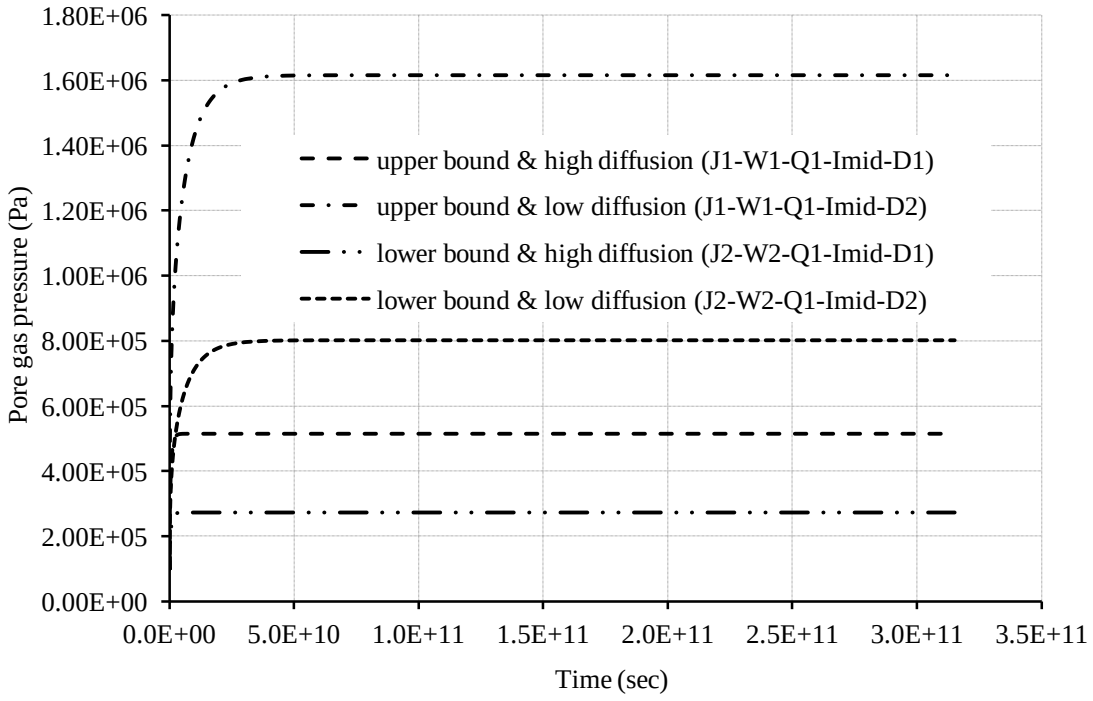

Figure 6.6: Pore gas pressure evolution with reference to changes in diffusion rate and realistic generation rates (upper and lower bound).

In all the simulations presented in this section, none have indicated any risk of fracture, since the maximum developed pressures are significantly less than the fracture pressure of 10 MPa.

6.4.1.4 Intrinsic permeability

In this section the effects of altering the intrinsic permeability have been investigated. Applying the upper realistic gas generation rate (J1) the difference in pore water pressure at steady state for the upper and lower bound of intrinsic permeability (I1 and I2) is shown in Figure 6.7. Only limited pore water pressure gradients are found even for the lower intrinsic permeability. At all times the buffer remains saturated. This indicates that the hydraulic pressure gradient within the sample is more than sufficient to allow for the water out-flux from the realistic upper bound gas corrosion process. Should either the bentonite be of much lower permeability or the gas flux greater then de-saturation may occur.

Similar analyses with over conservative generation rates (J3) are presented in Figures 6.8 and 6.9. Figure 6.8 presents the porewater pressure profile at steady state for the upper and lower bound intrinsic permeabilities. It has been seen that at the lower bound of permeability the sample de-saturates due to the water consumption process. A decrease in porewater pressure below zero indicates de-saturation and more pore space was available for advective gas flow and storage in the buffer at the onset of de-saturation.

Figure 6.9 presents simulation results from the conservative generation rate, the upper and lower bound of intrinsic permeability and upper and lower bound of diffusion. It is seen that where de-saturation occurs, in the lower intrinsic permeabilities (I2) then the gas pressure peak values are much reduced. This is due to advective flow occurring, extra storage being available and a reduced distance where the gas must be transported via diffusive flow through the pore water, i.e. a greater concentration gradient. Also of note, is the peak in the value of gas pressure in the low intrinsic permeability (I2) and high diffusion (D1) before the steady state conditions. This is due to the de-saturation/re-saturation not being at equilibrium at this point in time. The sample further de-saturates due to the water flux leaving the sample after the peak gas pressure has evolved.

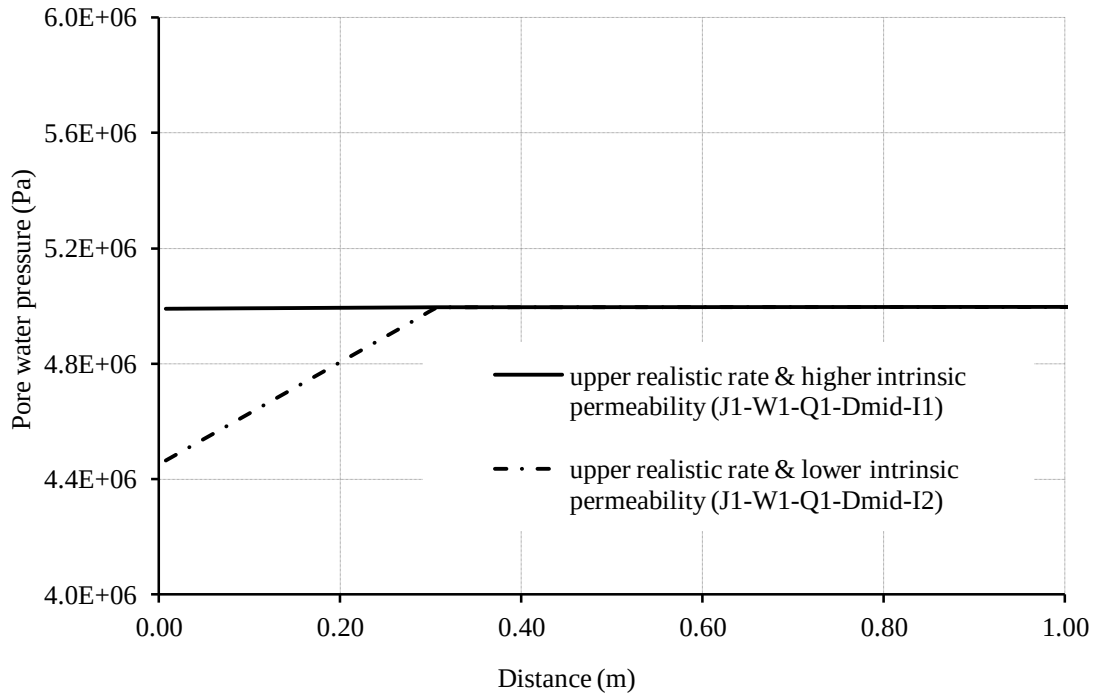

Figure 6.7: Porewater profile along buffer (300 mm) and rock in relation to change in intrinsic permeability with the upper realistic gas generation rate (J1) at steady state.

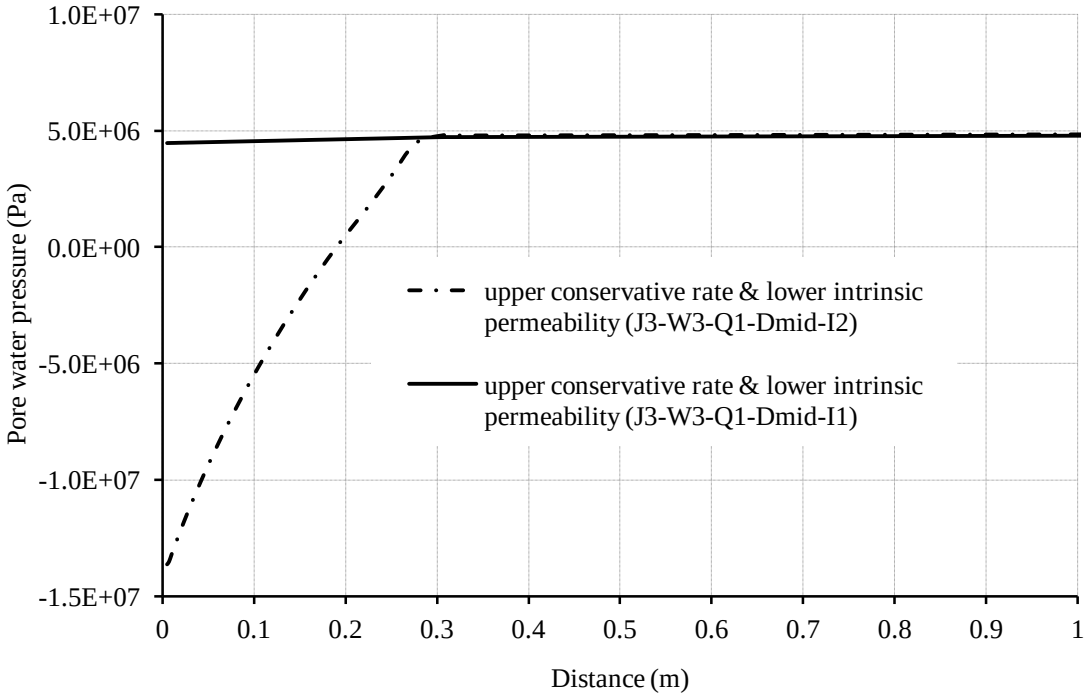

Figure 6.8: Porewater profile along buffer (300 mm) and rock in relation to change in intrinsic permeability with the upper conservative gas generation rate (J3) at steady state.

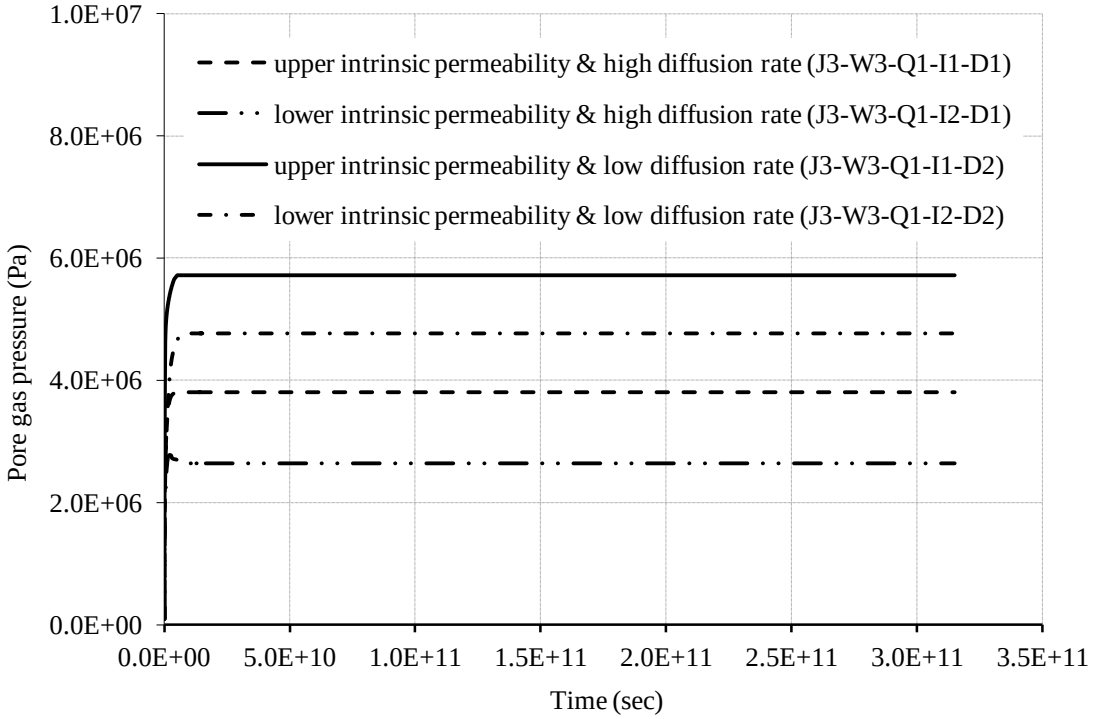

Figure 6.9: Pore gas pressure evolution in relation to change in intrinsic permeability with the upper conservative gas generation.

Therefore, it can be seen that it is important to understand the evolution of the gas pressures and the combination of material properties and variables for assessment of the gas pressures.

6.4.1.5 Boundary condition

It can be seen in section 6.4.1.4 that in all but the over conservative generation rate (J3) with low intrinsic permeability (I2) cases the buffer remains saturated. Therefore, no difference between the new flux boundary, which is related to saturation rate and the traditional flux boundary condition, is yielded.

In the case of the over conservative generation rate (J3) with low intrinsic permeability (I2) simulations the difference between the yielded pore gas pressures is small, although greater difference in the water content and cumulative boundary fluxes is greater. This is due to the response of the increased storage available if more water is removed. Additionally this would have an impact on the longevity of gas generation.

In the case with high intrinsic permeability (I1) the sample remains saturated. Interestingly the advective flow of water is able to retard the diffusive flow of gas and greater gas pressures are yielded than by using a gas only flux on the boundary. This is illustrated in Figure 6.10 below. This phenomenon clearly indicates that it is the combination of parameters that needs to be assessed. It is likely that with a low diffusion rate the effect of this phenomenon would be amplified. However, the realism of a material with high intrinsic permeability and low diffusive gas flow through porewater of that material would need to be investigated further.

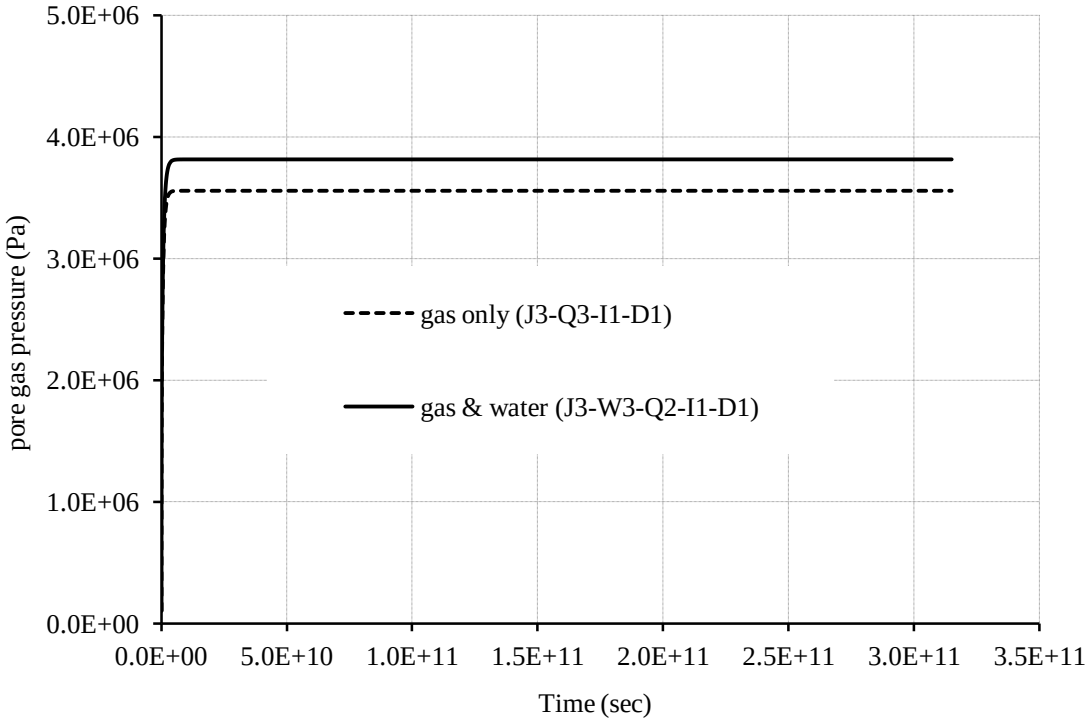

Figure 6.10: Pore gas pressure evolution in relation to different flux boundary conditions, with the over-conservative generation rate (J3), high diffusion rate (D1) and high intrinsic permeability (I1).

In contrast, by using the over-conservative (J3) gas generation rate and low intrinsic permeability (I2) the opposite trend is found. De-saturation, as discussed in section 6.4.1.4, increases storage for gas and therefore decreases pressures. These results are shown in Figure 6.11. The complimentary results of pore water pressure evolution are presented in Figure 6.12. Profiles of the de-saturation behaviour are presented at three times in Figure 6.13. The non-linear behaviour yielded is due to the water retention behaviour of the material.

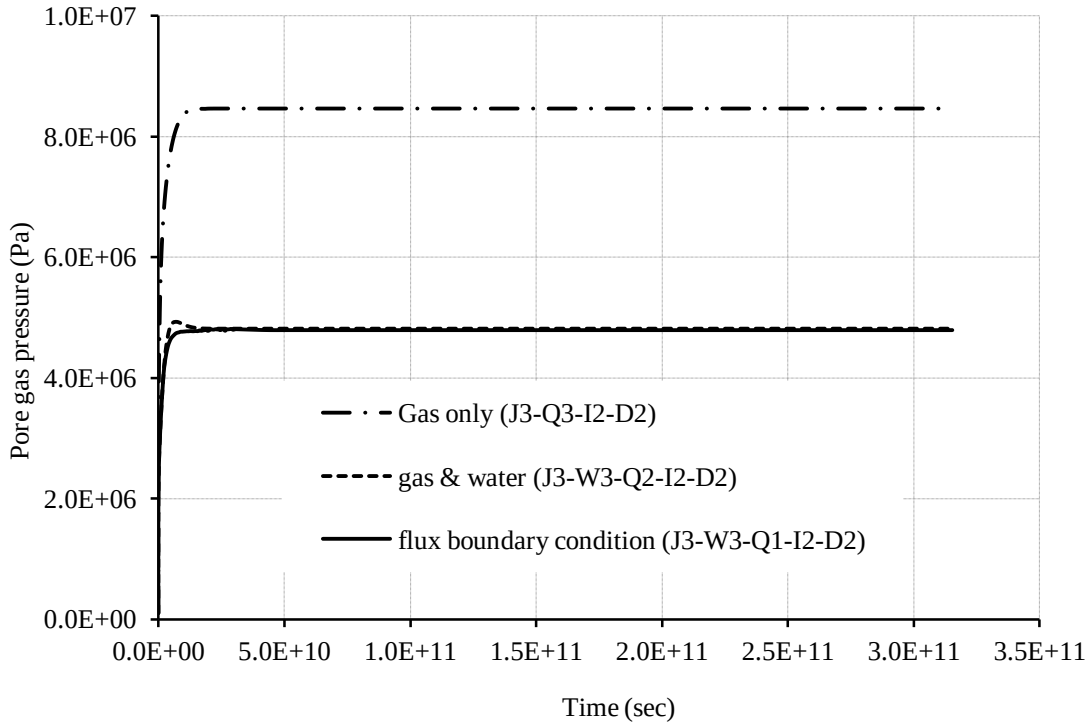

Figure 6.11: Pore gas pressure evolution in relation to different flux boundary conditions, with the over-conservative generation rate (J3), low diffusion rate (D2) and low intrinsic permeability (I2).

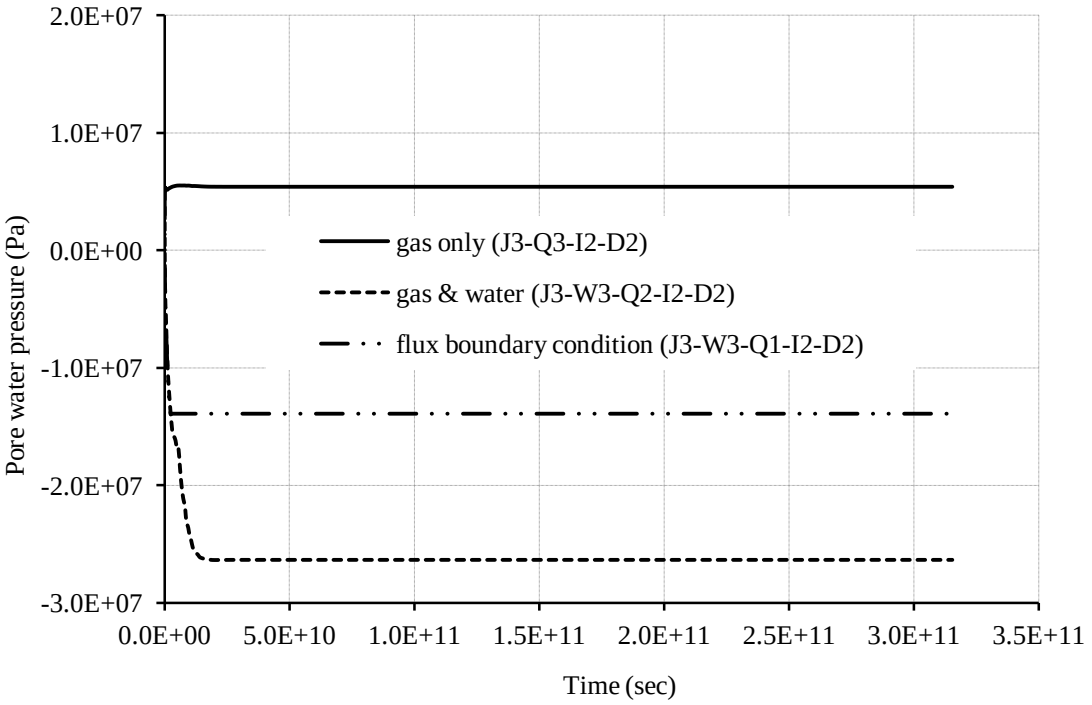

Figure 6.12: Porewater pressure evolution in relation to different flux boundary conditions, with the over-conservative generation rate (J3), low diffusion rate (D2) and low intrinsic permeability (I2).

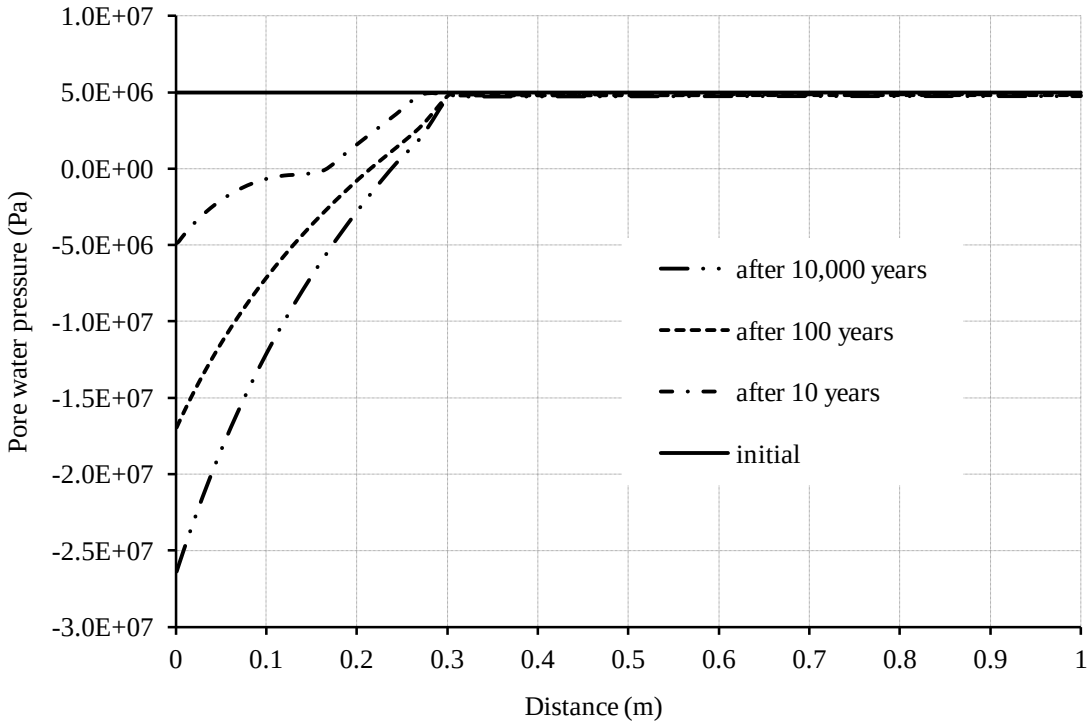

Figure 6.13: Porewater pressure profiles at steady state in relation to the water and gas flux traditional boundary condition (Q2), with the over-conservative generation rate (J3), low diffusion rate (D2) and low intrinsic permeability (I2).

6.4.1.6 Buffer thickness

Comparison in pore gas pressures along the 300 mm, 500 mm and 800 mm buffer has been provided in Figure 8.14 and Figure 8.15 for upper bound conservative and realistic gas generation rates respectively. It can be seen that in general the thicker the buffer the higher gas pressures evolve. This is due to the lower diffusion properties in the buffer than in the rock. However, it must be considered that a thicker buffer is likely to have greater resistance to the creation of preferential pathways and interconnected fissures. It is also noted that the increase in pressure is not equally proportional to the change in thickness of the buffer. For the upper realistic generation rate (J1) increasing the buffer thickness by over 150% yields an increase in pore gas pressure of just over 60%.

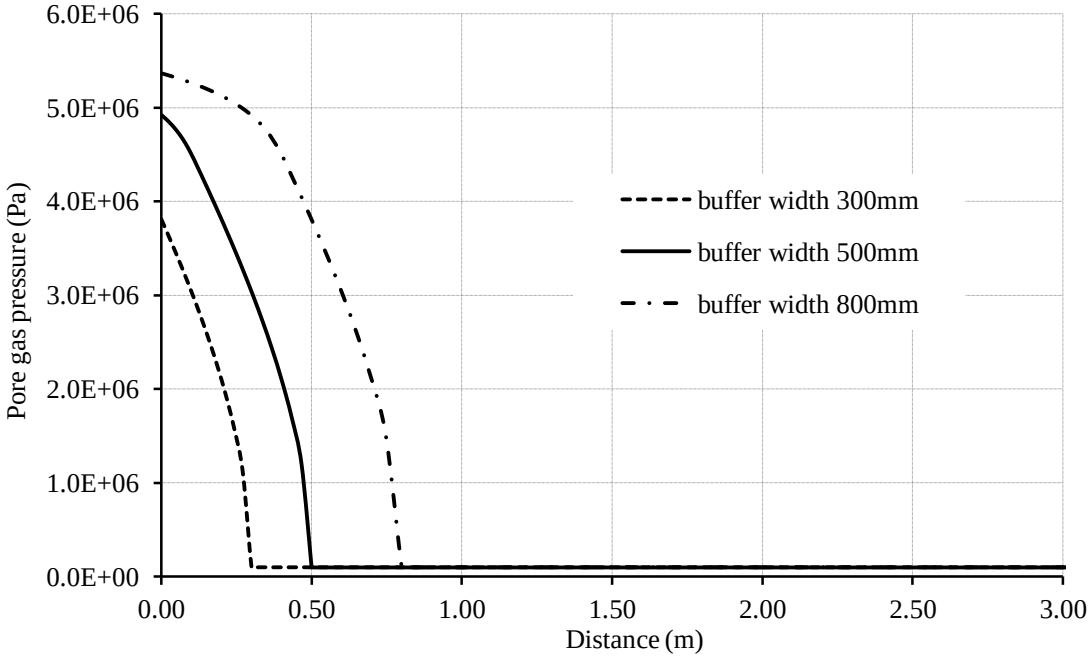

Figure 6.14: Pore gas pressure profiles at steady state in relation to differing buffer thicknesses, with the over-conservative generation rate (J3), high diffusion rate (D1) and high intrinsic permeability (I1).

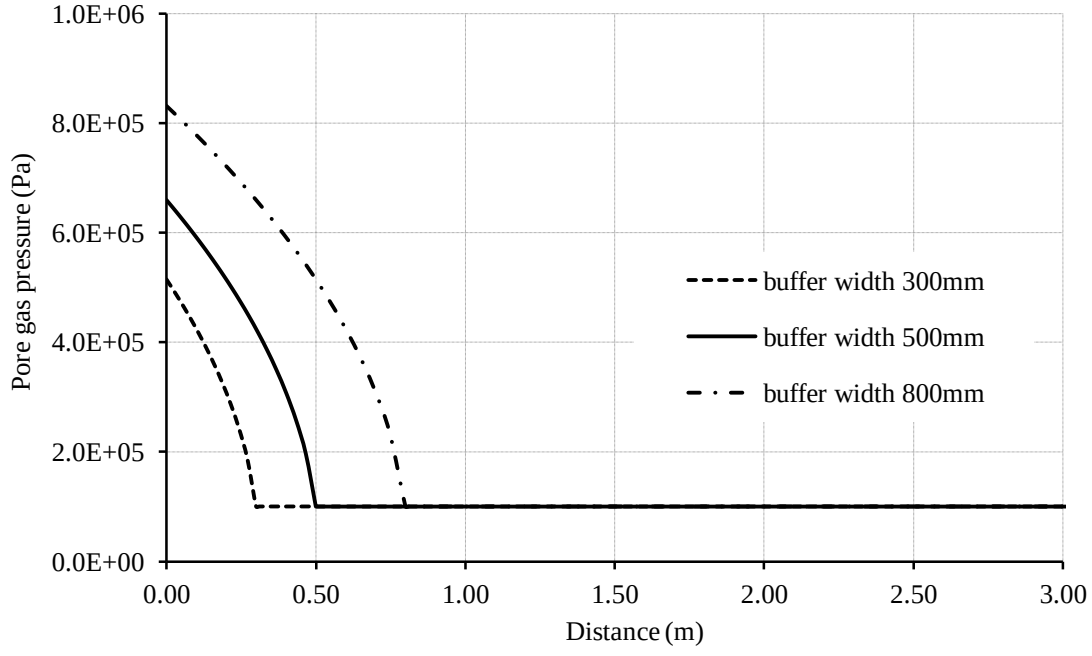

Figure 6.15: Pore gas pressure profiles at steady state in relation to differing buffer thickness, with the upper bound realistic generation rate (J1), high diffusion rate (D1) and high intrinsic permeability (I1).

6.4.2 Clay host rock (R2)

6.4.2.1 Base case

A realistic base case has been selected for the clay rock with the variables reported in Table 6.10. As with the Granite host rock the impact of various parameters will be investigated.

Table 6.10: Variable values for base case simulation for clay host rock.

Host rock	Clay	R2
Gas influx ($kg/m^2/s$)	$1.25x10^{-11}$ Realistic rate	Jmid
Water out-flux ($kg/m^2/s$)	$1.125x10^{-10}$	Wmid
Boundary conditions	saturation dependant flux	Q1
Diffusion coeff. (m^2/s)	1.1×10^{-11}	Dmid
Buffer thickness (mm)	300	B1
Degree of saturation (%)	100	S2
Intrns. perm. (m^2)	5.05×10^{-20}	Imid

The results are reported in Figure 6.16, as with the Granite rock concept the material is able to stay saturated throughout. The steady state value exceeds the steady state value for the base case in the Granite rock concept of 0.55 MPa at 1.8 MPa. This is due to the lower diffusive capability of the host rock. The steady state is reached in this case after approximately 30,000 years (9.5E+11 seconds). It is noted that the steel may be consumed by this point.

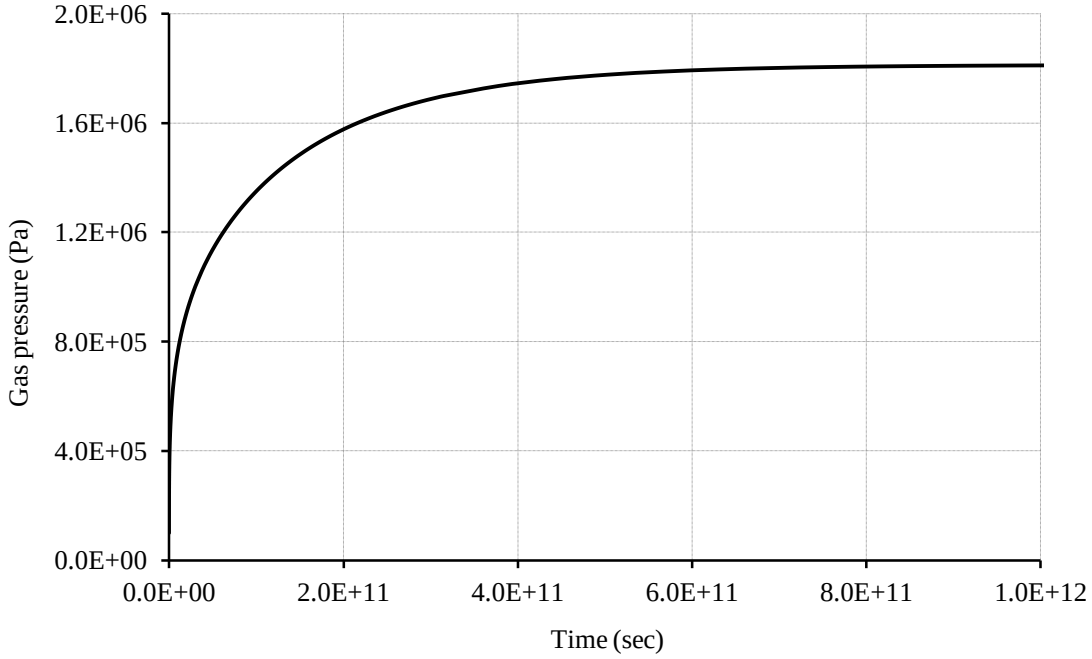

Figure 6.16: Pore gas pressure evolution of the base case scenario for clay host rock.

6.4.2.2 Generation rate

The effects of the generation rate are presented in Figure 6.17, where the upper realistic (J1) and upper (over-) conservative rates (J3) are shown. All other parameters are equal to the base case simulation in section 6.4.2.1. It can be seen with the over-conservative rate (J3) a steady state is reached at approximately 3,000 years (9.5E+10 seconds) and the upper bound realistic rate (J1) takes nearly 15,000 years (4.73E+11 seconds).

The effect of the intrinsic permeability and water supply condition on gas generation rate is illustrated in this example. The case of the conservative high rate (J3) with the low intrinsic permeability (I2) evolves a steady state quickly at a much reduced value to that of the mid intrinsic permeability (Imid). This is due to the water consumption and then lower water supply due to the low permeability host rock. For clay formations this is likely to be of importance in the safety assessment and design process.

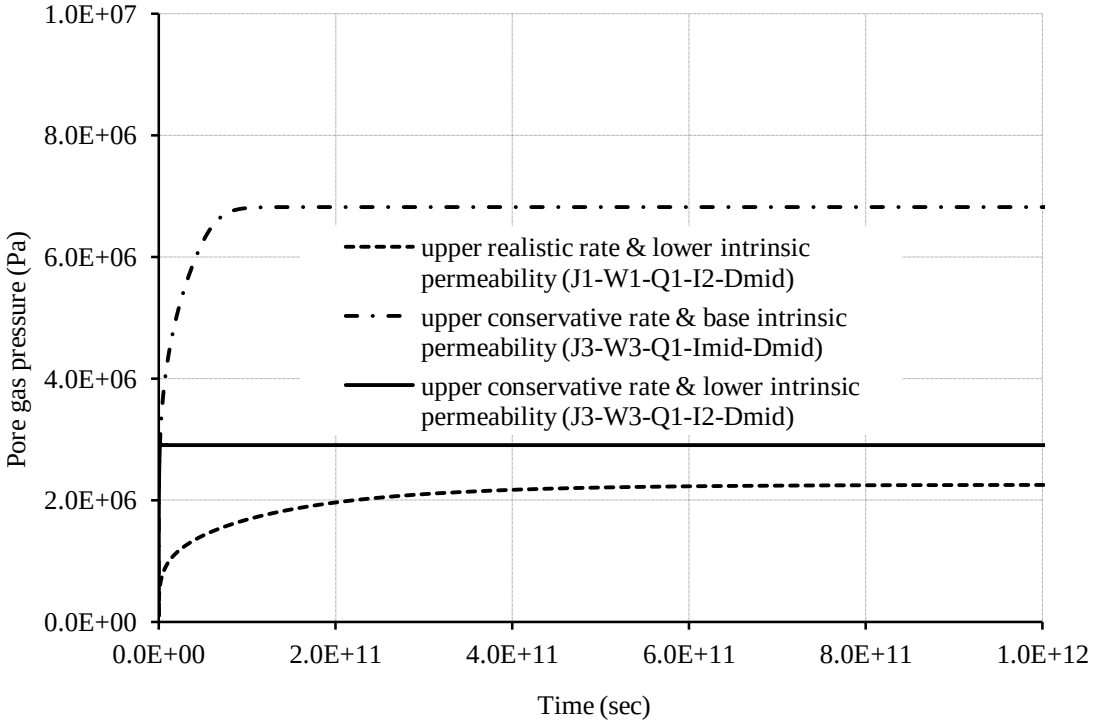

Figure 6.17: Pore gas pressure evolution for upper realistic (J1) and over-conservative (J3) gas generation rates, using the same parameter as the base case, with the exception of the single simulation with a lower intrinsic permeability for comparison.

6.4.2.3 Diffusion rate

Simulations investigating the diffusion rate are presented in this section. All other parameters are as the base case simulation presented in section 6.4.2.1. The gas pressure evolution is presented in Figure 6.18 for the upper and lower realistic rates of gas generation (J1 and J2) and for the upper and lower realistic bounds of gas diffusion through the pore water (D1 and D2). It is noted that is all cases the pressures evolved are higher than that in the Granite host rock case. In the upper realistic gas generation case (J1) the steady state conditions do not occur until almost 5,000 years (1.58E+11 seconds)..

For the upper realistic gas generation case (J1) the pressures evolved for the low diffusion rate case (D2) are 5.5 MPa and 1.8 MPa for the high diffusion rate. Clearly this indicates that the diffusion rate has a large impact and while in this case no risk of

fracture is found, more confidence is required in the diffusive capability of the clay rock and buffer in this concept. For the lower bound of the realistic rate 2.5 and < 1 MPa were found for the lower and higher bounds of diffusion respectively.

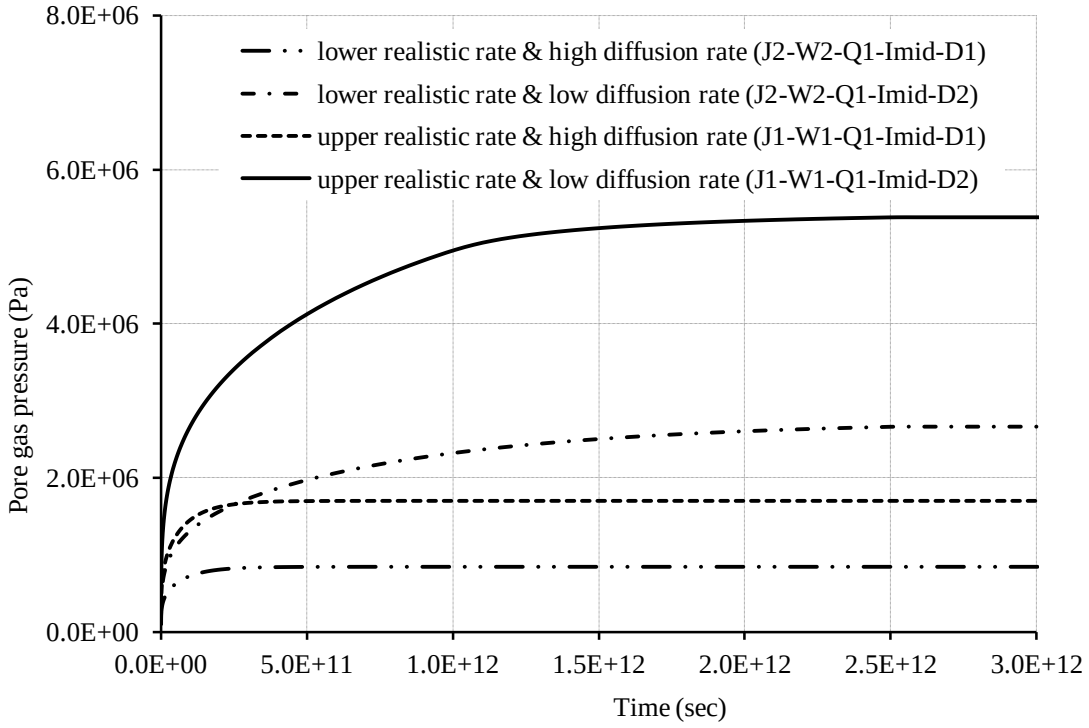

Figure 6.18: Pore gas pressure evolution with reference to changes in diffusion rate and realistic generation rates (upper and lower bound).

6.4.2.4 Intrinsic permeability

The effects of the range of intrinsic permeabilities are investigated in this section. Applying the upper realistic gas generation rate (J1) the difference in pore water pressure at steady state for the upper and lower bound of intrinsic permeability (I1 and I2) is shown in Figure 6.19, comparable to Figure 6.7 for Granitic rock. For higher permeabilities it is seen that the hydrostatic gradient is more than capable of maintaining saturation, whereas at the lower permeability (I2) there is risk of de-saturation.

Regarding the over conservative rate (J3) the results of the steady state porewater pressure profile are presented in Figure 6.20. It is seen that as with the Granitic case at the lower bound of permeability the sample de-saturates due to the water consumption

process. A decrease in pore water pressure below zero indicates de-saturation and more pore space was available for advective gas flow and storage in the buffer at the onset of de-saturation and the generation is stopped when the degree of saturation is below 0.85. It is also worth noting that even in the upper intrinsic permeability while a positive pore water pressure is maintained the excess gas pressure exceeds this greatly and the sample does not remain saturated. Therefore, the final pore gas pressure evolution is retarded if the water consumption was not considered.

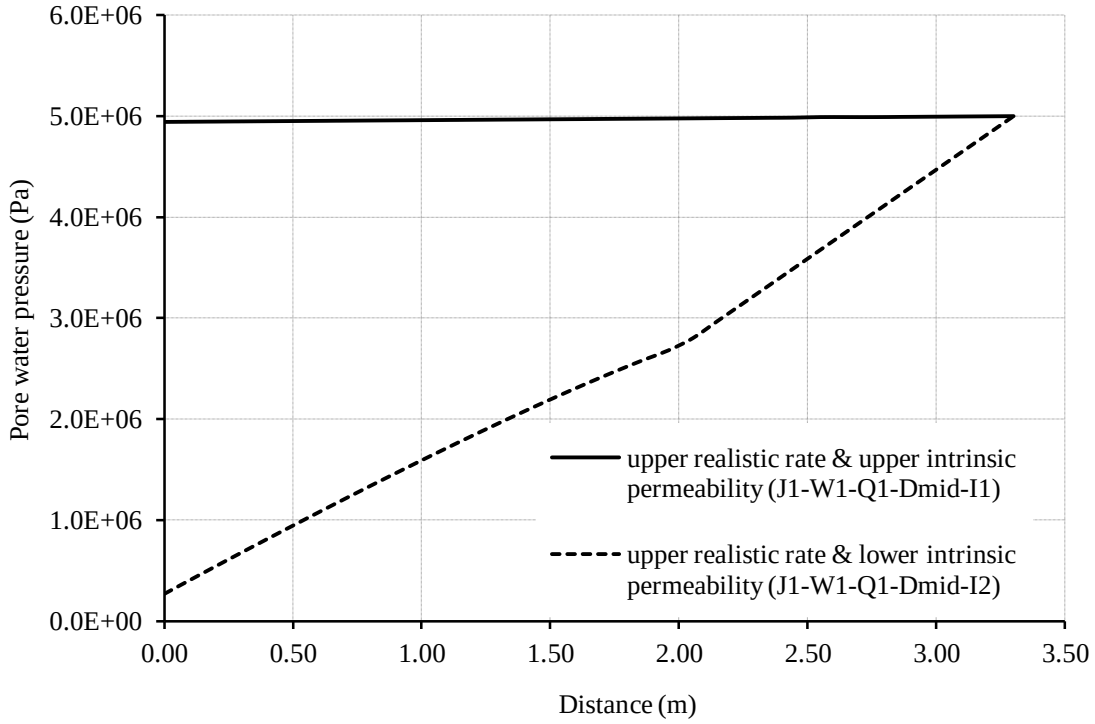

Figure 6.19: Porewater profile along buffer/rock in relation to change in intrinsic permeability with the upper realistic gas generation rate (J1) at steady state.

The pore gas profiles for the over conservative gas generation rate (J3) are presented in Figure 6.21. It can be seen that as expected the higher intrinsic permeabilities causes higher gas pressures and the low diffusion rates cause higher gas pressures. However, in comparison with Figure 6.9, it is seen that the relative effects are different, with the intrinsic permeability having a greater impact in the clay rock. The intrinsic permeability has more of an impact in the clay rock case than in the Granitic rock case as the permeability changes the entire rock system and not only the buffer. This needs to be considered when considering gas generation for disposal concepts in clay rock.

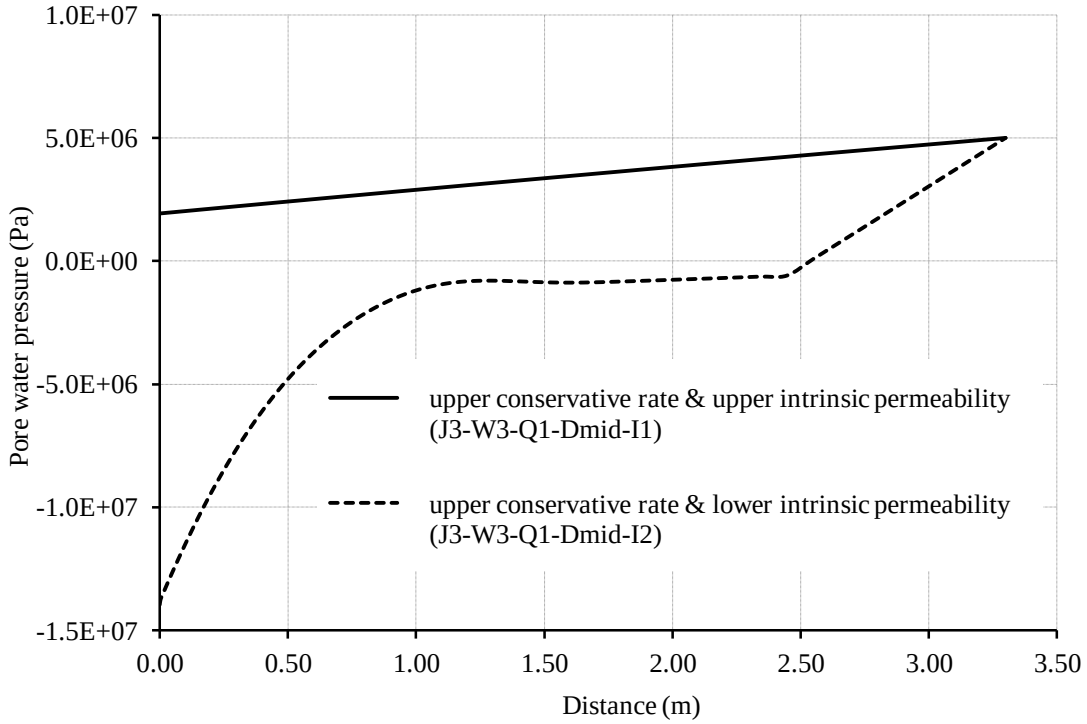

Figure 6.20: Porewater profile along buffer/rock in relation to change in intrinsic permeability with the upper conservative gas generation rate (J3) at steady state.

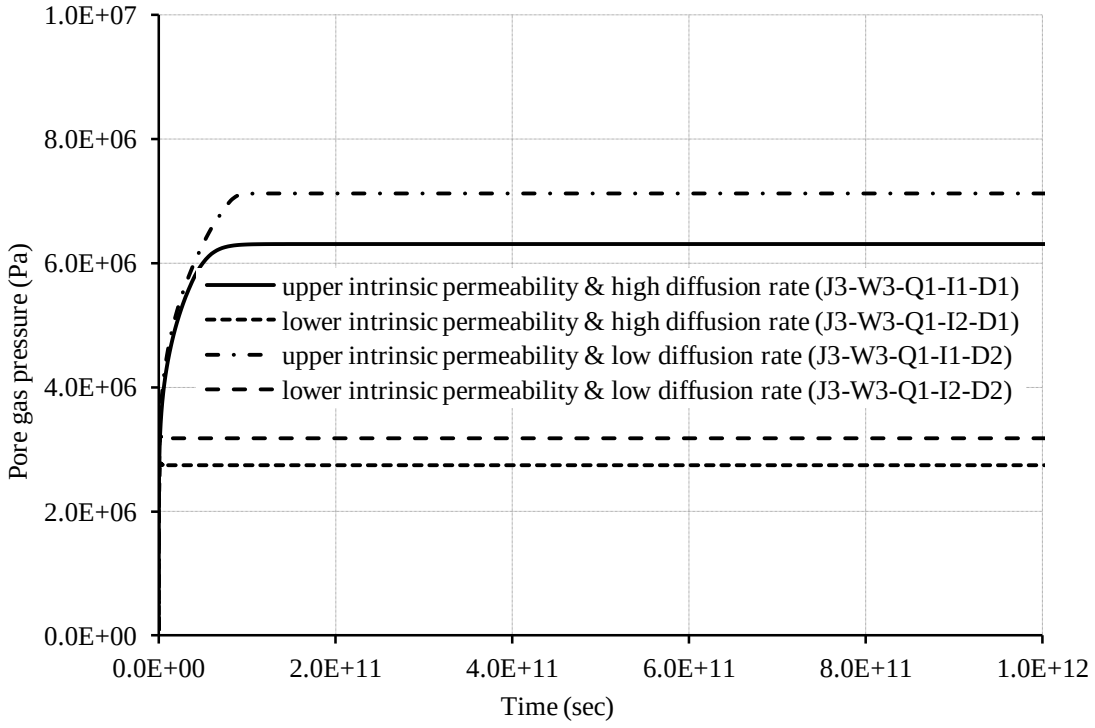

Figure 6.21: Pore gas pressure evolution in relation to change in intrinsic permeability with the upper conservative gas generation.

6.4.2.5 Boundary conditions

The evolution of pore gas pressures in relation to the different boundary conditions considered is presented in this section. Figure 6.22 presents the pore gas evolution with differing boundary conditions with over-conservative generation rate (J3), high diffusion rate (D1) and high intrinsic permeability (I1). As discussed in section 6.4.2.4, while a positive pore water pressure is maintained the gas pressure exceeds this value and saturation is not maintained. Therefore, the gas only generation boundary condition provides the worst case scenario. This was not the case for the Granitic rock where high water flows occurred and maintained saturation. It is noted that the results from the new boundary and traditional boundary conditions, both considering gas generation and water consumption, are identical as de-saturation past 0.85 was not achieved.

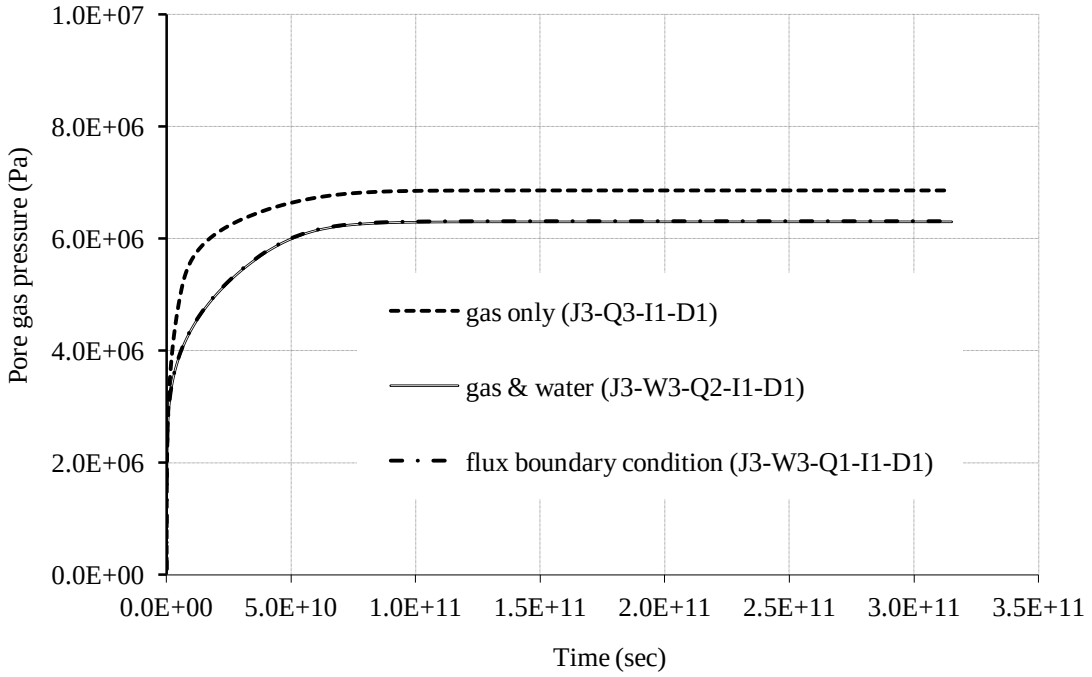

Figure 6.22: Pore gas pressure evolution in relation to different flux boundary conditions, with the over-conservative generation rate (J3), high diffusion rate (D1) and high intrinsic permeability (I1).

Figure 6.23 presents the results for the different flux boundary conditions, with the over-conservative generation rate (J3), high diffusion rate (D2) and low intrinsic permeability (I2). It can be seen with low intrinsic permeability and no water consumption (i.e. the gas only boundary condition, Q3) large gas pressures are generated, approximately 14 MPa. In this case it can be considered to be likely to

fracture. However with the more realistic new boundary condition, much lower values are predicted. This is due to i) water being removed, therefore increased storage capacity, and ii) the generation rate being inhibited by de-saturation. It is noted that for the traditional flux condition the material completely de-saturated and the model failed as this is beyond the conceptual limits of the model.

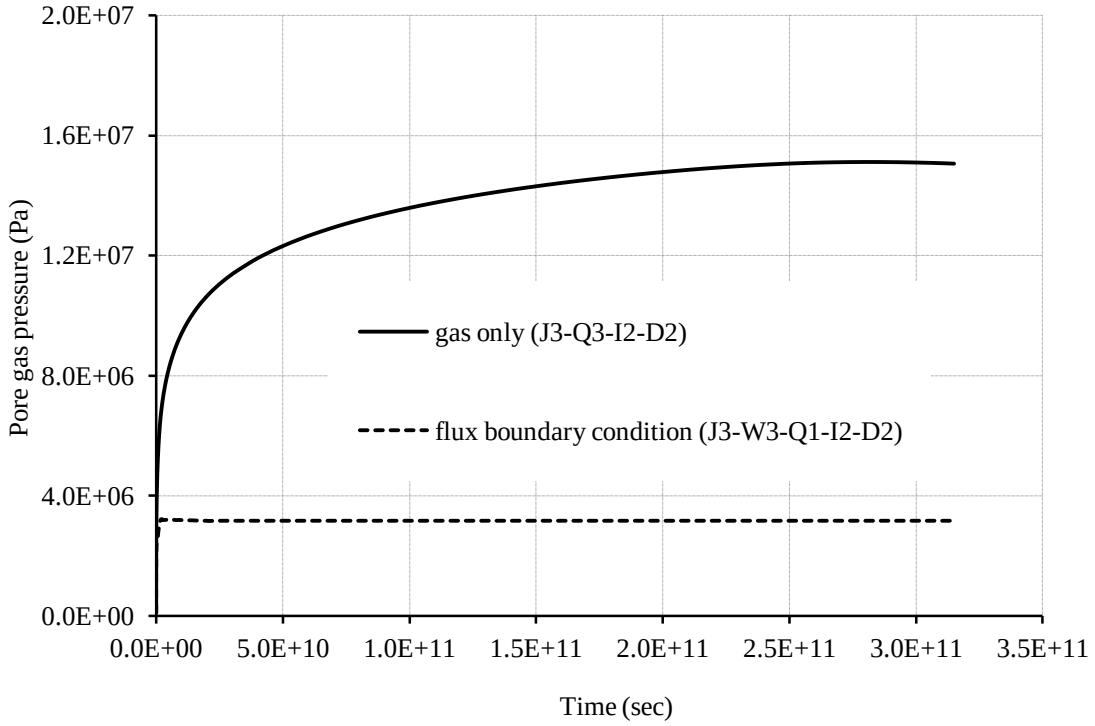

Figure 6.23: Pore gas pressure evolution in relation to different flux boundary conditions, with the over-conservative generation rate (J3), high diffusion rate (D2) and low intrinsic permeability (I2).

6.4.2.6 Initial condition and buffer thickness

The difference in initial conditions has been found to have very limited differences in the gas build-up. Only minor differences occur at the early stages when the buffer is still re-saturating under the initial hydraulic gradient. However the steady state conditions are identical. Therefore no results are reported in detail. The material parameters for clay buffer and clay host rocks has been considered identical and therefore, the buffer and host rock behaves as single unit rather than a domain of different materials, e.g. granite rock and clay buffer in crystalline host rock. Thus, the result for buffer thickness in clay host rock has not been presented separately.

6.5 Conclusion

Numerical simulations have been carried out to understand the gas migration through fully saturated buffer and the maximum pressure development in the domain. The realistic and conservative gas generation rates presented in literature review has been used in the simulations to observe the maximum values of developed pressures.

In most of the cases the risk of pneumatic fracture was found to be negligible. Specifically in all of the cases labelled 'realistic' no risk of fracture was found. The worst cases, using very conservative gas generation rates, ignoring water consumption and having lower bound diffusion in clay yielded pressures of up to 14 MPa, enough to present a risk of fracturing in repository conditions. However, these simulations are thought to be very conservative, in both boundary condition conceptualisation and gas generation rate. Further experimental work could confirm this is the case. The results of newly developed flux boundary condition for both gas generation and water consumption shows reduced gas pressure development comparing to the results where only gas injection has been considered

In the scenarios analysed clay rock was found to be less able to transport the gas away from the repository than granite rock but also prevent water from entering more easily. The buffer remains fully saturated in every simulation where realistic gas generation rates have been considered. The observation suggests that the diffusive flow plays significant role in case of fully saturated buffer. More experimental evidence is required to establish this process in long term and the diffusion coefficients require further investigation to confirm the appropriateness.

From the observation of the simulation results, it can be concluded that the development of excessive pressure and pressure driven fractures or preferential pathways are unlikely in fully saturated buffer. Moreover, the generated hydrogen exists for a very long period in the buffer which is highly sensitive to the surrounding chemical environment. Therefore, the important question arises about the flow behaviour and fate of gases in a buffer in presence of various chemicals and geochemical processes. This important issue has been addressed in the following chapter where the numerical simulation has been carried out to model the long term reactive flow of repository gases, in this case hydrogen.

References

Barden, L., Sides, G. R., (1967). "The diffusion of air through the pore water of soils". In proc, 3rd Asian Regional Conference on Soil Mechanics and Foundation Engineering 1, pp. 135-138.

Bonin, B., Colin, M., Dutfoy, A., (2000). "Pressure building during the early stages of gas production in a radioactive waste repository". *Journal of Nuclear Materials* **281,** No.1, pp. 1-14.

Brown, P.W., Masters, L.W., (1982). "Factors affecting the corrosion of metals in the atmosphere". Wiley, New York.

Cleall P.J., Melhuish T.A., Thomas, H.R., (2006). "Modelling of the three-dimensional behaviour of a prototype nuclear waste repository". *Engineering Geology* **85**, pp. 212-220.

EBS, (2005) "Specification of benchmark THM 1.1, bentonite THM mock-up experiments performed by CEA, Notes for Task Force on Engineered Barrier System".

Eriksen, T. E., Jacobsson, A., (1982). "Diffusion of Hydrogen, hydrogen sulphide and large molecular weight anions in bentonite". *SKB technical report TR*-82-17, Stockholm, Sweden.

Fredlund, D.G., Rahardjo, H., (1993). "Soil Mechanics for Unsaturated Soils", John Wiley & Sons, New York.

Galle, C., (2000). "Gas breakthrough pressure in compacted Fo-Ca clay and interfacial gas overpressure in waste disposal context". *Applied Clay Science* **17**, pp. 85-97.

Gens, A., Garcia-Molina, A.J., Olivella, S., Alonso, E.E., Huertas, F., (1998). "Analysis of a full scale in situ test simulating repository conditions". *International Journal for Numerical and Analytical Methods in Geomechanics* **22**, pp. 515-548.

Horseman, S.T., Harrington, J.F., Sellin, P., (1999). "Gas migration in clay barriers". *Engineering Geology* **54**, No. 1-2, pp. 139-149.

Nagra, (2002). "Canister options for the disposal of spent fuel". *Nagra Technical Report NTB 02-11*, Wettingen, Switzerland.

Neretnieks, I., Skagius, C., (1978). "Diffuisivitetsmatningar av metan och vate I vat lera", *SKB Technical Report TR-86*, Stockholm, Sweden.

Neretnieks, I., (1985). "Some Aspects of the Use of Iron Canisters in Deep Lying Repositories for Nuclear Waste". *Nagra Technical Report NTB 85-35*, Wettingen, Switzerland.

Norris, S., (2009). "Summary of gas generation and migration current state-of-the art". *FORGE Report D1.2-R-Draft.*

Rhén, I., Forsmark, T., (2001). "Äspö Hard Rock Laboratory, Prototype Repository, Summary report of investigations before the operation phase". *SKB, IPR-01-65*, Stockholm, Sweden.

Senger, R., Marschall, P., Finsterle, S., (2008). "Investigation of two phase flow phenomena associated with corrosion in an SF/HLW repository in Opalinus Clay, Switzerland". *Physics and Chemistry of the Earth* **33**, pp. 317-326.

SKB, (1999). "Post-closure safety SR-97". *SKB Technical Report TR-99-06*, Stockholm, Sweden.

THERESA., (2008). "THERESA project, Interface benchmark (1-D), Large scale test case, Description of the Canister Retrieval Test (CRT)", Unpublished report.

Vardon, P.J., (2009). "A three-dimensional numerical investigation of the thermo-hydro-mechanical behaviour of a large-scale prototype repository". Ph.D. thesis, Cardiff School of Engineering, Cardiff University, UK.

Werme, L., (1980). "Near field performance of the advanced cold process canister". *SKB Technical Report TR- 90-31*, Stockholm, Sweden.

Wikramaratna, R.S., Goodfield, M., Rodwell. W.R., Nash, P.J., Agg, P.J., (1993). "A preliminary assessment of gas migration from the copper/steel canister". *SKB Technical Report TR- 93-31*, Stockholm, Sweden.

7

Numerical simulation of reactive gas transport

7.1 Introduction

An application of multicomponent gas transport model to simulate non-reactive gas transport through fully saturated compacted clays has been presented in previous chapter. The modelling of reactive transport of gases through unsaturated soil has been presented in this chapter. It is expected that at the post closure stage of a high level nuclear waste disposal facility, the non-uniform saturation of bentonite buffer leads the groundwater to canister surfaces at various spots, causing local anaerobic corrosion to take place. The generated gas will therefore, flow through unsaturated portions of the buffer and involve in various geochemical processes with the available chemical components in the buffer. In this context, a series of numerical simulations of gas transport and reactions through partially saturated compacted clay has been carried out in this chapter. The main aim of the chapter is to represent capabilities of the developed model to simulate reactive gas transport in unsaturated soil and to investigate gas-chemical processes in determining the long term behaviour of bentonite buffer in context of high level nuclear waste disposal.

Since, the chapter is focused on to investigate the impact of reactive gas transport on the bentonite buffer; the contribution of host rocks in the total process has been ignored. Therefore, the influence of host rock chemical environment on the ground water chemical composition has not been considered.

Section 7.2 deals with the determination of porewater composition of compacted bentonite. The porewater composition has been for a compacted bentonite, i.e. MX-80 at different dry densities. A detail discussion on calculation procedures have been presented in this section. Geochemical model PHREEQC has been used to obtain the porewater composition in this study. Simulated results have been compared with the results reported by Bradbury and Baeyens (2002) for various dry densities.

Section 7.3 deals with development of simulation scenario including material parameters, initial and boundary conditions. A detailed discussion of the scenarios considered for the numerical simulations has been presented in this section. Two sets of tests have been carried out. The first set of simulations has been carried out considering hydrogen influx at the canister-buffer interface or the injection face. The simulation aims to investigate the transport and fate of the gas in the buffer for a long period of time. Since, the corrosion process generates magnetite alongside the hydrogen, second set of simulations have been performed by implementing both iron (Fe^{2+}) and hydrogen flux in the injection face of the buffer.

The results of simulation set-1 and simulation set-2 have been presented in section 7.4 and section 7.5 respectively. The simulations have been considered under isothermal and partially saturated conditions. It is noted that the focus has been on the understanding of the fate of gas and its impacts on chemical conditions of the system. Therefore, other coupled processes related to thermal, hydraulic and mechanical behaviour have not been investigated. An overall conclusion of this chapter has been presented in section 7.6.

7.2 Modelling of porewater chemistry

The important feature of reactive transport models includes the modelling capability of chemical reactions together with the transport processes. Reactive flow of a gas component, such as hydrogen through unsaturated soils e.g. compacted clay buffer, could possibly involve in chemical reactions at the individual phases or in between the phases, such as gas liquid interface. It has been mentioned previously, section 2.5, that the porewater of compacted clay soil contains significant amount of chemical components and the extent of reaction widely depends on the amount or composition of the chemicals. Therefore, chemical composition of the buffer porewater need to be determined prior to any geochemical reaction modelling. Porewater composition of compacted clay using laboratory experiments is difficult to obtain. On contrary, the modelling scheme provides an efficient way of measuring the porewater composition of compacted clay buffers for various dry densities and initial degree of saturations.

Bentonite MX-80 has been considered as the representative buffer material in this study. The material is widely accepted as a potential engineered barrier for disposal of higher activity radioactive waste and therefore, it has been subjected to in numerous experimental and numerical studies. The porewater composition of MX-80 bentonite compacted at various dry densities are available though literature which is beneficial since the results obtained in this study could be compared with the existing results.

In order to determine the porewater composition of the MX-80 bentonite, a similar approach adopted by Bradbury and Baeyens (2002) has been used in this work. The clay material has been characterised by Müller-Vonmoos and Kahr (1982, 1983) which has been used by Bradbury and Baeyens (2002) as well for modelling the porewater composition. The “as-received” bentonite MX-80 contains an initial gravimetric water content of 8-12 wt.%. At such a low water content direct water composition measurements are exceptionally difficult to carry out, since it requires hundreds to thousands bars to extract even small volumes of water from highly compacted bentonite samples and such high pressures could alter the porewater chemistry (Bradbury and Baeyens, 2002). Therefore, experimental results of porewater composition are inadequate at this level of water content. By using a geochemical model, simulation exercises can be carried out as an alternative technique to calculate the pore water chemistry if required material parameters such as realistic mineral compositions and selectivity coefficients are available.

The reported mineralogical analysis and compositions have been presented in Table 7.1. It is noticeable from Table 7.1 that the MX-80 bentonite contains large quantities of montmorillonite and therefore, the physical and chemical properties of this material are largely dominated by this clay mineral.

Table 7.1: Mineralogical composition of MX-80 bentonite (Bradbury and Baeyens, 2002)

Minerals	wt. %
Montmorillonite	75.0
Kaolinite	< 1.0
Mica	< 1.0
Quartz	15.2
Feldspar	5.0-8.0
Calcite	0.7
Siderite	0.7
Pyrite	0.3
Organic Carbon	0.4

Table 7.2: Chloride and sulphate inventories (Bradbury and Baeyens, 2002)

Minerals	mmol/kg
NaCl	1.35±0.1
$CaSO_4$	23.5±0.9

The material also contains some amount of quartz, feldspar, calcite, siderite and organic carbon which can influence the porewater chemistry of the bentonite (Bradbury and Baeyens, 2002). The chloride and sulphate minerals in porewater of MX-80 bentonite have been listed in Table 7.2.

The total specific surface area of montmorillonite has been reported approximately 7.5×10^5 m^2/kg with an external specific surface area of 31×10^3 m^2/kg determined by nitrogen adsorption (Bradbury and Baeyens, 2002). The surface of montmorillonite clay platelets comprises of negative charges which provides a high cation exchange capacity of 787±48 mEq/kg. Table 7.3 lists the exchangeable cation compositions.

Table 7.3: Exchangeable ions composition of MX-80 bentonite. Data has been obtained from (Bradbury and Baeyens, 2002)

Exchangeable Cations	Cation occupancies (mEq/kg)
Na^+	668±40
K^+	13±2
Mg^{2+}	40±3
Ca^{2+}	66±3
∑Cations	787±48

With a 10% of the cation exchange capacity, a secondary reactive surface sites located along the edges of clay platelets can potentially function as a powerful pH buffer (Bradbury and Baeyens, 2002). The surface groups are commonly known as amphoteric surface hydroxyl group (SOH) since the compounds can behave both as acid and as base. It has been suggested that the surface sites are able to protonate and de-protonate in such a way that the concentrations of neutral (SOH), protonated (SOH_2^+) and de-protonated (SO^-) edge sites changes as a function of pH. Table 7.4 and Table 7.5 represent the concentrations of surface sites and surface complexation reactions for MX-80 bentonite respectively.

Table 7.4: Initial states of amphoteric surface sites of MX-80 bentonite. $S^{w1}OH$ and $S^{w2}OH$ denote two weak site types (Bradbury and Baeyens, 2002).

SOH sites	Concentration (mol/ kg of soil)
$S^{w1}OH$	1.3×10^{-2}
$S^{w1}OH_2^+$	4.2×10^{-6}
$S^{w1}O^-$	1.7×10^{-2}
$S^{w2}OH$	3.0×10^{-2}
$S^{w2}OH_2^+$	9.4×10^{-5}
$S^{w2}O^-$	3.0×10^{-4}

Bradbury and Baeyens (2002, 2003) suggested that the charge on (SOH_2^+) and (SO^-) sites are compensated by outer sphere complexes, such as potassium (K^+), magnesium (Mg^{2+}) etc. and hence their contribution has been neglected in the modelling of porewater chemistry.

Table 7.5: Protolysis constants of Na-montmorillonite (Bradbury and Baeyens, 1997).

Surface complexation reactions	Log K
$S^{w1}OH + H^+ \leftrightarrow S^{w1}OH_2^+$	4.5
$S^{w1}OH \leftrightarrow S^{w1}O^- + H^+$	-7.9
$S^{w2}OH + H^+ \leftrightarrow S^{w2}OH_2^+$	6.0
$S^{w2}OH \leftrightarrow S^{w2}O^- + H^+$	-10.5

Simulations have been carried out to determine the porewater compositions of three samples compacted at dry densities of 1200, 1500 and 1600 kg/m^3. Geochemical model PHREEQC2 has been used to obtain the composition of the initial pore water, amount of minerals and exchangeable ions in water content values. The results have been compared with the reported results of Bradbury and Baeyens (2002, 2003) to achieve confidence for predicting the porewater composition of the representative sample at variable water content. Later the porewater composition of MX-80 bentonite compacted at 1600 kg/m^3 has been modelled for various solid to liquid ratios (i.e. water content of 10%, 15% and 18%).

Based on the suggestions proposed by Bradbury and Baeyens (2002) the simulations have been executed under following assumptions.

- During compaction the physico-chemical properties of the powdered bentonite remain unchanged and can directly be applied to determine the porewater composition of the compacted bentonite sample.
- The solid phase of the buffer plays dominant role to determine the initial porewater composition due to the very high solid to liquid ratio.
- pH in the moist bentonite powder is governed by the equilibrium of sulphate or carbonate minerals at air $P_{CO2} = 10^{-3.5}$ bar and the state of the amphoteric surface (SOH) sites corresponds to this pH.

The amount of minerals and exchangeable cations has been calculated from Table 7.1, Table 7.2 and Table 7.3 based on a mass balance which has been listed in Table 7.6. From Table 7.6 the mass balance inventories can readily be calculated for any chosen initial dry densities.

The equilibrium constant of mineral reactions have been obtained from the PHREEQC database (*phreeqc.dat*) presented by Parkhurst and Appelo (1999) which has been listed in Table 7.7. The selectivity coefficients for surface complexation reactions and exchange reactions have been adopted from the work of Bradbury and Baeyens (2002) and Bradbury and Baeyens (2003) which have been presented in Table 7.5 and Table 7.8 respectively.

Table 7.6: Amount of minerals and exchangeable cations in MX-80 adopted in the geochemical analysis by Bradbury and Baeyens (2002).

	Minerals/ Exchangeables	Quantity (mol/kg of dry soil)
Minerals	Calcite	0.07
	Gypsum	0.0235
	Halite	0.00135
Exchangeable cations	Na^+	0.668
	K^+	0.013
	Mg^{2+}	0.020
	Ca^{2+}	0.033

Table 7.7: Thermodynamic parameters of mineral dissolution/ precipitation reactions used n this study. The parameters have been obtained from PHREEQC2 database *phreeqc.dat* by (Parkhurst and Appelo, 1999)

Minerals reactions		Log k at 25°C
Calcite	$CaCO_3 = Ca^{2+} + CO_3^{2-}$	-8.480
Gypsum	$CaSO_4{:}2H_2O = Ca^{2+} + SO_4^{2-} + 2H_2O$	-4.580
Halite	$NaCl = Na^+ + Cl^-$	1.582

Table 7.8: Exchange reactions and equilibrium constants (Bradbury and Baeyens, 2003).

Exchange reactions	Log K at 25°C
Na-montmorillonite + $K^+ \leftrightarrow$ K-montmorillonite + Na^+	4.0±1.6
2Na-montmorillonite + $Mg^{2+} \leftrightarrow$ Mg-montmorillonite + $2Na^+$	2.2±1.1
2Na-montmorillonite + $Ca^{2+} \leftrightarrow$ Ca-montmorillonite + $2Na^+$	2.6±1.2

The results of geochemical modelling of the pore water composition of the MX-80 bentonite equilibrium with pure water have been presented in Table 7.9 for various dry densities. The results of a similar modelling carried out by Bradbury and Baeyens (2002) has been presented for comparison. The PHREEQC simulated results show a good agreement with the results obtained from Bradbury and Baeyens model. The results have been presented for an initial gravimetric water content of 10 wt. %. The calculated bentonite porewater has relatively high ionic strength varies from 0.295 to 0.356. At 1200 and 1500 kg/m^3 dry densities sodium (Na^+) and sulphates (SO_4^{2-}) dominates over the other ions in both studies. But at 1600 kg/m^3 dry density significant amount of chloride concentrations have been observed. Based on their results, Bradbury and Baeyens (2002) suggested that the porewater composition changed from a sodium sulphate (Na_2SO_4) water at 1200 kg/m^3 to a NaCl/ Na_2SO_4 water at 1600 kg/m^3. Similar results have been obtained from this study, suggesting that the modelling of porewater composition have been performed accurately. It is obvious from the results of porewater composition that a number of chemical components are present in the liquid phase which can undergo various geochemical reactions. The flow behaviour of gases in presence of such a chemical environment could be affected due to geochemical processes/ interactions. Therefore, in the following sections, numerical simulations have been carried out to observe the transport behaviour of a gas component coupled with geochemical reactions.

Table 7.9: Porewater composition of compacted MX-80 bentonite as a function of initial dry density

	PHREEQC This study	Bradbury and Baeyens (2002)	PHREEQC This study	Bradbury and Baeyens (2002)	PHREEQC This study	Bradbury and Baeyens (2002)
Dry density (Kg/m^3)	1200	1200	1500	1500	1600	1600
Log Pco_2 (bar)	-3.38	-3.38	-3.43	-3.43	-3.48	-3.48
Ionic strength (M)	0.318	0.295	0.34	0.314	0.356	0.327
pH	8.0	8.0	8.0	8.0	7.979	8.0
Na^+ (mol/l)	2.33×10^{-1}	2.20×10^{-1}	2.59×10^{-1}	2.43×10^{-1}	2.78×10^{-1}	2.61×10^{-1}
K^+ (mol/l)	1.26×10^{-3}	1.13×10^{-3}	1.39×10^{-3}	1.23×10^{-3}	1.49×10^{-3}	1.32×10^{-3}
Mg^{2+} (mol/l)	5.95×10^{-3}	6.11×10^{-3}	6.90×10^{-3}	7.06×10^{-3}	7.53×10^{-3}	7.69×10^{-3}
Ca^{2+} (mol/l)	9.33×10^{-3}	9.01×10^{-3}	9.87×10^{-3}	9.47×10^{-3}	1.06×10^{-2}	1.01×10^{-2}
Cl^- (mol/l)	2.70×10^{-2}	2.70×10^{-2}	6.75×10^{-2}	6.75×10^{-2}	1.08×10^{-1}	1.08×10^{-1}
SO_4^{2-} (mol/l)	1.19×10^{-1}	1.12×10^{-1}	1.13×10^{-1}	1.04×10^{-1}	1.03×10^{-1}	9.45×10^{-2}
HCO_3^- (mol/l)	9.45×10^{-4}	9.72×10^{-4}	8.59×10^{-4}	8.83×10^{-4}	7.71×10^{-4}	7.80×10^{-4}

Confidence achieved from the results of porewater chemistry modelling has been used to determine the porewater compositions of compacted bentonite for various water contents. The porewater compositions of MX-80 bentonite, compacted at 1600 Kg/m^3, have been obtained for 10%, 15% and 18% water content which has been presented in Table 7.10. During simulation, it has been assumed that all of the available water contributes in determining the porewater compositions.

Table 7.10: Porewater composition of MX-80 bentonite at various water content compacted at dry density of 1600 Kg/m^3.

Water content (wt. %)	**10.0%**	**15.0%**	**18.0%**
pH	8.03	8.03	8.03
Na^+ (mol/l)	2.14×10^{-1}	2.01×10^{-1}	1.95×10^{-1}
K^+ (mol/l)	1.16×10^{-3}	1.11×10^{-3}	1.07×10^{-3}
Ca^{2+} (mol/l)	9.21×10^{-3}	9.22×10^{-3}	9.25×10^{-3}
Mg^{2+} (mol/l)	5.14×10^{-3}	4.61×10^{-3}	4.39×10^{-3}
Cl^- (mol/l)	1.39×10^{-2}	0.89×10^{-2}	0.79×10^{-2}
SO_4^{2-} (mol/l)	1.14×10^{-1}	1.10×10^{-1}	1.07×10^{-1}
HCO_3^- (mol/l)	8.34×10^{-4}	8.23×10^{-4}	8.15×10^{-4}

7.3 Simulation scenario of reactive transport of gas

In this section numerical simulations of the reactive transport of gas has been presented in detail. Two sets of simulation have been carried out to observe the gas transport and reactions in clay buffer and its impact on the chemical state of clay-water system. Simulations have been performed under isothermal conditions, since it has been mentioned in the literature that the most of the hydrogen generation due to corrosion of the canister takes place when the system is in thermal equilibrium or at an ambient temperature. Therefore, in the simulations provided a constant ambient temperature of 25°C has been considered to prevail over the duration of simulation.

A detail discussion about the corrosion rate and consequent gas generation rate has been presented in literature review chapter. Based on the information reported in the literature a constant hydrogen influx of 2.0×10^{-11} kg/m^2/sec has been considered in this simulation which fits in the range of realistic gas generation rate in a higher activity radioactive waste disposal facility. Based on the constant corrosion rate and gas generation rate a hypothesis has been made to determine the duration of the simulation. The above mentioned gas generation rate a 20 cm thick canister will last for about 10,000 years. According to various disposal concepts, canister thickness for higher activity radioactive waste disposal facility has been suggested around 5 to 20cm (Bonin et al., 2000). A chronogram of the major phenomena affecting the repository and its geological environment has been presented in the literature (Figure 2.1). It has been suggested that from the point of repository closure the metallic corrosion and hydrogen production might continue for 10,000 years which also support the duration of numerical simulation.

In terms of saturation state of the clay, it has been assumed that a non-uniform re-saturation of the buffer leads the underground water to reach at various spots in the canister. As a result, metallic corrosion initiates which produce hydrogen due to local anoxic condition. The generated gas could possibly migrate through the unsaturated region and undergo various chemical processes, affecting the buffering properties in a long period of time. The portion of gas that might flow through the unsaturated buffer is yet to be determined. Since, gases predominantly flow through the paths of least resistance, it has been considered that the hydrogen gas inflows from canister-buffer interface to the unsaturated region at a rate which is similar to generation rate. The influence of host rock has been neglected in this chapter, as

the investigation is focused on to observe the gas-chemical interactions in the clay buffer. In presence of host rocks the groundwater chemical composition changes which ultimately alter the porewater composition of the clay buffer. Although this phenomenon might be important but the hydro-chemical processes are beyond the scope of this work and could be considered as a future work in this area of research.

The "as-received" bentonite powder contains around 10 wt.% water content and from the modelling of porewater composition the amount of chemical components can be obtained. At higher water contents, gas components usually have less space to flow and the amount of chemical components also varies. Therefore, to understand the extent of gas-chemical interactions and fate of gas in the buffer, a series of simulations has been carried out with various water contents or degree of saturations.

As it has been suggested in the literature, bentonite MX-80, a potential candidate as buffer material in a nuclear waste repository, compacted at a dry density of 1.6 Mg/m^3 has been considered as the buffer material for the simulations. The buffer thickness has been considered following the proposed KBS-3 concept by SKB as 0.35 m by 0.5m (Andersson et al., 2000).

In this study, two sets of conceptual simulations have been performed considering realistic material parameters and boundary conditions. The first set of simulation (section 7.4) considers only hydrogen influx at the canister-buffer interface (or the injection face), focusing on the gas flow behaviour and chemical reactions at various water contents. The second set of simulation (section 7.5) considers a condition in which both hydrogen and iron influx into the buffer. The simulation has aimed to study the flow and reactions of both gas and aqueous chemicals. The numerical model domain, boundary and initial conditions, time-step and material properties have been presented in the following sections.

7.3.1 Model domain and time-step

The 0.35 m long and 0.5 m high model domain has been discretised into 80 equally spaced finite elements of 4 noded quadrilaterals. A variable time step has been adopted in this work which allows a variation of time-step depending on the convergence criteria as it has been discussed in chapter 4. As mentioned previously, the simulations have been carried out for 10,000 years.

7.3.2 Material parameters for modelling thermal, hydraulic, gas and chemical processes

The material parameters used in this simulation have been detailed in this section. The important addition is the gas conductivity parameters and chemical reaction parameters.

7.3.2.1 Moisture retention behaviour

Water retention experiments carried out on MX-80 bentonite to characterise the water retention behaviour for a range of initial dry densities has been presented in EBS (2005). The moisture retention relationship has been adopted based on the van Genuchten expression, which can be represented as:

$$\theta_l = nS_r = \theta_{lr} + \left(\theta_{ls} - \theta_{lr}\right)\left[\frac{1}{1+(\alpha s)^n}\right]^m \tag{8.1}$$

where, θ_l is the liquid volumetric water content, θ_{lr} represents the saturated liquid volumetric water content, θ_{lr} is the residual liquid volumetric water content, α, n are m are constants and s is the matric suction measured in metres height. It was found that the best fit was achieved using the following constants for benontite of 1.6Mg/m^3: α = 0.00045, n=1.75 $m = 1 - \frac{1}{n} = 0.43$, $\theta_{lr} = 0.0001$, $\theta_{ls} = porosity$ = 0.4.

7.3.2.2 Unsaturated gas permeability

The saturation dependent gas conductivity has been used in the simulation. The gas conductivity relationship, equation (3.65), presented in chapter 3 has been adopted in this simulation. Recalling equation (3.65) yields:

$$k_g = \frac{K_{int} K_{rg}}{\mu_g} \tag{8.2}$$

Parker et al. (1987) proposed the relative gas conductivity, K_{rg} which is similar to the van Genuchten-Mualem characteristics curve which has been

$$K_{rg} = (1 - S_e)^{1/2}(1 - S_e^{1/m})^{2m} \tag{8.3}$$

For the value of n = 1.75 the van Genuchten relationship the value of m is close to 0.43. the effective saturation can be obtained from the equation

$$S_e = \frac{\left(S_l - S_{r,l}\right)}{\left(1 - S_{r,l}\right)} \tag{8.4}$$

where, $S_{r,l}$ is the residual degree of saturation. The intrinsic permeability has been obtained from FEBEX experiment (Huertas et al., 2000). The gas phase permeability has been determined using nitrogen at a low pressure on specimens with dry densities ranges from 1.5 to 1.7 Mg/m^3. In all of performed tests, the value of intrinsic permeability obtained in the range between 10^{-16} to 10^{-12} m^2. Since, the experimental values for compacted MX-80 bentonite are not available in literature, an intrinsic permeability value of 10^{-12} m^2 has been considered. The dynamic viscosity of hydrogen has been assumed to be equal to air viscosity at standard temperature and pressure condition. At 25°C and 1 atm pressure dynamic viscosity of hydrogen has been considered equal to 1.8×10^{-5} Ns/m^2 (Fredlund and Rahardjo, 1993).

7.3.2.3 Diffusion coefficients

The values of diffusion coefficients of ions in water and hydrogen through air has been presented in Table 7.11. The diffusion coefficients of ions in water has been obtained from Lasaga (1998) while the diffusion coefficient of hydrogen has been collected from the values reported by Cussler (1984). The diffusion coefficients of the Table 7.11 have been obtained in free flow condition, therefore in this simulation, the effective diffusion coefficients has been considered. The effective diffusion coefficient has been obtained by using the relationship proposed by Millington and Quirk (1961) which incorporates the effect of path tortuosity of a porous medium.

Table 7.11: Diffusion coefficients of dissolved chemical components and gas components.

Chemical/ gas components	Diffusion coefficients (m^2/s)
Cl^-	2.03×10^{-9}
SO_4^{2-}	1.07×10^{-9}
HCO_3^-	1.18×10^{-9}
Ca^{2+}	0.79×10^{-9}
Mg^{2+}	0.70×10^{-9}
Na^+	1.33×10^{-9}
K^+	1.96×10^{-9}
H^+	9.33×10^{-9}
$H_2(g)$	6.11×10^{-5}

The tortuosity relationship follows the previously mentioned in chapter 3 and for gas and liquid phase, it can be presented respectively as:

$$D_{ij}^0 = nS_g \tau_g D_{ij} \tag{8.5}$$

and,

$$D_{ij}^0 = nS_l \tau_l D_{ij} \tag{8.6}$$

For liquid phase and gas phase the factors can be presented as:

$$\tau_g = n^{1/3} S_g^{7/3} \tag{8.7}$$

$$\tau_l = \frac{(\theta_l)^{7/3}}{n^2} \tag{8.8}$$

7.3.2.3 Chemical reactions and equilibrium constant

The presence of hydrogen might influence a number of geochemical reactions. The important geochemical reactions in context of hydrogen flow, through the buffer, have been presented in Table 7.12 together with the equilibrium constants. Other chemical reactions of secondary importance have also been considered during the simulation, although have not been listed in the table. The possible mineral geochemical reactions that might occur in the buffer due to hydrogen influx have been presented in Table 7.13

Table 7.12: Redox half reactions in aqueous phase and thermodynamic constants. The equilibrium constants have collected from PHREEQC manual (Parkhurst and Appelo, 1999).

Aqueous complexes	Log K
$H_2(g) \leftrightarrow 2H^+ + 2e^-$	-3.150
$CO_3^{2-} + H^+ \leftrightarrow HCO_3^-$	10.329
$CO_3^{2-} + 2\,H^+ \leftrightarrow CO_2 + H_2O$	16.681
$CO_3^{2-} + 10\,H^+ + 8\,e^- \leftrightarrow CH_4 + 3\,H_2O$	41.071
$HS^- \leftrightarrow S^{2-} + H^+$	-12.918
$SO_4^{2-} + 9\,H^+ + 8\,e^- \leftrightarrow HS^- + 4\,H_2O$	33.65
$HS^- + H^+ \leftrightarrow H_2S$	6.994
$Ca^{2+} + H_2O \leftrightarrow CaOH^+ + H^+$	-12.780
$Ca^{2+} + CO_3^{2-} \leftrightarrow CaCO_3$	3.224
$Ca^{2+} + CO_3^{2-} + H^+ \leftrightarrow CaHCO_3^+$	11.435
$Ca^{2+} + SO_4^{2-} \leftrightarrow CaSO_4$	2.30
$Ca^{2+} + HSO_4^- \leftrightarrow CaHSO_4^+$	1.08
$Mg^{2+} + H_2O \leftrightarrow MgOH^+ + H^+$	-11.440
$Mg^{2+} + CO_3^{2-} \leftrightarrow MgCO_3$	2.98
$Mg^{2+} + H^+ + CO_3^{2-} \leftrightarrow MgHCO_3^+$	11.399
$Mg^{2+} + SO_4^{2-} \leftrightarrow MgSO_4$	2.370
$Na^+ + H_2O \leftrightarrow NaOH + H^+$	-14.180
$Na^+ + CO_3^{2-} \leftrightarrow NaCO_3^-$	1.270
$Na^+ + HCO_3^- \leftrightarrow NaHCO_3$	-0.25
$Na^+ + SO_4^{2-} \leftrightarrow NaSO_4^-$	0.70
$K^+ + H_2O \leftrightarrow KOH + H^+$	-14.460
$K^+ + SO_4^{2-} \leftrightarrow KSO_4^-$	0.850

Table 7.13: Reactions between minerals and thermodynamic constants. The equilibrium constants have been obtained from PHREEQC manual (Parkhurst and Appelo, 1999).

Minerals	Log K
$CaCO_3(s) + H^+ \leftrightarrow Ca^{2+} + HCO_3^-$	1.8487
$CaSO_4.2H_2O(s) \leftrightarrow Ca^{2+} + SO_4^{2-} + 2H_2O$	-4.4823
$CaMg(CO_3)_2(s) + 2H^+ \leftrightarrow Mg^{2+} + Ca^{2+} + 2HCO_3^-$	3.5676

7.3.3 Initial and boundary conditions

It has been assumed that the system is under isothermal condition and in equilibrium with the ambient temperature at 25°C or 298 K. Boundary conditions have been developed for two sets of simulations. Based on the geochemical analysis of porewater chemistry presented in previous section, the initial conditions for the primary dissolved chemical components have been presented in Table 7.10.

Table 7.14: Initial quantities of minerals and exchangeable ions for the numerical simulations.

Initial minerals and cation exchangesbles	**Water content (wt.%)**		
(mol/kg of soil)	10%	15%	18%
Calcite	0.069	0.069	0.069
Gypsum	0.012	0.007	0.004
Halite	0.0	0.0	0.0
Anhydrite	0.0	0.0	0.0
$Ca\text{-}X_2$	4.36×10^{-2}	4.82×10^{-2}	5.07×10^{-2}
$Mg\text{-}X_2$	1.95×10^{-2}	1.93×10^{-2}	1.92×10^{-2}
K-X	1.288×10^{-2}	1.288×10^{-2}	1.276×10^{-2}
Na-X	64.79×10^{-2}	63.90×10^{-2}	63.41×10^{-2}

The 7.10 contains porewater composition data of MX-80 bentonite for 10%, 15% and 18% water content. Simulation set-1 has been carried out at these three water contents. The initial amount of minerals and exchangeable cations for simulation set-1 has been listed in Table 7.14. The remaining void space has been assumed to be occupied by hydrogen gas at atmospheric pressure. Therefore, the initial concentration of hydrogen has been calculated at one atmospheric pressure in per cubic meter of $\theta_{g.}$

The simulation set-2 has been performed under the same material parameters for 10% water content and boundary conditions but considering both hydrogen and iron influx. Simulation set-2 considers no initial presence of Fe and Fe-exchangeable ions at the buffer in the initial condition. Based on the previous chapter, a realistic rate of hydrogen influx has been considered as 2.0×10^{-11} kg/m^2/sec and from the stoichiometric relationship the iron influx has been considered as 5.0×10^{-12} kg/m^2/sec. The opposite site of the injection face has been considered to be impermeable for any kind of gas and chemical components.

During saturation process the outer surface of the bentonite barrier becomes saturated with water and swelling of the buffer takes place. The high swelling pressure and water tight narrow flow channels restrict the movement of gas through the buffer. Therefore, the boundary opposite to injection face has been assumed to be impermeable for the gas to flow. Similarly, swelling of the buffer restricts or reduces further water flow towards the canister and as a result, the boundary at x = 0.35 has been considered impermeable to water and other chemicals flowing with it.

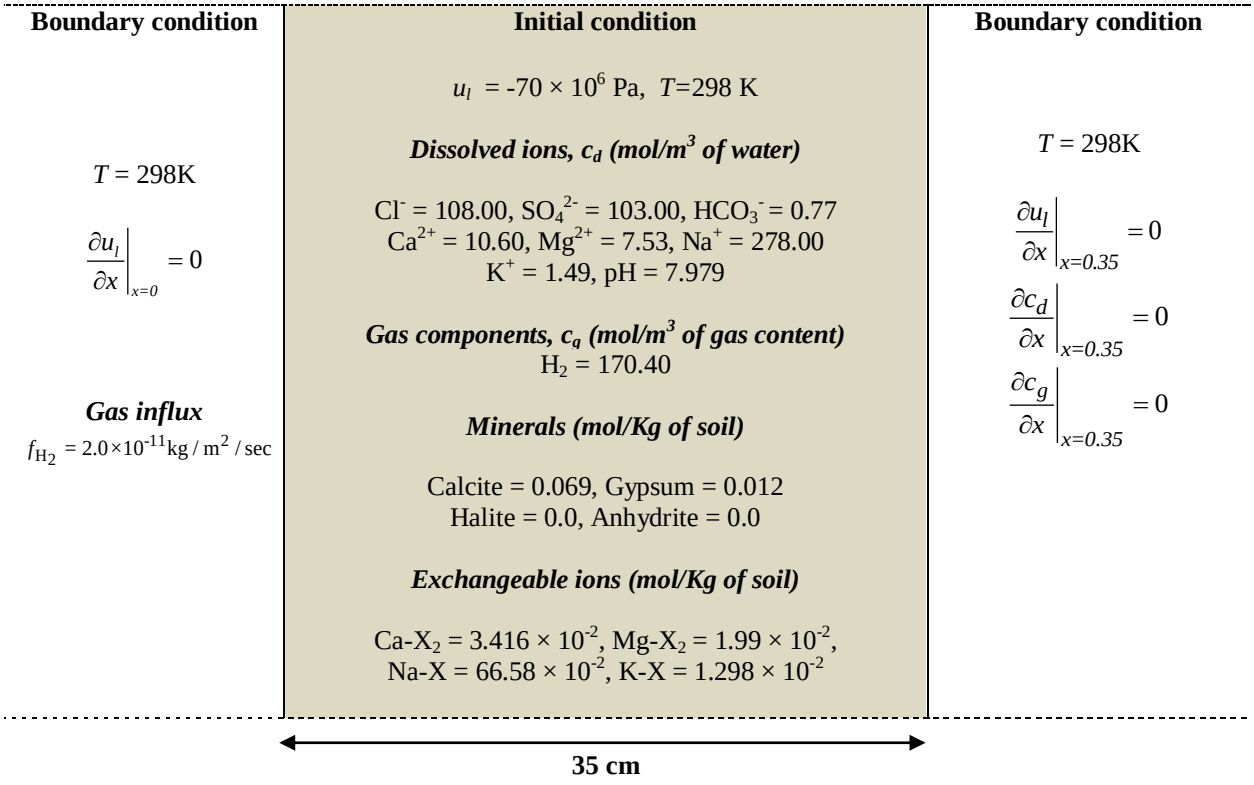

(a)

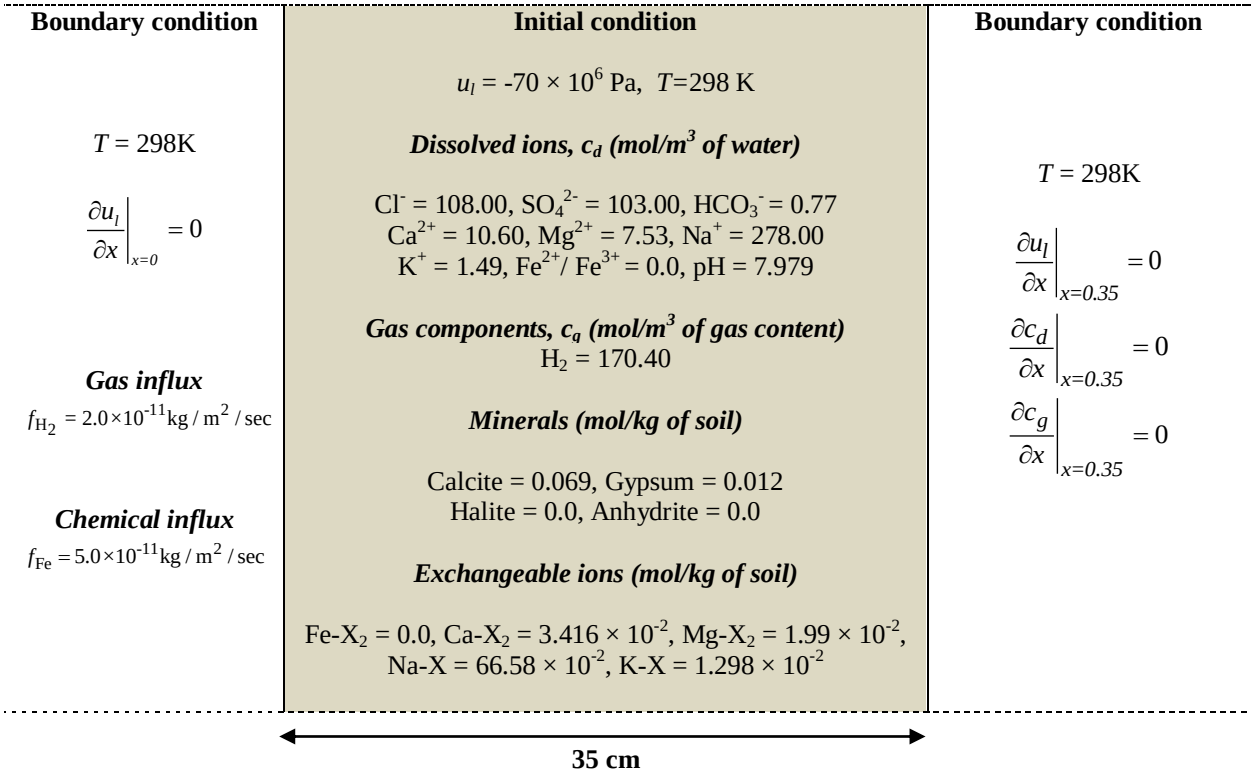

(b)

Figure 7.1: Schematic diagram of the boundary conditions (a) simulation set-1 for 10% water content with only hydrogen influx; (b) simulation set-2 for same water content with both hydrogen and iron influx.

7.4 Results and discussion of Simulation set-1

The first set of simulation considers only the influx of hydrogen in the buffer due to corrosion reactions. To observe the gas flow behaviour and chemical processes, simulations have been performed at three different water contents, such as 10 wt.%, 15 wt.% to 18 wt.% corresponds to degrees of saturation of 40%, 60% and 70% respectively. It has been assumed that at the unsaturated buffer, the porewater has been distributed uniformly at each of the gauss points in the model domain.

The results of numerical simulation in terms of gas flow and geochemistry of the gas and porewater including major cation, anions, minerals exchange capacity and pH have been presented in this section. The results have been plotted regarding the long term evolution of associated chemical and gas components in the system. The graphical results have been obtained from the injection face or the canister buffer-interface, since this part of the buffer receive maximum impact from the hydrogen influx due to corrosion. In case of similar type results (or graphical trends) one has been chosen as the representative for analysis and discussion that also applicable for the other results.

7.4.1 Evolution of hydrogen

The simulation results of hydrogen concentration at the gas injection face of the buffer have been presented in Figure 7.2. Results have been plotted for three different water content of 10%, 15% and 18% corresponding to degrees of saturation about 40%, 60% and 70% respectively. Since, the graphs of gas evolution are of similar pattern, the result of 10% water content has been analysed and the explanation is applicable for the other results.

The generated gas pressure is significantly less in the simulation where the pore water is comprised of various chemical components and minerals, such as calcite, gypsum than the simulation considering pure distilled water. A verification exercise was carried out for a similar gas influx and boundary conditions, presented in section 5.5, except the porewater being pure distilled water where the various minerals and chemical components are absent. The simulation with pure water reported a maximum gas pressure around 9.0 atmospheric pressure after 10,000 years (Figure 5.16) while in the current simulation the result is approximately 2.45 atmospheric pressure which suggests significant chemical processes might have been occurred. The reason of this type of behaviour can be explained as follows.

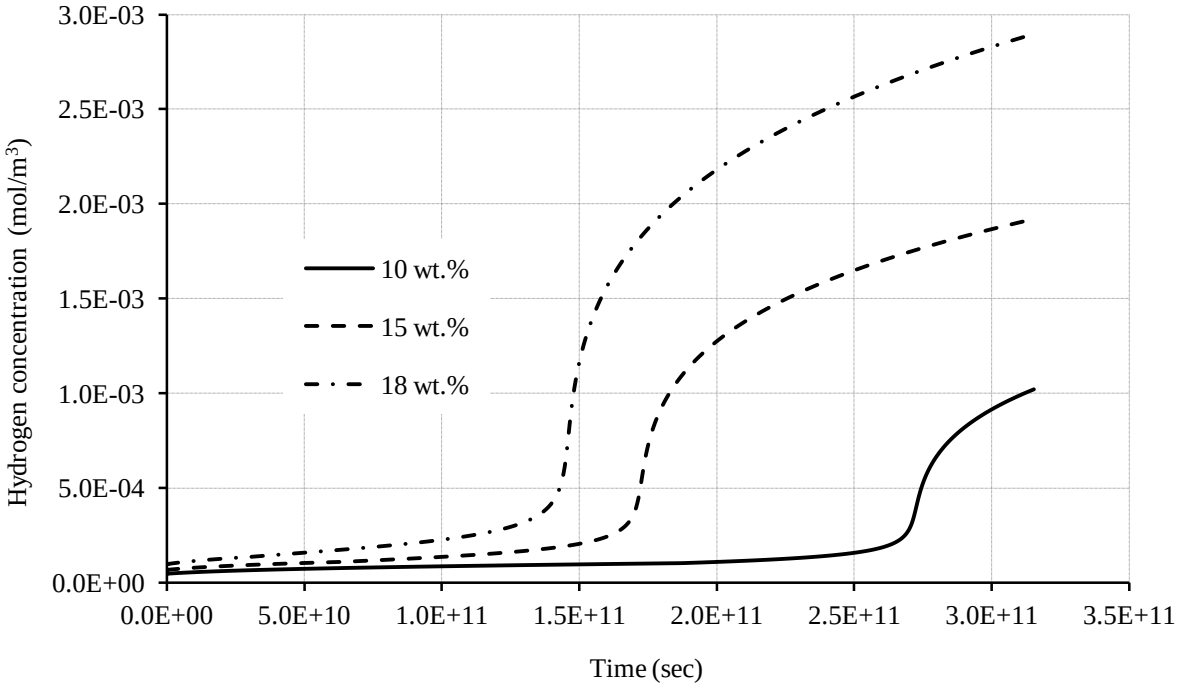

Figure 7.2: Evolution of hydrogen at various water contents for the duration of 10,000 years. The gas concentration is in mol per m^3 of gas content (θ_g).

Under equilibrium condition, hydrogen dissolves in pure water according to the following chemical reaction:

$$H_2(g) \leftrightarrow 2H^+ + 2e^-$$

To maintain the equilibrium from left to right of the chemical reaction, the influx of hydrogen increases the amount of H^+ ion and decrease the redox potential, Pe. The redox potential is a measure of electron activity, as the electrons do not present as an individual chemical component, such as H^+, it is normally expressed as a negative logarithm of electron activity e.g. $P_e = -\log a_e^-$. The lower the P_e, the higher the tendency of the solution to donate proton or H^+ to the system. The possible chemical reactions that might take place in the buffer has been listed in Table 7.12 and 7.13. A number of hydrogen impregnated species evolve and exist in the solution such as, HCO_3^-, H_2S, $CaHCO_3^+$, $CaHSO_4^+$ etc. The presence and evolution of these species in the solution consumes both hydrogen ion (H^+) and (e^-) which

affects the equilibrium position of the above mentioned chemical reaction for hydrogen dissolution into the porewater. Therefore, the equilibrium position shifts from left to right resulting in more hydrogen dissolves in the solution. The secondary solution species provide an alternative way for the generated hydrogen to flow through the buffer due to chemical processes.

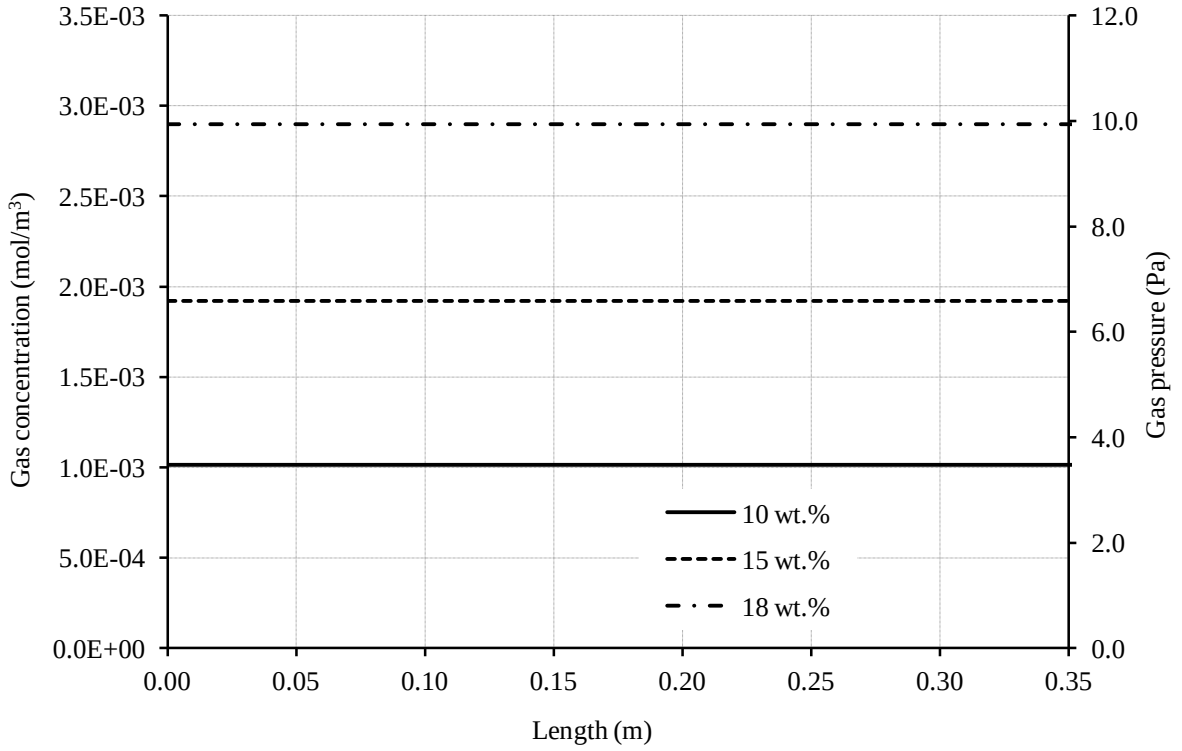

Figure 7.3: Hydrogen concentration and pressure profile along the buffer at various water contents after 10,000 years.

The saturation index or log (Ion activity/ solubility) (Appelo and Postma, 2005) of hydrogen after 10,000 years simulation shows a value of -6.43, suggesting the solution can accommodate more hydrogen. The simulation has been carried out to 100,000 years and it has been found after 60,000 years the pressure starts to build up rapidly in the system and a maximum pressure of 4.95 MPa has been recorded. The buffering capacity of the bentonite MX-80 can accommodate the amount of hydrogen generated in the system due to metallic corrosion. With the increasing water content, the available space for the gas decreases, resulting an increase in the gas concentration more rapidly and in a higher amount. The explanation for geochemical reactions remain similar and not been repeated. The hydrogen pressure and concentration profile along the buffer has been presented in Figure 7.3. It has

been noticed from Figure 7.3 that uniform distribution of hydrogen took place in the buffer at various water contents.

7.4.2 Evolution of Gypsum ($CaSO_4.2H_2O$)

The evolution of gypsum in the clay interface with gas influx has been presented in Figure 7.4. It has been found that with the increasing water content from 10% to 18%, the amount of gypsum in solution decreases from 0.0235 to 0.003 mol/kg of soil. At 10 wt. % water content the maximum amount of gypsum has been calculated at the beginning of the simulation. With time the mineral continuously dissolves in the porewater and consequently reaches to zero when total gypsum dissolves in the solution as calcium (Ca^{2+}) and sulphate (SO_4^{2-}) ions. In case of 10 % water content, all of the available gypsum dissolved in the porewater after 1.88E+11 seconds corresponds to 6000 years. The concentration profiles for gypsum has not been presented, since all of the gypsum has dissolved in the porewater before the end of simulation period.

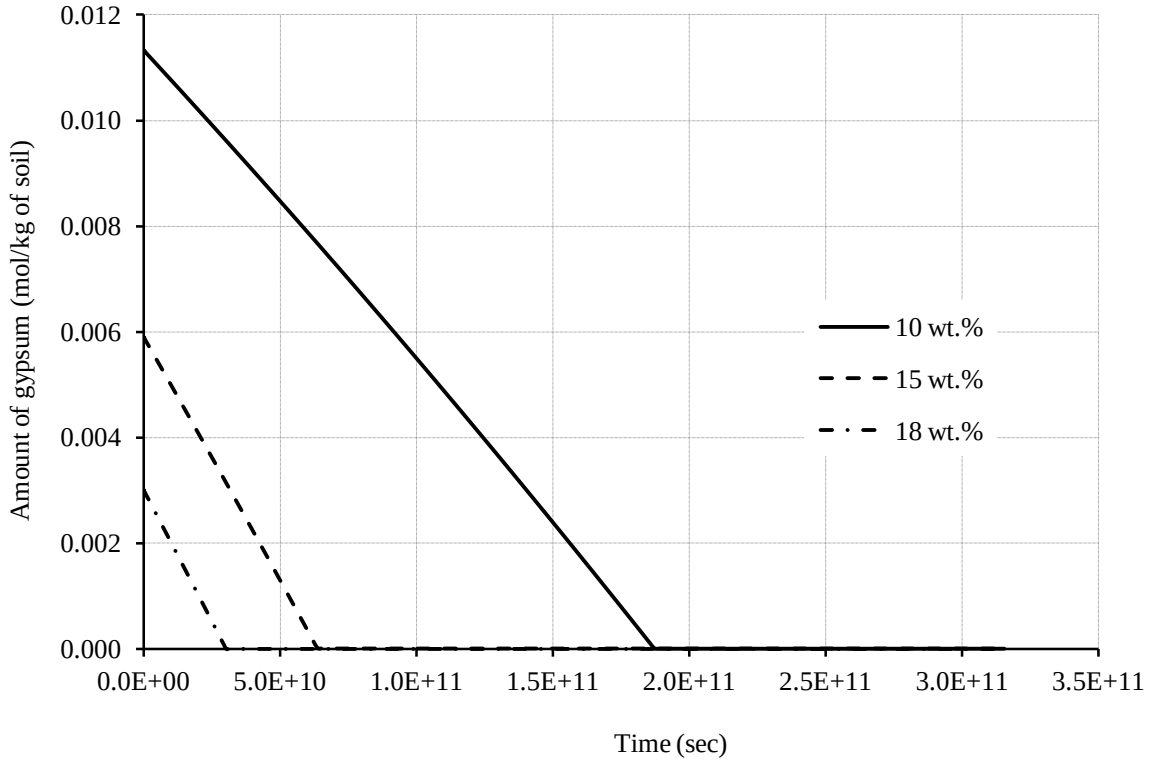

Figure 7.4: Evolution of gypsum in the buffer due to hydrogen influx. In case of 10% water content, total dissolution of gypsum takes place within first 6000 years of the simulation.

The proton donation capacity increases as the hydrogen influx in the system continues. The generation of chemical compounds, such as HS^-, H_2S (Table 7.12) increases the demand of sulphate ions in the solution and therefore the following reaction

$$CaSO_4.2H_2O \leftrightarrow Ca^{2+} + SO_4^{2-} + 2H_2O$$

moves from left to right, causing more dissolution of gypsum in the porewater. The Gypsum dissolution/ precipitation also affect the pH behaviour of the buffer and other cations and anions such as calcium and sulphate respectively.

7.4.3 Evolution of calcite ($CaCO_3$)

The quantity of calcite in a geochemical equilibrium reaction is governed by the precipitation/ dissolution of calcium and bicarbonate (HCO_3^-) ions. The evolution of calcite in the system has been presented in Figure 7.5. The behaviour of calcite evolution follows a similar pattern for various water contents. Therefore, the results have been discussed for a specific water content, such as 18 wt.%.

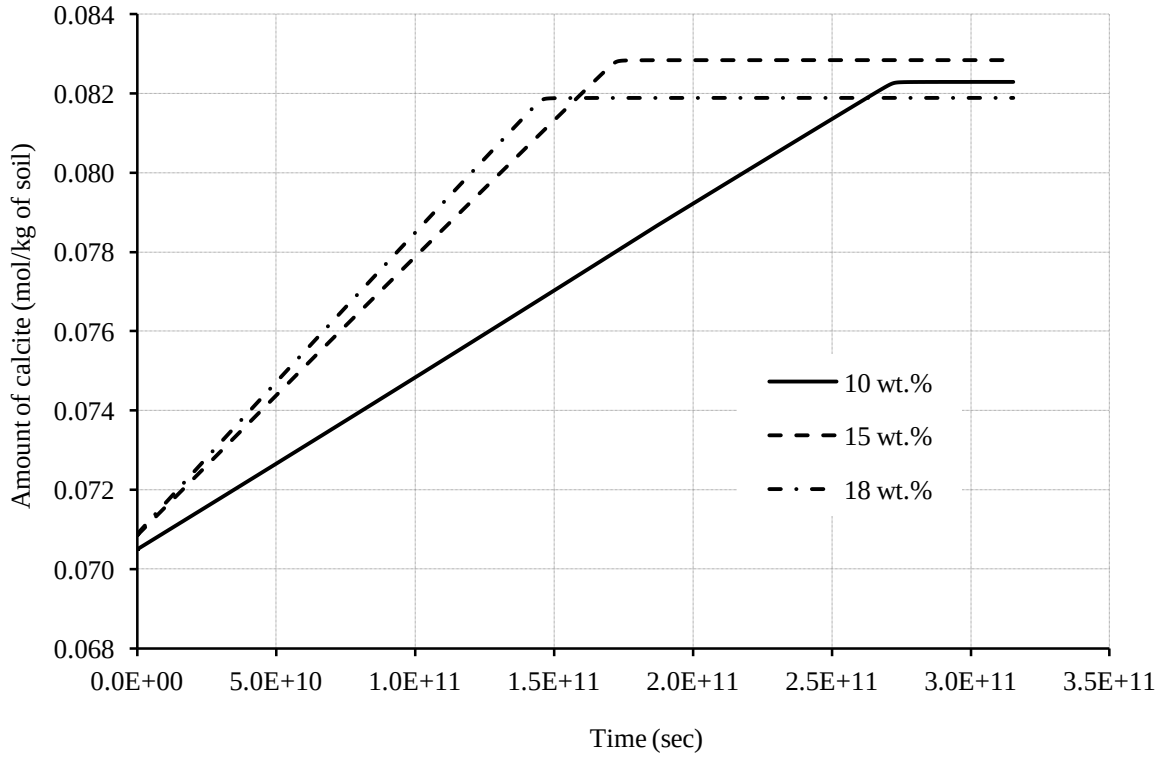

Figure 7.5: Evolution of calcite in the buffer due to hydrogen influx over a period of 10,000 years.

It is noticeable from Figure 7.5 that the precipitation of calcite continues for 1.48E+11 seconds or 4700 years until it reaches to a steady state in case of 18% water content simulation. The increasing precipitation of calcite results from the progressive dissolution of gypsum, as mentioned in Figure 7.4, which increases the amount of calcium ion in the solution. Together with bicarbonate ions the surplus calcium ions precipitate as calcites resulting in a drop off of bicarbonates in the system. It is obvious that the change in amount of calcite also affects the concentration of calcium, bicarbonates and exchangeable ions in the cation exchange zone of the buffer which have been presented later in this chapter. After 4700 years the saturation index of calcite reaches to zero suggesting that the porewater is saturated with calcite and the process of calcite precipitation ceases. The distribution profile of calcite over the domain has been presented in Figure 7.5. The results show a uniform distribution of calcite after the simulation period.

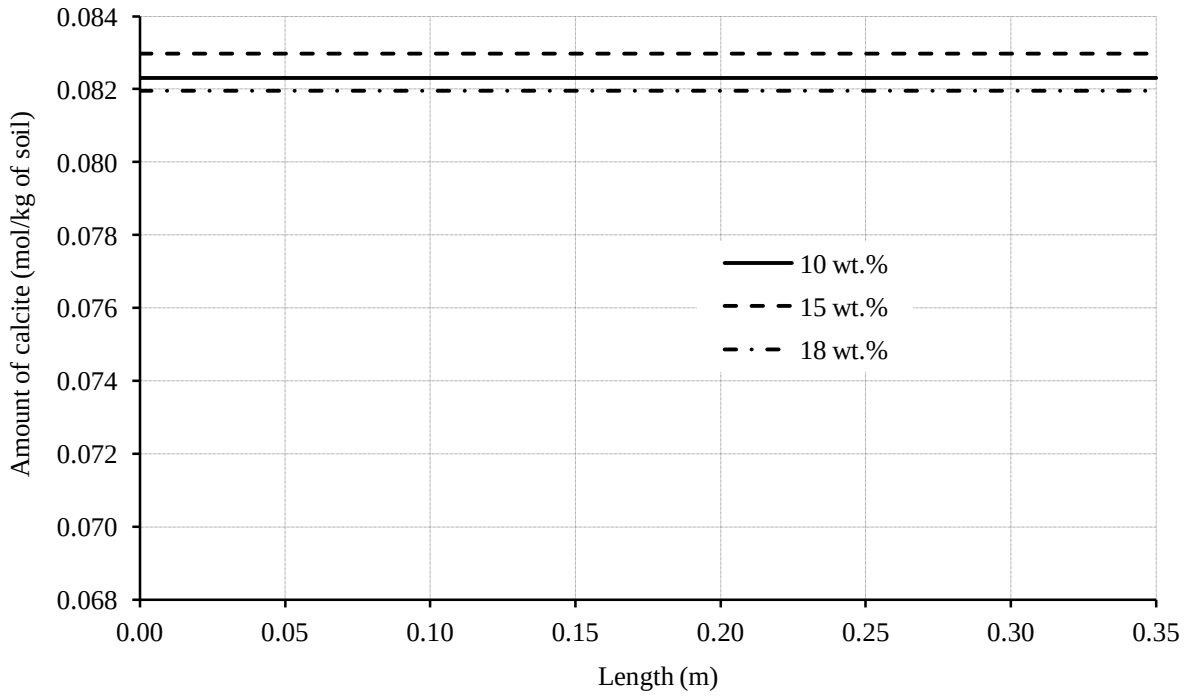

Figure 7.6: Distribution profile of calcite along the buffer due to hydrogen influx over a period of 10,000 years.

7.4.4 Evolution of redox potential or P_e in the buffer

The evolution of P_e or redox potential has been presented in the Figure 7.7. The constant flux of hydrogen reduces the redox potential of the system by increasing the electron activity. The redox potential plays significantly important role for the dissolution and precipitation of minerals. The initial changes in P_e curves at 10% and 15% water content take place after approximately 6000 years (1.89E+11 seconds) and 2000 years (6.31E+10 seconds) respectively.

Based on the results from gypsum variations, Figure 7.4, it can be found that the total dissolution of gypsum occurred for these two water contents at the same duration of the simulation. It is also noted that the oxidation tendency of the solution increases as the redox potential decreases which causes the gypsum to dissolve in the solution.

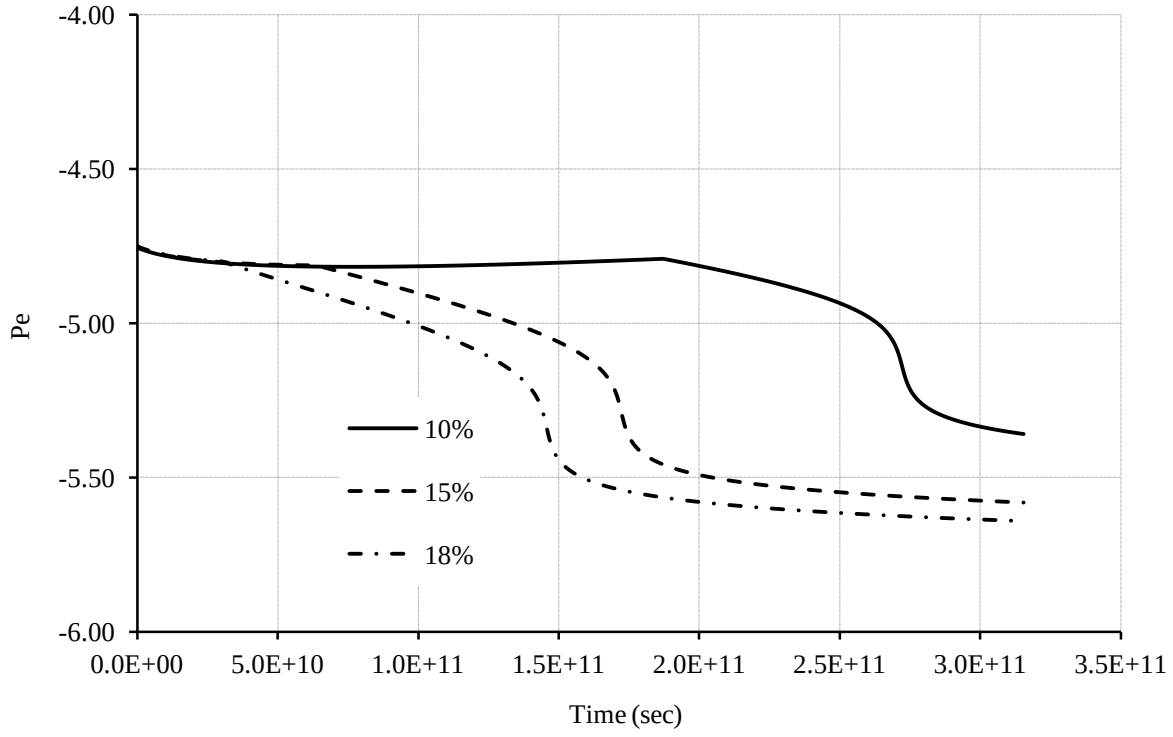

Figure 7.7: Redox behaviour during the simulation period of 10,000 years.

7.4.5 Evolution of pH in the buffer

The evolution of pH in the system has been presented in Figure 7.8. Several processes are involved to control the pH of the system, such as the influx of hydrogen, mineral precipitation and/or dissolution. In comparison with the results of gypsum and calcite behaviour, presented in Figures (7.4) and (7.5), it can be seen that the pH has initially been controlled dominantly by the dissolution of gypsum and later by the mineral calcite. The dissolution of gypsum has increased the demand of H^+ and e^- in the solution and more hydrogen has dissolved resulting in an increase of H^+ ions. Uniform distribution of pH has been observed from the results which has been presented in Figure 7.9.

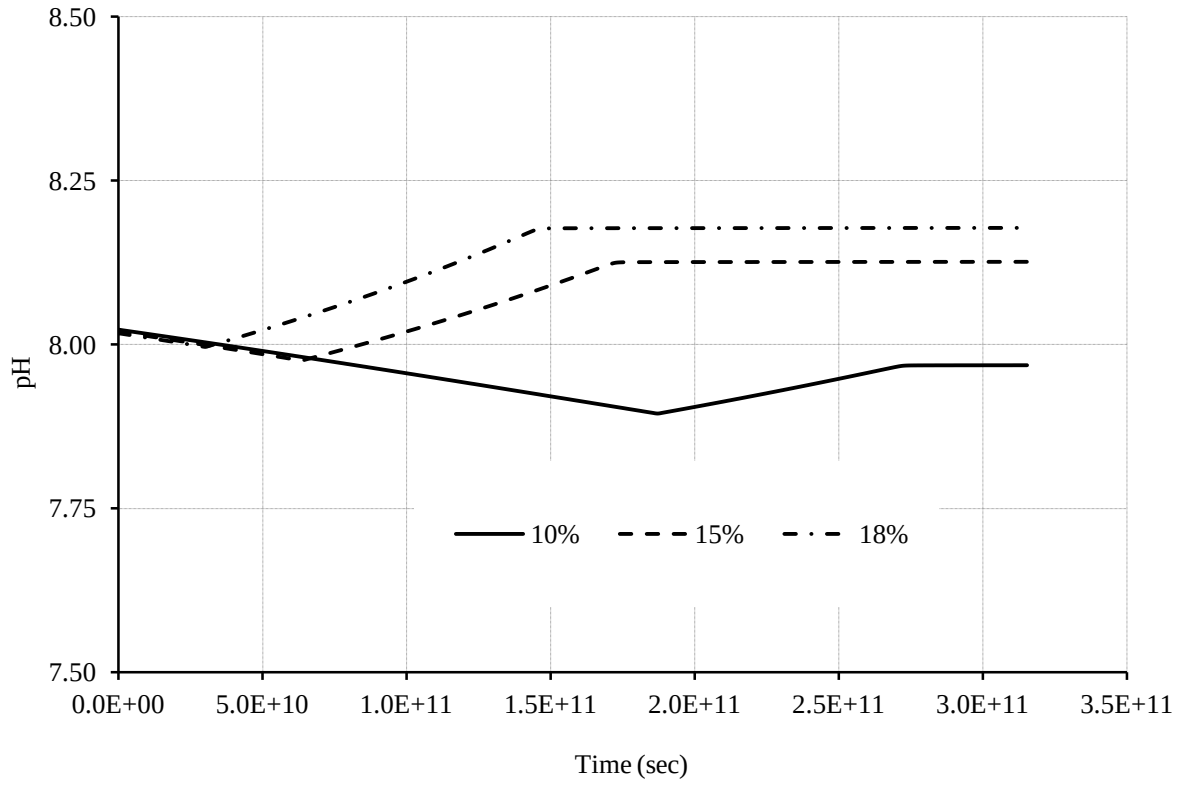

Figure 7.8: Evolution of pH in the buffer at various water contents.

The pH of the system increases when dissolution of gypsum stops and the increasing trend of pH follows that of the calcite. At this stage the demand for H^+ ions in the system reduces significantly and a sharp rise in the gas concentration (or pressure) is noticeable from Figure 7.2, suggesting a reduction of the hydrogen dissolution in the porewater. It is observable that over the duration of the simulation, pH of the buffer did not change significantly and just

varied from an initial value of 8.0 to a final value of 8.12. This in fact suggests that the pH is relatively stable for the bentonite MX-80 in case of hydrogen flow based on the boundary conditions of this simulation. As it has been mentioned in the literature that high pH condition is favourable for the buffer for its efficient performance.

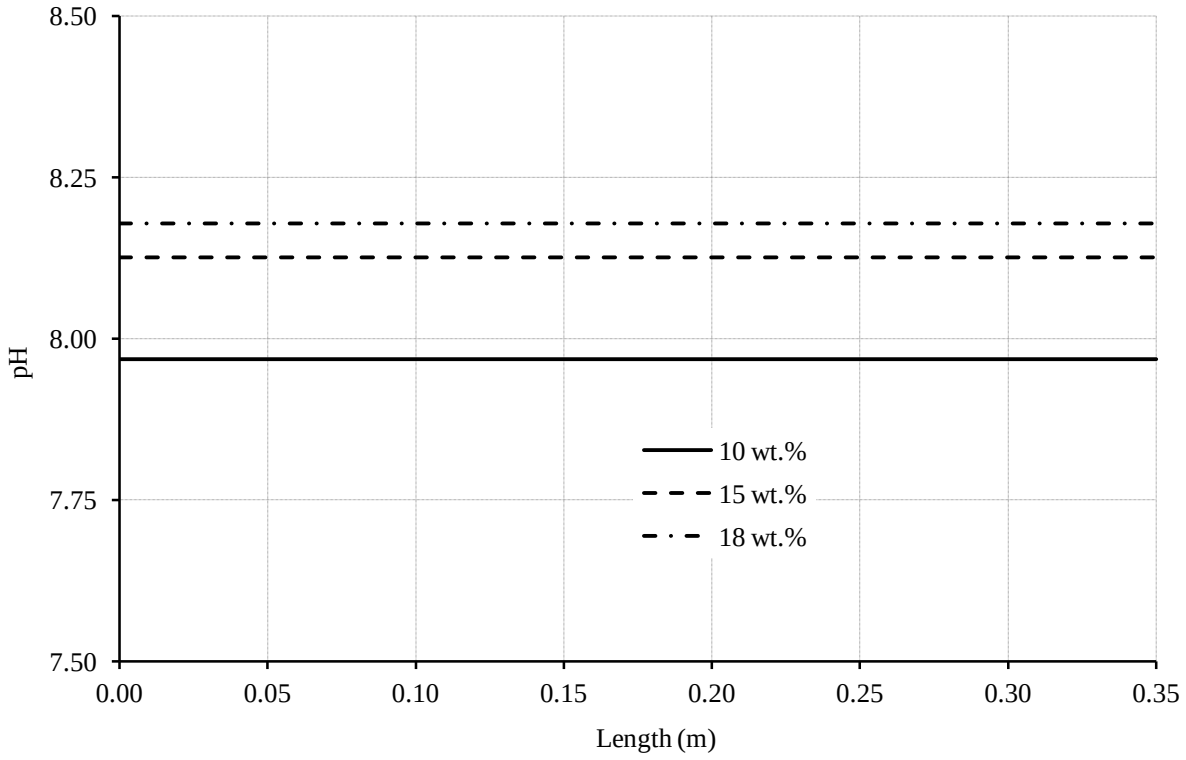

Figure 7.9: pH profile along the buffer at various water contents after 10,000 years.

7.4.6 Evolution of sulphate (SO_4^{2-})

The evolution of sulphate in the system has been presented in Figure 7.10. The sulphate evolution majorly depends on the dissolution of gypsum as this is the only source of this element in the solution. The results of 10%, 15% and 18% water content follows a similar trend. The sulphate concentration in the system increases as long as the gypsum dissolution occurs. The evolution reaches to a steady state after all of the gypsum dissolved in the solution.

After 6000 years which corresponds to 1.88E+11 seconds, all of the available gypsum has been dissolved in the pore water in case of 10% water content simulation. for the higher water content graphs the results shows a similar pattern but dissolve more quickly due to the less amount of gypsum is available for the reaction.

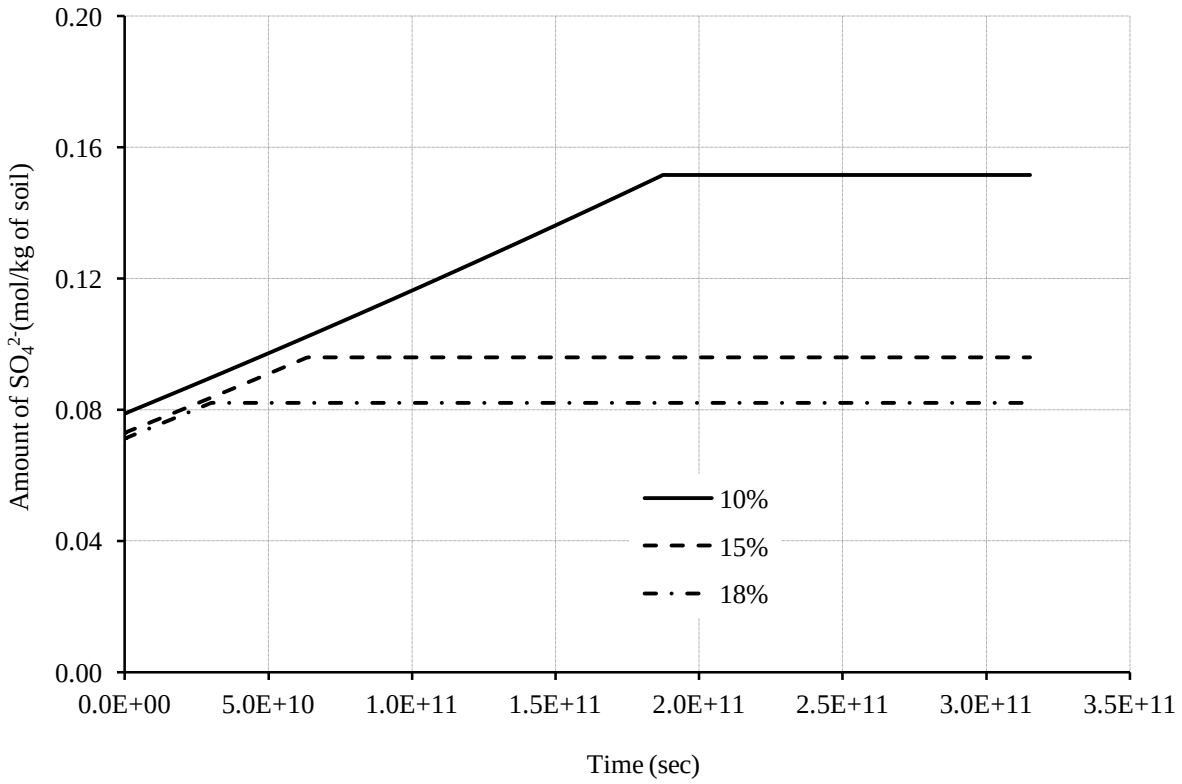

Figure 7.10: Sulphate evolution for various water content.

7.4.7 Evolution of bicarbonate (HCO_3^-)

Figure 7.11 represents the evolution of bicarbonate ions in the buffer. The concentration or amount of bicarbonate in the solution decreases with the calcite precipitation. It reaches to a steady state when the gypsum dissolution stops despite the fact that calcite precipitation continues based on the results presented in Figure 7.5

The possible explanation of this behaviour can be described as follows. The generation of bicarbonates follows the production of bicarbonic acid which is very unstable in the solution and it dissociate as bicarbonates.

The equilibrium reactions related to the above mentioned processes are as follows:

$$CO_2 + H_2O \leftrightarrow H_2CO_3$$

$$H_2CO_3 \leftrightarrow HCO_3^- + H^+$$

Since, the loss of bicarbonate due to the calcite precipitation shifts the equilibrium position of the second reaction equation from left to right, bicarbonate production continues by dissolving available carbon dioxide. Therefore, the rate of carbonates loss due to calcite precipitation and the rate of bicarbonic acid dissociation reach to an equilibrium position.

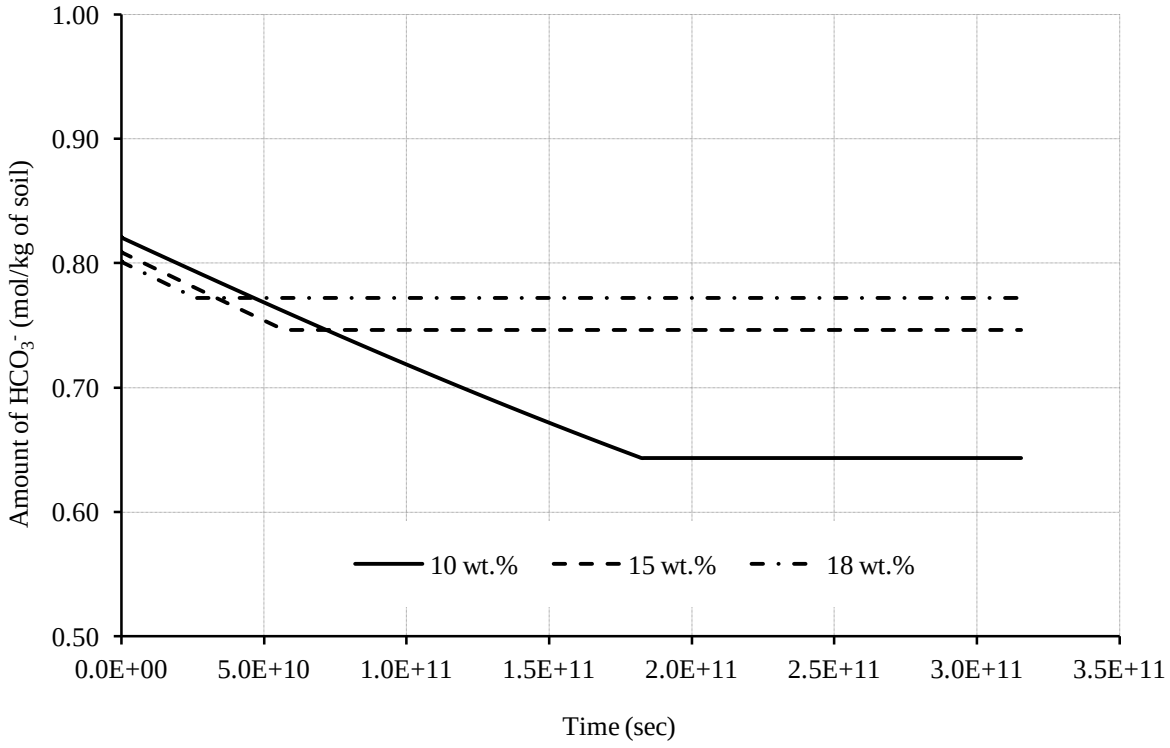

Figure 7.11: Evolution of bicarbonate (HCO_3^-) in the buffer.

7.4.8 Evolution of calcium (Ca^{2+})

Figure 7.12 presents the evolution of calcium ion in the solution resulted from the numerical simulation at various water content. The amount of calcium in the system increases due to the gypsum dissolution. After the gypsum completely dissolves in the porewater the continuous

precipitation of calcite reduces the amount of calcium from the system and reaches to a steady state when the solution becomes saturated with calcite. The evolution of calcite also influences the calcium exchangeable in the cation exchange zone.

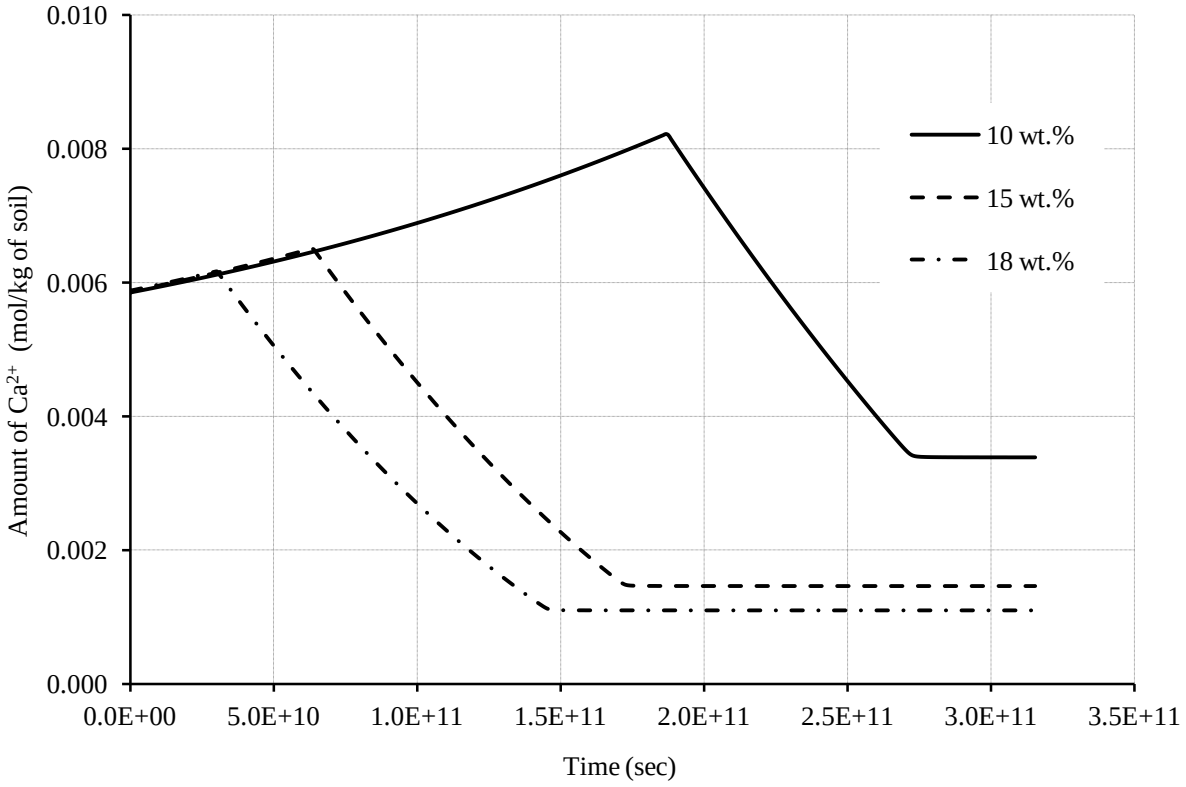

Figure 7.12: Evolution of calcium ion at different water content.

7.4.9 Evolution of sodium (Na^+)

The evolution of sodium in the solution has been presented in Figure 7.13. amount of sodium in the solution depends on the available Na-exchangeable in the buffer. The increasing calcium content replace Na-exchangeable from cation exchange zone resulting in an increase of Na^+ in the solution. Since the precipitation of calcite continues after the gypsum dissolution, there is a net reduction of calcium ion from the solution. Therefore, at high concentration sodium ion replaces calcium ions from cation exchange zone resulting in a reducing trend until it reaches to a steady state.

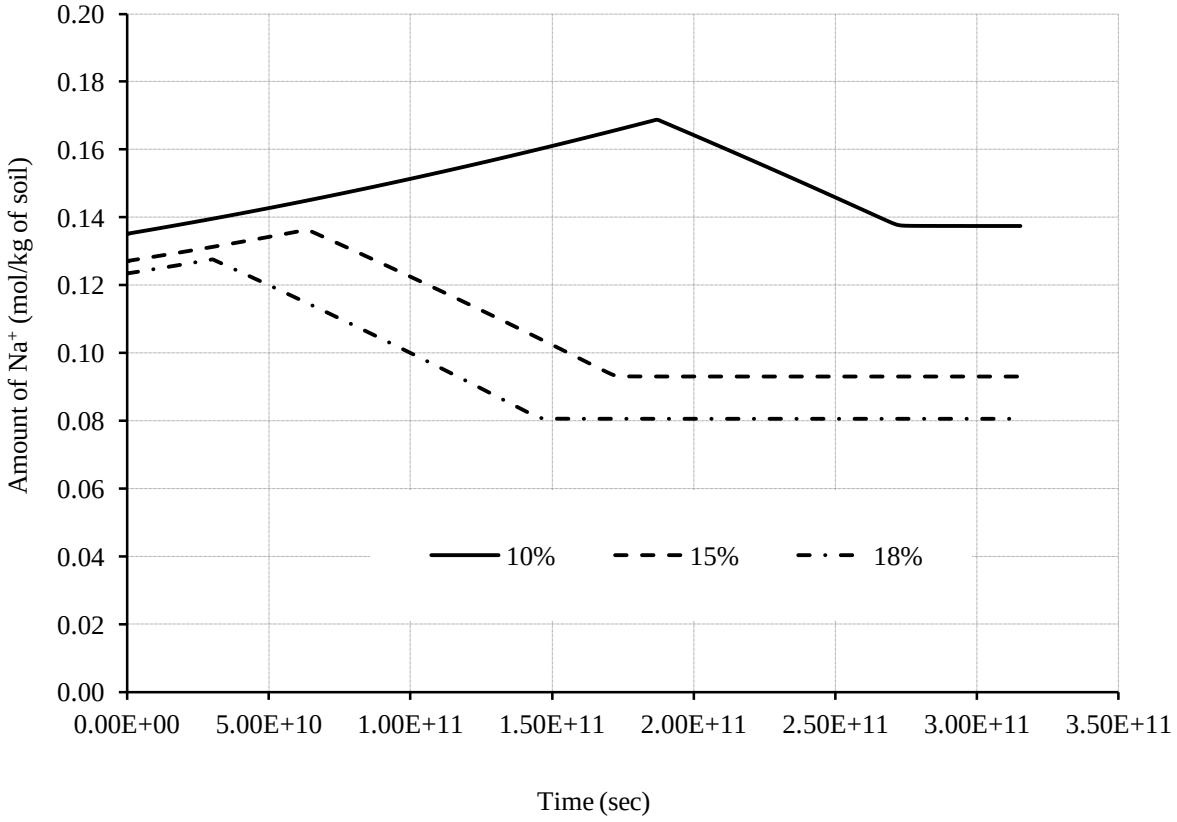

Figure 7.13: Evolution of sodium (Na^+) in the buffer.

7.4.10 Evolution of magnesium (Mg^{2+}) and potassium (K^+)

Figure 7.14 and 7.15 present the evolution of magnesium and potassium in the buffer respectively. The amount of magnesium and potassium in the solution is significantly less than the other aqueous species or minerals. Therefore, these components exert a secondary influence in determining the long term chemical behaviour. The variation patterns for these two ions are similar to the other cations present in the system. The amount of magnesium in the solution increases as the Mg-exchangeable decreases resulting in an increase of this ion in the system. Similarly, the amount of K-exchangeable affects the amount of K^+ ions in the solution. Higher amount of calcium and sodium ion could possibly influence these two species in the cation exchange zone.

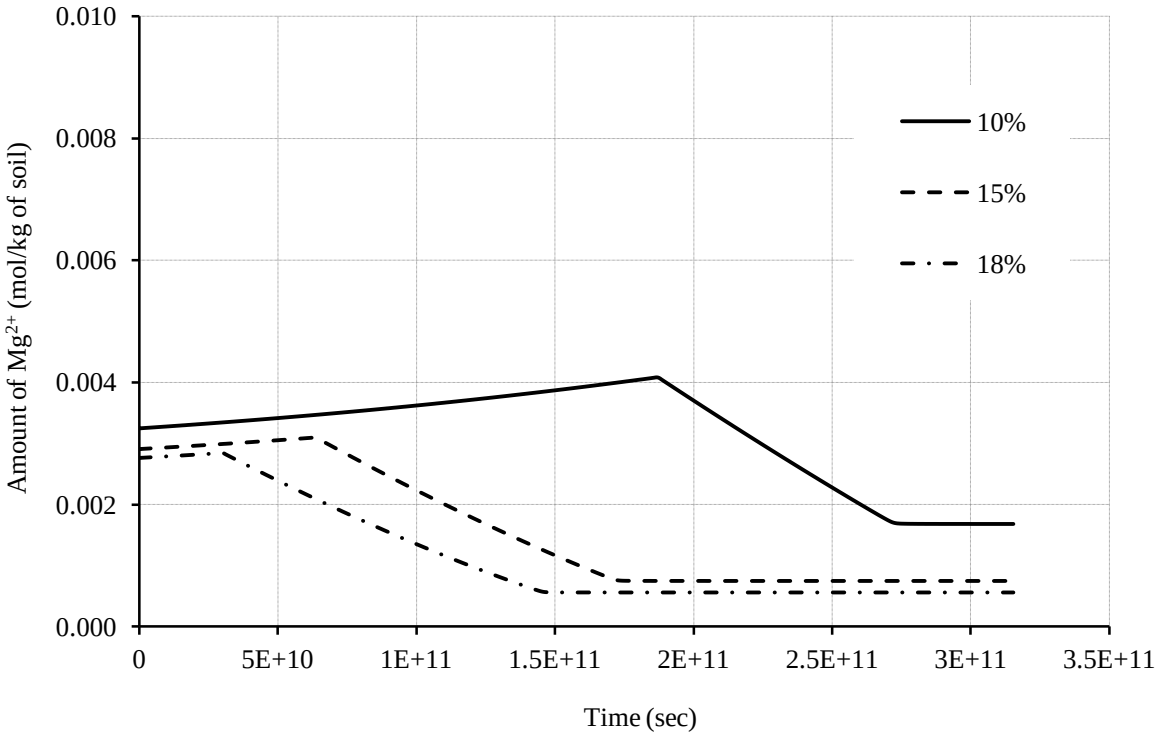

Figure 7.14: Evolution of Mg^{2+} in the solution for simulation period of 10,000 years.

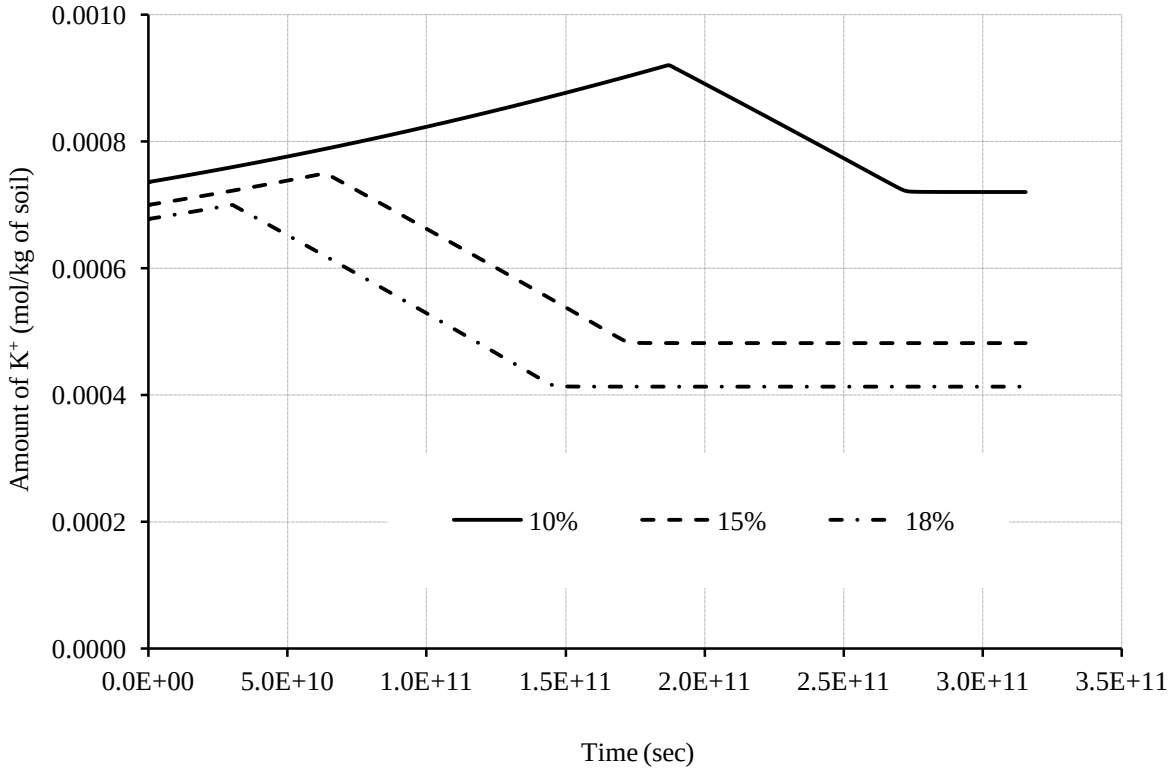

Figure 7.15: Evolution of K^{+} in the solution for simulation period of 10,000 years.

7.4.11 Evolution of exchangeable ions

The results of numerical simulation for the distribution of Ca, Na, Mg, and K exchangeable cations have been presented in Figures 7.16, 7.17, 7.18, 7.19 respectively. From Figure 7.16 it can be shown that for any amount of water content, the amount of Ca-exchangeable increase by time .This is mainly because of the continuous dissolution of gypsum which provides Ca^{2+} ions in the solution. Since the concentration of calcium ion increases in the system, it replaces the other ions, such as Na^{+}, Mg^{2+} and K^{+}, in the cation exchange zone. This phenomenon is noticeable in from Figure 7.17, 7.18 and 7.19 where the amount of Na^{+}, K^{+} and Mg^{2+} exchangeable ions decreases over the duration of gypsum dissolution. Therefore, the amount of these ions increases in the solution which has been presented in Figure 7.13, 7.14, 7.15 for Na^{+}, Mg^{2+} and K^{+} respectively. At the end of gypsum dissolution the calcite precipitation continues and reduces the amount of Ca^{2+} in the solution.

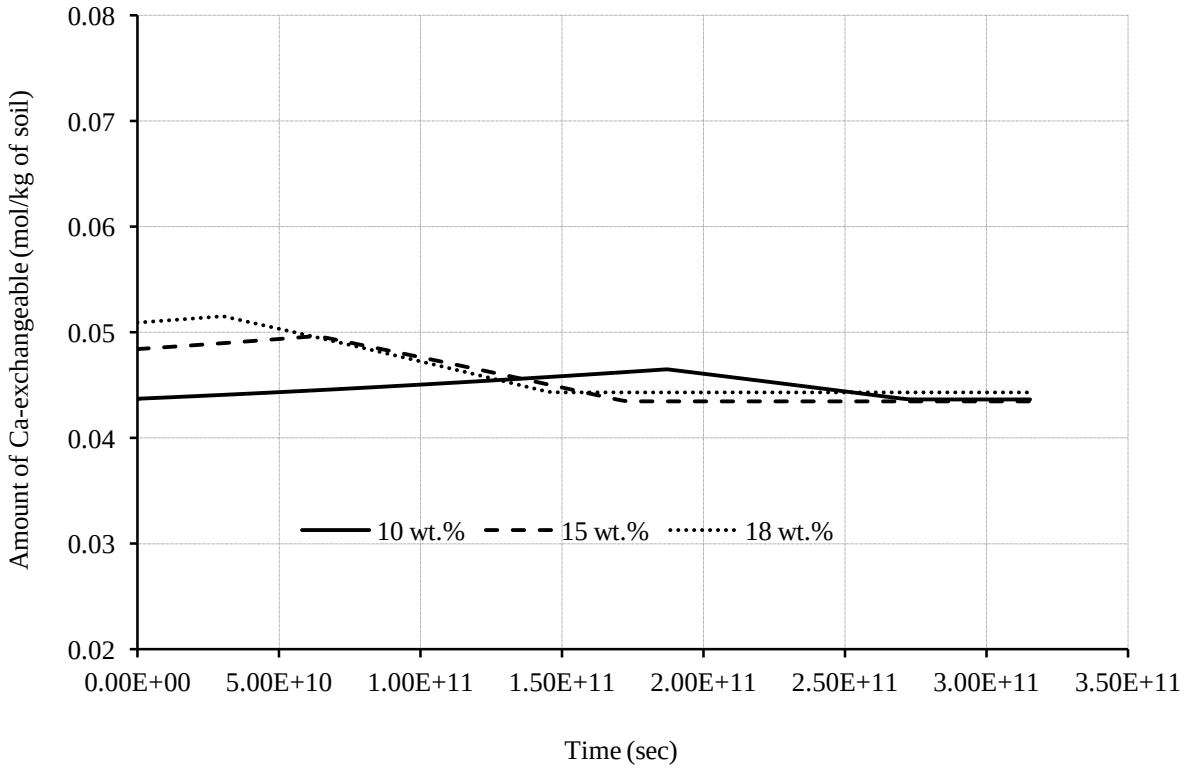

Figure 7.16: Evolution of Ca-exchangeable.

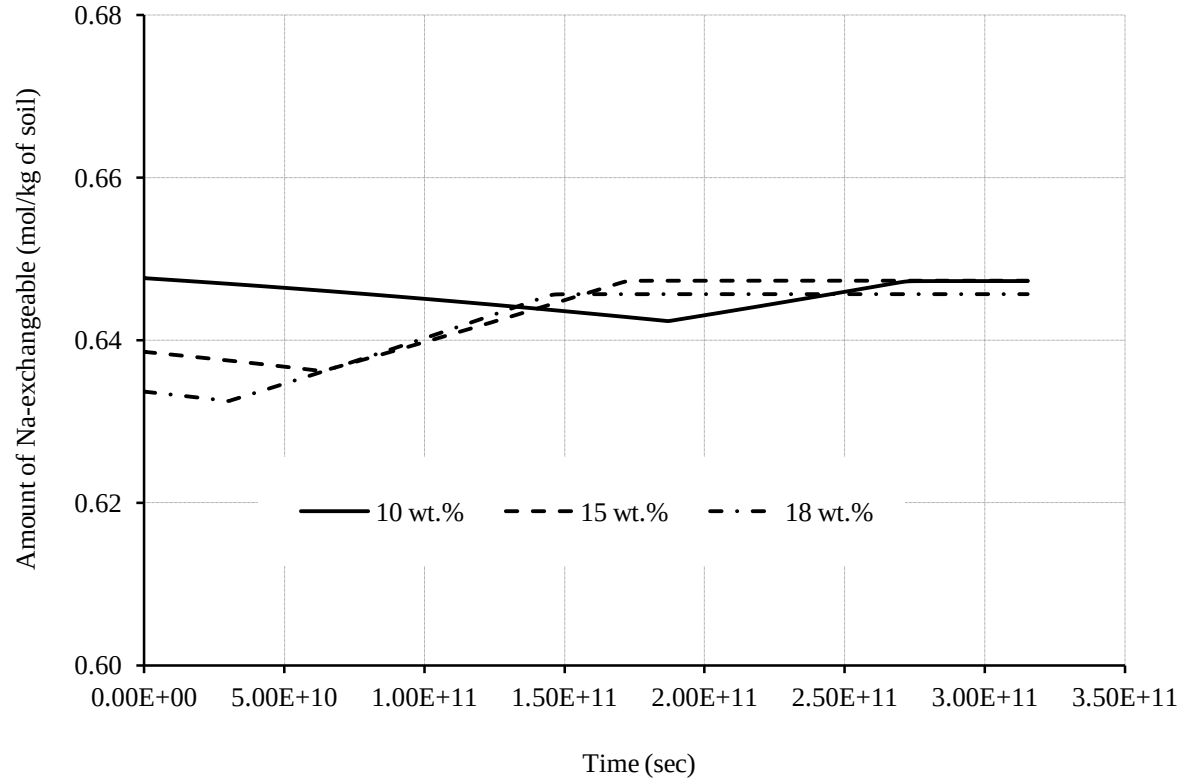

Figure 7.17: Evolution of Na-exchangeable.

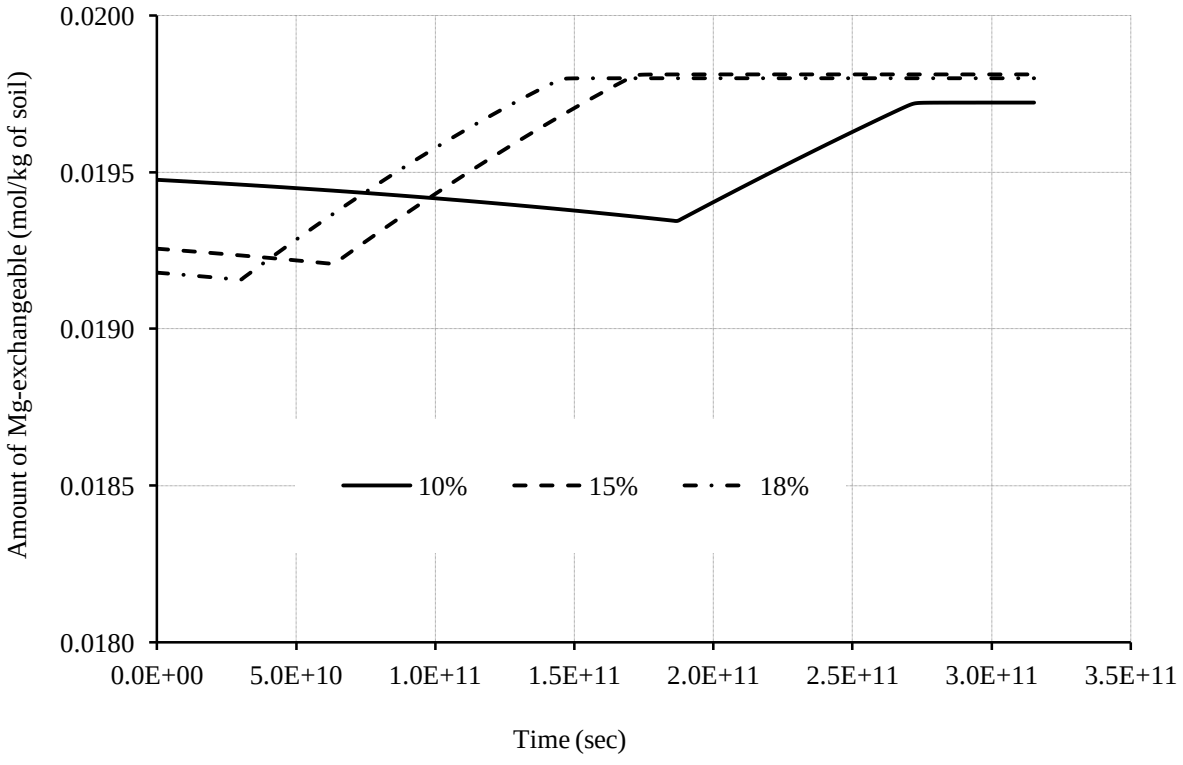

Figure 7.18: Evolution of Mg-exchangeable.

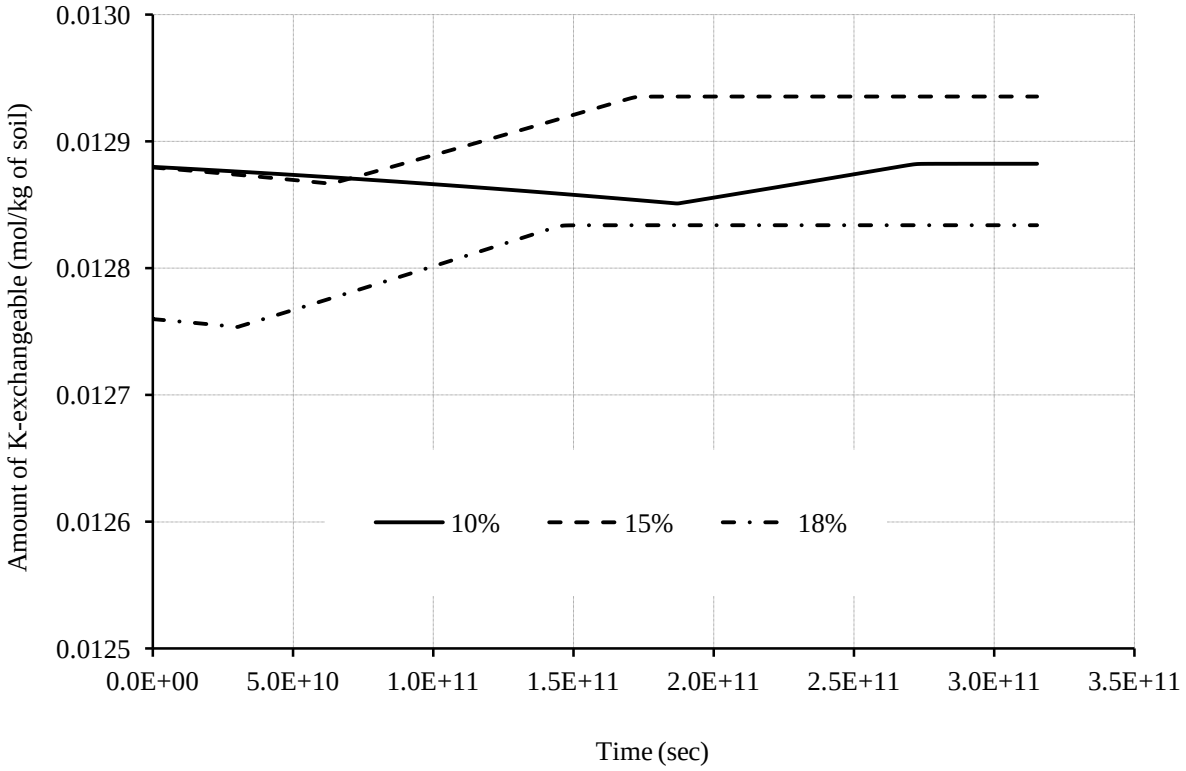

Figure 7.19: Evolution of K-exchangeable.

At lower concentration of calcium ions, comparatively higher Na^+, K^+ and Mg^{2+} ions starts to replace Ca-exchangeable from the cation exchange zone, resulting a decreasing trend in Figure 7.16 until reach to a steady state.

The Mg-exchangeable and K-exchangeable shows a similar behaviour to that of Na-exchangeable. Although, the amount of these two exchangeable is significantly lower than the others.

7.4.12 Evolution of chloride (Cl^-) in the system

The chloride concentration in the system remains unchanged over the duration of the simulation. As the solution do not contain any halite and all of the halite has been dissolved prior to the simulation. The evolution of chloride at various water content has been presented in Figure 7.20.

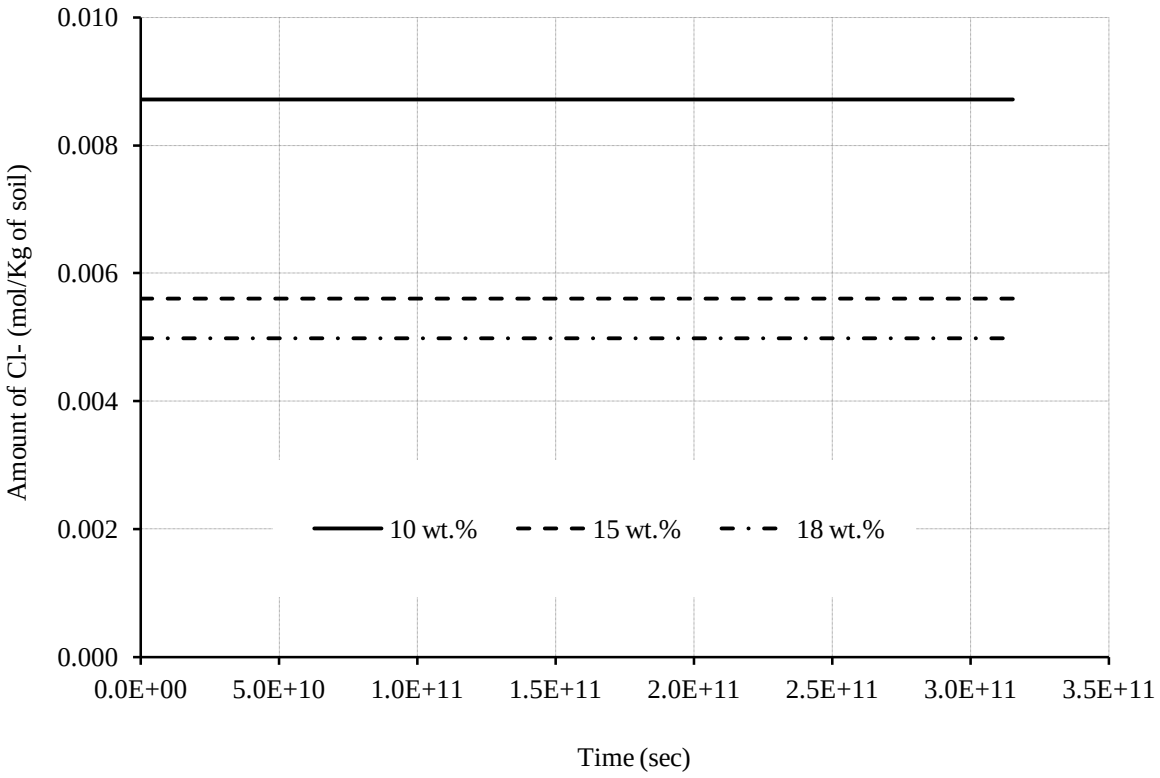

Figure 7.20: Evolution of chloride.

7.4.2 Conclusion

The results of simulation set-1 have been discussed in details in this section. The recorded gas concentration at gas phase in the buffer after the simulation period of 10,000 years is very negligible comparing to the simulation where porewater has been considered as distilled water. Most of the gas has been used by the chemical processes involved in the near field of the buffer. The pH of the buffer remains close to its initial value suggesting that the bentonite buffer provides sufficient resistant towards the pH change due to hydrogen influx. Minerals, such as gypsum and calcite plays important role on the evolution of cations and anions present in the solution.

7.5 Results and discussion of simulation set-2

The corrosion of metallic canisters generates both hydrogen gas and magnetite which are known as the corrosive products. The previous simulation considered only the influx of hydrogen gas while in this simulation both hydrogen and iron, Fe^{2+} (from magnetite) influx has been considered. Using the stoichiometry of corrosion reaction, the iron influx has been calculated. The material parameters and boundary conditions remain similar to the previous simulation. Initially, the clay porewater system contained no iron ions and the iron flux has been considered at the same boundary as the gas is injected. As it has been found from previous simulation that the flow and reaction behaviour of gas and chemical components are of similar type at various water contents, the simulation has been carried out for a single water content, i.e. 10 wt.% over a period of 10,000 years.

The results of numerical simulation in terms of gas flow and geochemistry of the system including major ions, minerals, exchangeable ions and pH have been presented in this section. The results have been plotted regarding the long term evolution of associated chemical and gas components present in the system. The graphical results have been obtained from the injection face or the canister buffer-interface, since this part of the buffer receive maximum impact from the hydrogen and iron influx due to corrosion. The discussion on the results achieved has been limited to the major chemical components and minerals and changes related to less abundant ions and exchangeable ions such as magnesium, potassium have not been presented here.

7.5.1 Evolution of hydrogen (H_2)

The simulated result of hydrogen evolution has been presented in Figure 7.21. At the end of 10,000 years simulation period the maximum gas concentration has been obtained 1.8×10^{-3} mol/m^3 of θ_g. Comparing this value with the previous simulation result, Figure 7.2 (maximum gas concentration was calculated 1.0×10^{-3} mol/m^3 of θ_g) where only hydrogen influx has been considered at the canister buffer interface or injection face, only a slight increase has been noticed. Therefore, considering both iron and hydrogen influx the amount of hydrogen at gas phase in the buffer did not show much variation, suggesting that the presence of iron does not significantly affect the flow behaviour of hydrogen in the gas phase.

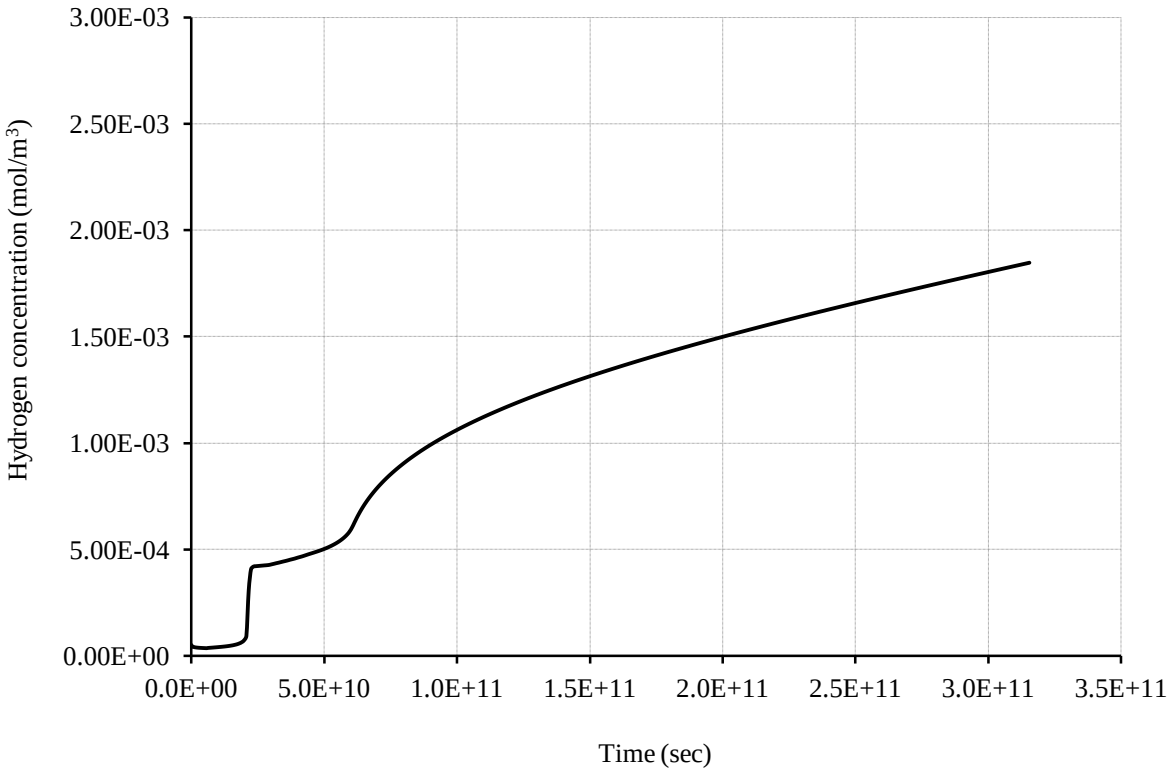

Figure 7.21: Evolution of hydrogen concentration. Simulation considers both hydrogen influx and iron (from magnetite) influx due to corrosion.

7.5.2 Evolution of iron and Fe-exchangeable

Figure 7.22 and 7.23 represent the evolution of iron and Fe-exchangeable respectively in the buffer due to a constant flux at the canister buffer interface. Since, the system is not subjected to a porewater pressure gradient; the main mechanism for flow is due to diffusion. Over the simulation period amount of iron in the buffer has significantly increased from zero to a maximum of 0.74 mol/kg of soil. it is noted that the iron presented as the result of the simulation describes the total iron which includes ferrous (Fe^{2+}) ions, ferric (Fe^{3+}) ions and their compounds, such as $FeSO_4^+$, $Fe(HS)_2$, $FeSO_4$, $FeCO_3$ etc.

It has been presented in Figure 7.21 that the presence of iron did not affect the flow of hydrogen gas in the buffer but significant variation has been observed in case of aqueous species, minerals and exchangeables in the solution. In the following section some of the results have been discussed in detail. Figure 7.23 shows a gradual increase of Fe-exchangeable in the buffer. Due to constant iron (Fe) flux, the amount of ferrous (Fe^{2+}) ion increases in the solution which starts to react with other chemicals present in the exchange sites, such as Ca^{2+}, Mg^{2+}, Na^+, K^+ and replace these ions from the exchange zone.

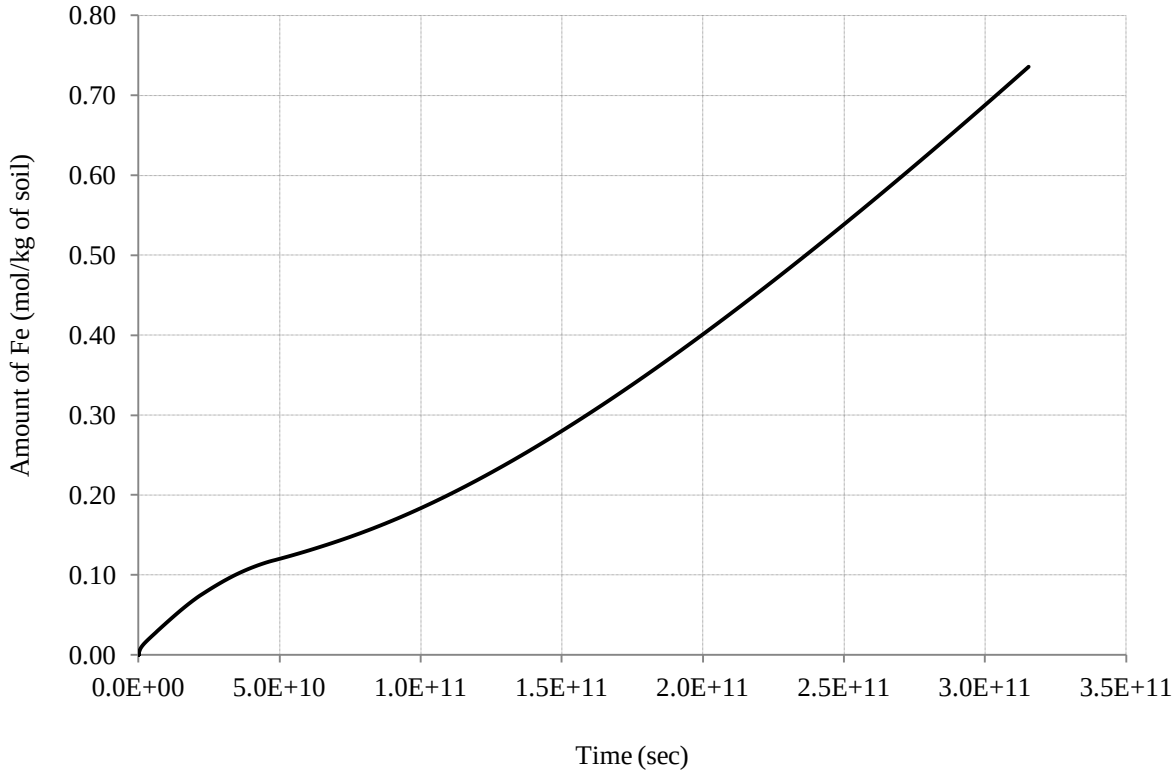

Figure 7.22: Evolution of Fe^{2+} concentration. Simulation considers both hydrogen influx and iron (from magnetite) influx due to corrosion.

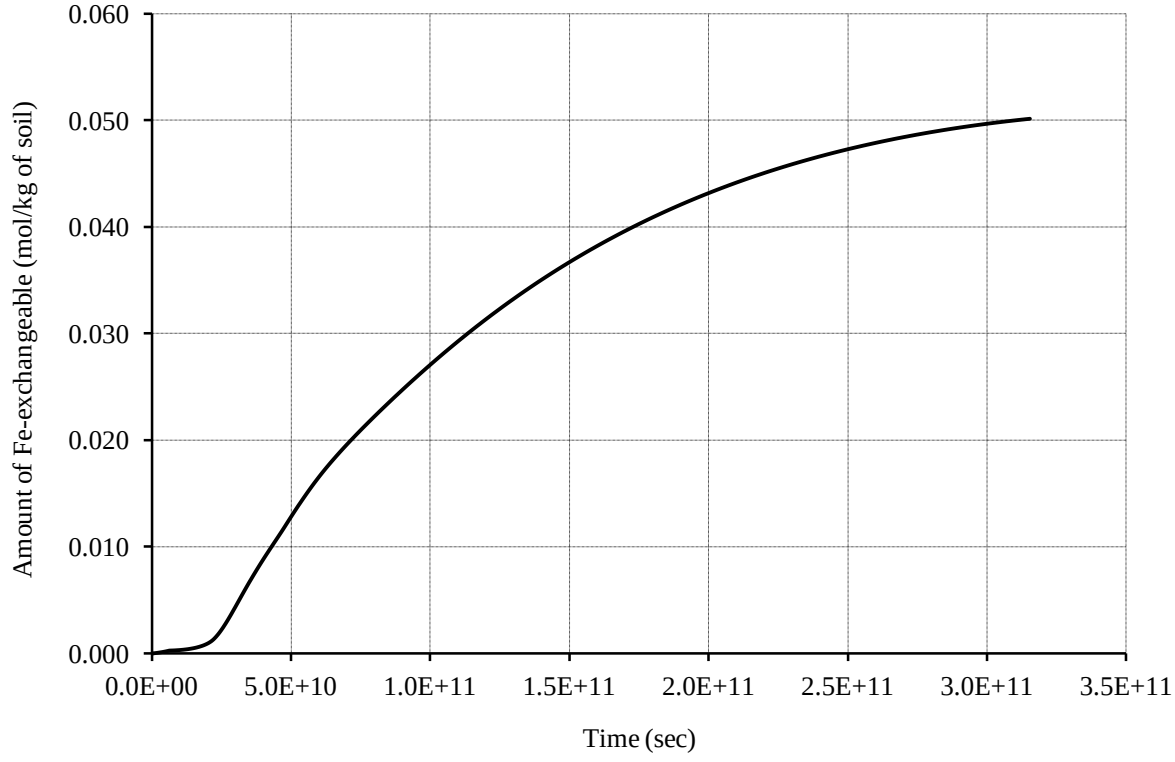

Figure 7.23: Evolution of Fe-exchangeable.

7.5.3 Evolution of pH

The simulated result of pH behaviour of the simulation has been presented in Figure 7.24. Comparing to previous simulation result where pH value varies only 8.0 to 7.979 in this simulation it varies from 8.0 to 7.15. The ferrous and ferric ions react with the hydroxyl ions, causing to form ferrous or ferric hydroxides. The iron compounds also react with bicarbonate and carbonate as a result the pH of the solution decreases (Sharma and Reddy, 2004). The chemical processes can be written as chemical equilibrium reactions as follows:

$$Fe^{2+} + HCO_3^- \leftrightarrow FeCO_3 + H^+ + e^-$$

$$Fe^{2+} + H_2O \leftrightarrow Fe(OH)_3 + 3H^+ + e^-$$

From the reactions it can noticed that the hydroxyl ions and bicarbonate ions reduces and produce more H^+ in the solution.

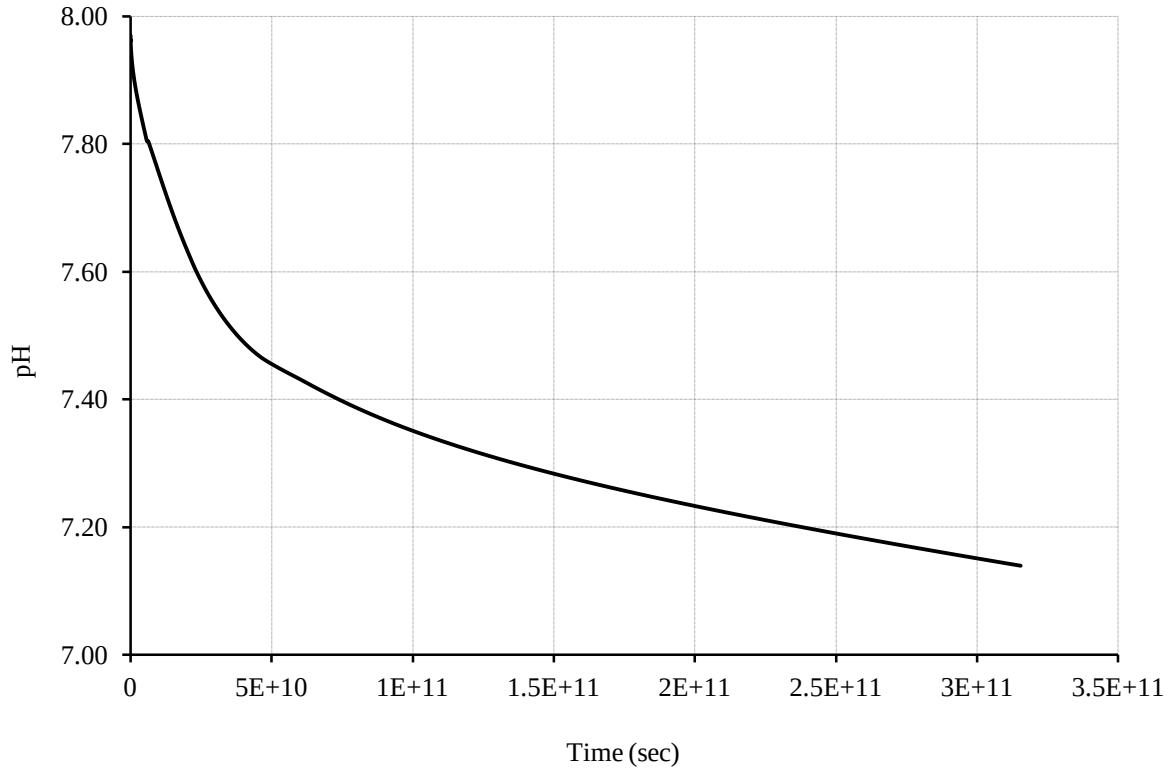

Figure 7.24: Evolution of pH.

7.5.4 Evolution of calcium (Ca^{2+}) ion and Ca-exchangeable

Figure 7.25 represents the evolution of calcium ion in the buffer due to hydrogen and iron influx in the buffer. The amount of calcium ion in the buffer has increased significantly which is initially due to the dissolution of gypsum. At the early stages the curve shows some little drop which occurs due to the calcite precipitation causing the amount of calcium ion to drop. As the iron content in the solution increases, it starts to replace the Ca-exchangeable from the cation exchange zone causing more calcium ions to come into the solution. After the gypsum dissolution, cation exchange and calcite dissolution dominates the supply of calcium ion in the solution. Figure 7.26 represents the evolution of Ca-exchangeable in the buffer. Figure 7.26 suggests an increase of Ca-exchangeable at the early stages of simulation which is due to the dissolution of gypsum in the solution.

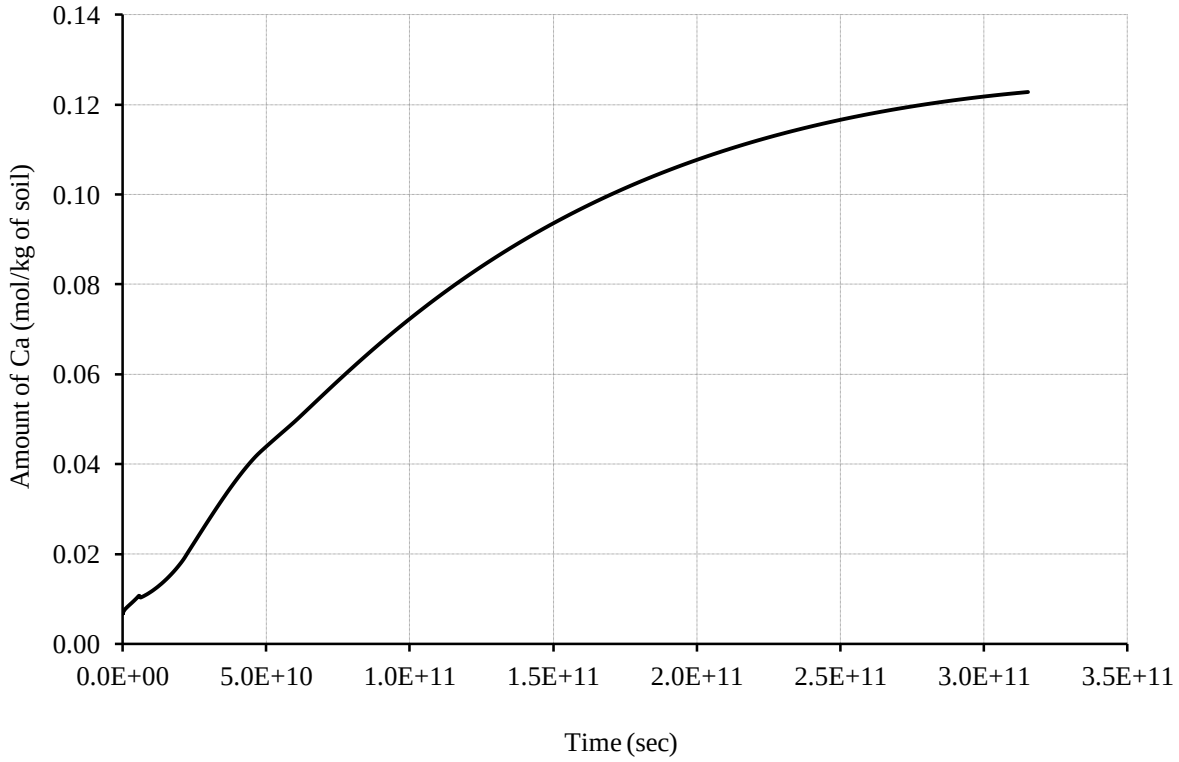

Figure 7.25: Calcium ion evolution.

Due to the constant influx of iron in the system, the solution builds up a higher concentration of ferrous and ferric ions which ultimately causes the calcium ions to replace from the cation exchange zone therefore a significant drop has been observed.

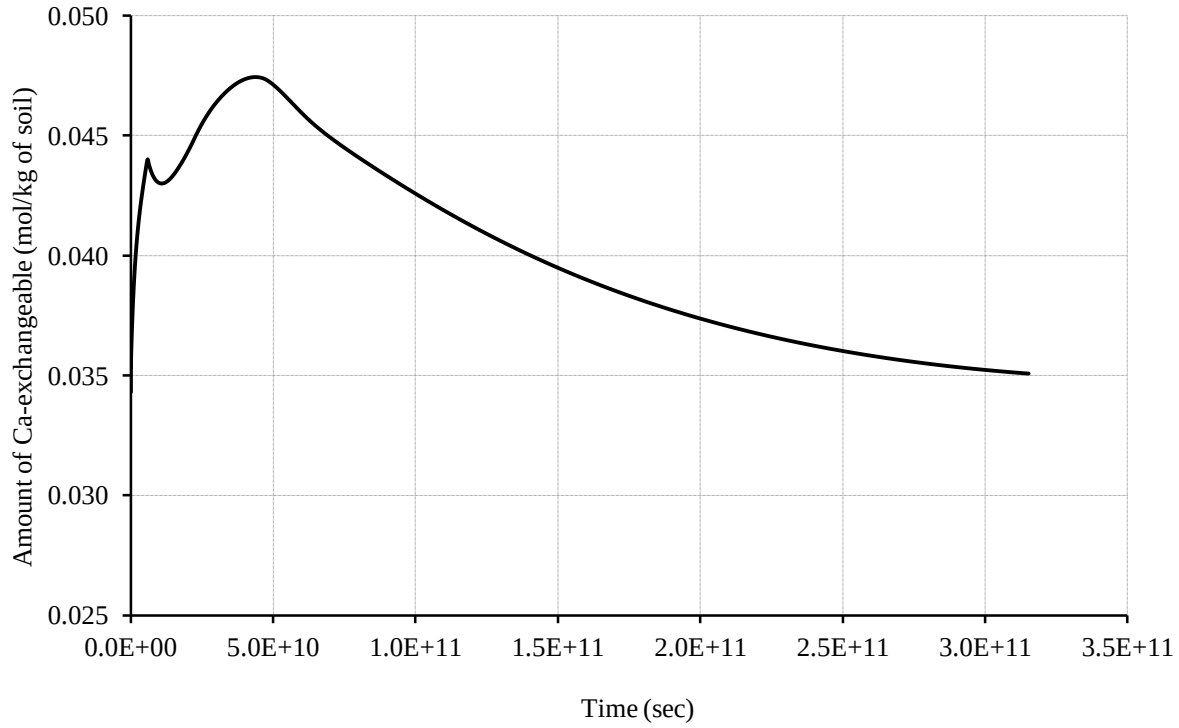

Figure 7.26: Evolution of Ca-exchangeable.

7.5.5 Evolution of sodium (Na^+) ion and Na-exchangeable

The amount of sodium ion in the solution increased from the initial amount. The evolution of sodium in the solution has been presented in Figure 7.27. The continuous increment of sodium ion arises from the replacement of this ion from cation exchange zone. As the iron concentration increases in the solution, it starts to replace Na-exchangeables similar to the Ca-exchangeable which has been presented in Figure 7.26. The evolution of Na-exchangeable has been presented in Figure 7.28. In this simulation the Na-exchangeable act as the source for the sodium ion in the solution.

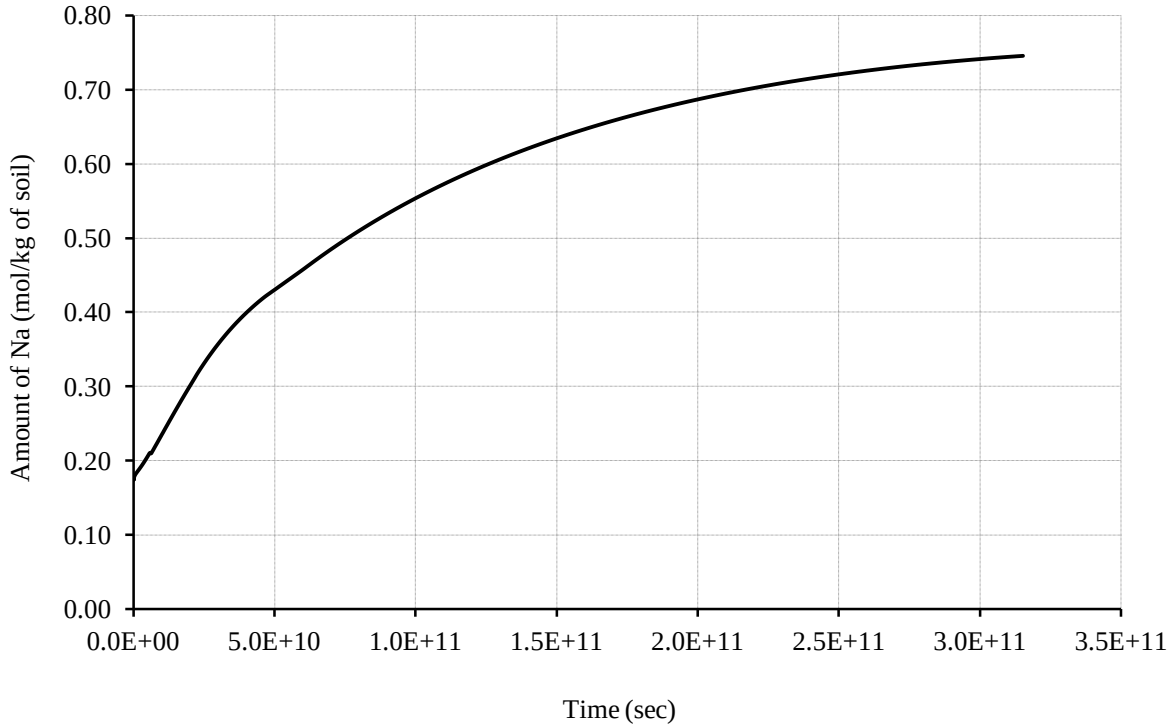

Figure 7.27: Evolution of sodium (Na^+) ion due to hydrogen and iron influx for a simulation period of 10,000 years.

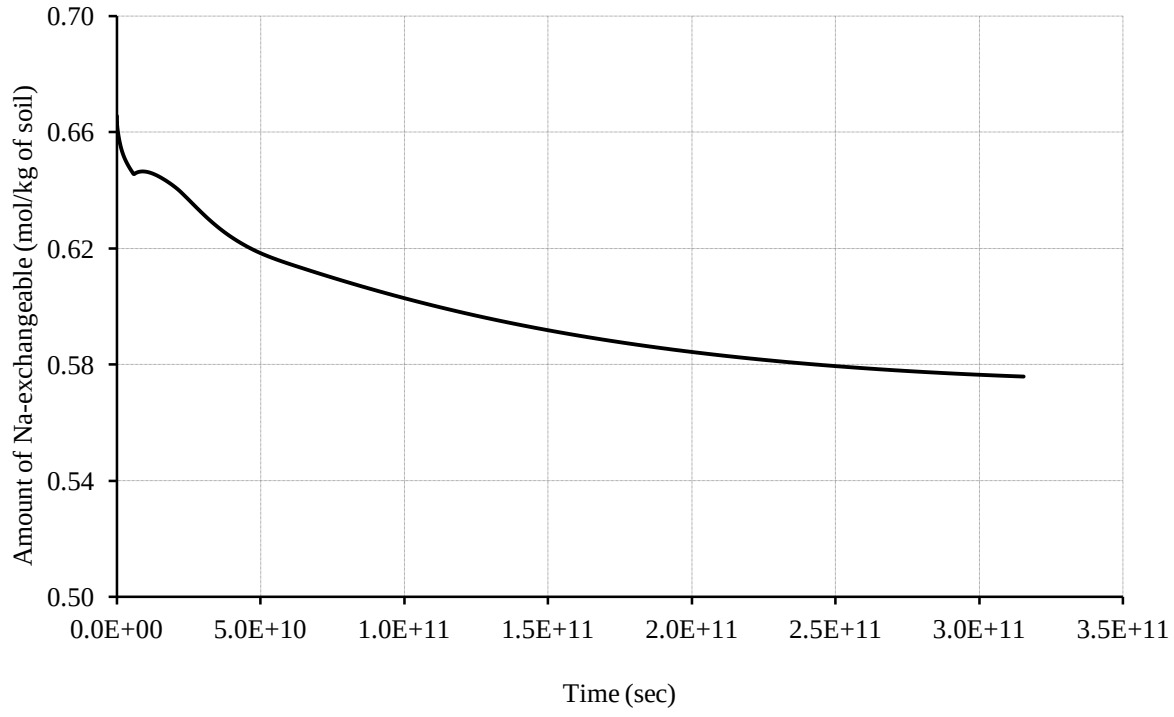

Figure 7.28: Evolution of Na-exchangeable for a simulation period of 10,000 years.

7.5.6 Evolution of calcite and gypsum

The evolution of gypsum and calcite has been presented in Figure 7.29 and Figure 7.30. Figure 7.29 shows that the dissolution of gypsum took place at very early stage of the simulation comparing to the result of previous simulation, Figure 7.3.

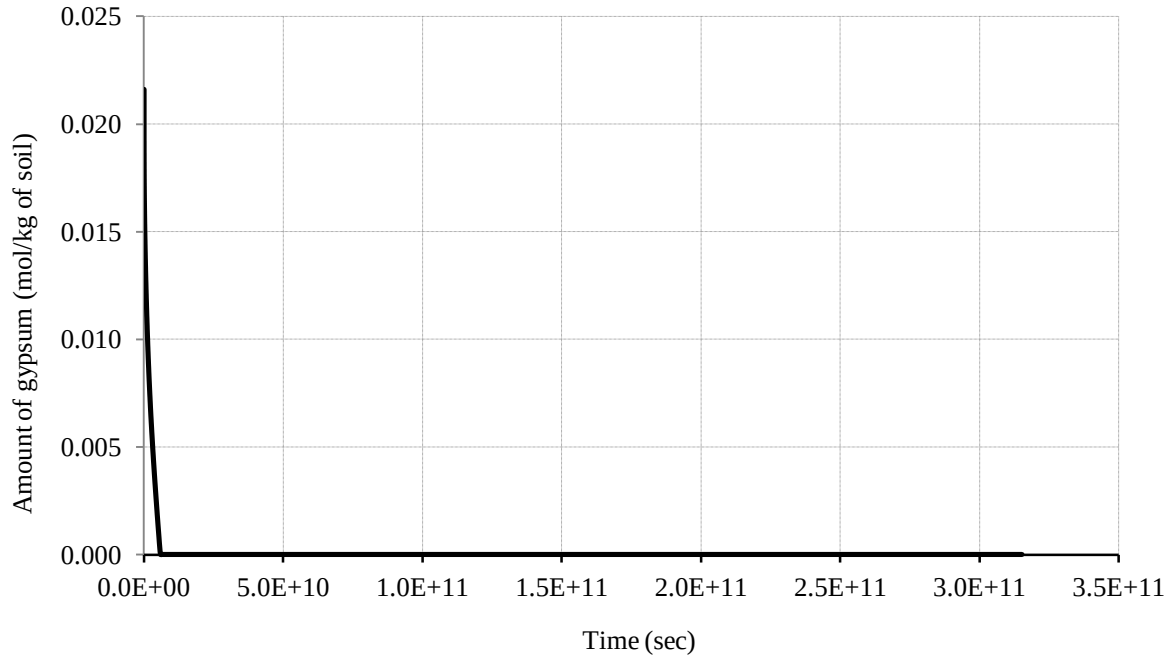

Figure 7.29: Evolution of gypsum for a simulation period of 10,000 years.

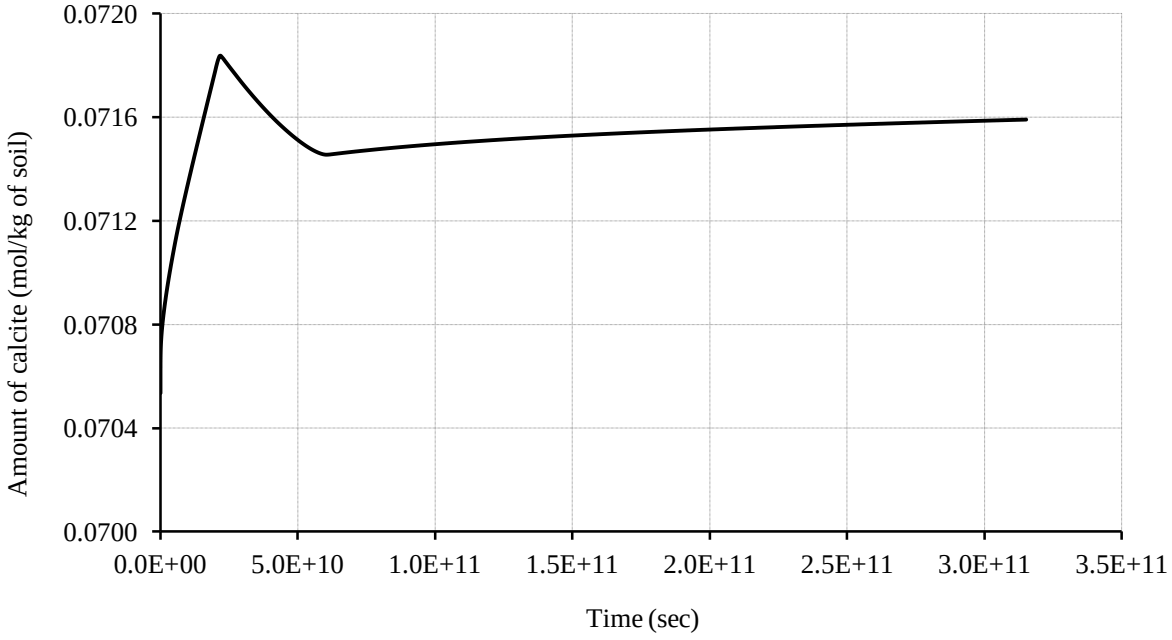

Figure 7.30: Evolution of calcite in the buffer for a simulation period of 10,000 years.

The presence of ferrous ions in the solution reacts with sulphate and precipitate as ferrous sulphate. Therefore, in this simulation the dissolution of gypsum was very rapid. The evolution of calcite has been presented in Figure 7.30. The evolution behaviour is different than that of the previous simulation. This is due to the present of ferrous and ferric ions which react with the calcites and exchange the calcium ion for ferrous/ ferric ions. As a result the sharp rise of calcite mineral follows by a slight drop and starts to rise again, as long as the chemical processes continues.

7.5.7 Conclusion

The results of simulation set-2 have been presented in detail in this section. From the results of this simulation, it has been observed that the flow and chemical processes of the gas component remain similar to the previous simulation which considers only hydrogen influx at the injection face. The influx of iron has dramatically increased the amount of ferrous ions in the solution. Fe-exchangeable has replaced the other cations from the cation exchange zone due to its higher concentration and activity in the solution. The pH of the system in this simulation has decreased a considerable amount in comparison with the result of previous simulation.

7.6 Overall conclusion

Numerical simulations have been carried out to observe the reactive gas flow through a partially saturated bentonite buffer and its impact on the chemical behaviour of the medium.

Since the geochemical processes of gas components directly related to the chemical composition of the porewater, simulations have been carried out to obtain the porewater compositions for the material at various water contents. The widely used Bradbury and Baeyens model has been used to determine the porewater composition of compacted bentonite samples. Geochemical model PHREEQC has been used in this study to calculate the porewater composition. The results of porewater composition for various dry densities have been compared with the results provided by Bradbury and Baeyens and a good agreement between the results have been obtained. To observe the impact of gas pressure on the porewater composition, batch reaction calculations have been carried out which further increases the understanding of the chemical behaviour of the buffer.

The results of two simulation sets have been presented in great details. In case of gas influx only simulations, the recorded gas concentration at gas phase in the buffer after the simulation period of 10,000 years is very negligible comparing to the simulation where porewater has been considered as distilled water. Due to the chemical components and processes involved in the buffer, most of the gas has been used in the near field of the buffer suggesting that the buffering capacity of compacted bentonite sample is sufficient enough to prevent the development of high gas pressure in the buffer. Another important conclusion can be drawn from the simulation pH results. The pH of the buffer remains close to its initial value suggesting that the bentonite buffer also provides sufficient resistant towards the pH change due to hydrogen influx. Minerals, such as gypsum and calcite plays important role on the evolution of cations and anions present in the solution. It has been found that the flow of gas through the buffer influence the concentrations of dissolved chemical components and exchangeable cations in the cation exchange zone.

From the results of the second set of simulation, where both hydrogen and iron influx has been considered, it has been observed that the flow and chemical processes of the gas component remain similar to the previous simulation which considers only hydrogen influx at the injection face. Therefore, it can be suggested that in presence of iron influx gas pressure of hydrogen did not increase significantly. The influx of iron has dramatically increased the

amount of ferrous ions in the solution. Fe-exchangeable has replaced the other cations from the cation exchange zone due to its higher concentration and activity in the solution. The pH of the system in this simulation has decreased a considerable amount in comparison with the result of previous simulation

References

Andersson C., Bárcena, I., Bono, N., Boergesson, L., Cleall, P., Forsmark, T., Gunnarsson, D., Johannesson, L.E., Ledesma, A., Liedtke, L., Luukkonen, A., Pedersen, K., Puigdomenech, I., Pusch, R., Rhén, I., Rothfuchs, T., Sandén, T., Sineriz, J.L., Sugita, Y., Svemar, C., Thomas, H.R., (2000). "Full-Scale Testing of the KBS-3V Concept for the Geological Disposal of High-Level Radioactive Waste PROTOTYPE REPOSITORY". Nuclear science and technology, Final Report, EUR 21924.

Bradbury, M., Baeyens, B., (1997). "A mechanistic description of Ni and Zn sorption on Na–montmorillonite: Part II. Modelling". *Journal of Contaminant Hydrology* **27**, pp. 223–248.

Bradbury, M., Baeyens, B., (2002). "Porewater chemistry in compacted re-saturated MX-80 bentonite: physicochemical characterisation and geochemical modelling". PSI Bericht 02–10, Villigen PSI and NTB 01– 08,Nagra, Wettingen, Switzerland.

Bradbury, M., Baeyens, B., (2003). "Porewater chemistry in compacted re-saturated MX-80 bentonite". *Journal of Contaminant Hydrology* **61**, pp. 329 - 338

Bonin, B., Colin, M., Dutfoy, A., (2000). "Pressure building during the early stages of gas production in a radioactive waste repository". *Journal of Nuclear Materials* **281,** No.1, pp. 1-14.

Cussler, E.L., (1984). "Diffusion: Mass Transfer in Fluid Systems". Cambridge University Press, Cambridge.

EBS, (2005) "Specification of benchmark THM 1.1, bentonite THM mock-up experiments performed by CEA, Notes for Task Force on Engineered Barrier System".

Fredlund, D.G., Rahardjo, H., (1993). "Soil Mechanics for Unsaturated Soils". John Wiley, New York.

Huertas F., Fuentes-Cantillana J.L., Jullien F., Rivas P., Linares J., Farina P., Ghoreychi M., Jockwer N., Kickmaier W., Martines M.A., Samper J., Alonso E., Elorza F.J., (2000). "Full-scale engineered barriers for a deep geological repository for high-level radioactive waste in crystalline host rock (FEBEX project)". European Commission, Nuclear science and technology series, Report EUR 19147 EN.

Lasaga, A.C., (1998). "Kinetic Theory in the Earth Science". Princeton Series in Geochemistry, Princeton University Press.

Millington, R.J., Quirk, J.M., (1961). "Permeability of porous solids". *Transactions of Faraday Society* **57**, pp 1200–1207.

Müller-Vonmoos, M., Kahr, G., (1982): "Bereitstellung von Bentoniten für Laboruntersuchung". *Nagra Technical Report NTB 82-04*, Wettingen, Switzerland.

Müller-Vonmoos, M., Kahr, G., (1983): "Mineralogische Untersuchungen von Wyoming Bentonite MX-80 und Montigel". *Nagra Technical Report NTB 83-13*, Wettingen, Switzerland.

Parker, J.C., Lenhard, R.J., Kuppusamy, T., (1987). "A Parametric Model for Constitutive Properties Governing Multiphase Flow in Porous Media". Water Resources Research, **23**, No. 4, pp 618–624.

Parkhurst, D.L., Appelo, C.A.J., (1999). "User's guide to PHREEQC (version 2)", U.S. Geological Survey, Water Resource Investigation Report, 99-4259.

8

Conclusions and Suggestions for Further Research

8.1 Introduction

Specific conclusions pertinent to each chapter have been presented at the end of each chapter. This chapter aims to synthesise the conclusions relevant by this research relate to the objectives presented at the start of this work. Key contributions and advancements will be highlighted throughout this chapter followed with opportunities for further work.

8.2 Summary and conclusions of the work

In order to investigate the reactive gas transport processes in variably saturated soils a coupled thermo-hydro-chemical-gas-mechanical model has been developed in the scope of this work and has been presented in this thesis. The summary and conclusion of individual chapters have been presented briefly in this section.

8.2.1 Literature review

A selective literature review has been carried out to address the gas generation and migration issues in chapter 2. Throughout the review various aspects related to the transport and fate of gases has been identified and the importance of this work has been established.

It has been suggested that gas transport processes are directly related to the generation rates. Since gas generation due to metallic corrosion is an important issue in context of nuclear waste disposal, the corrosion process has been initially examined, with the overall reactions and a kinetic method to determining gas generation rate reported. It has also been reported that the presence of buffers could enhance the corrosion process. It has been found that the gas generation rates entirely depend on corrosion rates in a deterministic manner. A range of corrosion rates and therefore gas generation rates have been presented in this section from experimental work.

Gas flow through unsaturated buffer has been reviewed to understand the principle flow mechanisms. Most of the gas migration experiments related to high level waste disposal has been undertaken for saturated buffer. It has been reported that the gas migration through saturated buffer is ambiguous where a number of mechanisms has been deemed to exist with the some debate over the dominant mechanism.

Since migration of gases might influence the chemical behaviour of the buffer, gas-liquid interface has been considered as the principle zone for geochemical reactions. A review of geochemical reactions and processes of special interests, associated with gas flow, has been presented. The structure of the buffer and controlling factors of porewater compositions have been reviewed briefly. It has been known that the bentonite porewater contains various chemicals and minerals in considerable amount.

A comprehensive review on the computational aspects of the reactive transport of gas has been presented in chapter 2. The sequential non-iterative approach has been found more efficient to solve the governing equations for transport and chemical reactions.

8.2.2 Theoretical and numerical formulation

Theoretical and numerical formulations of governing flow and deformation behaviour have been developed in the framework of coupled THCM modelling which have been presented in chapter 3 and chapter 4 respectively. In particular, the framework has been extended by implementing the newly developed multicomponent reactive gas transport as being one of the major objectives in this work.

The governing gas flow equation has been developed by adopting the law of conservation of mass via molar form. The concentration or pressure gradient has been defined as the principle driving potential for gas flow. Multicomponent advective and diffusive gas flow have been characterised using Darcy's law and Fick's law respectively. At equilibrium, various chemical/geochemical reactions have been calculated using geochemical model PHREEQC2 and the results have been incorporated in the governing equation using a sink/source term. Geochemical reactions, such as precipitation/dissolution, ion-exchange, redox processes, phase equilibrium etc. have been considered. The formulation has been developed for both isothermal and non-isothermal condition although isothermal condition has been prioritised over non-isothermal in this study. The theoretical development of moisture flow, heat flow, dissolved chemical flow and deformation has been adopted in this work from previous developments.

To solve the series of the governing equations, a numerical approximation has been adopted for all primary variables related to the flow and deformations. In particular, the finite element method has been used to provide a spatial solution and the finite difference method used to provide a temporal solution. A finite element solution for spatial discretisation has been employed based on Galerkin weighted residual method. A finite difference scheme for temporal discretisation has been considered based on a forwards difference, mid-interval time stepping algorithm. Based on the comprehensive review on the computational aspects of the reactive transport of gas and dissolved chemicals, presented in chapter 2, sequential approach has been found to be efficient to solve the governing equations for transport and chemical reactions. Therefore, the coupling between the transport and geochemical models has been achieved with adaptation of a sequential non-iterative approach. The developed theoretical formulation and the numerical solution present a robust and advanced computational approach to study the reactive gas transport processes in the framework of coupled THCM behaviour.

8.2.3 Verification of theoretical developments

A number of verification exercises have been presented in chapter 5, following the objective of this work, to test the implementation of governing equations of multicomponent gas flow in the THCM model. The key components of gas transport including advective flow, diffusive flow and the geochemical sink/source term of the governing equations of gas transport have been verified with available Analytical solutions, alternative numerical solutions.

Two sets of simulations have been carried out to verify transport of a single gas through unsaturated porous medium. The developed model has been verified against an analytical solution, for a single gas, in case of pure diffusion and advective-diffusive flow. A good agreement between the simulated results and analytical solutions has been achieved. To verify the multicomponent advective flow, two sets of verification exercise have been presented. Verification of three gas components has been detailed by employing an analytical approach and the results of two gas system have been compared with the results of an alternative numerical model. Verification exercises of multicomponent diffusion have been demonstrated. It has been found that the multicomponent diffusive gas flow is dominated by the diagonal elements of the multicomponent diffusion coefficient matrix and these values are similar to the binary diffusion coefficients. The simulation considering binary diffusion has shown a similar flow pattern to the multicomponent diffusive flow pattern. In case of similar order diffusion coefficients, negligible difference in flow pattern has been observed in both binary diffusion and multicomponent diffusion. The implementation of the geochemical sink/source term of the governing equation has also been presented. Good agreement has been obtained between the simulation results and the manual calculation, transport model simulation and transport model - chemical model simulations. Therefore, the accuracy of the sink/source term as well as the efficient implementation of sequential non-iterative approach adopted for coupling the transport and reaction formulations have been verified.

8.2.4 Gas migration and pressure development in saturated clay buffer

As an implementation of the model to simulate non-reactive gas flow through fully saturated buffer, numerical simulations have been carried out which have been detailed in chapter 6. It has been understood that the saturated clay buffer in a high level nuclear waste disposal facility is subjected under pressure development due to corrosion of metallic canisters. At an elevated pressure pneumatic fracture could possibly develop in the buffer, affecting the safety

and performance of the system. Therefore, investigations have been focused on the development of maximum pressure and the dominant flow mechanisms in the buffer.

Simulations have been undertaken based on a number of scenarios including host rock geology, disposal concept, buffer thickness, material parameters, boundary conditions and gas generation rates. The realistic and conservative gas generation rates collected from the literature have been used at the gas injection boundary in the simulations. From the results of numerical simulation, it has been observed that in all cases of realistic and most cases of conservative rates, the risk of development of pneumatic fracture has been found negligible. In a worst case, using over conservative gas generation rate, ignoring water consumption and having lower bound diffusion in clay yielded a pressure higher than that require for the development of fracture. However, these simulations are thought to be very conservative, in both boundary condition conceptualisation and gas generation rate. Further experimental work could confirm this is the case. In most simulations, pressure development considering gas influx and water outflow has been found less than that of gas influx condition only. The results of simulations suggest that the diffusive flow plays significant role in case of fully saturated buffer. More experimental evidence is required to establish this process in long term and the diffusion coefficients require further investigation to confirm the appropriateness.

8.2.5 Gas transport and reactions in unsaturated clay buffer

Chapter 7 deals with the implementation of the model to simulate reactive gas flow through a partially saturated clay buffer and its impact on the chemical behaviour of the medium. Investigation has been carried out to observe the long term flow behaviour of gas through partially saturated buffer in presence of various chemicals. The porewater of bentonite buffer contains significant amount of chemicals depending on the material condition. Therefore, modelling of porewater composition has been carried out prior to reactive transport simulations. Geochemical model, PHREEQC2 has been used to calculate the porewater composition at various water contents. Two sets of simulations have been conducted to address the aforementioned investigation. Details of parameters and boundary conditions have been presented in chapter 7. The first simulation set considers the influx of hydrogen at the injection boundary whilst in the second set of simulation both hydrogen and iron influx has been adopted, since the process of corrosion produces both hydrogen and magnetite.

The results of two simulation sets have been presented in great details. In case of gas influx only simulations, the recorded gas concentration at gas phase in the buffer after the simulation period has been observed negligible in comparison to the simulation where porewater has been considered as distilled water. The results of pH evolution and distribution remain close to its initial value suggesting that the bentonite buffer provides sufficient resistant towards the pH change due to hydrogen influx. Minerals, such as gypsum and calcite plays important role on the evolution of cations and anions present in the solution. It has been found that the flow of gas through the buffer influences the concentrations of dissolved chemical components and exchangeable cations in the cation exchange zone. The results suggest that the gas has been broadly involved in chemical reactions with the other components present in the buffer. The buffering capacity of compacted bentonite sample is sufficient enough to accommodate the hydrogen generated due to corrosion and prevent the development of high gas pressure.

From the results of the second set of simulation, it has been observed that the flow and chemical processes of the gas component remain similar to the previous simulation which considers only hydrogen influx at the injection face. Therefore, it can be suggested that the presence of iron did not significantly alter the reactive flow of hydrogen. The amount of ferrous ions and Fe-exchanges in the buffer has increased considerably due to iron influx. Comparing to the previous simulation, a reduced level of pH has been recorded in this simulation.

8.2.6 Analysis of the assumptions and limitations of the work

The research has been carried out to advance the knowledge and understanding of multicomponent reactive gas transport through unsaturated soil. Some of the major issues in this subject area have been addressed in the scope of this work. But similar to any other research work, this study also is enclosed by some limitations or assumptions those have been made due to inadequate information or just to simplify the complexities of the associated problems. Some of the assumptions and limitations have been highlighted below:

- The study considers soil as a homogeneous isotropic material which is rare in practical scenarios. The substitution of soil heterogeneity with homogeneity could potentially under estimate some of its key properties while the others could be overestimated.

- The simulations in this study have been carried out at constant volume conditions with the assumptions of a constant void ratio or porosity. The change in void ratio of the medium is time dependent because of mineral precipitation or dissolution in case of reactive gas transport. Due to lack of information and limited time, it has been beyond the scope of this work which can be considered in a future work of multicomponent reactive gas transport.

- The flow of water vapour has been considered with the liquid water in the governing equation of moisture transfer, although the flow behaviour is similar to any other atmospheric gases. Sink/source term of the vapour flow equation which arises due to evaporation/ condensation is yet to be fully understood in case of long term vapour transport. Since, the combined flow of water and vapour revoke the sink/source term, conservation of mass is balanced at all time during the simulation. Therefore, the computational complexity associated with the water vapour sink/source term can be overcome, although the inclusions of vapour phase in the governing equation of multicomponent reactive gas transport would be more appropriate.

- The geochemical reactions have been modelled at equilibrium conditions. In case of long term simulations both equilibrium and kinetically controlled reactions are important. The combined feature provides an efficient and rigorous modelling of reactive transport of chemical/gas components. Although the developed multicomponent reactive gas transport model is able to simulate kinetically controlled reactions, due to insufficiency of knowledge/information in this particular research area, such modelling capability could not be demonstrated.

8.3 Overall conclusions

The overall conclusions of the research can be presented as:

- Several aspects relating to the theoretical modelling of the multicomponent reactive gas flow behaviour of unsaturated soils have been developed in this thesis. The newly developed gas transport equation has extended the modelling capability of coupled THCM behaviour of compacted clays.

- The coupling of robust geochemical model PHREEQC2 to the THCM model significantly improves the capability to simulate the reactive transport of gas and chemicals under equilibrium controlled chemical reactions. Advanced geochemical features are therefore, introduced into the coupled thermo-hydro-gas-chemical-mechanical model.

- Verification exercises of the developed model have been carried out, exploring the accuracy of the theoretical formulations and the numerical approach. The results indicated that the techniques, adopted to solve the governing equations for flow and deformation, and the sequential scheme, implemented to solve the governing equations for reactive transport of chemicals, provide an efficient solution for the problems considered.

- In a mixture of multicomponent gases, advective flow of an individual component takes place due to the bulk flow and the direction of flow is from the region of higher pressure (or concentration) to that of the lower pressure (or concentration). In a multicomponent gas mixture, change in concentration or pressure of a particular component influence the bulk flow which ultimately alters the flow of all gas components present in the system.

- Multicomponent diffusion of gases can be explained using the extended form of Fick's law which was originally developed for binary diffusion. The multicomponent diffusion is dominated by the diagonal terms of the multicomponent diffusion matrix. The values of the diagonal diffusion matrix have been obtained similar to that of the binary diffusion coefficients. Gases with higher order of diffusion coefficients might affect the diffusive flow of other components with lower value of diffusion

coefficients. On the other hand, gases with similar order diffusion do not influence the movement of other components present in the system. In case of similar order diffusion coefficients, the results based upon multicomponent diffusion are identical to the results of binary diffusion.

- Maximum pressure development in saturated compacted buffer in case of realistic gas generation rate has been found significantly less than the pressure required for developing pneumatic fracture. Therefore, development of such elevated gas pressures and consequent gas flow through pressure induced preferential pathways in saturated buffer is unlikely.

- Diffusive flow has been identified as a principal transport mechanism in saturated clay buffer at realistic gas generation rates.

- From the simulations of reactive gas transport through unsaturated soil repository gases, such as hydrogen has been found more reactive in presence of a compacted clay i.e. sodium bentonite buffer. At normal pressure and temperature hydrogen is less soluble in pure water but more soluble in the porewater of compacted bentonite which contains a considerable amount of dissolved chemicals and minerals in it. In presence of hydrogen various geochemical reactions such as gypsum dissolution, calcite precipitation and cation exchange are accelerated due to an increase of redox potential of the solution or porewater. The execution of these chemical reactions increases the demand of hydrogen ion in the solution which is supplied by the available hydrogen in gas phase. The presence of iron in the buffer due to corrosion does not affect the flow behaviour of hydrogen gas, although it significantly manipulates the other chemicals present in the system.

- The buffering capacity of bentonite buffer is sufficient to accommodate the amount of gas generated at a realistic generation rate over a period of thousand years.

- Therefore, from the result of this study, it can be claimed that the newly developed model is an advanced tool for assessing multicomponent reactive gas transport processes under variable physical, chemical and mechanical conditions in variably saturated porous mediums. Applications of the work to the case of compacted swelling clays have been carried out throughout this thesis. The developed model can be applicable in the research area of carbon sequestration, coal gasification, shale gas extraction etc.

8.4 Suggestions for further research

The developed model has been implemented in this thesis to simulate the reactive gas transport processes under coupled THCM behaviour of compacted clay buffers. However, the numerical code is under constant development to improve its efficiency and capabilities. The following suggestions are made for further research and developments especially for modelling the coupled processes in a porous medium, such as compacted bentonite:

Laboratory experiments of gas migrations predominantly focused on saturated buffer condition. The short term experiments often consider a very high gas injection rate comparing to the real rates. This could possibly lead the understanding of flow behaviour for a very special case rather than the general conditions. Therefore, long term experiments using realistic gas generation rates in case of fully saturated buffer should be carried out.

Large scale experiments should be carried out using real generation rates to identify the dominant flow mechanism in a saturated buffer. Particularly, the diffusive flow mechanisms should be investigated in great details. More experimental effort is required to determine the diffusion coefficients of gas components through porewater. Laboratory experiments often consider helium or nitrogen as a safe replacement of hydrogen which are more inert in nature. But hydrogen can be involved in various chemical processes due to its chemical activity. Therefore, more experimental and numerical study is required to understand the behaviour of hydrogen in variably saturated clay buffers.

In case of unsaturated buffer, both reactive and non-reactive gas flow experiments have rarely conducted. Therefore, to understand the flow processes and to calculate the material parameters more experimental research should be carried out. Long term corrosion experiments are required to identify the real corrosion rate of metallic canisters of high level waste disposal facility

The variability of material parameters is not well known. This is possibly due to the time and expense required to undertake multiple experiments. However, this is key to understanding the predictive capabilities of numerical simulation. Only when the reliability of models and the material variability has been established and quantified may the models be used in a truly predictive capacity.

The buffer has always been considered as a homogenous material ignoring the natural heterogeneous properties. Inclusion of more heterogeneity into numerical models is required to be able to fully predict various flow processes in buffers.

Information about chemical/geochemical reactions related to reactive gas transport is insufficient. Available reaction database should be extended by incorporating more such chemical reactions. The geochemical reactions consider equilibrium constant measured at a particular pressure and temperature condition. But in case of long term simulations the equilibrium constants may change with time resulting in wrong prediction of the behaviour of the whole system. More research effort is required to enrich the knowledge in this subject area.

Hydro-chemical and thermo-hydro-chemical processes influence the compositions of porewater. Since porewater remains as the most important phase for gas-chemical interactions, further research is essential including all of the important processes.

Extensive verification and validation tests should be carried out to ensure accuracy and efficiency of the multicomponent reactive transport model. Due to lack of information the results of developed model could not compare with other experimental/ numerical results. Laboratory experiments are essential to enrich the multicomponent reactive gas transport research.

The initial development of reactive gas model has been limited to isothermal condition only. Further work should consider non-isothermal condition, since the transport of gas and the extent of reaction are subjected to temperature change. In this context more work is required to update the reaction database, such as the temperature effect on equilibrium constants.

Computer technology that enables the simulations to be undertaken is transient and as such the ability to undertake large scale or complex analyses generally increases with time. New algorithms must be developed and adopted for faster and efficient computing.